PROGRAMA DE DOCTORADO INTERUNIVERSITARIO EN ARQUEOLOGÍA PREHISTÓRICA

TESIS DOCTORAL

EL BAJO VALLE DEL SADO DURANTE EL HOLOCENO

EVOLUCIÓN PALEOAMBIENTAL, GEOMORFOLOGÍA Y ADAPTACIONES DE LOS CAZADORES RECOLECTORES TARDÍOS

PhD THESIS

THE LOWER SADO VALLEY DURING THE HOLOCENE

PALAEOENVIRONMENTAL EVOLUTION, GEOMORPHOLOGY AND LATE HUNTER-GATHERERS' ADAPTATIONS

AUTORA

Ana Maria Caixado Novo da Costa

DIRECTORES

Pablo Arias Cabal

Maria da Conceição Pombo de Freitas

UNIVERSIDAD DE CANTABRIA

UNIVERSITAT AUTÒNOMA DE BARCELONA

Escuela de Doctorado de la Universidad de Cantabria

Santander 2022

UNIVERSIDAD DE CANTABRIA

UNIVERSITAT AUTÒNOMA DE BARCELONA

Programa de Doctorado en Arqueología Prehistórica

TESIS DOCTORAL

EL BAJO VALLE DEL SADO DURANTE EL HOLOCENO

EVOLUCIÓN PALEOAMBIENTAL, GEOMORFOLOGÍA Y ADAPTACIONES DE LOS CAZADORES RECOLECTORES TARDÍOS

PhD THESIS

THE LOWER SADO VALLEY 8000 YEARS AGO

RELATIONS BETWEEN ENVIRONMENTAL EVENTS AND CULTURAL ADAPTATIONS

Realizada por: Ana Maria Caixado Novo da Costa

Dirigida por: Pablo Arias Cabal

Codirigida por: Maria da Conceição Pombo de Freitas

Escuela de Doctorado de Universidad de Cantabria

2022

Costa, AM, 2022
El bajo valle del Sado durante el Holoceno: evolución paleoambiental, geomorfologia y adaptaciones de los cazadores recolectores tardios.
The lower Sado valley 8000 years ago: relations between environmental events and cultural adaptations.

Back cover photo CC BY-NC-ND José Vicente, Agência Calipo, 2020

To:
Avô Chico and Avó Maria
mãe and pai
Alice, André and Zé

ABSTRACT

Abstract

Between ca. 8400-7000 cal BP (6450 and 5050 cal BC) Late Mesolithic communities occupied the Sado valley embankments, upstream Alcácer do Sal, Portugal. The consumption of marine resources is attested by the shell waste abandoned in several sites (known as shell middens) and later confirmed by isotopic analyses on bone collagen from individuals buried in these locations.
During the time-period of Late Mesolithic occupation, the sea level was rising, mostly in response to global warming, allowing for the flooding of the pre-incised Sado valley by marine water and forming an extensive estuarine area. Consequently, several questions arose: Did these communities colonize the margins of an estuarine environment where marine resources were available? How was the environmental context in the Sado valley during the Late Mesolithic? How did it evolve through time?
In order to solve those questions, a geophysical survey using the Electrical Resistivity Tomography (ERT) method was performed to characterize the subsurface configuration of the Sado valley and its tributaries, close to the area where shell-middens are located. Additionally, sediment cores were collected in the proximity of the ERT profiles and the sediments analysed for multi-proxies and radiocarbon dated contributing to reconstruct the Mesolithic environmental conditions and landscapes, and its evolution through the Holocene.
The ERT model's interpretation allowed recognising a deeply incised valley (between ca. 40 and 30 m depth) in the occupied area of the Sado channel and less deep valleys in the tributaries (ca. 15 m).
The multi proxy analyses (texture, magnetic susceptibility, organic composition and chemistry, *n*-alkanes and palynology) performed in the 13.5 m-long sediment core (Arez3) collected at the Carrasqueira stream, a tributary of the Sado located near the most downstream shell midden and with a palaeovalley depth of ca. 15 m, point to the presence of an estuarine environment in the area until 7040 cal BP (5090 cal BC; -390 cm MSL). Higher marine influence was identified between ca. 8850 cal BP (ca. 6900 cal BC; at the core base) and ca. 7450 cal BP (ca. 5500 cal BC; at -750 cm MSL) revealing an estuarine environment similar to the present-day central estuarine basin, suitable for the development of shellfish banks. This fact is evidenced by the presence of foraminifera shells (usually not preserved in Sado sediments due to under saturated $CaCO_3$ conditions) and marine and brackish diatoms. By then, the sedimentation rates were lower than the rate of sea level rise forming a drowned area with intertidal environments developing the less incised margins. After 7040 cal BP (5090 cal BC), slightly coincident with the deceleration of the sea level rise rate, the contribution of OM from terrestrial plants and freshwater phytoplankton

to the sediment starts to increase reflecting changes in the sedimentary pattern, with the estuarine environment progressively giving way to freshwater environments. Since the Middle Holocene (ca. 6530 cal BP; 4580 cal BC), negative shifts of $\delta^{15}N$ to values ~0‰ point to hypereutrophication and cyanobacteria bloom episodes under backswamp conditions in the Carrasqueira valley.

The sediment cores collected in the Sado channel at Arapouco (7 m-long), near the most downstream shell midden and at Laxique (10.5 m-long), at the proximity of Cabeço das Amoreiras, one of the shell middens located more upstream, allowed for the palaeoenvironmental reconstruction of the area only during the Middle-Late Holocene transition and through the Late Holocene.

At the most upstream location, Laxique, located at ca. 65 km of the present-day estuarine inlet and ca. 15 km upstream the present-day estuarine limit, the multi-proxy analyses allowed to concluded that: i) the organic matter is mostly sourced in terrestrial/freshwater environments even during periods with marine influence suggested by the occurrence of marine benthic diatoms between 4300 and 4200 cal BP (between 2350 and 2250 cal BC); ii) the fluvial-estuarine boundary retreat for a short period during the Middle to Late Holocene transition (4350-4000 cal BP; 2400-2050 cal BC) reaching Laxique; iii) modifications on the location of the fluvial-estuarine boundary are mostly derived from drier climatic conditions and consequent flow river discharges; iv) the aggradation and progradation of the alluvial plain started at ca. 4000 cal BP (2050 cal BC).

At the most downstream location, Arapouco, located ca. 50 km upstream the present-day estuarine inlet and coinciding with the present estuarine limit, the lithofacies, geochemistry and diatom assemblages in the sediments accumulated between 3570 and 3240 cal BP (1620 and 1290 cal BC) point to: i) mixture between terrestrial and marine organic matter sources that varied through time as sedimentation progressed in a low intertidal to high subtidal and low-energy accreting tidal flat; ii) a general pattern of drier and higher aridity conditions, punctuated by century-long changes of the rainfall regime that mirror an increase in storminess that affected SW Portugal and Europe; iii) downstream displacement of the estuarine/freshwater transitional boundary between 3570-3400 (1620-1450 cal BC) and 3300-3240 cal BP (1350-1290 cal BC), intercalated by one episode where marine influence shifted upstream; and iv) exceptional high sedimentation rates due to high terrestrial sediment delivery to this location. The aggradation of the alluvial plain started at ca. 3240 cal BP (1290 cal BC) accompanied by a pronounced change in sedimentation rate that decreased by two orders of magnitude. The abrupt changes in the sedimentation rates and sedimentation pattern before and after the beginning of the alluvial plain

aggradation at both locations reflects essentially changes in the fluvial activity and the loss of accommodation space.

According to these results, brackish conditions prevailed in the Sado estuary (including the lower valleys of some tributaries) during the Late Mesolithic occupation of the area (ca. 8400-7000 cal BP; 6450-5050 cal BC), offering suitable environmental conditions for the development of molluscs and thus conditions for the exploitation of these resources by Mesolithic people. Estuarine conditions were present, at least, since ca. 8850 cal BP (ca. 6900 cal BC) and prevailed until ca. 7040 cal BP (ca. 5090 cal BC). Saltmarshes developed in the area as revealed by the high percentage of Chenopodiaceae pollen, while freshwater wetlands certainly occurred in upstream areas of the valley as proven by the appearance of *Isoetes*. In the emerged landscape, the abundance of mesophilous trees, such as evergreen and deciduous *Quercus*, suggest mostly the existence of a moist climate during the Late Mesolithic occupation.

From 7450 cal BP (5500 cal BC) onwards, still during the last phases of the Late Mesolithic, the marine influence seems to retreat in the Carrasqueira valley, but estuarine conditions were present in this tributary, at least, until ca. 7040 cal BP (5090 cal BC). Estuarine environments certainly developed in the Sado channel, at least, until ca. 57 km upstream the present-day estuarine inlet, coinciding with the middle of the occupied section of the river. At this location the Sado has a deeply incised valley (ca. 38 m, i.e. -34 m MSL) that was certainly flooded by marine waters during the Mesolithic occupation period, given the contemporaneous depth of the MSL (ca. -8.9 m at 8300 cal BP (6350 cal BC) and -1.6 m at 6900 cal BP (4950 cal BC) below present) and the radiocarbon age of the sediments in depth (2288-1995 cal BP; 338-45 cal BC; at -9.4 m MSL).

The maximum extension of the estuarine area during the Mesolithic occupation is still unknown. Despite being possible to indicate the depth of the palaeovalley at Laxique (ca. 30 m depth, i.e. -23 m MSL) based on abrupt differences in the electric resistivity signal, the relation between the resistivity values and the valley infilling is difficult to access. The sedimentary association to geophysical response points to coarse sediments fulfilling the Sado valley at that location. Such coarse materials could correspond to alluvial fan deposits that impeded the marine front to advance or to sediments related to an old bay-head delta that today is not identifiable at the surface. Further analyses are needed to disentangle between those two hypotheses.

Keywords: Geoarchaeology; Late Mesolithic; Holocene; High-resolution multi-proxy analyses; Sensitive-environmental proxies; Palaeoestuary; Landscape; SW Iberia; Sado Valley

Resumen

Entre ca. 8400 y 7000 cal BP (6450 y 5050 cal BC), las comunidades del Mesolítico final ocuparon las riberas del río Sado aguas arriba de Alcácer do Sal (Portugal). Las acumulaciones de restos de moluscos marinos en diversos sitios (conocidos como concheros) permite constatar el consumo de recursos marinos por parte de esos grupos, lo que se ha visto confirmado por los análisis isotópicos sobre colágeno óseo procedente de individuos enterrados en esos lugares.

Durante el lapso temporal del Mesolítico final, el nivel del mar estaba elevándose, en gran medida como consecuencia del calentamiento global, dando lugar a la inundación del previamente inciso valle del Sado por las aguas del mar, y creando un extenso estuario. En consecuencia, se plantean diversas cuestiones: ¿Colonizaron estas comunidades los márgenes de un ambiente estuarino en el que estaban disponibles los recursos marinos?; ¿qué características presentaba el contexto medioambiental del valle del Sado durante el Mesolítico final?; ¿cómo evolucionó a lo largo del tiempo?

Para resolver esas cuestiones se ha desarrollado una prospección geofísica empleando el método de la tomografía por resistividad eléctrica (ERT) para caracterizar la configuración subterránea del valle del Sado y sus afluentes en la zona donde se localizan los concheros. Así mismo, se obtuvieron testigos sedimentarios en las proximidades de los perfiles de resistividad eléctrica, y los sedimentos han sido objeto de análisis de diversos indicados y datados por radiocarbono para reconstruir las condiciones medioambientales y los paisajes del Mesolítico, así como su evolución a lo largo del Holoceno.

La interpretación del modelo de ERT permitió constatar la existencia de un valle profundamente encajado (entre unos 30 y 40 m de profundidad) en la zona ocupada del canal del Sado, y valles menos profundos en los afluentes (ca. 15 m).

Los análisis *multi-proxy* (textura, susceptibilidad magnética, composición y química orgánica, n-alcanos y Palinología) realizados en el testigo sedimentario de 13,5 m de longitud Arez3, recogido en el arroyo de Carrasqueira, un afluente del Sado situado cerca del conchero situado en la posición más baja, con una profundidad del paleovalle de ca. 15 m, apunta a la presencia de un ambiente estuarino en esta zona hasta 7040 cal BP (5090 cal BC; -390 cm MSL). Se observó mayor influencia marina entre ca. 8850 cal BP (ca. 6900 cal BC; base del testigo) y ca. 7450 cal BP (ca. 5500 cal BC; a -750 cm MSL), mostrando un ambiente estuarino similar a la parte central de la cuenca estuarina, adecuado para el desarrollo de colonias de marisco. Este hecho ha sido confirmado por la presencia de conchas de foraminíferos (que normalmente no se conservan en los sedimentos del Sado por las condiciones infrasaturadas de $CaCO_3$) y diatomeas de aguas

marinas y salobres. En aquel momento, las tasas de sedimentación eran inferiores a las de elevación del nivel del mar, dando lugar a una zona inundada con ambientes intermareales desarrollándose en los márgenes menos incisos. Después de 7040 cal BP (5090 cal BC), coincidiendo aproximadamente con la deceleración de la tasa de ascenso del nivel marino, la contribución de materia orgánica (OM) procedente de plantas terrestres y de fitoplancton de agua dulce a los sedimentos comienza a incrementarse, reflejando cambios en el patrón sedimentario, al tiempo que el ambiente estuarino da paso progresivamente a ambientes de agua dulce. A partir del Holoceno medio (en torno a 6530 cal BP; 4580 cal BC), las variaciones negativas del $\delta^{15}N$ a valores ~0‰ apuntan a episodios de hipereutroficación y explosiones de cianobacterias bajo condiciones pantanosas en el valle de Carrasqueira.

Los testigos de sedimento recogidos en el canal del Sado en Arapouco (7 m de longitud), cerca del conchero situado más aguas abajo, y en Laxique (10,5 m de longitud), en las cercanías de Cabeço das Amoreiras, uno de los concheros situados más aguas arriba, han permitido la reconstrucción paleoambiental del área durante la transición del Holoceno medio al final y durante esta última edad.

En la localidad más elevada, Laxique, situada a unos 65 km de la actual boca del estuario y a unos 15 km aguas arriba del límite de la zona estuarina, los análisis *multi-proxy* nos han permitido concluir que i) la materia orgánica proviene fundamentalmente de ambientes terrestres o de agua dulce, incluso en períodos en los que existen indicios de influencia marina como la aparición de diatomeas bentónicas entre 4300 y 4200 cal BP (2350-2250 cal BC); ii) el límite fluvio-estuarino retrocede por un corto período durante la transición del Holoceno medio al final (4350-4000 cal BP; 2400-2050 cal BC), llegando hasta Laxique; iii) las modificaciones en la localización del límite fluvio-estuarino derivan fundamentalmente de condiciones climáticas más áridas, con las consecuentes descargas fluviales; iv) la agradación y progradación de la llanura aluvial comenzó en torno a 4000 cal BP (2050 cal BC).

En Arapouco, la localidad situada más aguas abajo, a unos 50 km de la actual boca del estuario y en el límite estuarino, las litofacies, la geoquímica y los conjuntos de diatomeas acumulados entre 3570 y 3240 cal BP (1620-1290 cal BC) apuntan a i) variaciones en las proporciones de materia orgánica de origen terrestre y marino según progresaba la sedimentación en una llanura mareal acreciente; ii) un patrón general de condiciones más secas y de mayor aridez, puntuadas por cambios seculares del régimen de lluvias que reflejan un incremento en la tasa de tormentas que afectó al sudoeste de Portugal y a Europa en su conjunto; iii) un desplazamiento aguas abajo del límite transicional estuario/agua dulce entre 3570 y 3400 cal BP (1620-1450 cal BC) y 3300 y 3240 cal BP (1350-1290 cal BC), con un episodio intercalado en el que la influencia marina

ascendió aguas arriba; y iv) tasas de sedimentación excepcionalmente altas, debido al elevado acarreo sedimentario terrestre a esta localización. La agradación de la llanura aluvial comenzó en torno a 3240 cal BP (1290 cal BC), acompañada de un pronunciado cambio en la tasa de sedimentación, que se redujo unos dos órdenes de magnitud. Los abruptos cambios en las tasas y patrones de sedimentación antes y después de la agradación de las tasas de sedimentación en ambas localizaciones reflejan esencialmente cambios en la actividad fluvial y la falta de espacio de acomodación.

Estos resultados indican un predominio de las condiciones salobres en el estuario del Sado (incluyendo los tramos bajos de los valles de algunos afluentes) durante la ocupación mesolítica del área (ca. 8400-7000 cal BP; 6450-5050 cal BC), que ofrecían condiciones medioambientales adecuadas para el desarrollo de moluscos y, por lo tanto, para la explotación de esos recursos por parte de las poblaciones de cazadores-recolectores. Las condiciones estuarinas estuvieron presentes desde al menos ca. 8850 cal BP (ca. 6900 cal BC) y fueron predominantes hasta ca. 7040 cal BP (ca. 5090 cal BC).

El alto porcentaje de Chenopodiaceae revela que se desarrollaron marismas en esta zona, al tiempo que en áreas situadas aguas arriba en el valle existían zonas pantanosas de agua dulce, tal como prueba la aparición de *Isoetes*. En el paisaje emergido, la abundancia de árboles mesófilos, como *Quercus* perennifolios y caducifolios, sugiere que el clima era relativamente húmedo durante la ocupación del Mesolítico final.

A partir de 7450 cal BP (5500 cal BC), aún en las últimas fases del Mesolítico, la influencia marina parece disminuir en el valle de Carrasqueira, pero las condiciones estuarinas estuvieron presentes en este afluente hasta, al menos, ca. 7040 cal BP (5090 cal BC). Se ha podido establecer con seguridad que los ambientes estuarinos se desarrollaron en el canal del Sado hasta, al menos, unos 57 km aguas arriba de la actual boca del estuario, coincidiendo con el centro del sector del valle ocupado durante el Mesolítico final. En esta localización, el Sado tiene un valle profundamente inciso (ca. 38 m, equivalente a -34 m MSL) que fue con toda certeza inundado por las aguas marinas durante el período de ocupación mesolítica, dadas la profundidad contemporánea del nivel medio del mar (ca. -8.9 m en 8300 cal BP [6350 cal BC] y -1.6 m en 6900 cal BP [4950 cal BC]) y la edad radiocarbónica de los sedimentos (2288-1995 cal BP [338-45 cal BC] a -9.4 m MSL).

Se desconoce aún la extensión máxima del área estuarina durante el Mesolítico. Aun siendo posible establecer la profundidad del paleovalle en Laxique (unos 30 m, equivalentes a -23 m MSL) a partir de abruptas diferencias en la señal de resistividad eléctrica, la relación entre los valores de la resistividad y el relleno del valle es difícil de determinar. La asociación sedimentaria a

la respuesta geofísica sugiere la existencia de sedimentos gruesos en esa localización. Dichos materiales podrían corresponder a un abanico sedimentario que habría impedido el avance al frente marino o a sedimentos relacionados con un antiguo delta no identificable actualmente en la superficie. Serán necesarios nuevos análisis para verificar cuál de estas hipótesis es la mejor explicación para estos datos.

Palabras clave: Geoarqueología; Mesolítico final; Holoceno; Análisis *multi-proxy* de alta resolución; métodos ambientales sensitivos; paleoestuario; paisaje; Sudoeste Ibérico; Valle del Sado

ACKNOWLEDGEMENTS

Support and funding

This work was developed in the framework of the following projects:
a) COASTTRAN - *Coastal Transitions - A comparative approach to the processes of neolithisation in Atlantic Europe* (HAR2011-29907-C03-00), funded by the Ministerio de Ciencia e Innovación, Spain;
b) Back to Sado - *A case study between last hunter-gatherers and first agro-pastoralist societies in southern Portugal* (PTDC/HISARQ/121592/2010), funded by Fundação para a Ciência e Tecnologia (FCT), Portugal;
c) CoChange - *Coastal societies in a changing world: A diachronic and comparative approach to the Prehistory of SW Europe from the late Palaeolithic to the Neolithic* (HAR2014-51830-P) financed by the Ministerio de Ciencia e Innovación, Spain;
d) SimTIC - *Symbols below the ground: An approach to the thinking of late Glacial hunter-gatherers using information technology* (HAR2017-82557-P), funded by Ministerio de Economía y Competitividad, Spain.

Ana Maria Costa was supported by the FCT grant SFRH/BD/110270/2015 between 2016-2019.

Instituto Dom Luiz - IDL (UID/GEO/50019/2013 and UIDB/50019/2020) also supported the work presented in the thesis.

Acknowledgements

A PhD is a *long and winding road*[*], but the task is easier due to some people we find in the way.
I would like to express my thanks to my director and supervisor, Pablo Arias, by the opportunity to work in the Portugal SadoMeso projects and the trust in my capability to bring this work to a successful conclusion.
I am very grateful to my co-supervisor, Maria da Conceição Freitas, for the trust, attentiveness, activeness, availability and for give me the opportunity to learn more about coastal areas.
I must thank Mariana Diniz, also responsible for the Portuguese SadoMeso projects, who gave me the change to participate in the archaeological excavations and to develop this work concerning the environmental context of Late Mesolithic people.
My gratitude goes also to Ana Cristina Araújo, Catia, my colleague and friend, with whom I have learned so much about the Mesolithic in Portugal and archaeology, and an unofficial supervisor of this thesis.
I acknowledge the help of all the researchers (other then the aforementioned) and respective institutions who were responsible for some of the analyses presented in this work and for general discussions concerning geological, climatic and archaeological issues (in alphabetically order): Aurora Rodrigues (Instituto Hidrográfico), César Andrade (Faculdade de Ciências da Universidade de Lisboa (FCUL) and IDL - Instituto Dom Luiz), Cristina Barroca Dias (HERCULES Laboratory), Cristina Val-Péon (Institute of Neotectonics and Natural Hazards, RWTH Aachen University), Francisco Fatela (FCUL and IDL) João Duarte (Instituto Hidrográfico), Klaus Reicherter (Institute of Neotectonics and Natural Hazards, RWTH Aachen University), Manel Leira (Universidad La Coruña and IDL), Marco A. Jiménez-González (HERCULES Laboratory and Universidad Autónoma de Madrid), Mário Cachão (FCUL and IDL), Nicasio T. Jiménez-Morillo (Universidade de Évora), Nuno Pimentel (FCUL and IDL), Pedro J. M. Costa (Universidade de Coimbra and IDL), Rita Fonseca (Laboratório de Biogeoquímica Ambiental and Universidade de Évora), Roberto Bao (Universidad La Coruña), Rogério Mota (Laboratório Nacional de Engenharia Civil - LNEC), Sónia Gabriel (Laboratório de Arqueociências - LARC-DGPC and UNIARQ - Centro de Arqueologia de Lisboa), Susana Costas (CIMA, Universidade do Algarve).
I should also thank my PhD colleagues, Ana Cunha, Miguel Inácio and Vera Lopes, for all the weekly meetings and discussions about the Sado estuary, organized by our common adviser Maria da Conceição Freitas.

Concerning core sampling, I would like to acknowledge Santa Casa da Misericórdia de Alcácer do Sal and Eng. Custódio Lutas who made possible the recovery of Arapouco cores on Herdade de Arapouco, Santa Casa da Misericórdia de Alcácer do Sal who allow the recovery of Arez cores at Carrasqueira and José Luís Passanha Guedes that gave us permission to collect the core at Laxique at Herdade Vale de Laxique. My acknowledgements also go to Alexandra Amorim, Ana Cristina Araújo, Ana Filipa Fernandes, Barbara Wagner, César Andrade, Francisco Fatela, Hannes Laermanns, Lukas Kienzler, Marcelo Fernandes, Maria Alexandra Oliveira, Marcelo Fernandes, Nuno Pimentel, Patrícia Mendes, Pedro Costa, Randi Danielsen, Sebastian Frank, Tiago Silva and Vera Lopes who helped on the core collection.

In what respect lab work, I acknowledge the help of Vera Lopes, Ana Filipa Fernandes and Ricardo Santos, who processed some sample analyses.

At last, but not least, I am very grateful to my family, in particular to Alice, André and José Vicente for being always there, even in the days I was completely immerse in the environmental issues of 8000 years ago.

* Caetano Veloso, after The Beatles

SUMMARY OF CONTENTS

SUMMARY OF CONTENTS

1. INTRODUCTION

1. Introduction and objectives

1.1 Preliminary notes

On the onset of the Holocene, in response to climate warming and changes on coastal morphology due to sea level rise, hunter-gatherer communities intensified the exploitation of the coastal areas and of marine resources, which became an important component of their diets (e.g Jackes and Lubell, 2012; Umbelino and Cunha, 2012; Peyroteo-Stjerna, 2016; 2020; Araújo et al., 2019 - isotopic data from Portuguese shell middens). As a result, the archaeological record from the Early to the beginning of the Middle Holocene is enriched in shell middens sites, that stretch along the European Atlantic coast, from the south of Spain to Norway (e.g., Gutiérrez-Zugasti et al., 2011; Dupont, 2016). The size and number of shell middens become more relevant from the Early-Middle Holocene transition onwards suggesting an intensification in the exploitation of coastal environments (e.g.,, Araújo, 2016a; Astrup et al., 2020). Nevertheless, in what concerns the Portuguese Early Holocene archaeological record, sites are also essentially of shell midden type, and shell deposits are systematically identified in inland sites located distant from the shoreline (ca. 40-50 km), reflecting the importance of marine resources to these hunter-gatherer groups (e.g.,, Zilhão, 2004a; Araújo, 2016a). This pattern reveals a shift in human subsistence strategies at the transition to the Holocene (e.g.,, Carvalho, 2010; Araújo, 2015; 2016a; 2016b). This behaviour characterizes the Mesolithic way of life at a worldwide scale, among other innovative solutions that were triggered by hunter-gatherer populations that passed through to the Holocene.

The recognition of a period between the Palaeolithic and the Neolithic was presented initially after the first identification of shell midden deposits in Denmark in the 19th century (the so-called *Kokkenmøddiger*, Krabbelsholm site). The definition of the period has, since then, a long and controversial history (e.g., Zvelebil, 1986a, particularly Zvelebil, 1986b). Despite the general acceptance of the Mesolithic by the scientific community, its chronological boundaries and definitions are still a matter of debate according to the different teorethical perspectives on the issue (e.g., Milner and Woodman, 2005).

In Portugal, the Mesolithic is separated in two different phases: the Early Mesolithic or Epipalaeolithic (ca. 11500 and 8400 cal BP; ca. 9500 and 6450 cal BC) and the Late Mesolithic (e.g., 8400 and 7000 cal BP; 6450 and 5050 cal BC). Both Early Mesolithic and Epipalaeolithic terms are used to define the archaeological record of the Early Holocene. Its use depends on the perspective of the researcher and the emphasis given to some aspects of the archaeological record, that, respectively, consider i) a deviation in the behaviour patterns of Early Holocene

hunter-gatherers in relation to their ancestors, materialized, among other aspects, on the great reliance upon marine resources and the creation of innovative technological solutions that triggered new mobility and settlement strategies (e.g., Araújo, 2015; 2016a; 2016b). According to this view the Mesolithic lower frontier is concomitant with the Pleistocene-Holocene transition; ii) from a different perspective, a continuity of the Palaeolithic way of life (subsistence, settlement, technology) characterizes the behaviour of human groups during the first millennia of the Holocene until ca. 8200 cal BP. This perspective considers this date as the lower limit for the Mesolithic (e.g., Bicho, 2004), when the valleys of the major Portuguese rivers are occupied by the last hunter-gatherer societies. In both terminologies, this chronological period finds an end at ca. 7000 cal BP, roughly coincident with the last burials associated to the Mesolithic communities occupying the Tagus and Sado valleys (Peyroteo-Stjerna, 2016; 2020).

A major description of the differences identified between the Early and Late Mesolithic communities was published by Araújo (2015; 2016b). In the following sections of this work, the chronology, settlement pattern and environmental context of both phases are presented.

In this thesis, the Mesolithic was considered in the interval between 11500 and 7000 cal BP (between ca. 9500 and 5050 cal BC), separated in two (Early and Late) phases, established at 11500-8400 cal BP (9500-6450 cal BC) and 8400-7000 cal BP (6450-5050 cal BC), respectively.

As mentioned above, most Mesolithic sites are shell midden type, and thus these archaeological records are important archives that contribute to the knowledge of the last hunter-gatherer communities. Considering the Portuguese context, advances have been made concerning the study of lithic technology (e.g. Roche, 1951; 1970; Araújo, 1995-1997; 2016a; Marchand, 2001; 2005; Diniz and Nukushima, 2014; Araújo et al., 2015; Cascalheira et al., 2015; Nukushima, 2015), faunal remains (e.g., Lentacker, 1986; Le Gall et al., 2002; 2004; Detry, 2007; Valente, 2008; Dupont, 2011; Gabriel, 2011; Moreno, 2011; Valente, 2014; Dias et al., 2016; 2019), seasonality (e.g., Rowley-Conwy, 2015; Dias et al., 2019), palaeodiets (e.g., Umbelino et al., 2007; Jackes and Lubell, 2012; Umbelino and Cunha, 2012; Fontanals-Coll et al., 2014; Guiry et al., 2015; Peyroteo-Stjerna, 2016; 2020; Araújo et al., 2019), burial practices (e.g., Roksandic, 2006; Umbelino, 2006; Cunha and Cardoso, 2001; Cunha and Umbelino, 2001; Jackes and Lubell, 2012; Jackes et al., 2014; Peyroteo-Stjerna, 2016), palaeodemography (e.g., Jackes and Meiklejohn, 2008; McLaughlin et al., 2021) and site formation processes (Aldeias and Bicho, 2016; Duarte et al., 2017; 2019; Duarte, 2019) from materials recovered from shell middens sites. Late Mesolithic sites are also important archives that can bring information concerning the processes of transition to the Neolithic (e.g., Lubell et al., 1994; Zilhão, 2004a; Jackes and Meiklejohn, 2008;

Carvalho, 2010; Diniz and Cubas, 2015; Arias et al., 2021). Despite the reliance of these communities on marine resources and their relation to the sea and the coastal areas (including estuaries), the characterization of the local environments, and, at a large extent, their regional environmental contexts still lack in information. If Portuguese environmental conditions and its evolution through the Holocene have been extensively studied by the analyses of long-sediment cores collected in coastal areas (e.g., Queiroz, 1999; Cearreta et al., 2003; Santos and Sánchez-Goñi, 2003; Fletcher et al., 2007; 2013; Chabaud et al., 2014; Gomes et al., 2020), few works have been published concerning the maximum inland extension of estuarine areas and the coastal and fluvial morphology during the Holocene transgression (e.g., van der Schriek et al., 2007a; Vis et al., 2008; Lord et al., 2011; Dambeck et al., 2015).

The occurrence of most of Late Mesolithic shell middens in the Tagus and Sado valleys, located in the innermost areas of contemporary large estuaries, makes those sites of extremely importance in what respects to the behaviour of the last hunter-gatherer communities and their relationship with the estuarine environments. The environmental conditions of the Tagus valley during the Mesolithic occupation have already been studied (e.g., van der Schriek et al., 2007a; Vis et al., 2008). Nevertheless, the Sado environmental context and the maximum limit of the estuarine basin are still unknow. In this sense, this thesis focuses on: i) the environmental context and fluvial morphology of the Sado valley during the Late Mesolithic occupation, established between 8400 and 7000 cal BP (6450-5050 cal BC); ii) its implications to the Mesolithic communities; and iii) the palaeoenvironmental evolution of the area through the Holocene.

1.2 The Mesolithic in Portugal: chronology, settlement pattern and environmental context

The consumption of marine foods and the exploitation of molluscs have been documented in the archaeological record since the Middle Palaeolithic, being the archaeological sites of Figueira Brava (Zilhão et al., 2020) and Vale Boi (Bicho et al., 2013b) a good example of the exploitation of coastal environments during the Late Pleistocene in Portugal. However, it is from the Holocene onwards that the exploitation of marine resources assumed a major role in the diet of hunter-gatherer's communities, leading to the formation of several shell middens sites along Atlantic Europe (e.g., Lentacker, 1986; Zilhão, 2004b; Gutiérrez-Zugasti et al., 2011; Araújo, 2016a; Dupont, 2016; Dupont and Marchand, 2021). This particularly type of archaeological context contains a miscellaneous of marine species, particularly molluscs (e.g., Valente, 2014; Dupont, 2016; Fernández-López de Pablo and Gabriel, 2016) evidencing important changes in human behaviour (Araújo, 2015; 2016a; 2016b).

In Portugal, Mesolithic sites are concentrated in SW regions, south of the Mondego River (Figures 1.1 and 1.2). Despite the reliance of Mesolithic people upon marine foods, different aspects of culture as technology, settlement patterns, social organization and attitudes facing death divide this chronological period in two phases (e.g., Araújo, 2015; 2016; Araújo et al., 2019): the Early (ca. 11500-8400 cal BP; 9500-6450 cal BC) and the Late Mesolithic (ca. 8400-7000 cal BP; 6450-5050 cal BC).

Portuguese Early Mesolithic shell middens crop up essentially along the present coastline. Even though the distance to the sea and the coastal morphology at the time of occupation are still deficiently known, sites are presently located near the mouth of small rivers flowing to the Atlantic and freshwater springs (e.g., Araújo 2015; 2016; Figure 1.1). Sites tend to be small in size and thickness and are frequently interpreted as the result of repeated short-term occupations acting as logistical sites related to shellfish consumption (Carvalho and Valente, 2005; Araújo, 2016b; 2015).

The largest shell middens known in Portugal dating from the Late Mesolithic are clustered in the innermost areas of large estuaries such as the Tagus and Sado, formed during the Early to Middle Holocene sea level rise or bordering its tributaries, taking advantage of the new boundary spaces formed at the interface between the land and the sea (e.g., Arnaud, 2000; Carvalho, 2009; Gutiérrez-Zugasti et al., 2011; Diniz and Arias, 2012; Araújo, 2015; Figure 1.2).

Most of sites are of shell midden type (Figure 1.2) constituted mainly by shells and shell fragments of molluscs consumed and accumulated during long-term Mesolithic stays (Zilhão, 2004a; Carvalho, 2009; Gutiérrez-Zugasti et al., 2011; Bicho et al., 2013a; Araújo, 2015). Some sites are large in area and in thickness and have been interpreted as seasonal (Rowley-Conwy, 2015) basecamps of residential nature, where different types of activities were performed (e.g., Carvalho, 2009; Gutiérrez-Zugasti et al., 2011). In most cases, associated burials were found, which corroborates the idea of a strong relationship between living people, their territory and their dead relatives (Zilhão, 2004a; Gutiérrez-Zugasti et al., 2011). Until the moment, 376 Late Mesolithic burials (Peyroteo-Stjerna, 2020) were identified in the Tagus and the Sado valleys, being the largest burial grounds known for hunter-gatherer societies of SW Europe (e.g., Jackes and Lubell, 2012; Umbelino and Cunha, 2012; Peyroteo-Stjerna, 2020).

Many interpretations about Late Mesolithic communities relate the proximity to the estuaries as an important surviving strategy allowing to the exploitation of terrestrial areas and aquatic environments (e.g., Arnaud, 2000; Zilhão, 2004a) with marine resources still playing an important role in their diets (e.g., Lubell et al., 1994; Cunha and Umbelino, 2001; Jackes and Lubell, 2012; Umbelino and Cunha, 2012; Fontanals-Coll et al., 2014; Peyroteo-Stjerna, 2020). Indeed,

demographic studies of human populations from Atlantic Iberia reflect a grew during the Early to Middle Holocene transition, starting at ca. 8700±100 cal BP (6750±100 cal BC) to reach maximum population at 7750±50 cal BP (5800±50 cal BC) due to an increase dependence of marine and estuarine food resources (McLaughlin et al., 2021).

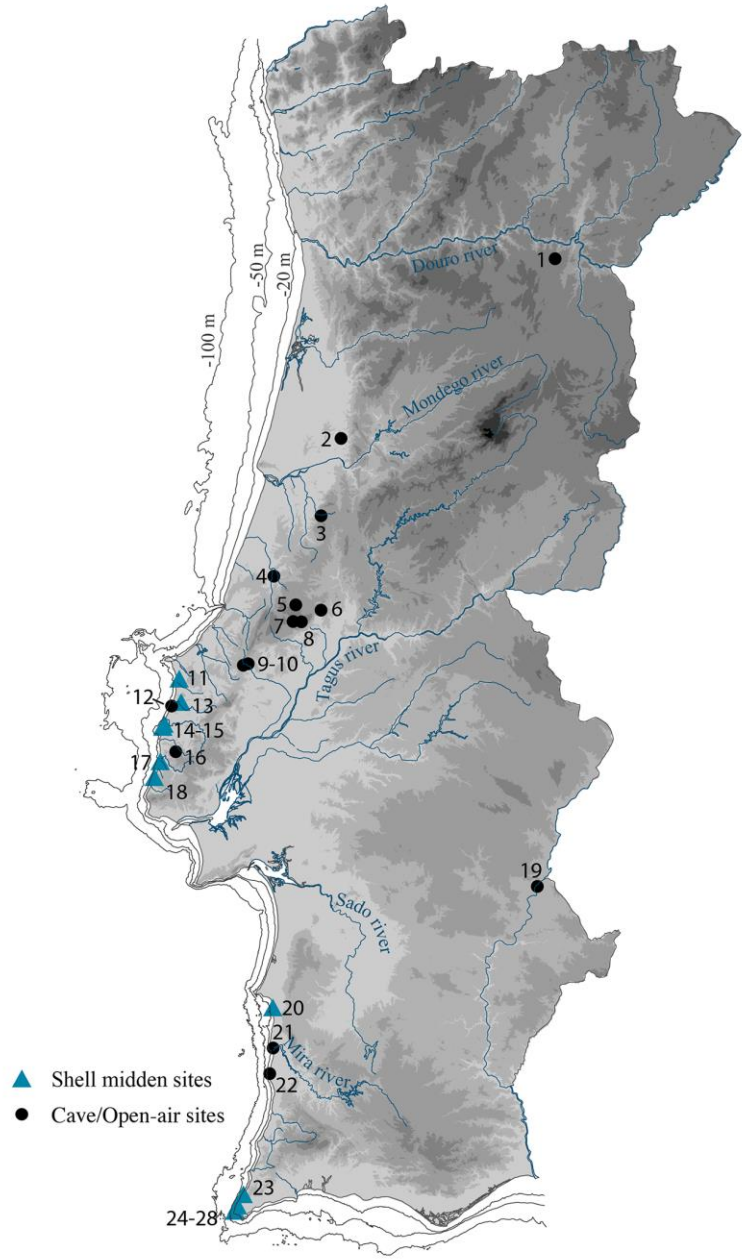

Figure 1.1 - Early Mesolithic sites in Portugal: 1 - Prazo; 2 - Vale Sá; 3 - Buraca Grande; 4 - Cruz da Areia; 5 - Casal Papagaio; 6 - Abrigo da Pena D'Agua; 7 - Abrigo da Pena de Mira; 8 - Lapa do Picareiro; 9 - Abrigo Grande das Bocas (Abrigo I das Bocas); 10 - Areeiro 3; 11 - Vale Frade; 12 - Ponta da Vigia; 13 - Toledo; 14 - Cabeço do Curral Velho; 15 - Pinhal da Fonte; 16 - Cova da Baleia; 17 - Concheiro de São Julião; 18 - Magoito; 19 - Barca do Xerês de Baixo; 20 - Praia da Oliveirinha; 21 - Pedra do Patacho; 22 - Palheirões do Alegra; 23 - Castelejo; 24-28 - Rocha das Gaivotas e Barranco das Quebradas 1, 3, 4 e 5. Information from ENDOVELICO database (DGPC).

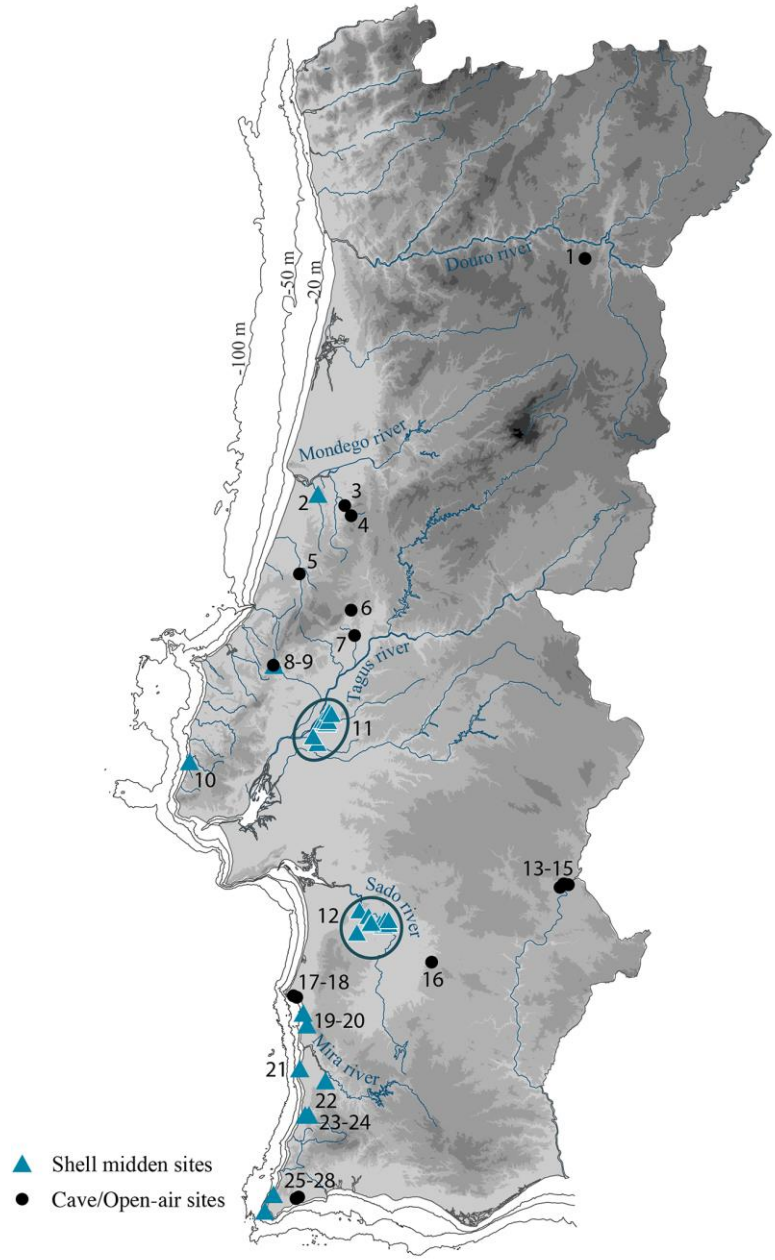

Figure 1.2 - Late Mesolithic sites in Portugal: 1 - Prazo; 2 - Forno da Cal; 3 - Pelonia; 4 - Buraca Grande; 5 - Quinta do Bispo; 6 - Costa do Pereiro; 7 - Pessegueiros; 8 - Forno da Telha; 9 - Abrigo Grande das Bocas (Abrigo I das Bocas); 10 - Concheiro de São Julião; 11 - Tagus shell middens; 12 - Sado shell middens; 13 - Carraça 1; 14 - Xerez 4; 15 - Fonte dos Sapateiros; 16 - Monte do Carrascal; 17 - Vale Pincel; 18 - Vale Marim 1; 19 - Samouqueira 1; 20 - Vidigal; 21 - Medo Tojeiro; 22 - Fiais; 23 - Montes de Baixo; 24 - Paço Velho 2; 25 - Castelejo; 26 - Rocha das Gaivotas; 27 - Monte do Azureque; 28 - Vale Boi. Information from ENDOVELICO database (DGPC).

Since the Last Glacial Maximum (LGM) several environmental and landscape changes occurred in response to major climate re-organisations. Some researchers have hypothesised that environmental factors, such as the 8.2 ka cal BP cold event, whose impact in the landscape and in the availability of resources would have been abrupt in these southern latitudes, were responsible for this twist in human strategies (Zilhão, 2003; Monge Soares, 2004; Carvalho, 2009; Bicho et al., 2010; McLaughlin et al., 2021). However, at least in what concerns SW Iberia, this correlation still lacks in comprehension (e.g., Carvalho et al., 2009; Evans, 2021) and new approaches are being developed to support Early to Late Mesolithic settlement changes (Araújo et al., 2021; Costas et al., 2021). The environmental and landscape changes are particularly visible in the coastal areas that were flooded due to the sea level rise induced by global warming. Previously incised palaeovalleys and other lowland areas in Iberia and elsewhere were flooded (Freitas et al., 2002; 2003; Freitas and Andrade, 2005; Andrade et al., 2006b; Boski et al., 2008; Vis et al., 2008; Hijma et al., 2009; Chaumillon et al., 2010), leading to the formation of new spaces at the interface between land and sea and offering new conditions for the Late Mesolithic communities.

In Portugal, the palaeoenvironmental conditions of the Tagus estuary since the Late Glacial have been significantly studied (e.g., Vis et al., 2008). The maximum marine flooding occurred ca. 7000 cal BP (5050 cal BC; Vis et al., 2008), forming a large estuarine area of nearly 1300 km^2 (more than 4 times larger than the present-day estuary) that extended for more than 100 km upstream the estuary inlet, until Torres Novas (Taborda et al., 2009; Figure 1.3A).

Late Mesolithic Tagus shell middens occur on three southeast-bank tributaries of the Tagus, named Magos, Muge and Vale da Fonte da Moça (e.g., Arnaud, 1987; Bicho et al., 2013a; Figure 1.3A), that locate up to more than 65 km from the present-day estuary inlet. The streams drain the central area of the Pre-Quaternary and Pleistocene Lower Tagus Basin (Figure 1.3B), mostly constituted by sandstones, conglomerates, siltstones, claystones and limestones (only present in the Miocene deposits; Figure 1.3B). The lower valleys of these streams were flooded during the Holocene transgression as demonstrated by the sedimentary record of the Muge tributary (Figure 1.3A). According to this record (van der Schriek et al., 2007b; 2008), a fluvial channel system was established in the Muge valley previously to 8050 cal BP (6100 cal BP). From that date onwards, i.e., during the Late Mesolithic occupation, the intertidal environments (saltmarsh and tidal flats) abruptly replaced the fluvial system, reaching up to 4 km river upstream during the maximum marine influence period, that took place between 7750 and 7500 cal BP (5800 and 5550 cal BC). Tidal flat environments and salt marsh communities developed in the area until ca. 5750 cal BP (ca. 3800 cal BC; van der Schriek et al., 2007b), long after the disappearance of the last hunter gatherer Mesolithic communities.

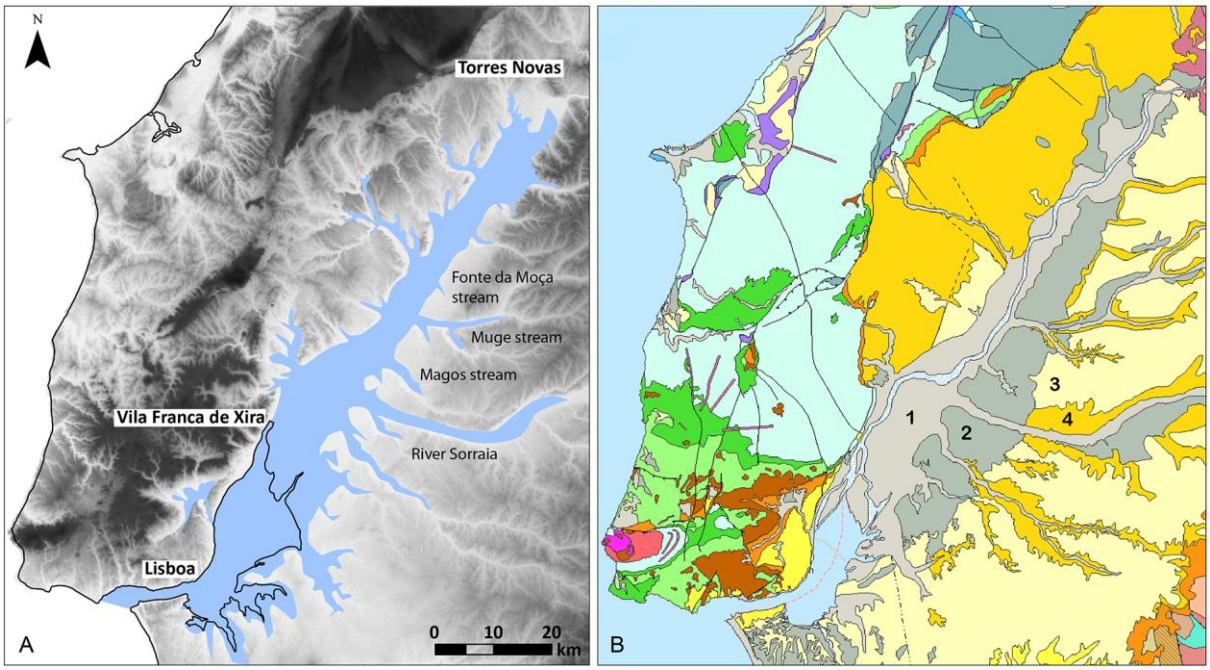

Figure 1.3 - A - Present-day Tagus estuary (black line) and palaeoestuary (blue area) indicating the maximum extension of brackish environments (adapted from Vis et al., 2008) and indication of the left margins tributaries of the Tagus river where Late Mesolithic occupation took place. B - Simplified geological map (Geological Map of Portugal, scale 1:1000000, LNEG, 2010, Geoportal Energia e Geologia, geoportal.lneg.pt, consulted in November 2021) representing the Lower Tagus Valley sedimentary infilling. 1 - Holocene alluvial sediment constituted by sand, gravel, silt and clay; 2 - Pleistocene alluvial terraces constituted by conglomerates, sandstones, siltstones and claystones; 3 - Pliocene sedimentary rocks constituted by sandstones, conglomerates and siltstones; 4 - Miocene sedimentary rocks constituted by sandstones, claystones, conglomerates and limestones from continental environments. Other lithology descriptions can be consulted at geoportal.lneg.pt.

Similarly, to the environmental context characterized for the Tagus valley during the Late Mesolithic occupation, estuarine environments were previously predicted for the section of the Sado valley occupied by these groups (e.g., Arnaud, 1987; 1989; 2000; Diniz and Arias, 2012; Araújo, 2015). Previous studies have been published inferencing about the Holocene evolution of the estuarine area (e.g., Andrade et al., 2013), and focused on the development of recent saltmarshes (e.g., Moreira, 1992; Psuty and Moreira, 2000). Notwithstanding, the i) Sado estuary palaeomorphology, ii) maximum extension of the palaeoestuary, iii) environmental conditions and evolution throughout the occupation and through the Holocene, and iv) fluvial and estuarine responses to sea level changes have never been investigated, being still poorly known.

According to geotechnical information, the total thickness of Sado post-Late glacial alluvial sediments reach depths of 40 m near Alcácer do Sal (GRID, 1989; ENGIVIA, 1995). Preliminary

data (Freitas et al., 2013) indicate that the sedimentary infilling of the Sado valley could be an important source of information concerning environmental conditions of the area during the Late Mesolithic occupation.

The relationship between Man and Environment plays an important role in the comprehension of culture, in a broader perspective. Nowadays the topic attracts significant attention from researcher, political and general public groups, given the environmental issues lived by present-day populations, particularly in the coastal areas, and the environmental changes that promote more frequent extreme weather and climate-related events, making climatic change adaptation one of the top priorities for, e.g.,, the European Environmental Agency (https://www.eea.europa.eu/themes/climate-change-adaptation, consulted in November 2021). The approach between cultural anthropology and Prehistoric ecology is one of the most auspicious fields of research of Past human societies, and considering the objectives of the present work, particular emphasis is given to the Portuguese Mesolithic groups, the last hunter-gatherer societies of SW Iberia.

The aim of this thesis is to characterize the environmental conditions of the Sado valley during the Mesolithic occupation and to evaluate the opportunities offered by the palaeoestuary to people, which settled and stayed in this area for ca. 1500 years.

This research will be based on high-resolution multy-proxy analyses of environmental sensitive (sedimentological, geochemical, ecological) indicators obtained from sediment cores retrieved from the Sado alluvial plain, combined with geophysical methods that allow to characterize the valley morphology, and a high-resolution chronological framework. The study of these alluvial sediments is crucial to understand Mesolithic behaviours, their relationship with the surrounding environment and with marine resources that featured the archaeological contents of their sites.

The main questions to be addressed are the following:

1. Did marine influence reach the occupied area of the Sado valley during the Mesolithic?
2. Did Mesolithic groups had conditions to exploit marine resources in the vicinity of their habitats or did they carry them from other locations closest to the Sado mouth?
3. What was the maximum flooding extension on the Sado valley?
4. How did the estuarine border evolved through the Holocene?
5. Which conditions characterised the Sado valley during Late Mesolithic times?

Based on these questions, the specific objectives of the work are:

i) to characterize the Sado valley palaeomorphology in the section occupied by the Mesolithic groups;

ii) to establish the environmental conditions in the Sado valley during the Early / Middle Holocene;

iii) to characterize the local /regional environmental changes during the Mesolithic occupation;

iv) to comprehend the palaeoenvironmental evolution of the Sado valley during the Middle / Late Holocene;

v) to establish the environmental context of Late Mesolithic communities in the Portuguese estuaries, particularly those of the Tagus and the Sado.

1.3 The Late Mesolithic shell middens in the Tagus and Sado valleys

The Tagus valley

The Tagus river, with ca. 1000 km in length, originates in the Sierra de Albarracín (Spain) and flows westwards into the Atlantic Ocean, forming an estuary, the most important in the Iberian Peninsula, with an area of ca. 325 km^2 (Bettencourt and Ramos, 2003; Figure 1.3). The estuary reaches the Atlantic Ocean through a deep and narrow (2 km wide) tidal inlet. Upstream, the estuary corresponds to a shallow tide-dominated basin with ca. 40% of the area covered by tidal flats and marshes (e.g., Bettencourt and Ramos, 2003). Tides vary between 1.5 m (neap) and 3.2 m (spring) (Bettencourt and Ramos, 2003) but resonance amplifies the semi-diurnal constituents within the estuary (Fortunato et al., 1999). The average discharge of the Tagus river is ca. 400 $m^3 s^{-1}$ (e.g., Neves, 2010) presenting extreme seasonal and annual variability with flood peak discharges that sum-up to more than 30 times the mean flow, being influenced by Atlantic fronts that cross the Iberian Peninsula mostly during the winter (Benito et al., 2003).

Thirteen shell middens were identified in the Tagus valley, scattered over the margins of Fonte da Moça, Muge and Magos streams, three tributaries of the left margin of the Tagus (Figure 1.4; Table 1.1) located more than 65 km upstream from the present-day estuary inlet (Figure 1.3).

The Tagus shell middens were discovered in 1863 by Pereira da Costa and Carlos Ribeiro (e.g., Roche and Veiga Ferreira, 1957) and have been intensively studied over the last 150 years during which several works were published focusing in diverse topics (e.g., Roche, 1989; Cardoso and Rolão 1999-2000; Rolão et al., 2006; Rolão and Roksandic, 2007; Bicho, 2009; Bicho et al., 2010; 2013; Peyroteo-Stjerna, 2016, just to mention some that present synthesis concerning the development of archaeological work and recent chronological models; see also Table 1.1).

The shell middens are placed at the edge of Pleistocene fluvial terraces (Q1 to Q4) and Pleistocene / Holocene (?) superficial fluvial / aeolic sands (As) that cover the terraces preserved at the lower sections of the three streams, at their confluence with the Tagus (Figure 1.3; Zbyszewski et al., 1967; Zbyszewski and Veiga Ferreira, 1968), at heights between 10 and 20 m in relation to present-day mean sea level (MSL) (Table 1.1; Gonçalves, 2014). Cabeço dos Môrros is the only exception to this pattern (Figure 1.4), located at a lower height of ca. 7 m (Gonçalves, 2014), ca. 2.5 m above the Magos present-day alluvial plain surface, what seems to allow the flooding of the site during winters with high precipitation rates (e.g., Detry, 2008).

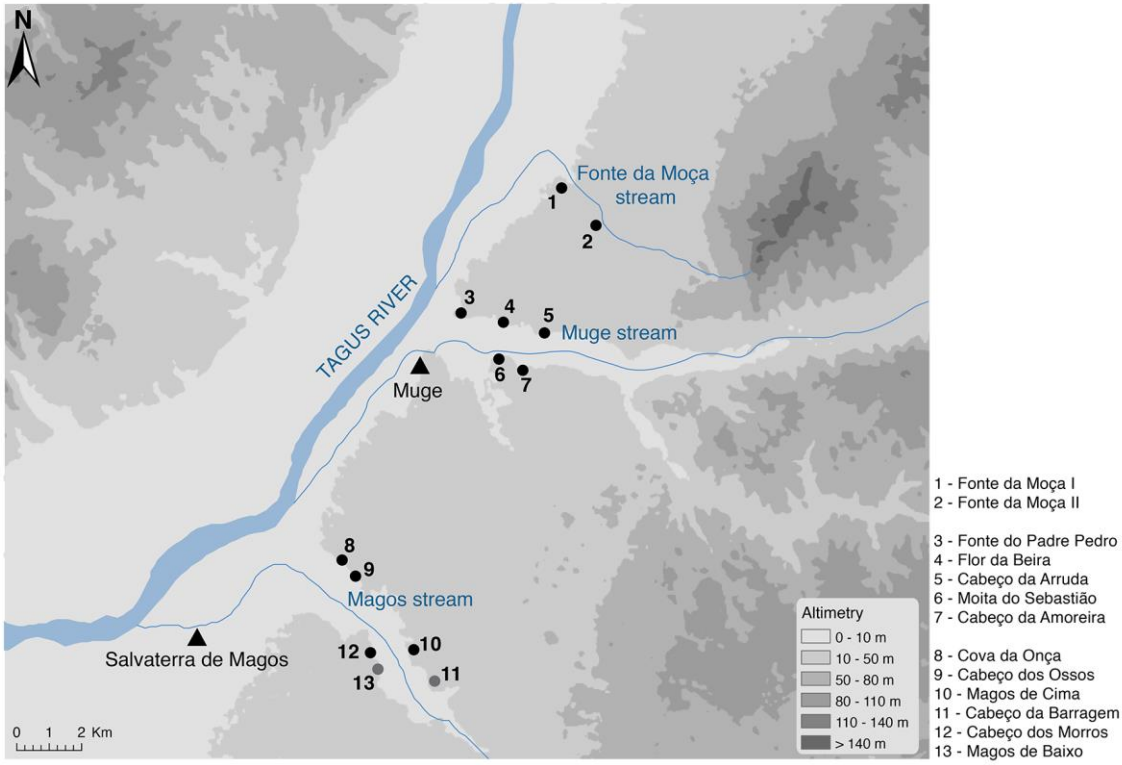

Figure 1.4 - Location of the Tagus Late Mesolithic shell middens. For location in Portugal, see Figure 1.2. Black circles correspond to the sell middens with known coordinates. Grey circles correspond to the shell middens whose location is uncertain. Coordinates and altimetry are presented in Table 1.1.

The Pleistocene terraces Q1, Q2, Q3 and Q4 (Zbyszewski et al., 1967) were tentatively correlated with the terraces T2, T3, T4 and T5 defined at upstream reaches (from ca. 120 km from the Atlantic Ocean river up) of the Tagus (Martins and Cunha, 2009). According to Martins et al.

(2009), T2 is beyond the upper range for luminescence dating, T3 has a minimal age of ca. 300 ky and T4 and T5 were luminescence dated from 107-222 ky and 42-99 ky, respectively (Martins et al., 2009). At a local scale, van der Schriek et al. (2007a) identified 7 terrace levels bordering the Muge valley varying in its constitution and height, corresponding to the fluvial terraces and fluvial / aeolic sands identified as Q1 to Q4 and As, respectively, in the geological map (Zbyszewski and Veiga Ferreira, 1968). The description of these geomorphological units is resumed in Table 1.2. At present, most of the shell middens located in the Tagus valley are total or partially destroyed (Table 1.1), mostly due to agriculture and other anthropic activities and are difficult to identify (Gonçalves, 2014).

Table 1.1 - Coordinates, altimetry and area of the Tagus Late Mesolithic shell middens. *Data from Geoportal DGPC (consulted in December 2021). Coordinate system WGS84. Altimetry retrieved from Gonçalves, 2014, reported in height in relation to MSL. ID corresponds to the identification of the sites in figure 1.4. Area was retrieved from Detry, 2007. ** Information retrieved from the ENDOVELICO database (DGPC), when possible. Other references are from bibliography. To be continued.

Loc	ID	Name	Latitude*	Longitude*	Altimetry (m)	Area (m^2)	Preservation state	Excavation years**	Responsible for the archaeological works**
Fonte da Moça stream	1	Fonte da Moça I	39.159491	-8.671842	14	1000	Partially destroyed	1981 (test pit), 1982, 1983, 1984	Manuel Farinha dos Santos
	2	Fonte da Moça II	39.143807	-8.648415	20	2500	Partially destroyed	1984 (test pit)	José Rolão e Manuel Farinha dos Santos
Muge stream	3	Fonte do Padre Pedro	39.116724	-8.697218	12	?	Destroyed	1880 (test pit), 1930 (test pit)	Carlos Ribeiro; Mendes Corrêa
	4	Flor da Beira	39.114880	-8.684675	16	?	Destroyed	-	-
	5	Cabeço da Arruda	39.111495	-8.664779	10	5400	Partially excavated	1864, 1880, 1884, 1933, 1937, 1964, 1965, 2000, 2013	Carlos Ribeiro; Francisco de Paula e Oliveira; Mendes Corrêa; Jean Roche and Octávio da Veiga Ferreira; José Rolão; João Marreiro, João Cascalheira, Nuno Bicho and Telmo Pereira
	6	Moita do Sebastião	39.106428	-8.682857	20	3500	Destroyed	1880, 1884, 1952, 1953, 1954	Carlos Ribeiro; Francisco de Paula e Oliveira; Jean Roche and Octávio da Veiga Ferreira; Mendes Corrêa

Table 1.1 - Continuation.

Loc	ID	Name	Latitude*	Longitude*	Altimetry (m)	Area (m^2)	Preservation state	Excavation years**	Responsible for the archaeological works**
Muge stream	7	Cabeço da Amoreira	39.103338	-8.674119	20	4500	Partially excavated	1930, 1931, 1933, 1962, 1963, 1964, 2000, 2002, 2003, 2008, 2009, 2010, 2011, 2012, 2013, 2014, 2015	Mendes Corrêa; Jean Roche and Octávio da Veiga Ferreira; José Rolão; Nuno Bicho; João Marreiro, João Cascalheira, Nuno Bicho and Telmo Pereira; Célia Gonçalves, João Marreiro, João Cascalheira, Nuno Bicho and Telmo Pereira
Magos stream	8	Cova da Onça	39.050055	-8.748809	20	?	Partially destroyed		
	9	Cabeço dos Ossos	39.021763	-8.717710	10	?	Destroyed		
	10	Magos de Cima	-	-	-	?	Destroyed		
	11	Cabeço da Barragem	38.995034	-8.689037	10	?	Destroyed		
	12	Cabeço dos Môrros	39.020246	-8.724060	7	600	Partially destroyed	1997, 1998, 1999, 2001	José Rolão
	13	Magos de Baixo	-	-	-	?	Destroyed		

*https://patrimoniodgpc.maps.arcgis.com/apps/webappviewer/index.html?id=5cb4735d7d7743a39a16d7269a753a4a

Table 1.2 - Description of the terrace levels identified and described in the Muge valley area by van der Schriek et al. (2007a). Altimetry reported in height in relation to MSL. Ages are inferred. ID corresponds to the identification of the deposit in the geological map 31-C, Coruche (Zbyszewski and Veiga Ferreira, 1968).

Terrace levels	Altimetry	Age	ID	Description
T1	95-88 m	Late Pliocene / Early Pleistocene	Q1	Lack in outcrops in the Muge area. Correspond to a sequence of gravel, sand, clayey silt and clay (Zbyszewski et al., 1967; Zbyszewski and Veiga Ferreira, 1968)
T2	68-64 m	Pleistocene	Q2	
T3a	55-47 m	Pleistocene	Q3	Stacked series of tabular gravel and sand layers and reddish coarse sands and gravels at the base
T3b	42-37 m	Pleistocene	Q3	
T4	30-20 m	Pleistocene	As; Q3	Stacked series of cross-bedded sand sheets, locally comprising tabular gravel bodies and organic-rich fine-grained deposits
T5	12-15 m	Late Pleistocene	Q4	Bedded sandy silt and clay or cross-bedded sand bodies
T6	7-9 m	Late Pleistocene	Q4	Bedded coarse sand and some gravel

Cabeço da Arruda and Cabeço da Amoreira, located in the Muge valley, are somewhat preserved and target of archaeological works since 2006 by Nuno Bicho and his team in the framework of three projects financed by Fundação para a Ciência e Tecnologia: *The last hunter-gatherers in the Tagus valley - The Muge shell middens* (PTDC/HAH/64185/2006; IP Nuno Bicho); *The last hunter-gatherers of Muge (Portugal): the origins of social complexity* (PTDC/HIS-ARQ/112156/2009; IP Nuno Bicho); and *The Muge shell middens project: a new portal to the last hunter-gatherers of the Tagus valley, Portugal* (PTDC/HAR-ARQ/29680/2017; IP Célia Gonçalves).

Cabeço da Arruda, Moita do Sebastião and Cabeço da Amoreira (Muge stream; Figure 1.5) are the largest shell midden of the Tagus complex (Table 1.1) reaching a thickness of 5 m at Cabeço da Arruda and extending, in some cases, for ca. 100 m (e.g., van der Schriek et al., 2007b; Bicho et al., 2010; 2013; Gonçalves, 2014), forming artificial mounds that modify and severely impact the landscape (e.g., Arnaud, 1987; Bicho et al., 2013a).

Sites resulted from the development of anthropic activities and accumulation of materials deposited during several occupations, being the complex stratigraphic record marked by different evidence of use (e.g., post-holes, hearths, pits, burials, shell tossing events) and abandonment (e.g., sedimentary hiatuses, geogenic sedimentation) at a macro and micro scale (Arnaud, 1989; Roche, 1989; Bicho et al., 2013a; Aldeias and Bicho, 2016).

The shell middens are constituted by a matrix of shells and shell fragments, mostly of cockle (*Cerastoderma edule*) and peppery furrow shell (*Scrobicularia plana*) (Lentacker, 1986; Detry, 2007), marine species frequently found in shallow areas of saline lagoons and estuaries (MarLIN - The Marine Life Information Network, www.marlin.ac.uk, consulted in January 2022) and characterized by rich terrestrial and aquatic (other than aforementioned shellfish) assemblages. Although the predominance of *C. edule* and *S. plana* are predominant in the shell midden record, razor clam (*Solen* sp.) and oyster (*Ostrea* sp.) were also identified. The mammal fauna collection is mainly composed by red deer (*Cervus elaphus*), wild boar (*Sus scrofa*), roe deer (*Capreolus capreolus*), aurochs (*Bos primigenius*) and rabbit (*Oryctolagus cunniculus*) and the most represented taxon among the avian fauna is mallard (*Anas platyrhynchos*) (Lentacker, 1986; Detry, 2007).

Figure 1.5 - Cabeço da Amoreira shell midden (Muge) during the fieldtrip done in the framework of Muge 150th: the 150th Anniversary of the Discovery of Mesolithic Shell middens, 2013.

Fish was also intensively exploited (Dias et al., 2016; 2019). In the Cabeço da Amoreira record, mullets (Mugilidae) predominates and, at least, *Liza ramada*, *Cheron labrosos*, *Mugil cephalus* and *Liza aurata* were identified (Dias et al., 2019). European seabass (*Dicentrarchus labrax*), common eagle ray (*Myliobatis aquila*), meagre (*Argyrosomus regius*), river herrings (*Alosa* sp.) and gilthead seabream (*Sparus aurata*) are also well represented in the Cabeço da Amoreira fish assemblage (Dias et al., 2019). Still in the faunal record, it is important to mention the presence of amphibian (e.g., *Anura* (frog), *Ranidae* (true frog), *Bufo bufo* (common toad), *Discoglossus pictus* (painted frog), *Salamandra salamandra* (fire salamander); Lentacker, 1986) and reptilian remains (e.g., *Emys orbicularis* (swamp turtle), *Mauremys leprosa* (Spanish pond turtle); Lentacker, 1986; Detry, 2007) that evidence the proximity of the sites to aquatic systems (Detry, 2007). Remains of domestic dog were also identified, including a complete canid skeleton from Cabeço da Arruda (Detry and Cardoso, 2010).

The Tagus (and the Sado, see below) Late Mesolithic shell middens were also a place for the dead (Peyroteo-Stjerna, 2016). Several human burials were found corresponding to, at least, 263 individuals (Cunha and Cardoso, 2001; 2002-2003; Roksandic, 2006; Jackes and Meiklejohn, 2008; Meiklejohn et al., 2009; Bicho et al., 2013a; data resumed in Peyroteo-Stjerna, 2016; Table 1.3). The anthropological and isotopic ($\delta^{13}C$ and $\delta^{15}N$) analyses of the skeletons (e.g., Cunha and Cardoso, 2001; 2002-2003; Cunha and Umbelino, 2001; Cunha et al., 2003; Umbelino, 2006; Umbelino et al., 2007; Bicho et al., 2013a; Peyroteo-Stjerna, 2016), together with the faunal assemblages recovered from the sites (Lentacker, 1986; Detry, 2007; Dias et al., 2016; 2019) evidence the consumption of a wide varied mixed diet composed by diverse terrestrial and marine components, exploited in the terrestrial and aquatic surrounding environments.

A considerable number of radiocarbon dates were performed on diverse materials (human and fauna bones, charcoal and shells) from the Tagus shell middens. Table 1.4 (with respective references) compiles the available conventional radiocarbon dates and other available data concerning stable isotopic results for C and N. In the present work, the conventional dates were calibrated in a simple scientific dating mode using the InCatl13 and Marine13 calibration curves (Reimer et al., 2013) for terrestrial and marine samples, respectively, and OxCal 4.4 (© Bronk Ramsey). IntCal13 and Marine 13 were chosen instead of IntCal20 (Reimer et al., 2020) and Marine20 (Heaton et al., 2020), once that, to our knowledge, the ΔR value was not yet recalculated using the more recent marine curve. For the calibration of marine samples, a ΔR value of 140 ± 40 ^{14}C years was applied (Martins et al., 2008) as determined for the Tagus valley Late Mesolithic. For human dates, a mixed curve was used, draw considering the % of marine diet and the aforementioned ΔR value. However, the dating set, particularly in what concerns the

older dates, present some issues in what respects provenance, charcoal species identification (to avoid old carbon effect), large BP associated errors (e.g., Bicho et al., 2013a), AMS stable isotopic values (not suitable for diet determinations) instead of IRMS measurements (Peyroteo-Stjerna, 2020), among other, making difficult to analyse the chronological framework of Late Mesolithic records.

Table 1.3 - Late Mesolithic human remains in the Tagus shell middens. Resumed by Peyroteo-Stjerna, 2016.

Loc	ID	Name	MNI	Reference
Fonte da Moça stream	1	Fonte da Moça I	fragments of bones and teeth	Santos et al., 1990
	2	Fonte da Moça II	fragments of bones	Santos et al., 1990
Muge stream	3	Fonte do Padre Pedro	2/3	Meiklejohn et al., 2009
	4	Flor da Beira	4/5	Meiklejohn et al., 2009
	5	Cabeço da Arruda	110	Cunha and Cardoso, 2002-2003; Roksandic, 2006
	6	Moita do Sebastião	85	Jackes and Meiklejohn, 2008
	7	Cabeço da Amoreira	29	Cunha and Cardoso, 2001; Roksandic, 2006; Bicho et al., 2013a
Magos stream	8	Cova da Onça	32 ou 36	Cunha and Cardoso, 2002-2003; Meiklejohn et al., 2009
	9	Cabeço dos Ossos	-	
	10	Magos de Cima	-	
	11	Cabeço da Barragem	-	
	12	Cabeço dos Môrros	1 (1 cranium)	Paço, 1938
	13	Magos de Baixo	-	

The Bayesian model recently draw by Peyroteo-Stjerna (2020) based on the radiocarbon dates from human collagen give evidence of a first burial activity phase occurring at ca. 8300-7900 cal BP (6350-5950 cal BC) for the Tagus valley (Moita do Sebastião; Peyroteo-Stjerna, 2020) receding the chronology previously established for the first occupations of the area (at ca. 8000 cal BP; ca. 6050 cal BC; Bicho et al., 2013a). A more frequent and synchronous (between sites) activity took place between 7800 and 7600 cal BP (5850 and 5650 cal BC), with the final burials occurring between ca. 7400 and 7000 cal BP (5450 and 5050 cal BC; Peyroteo-Stjerna, 2020.

Table 1.4 - Radiocarbon dates for the Tagus shell midden sites. Conventional dates, isotopic results and % of non-terrestrial carbon (% marine) for human samples retrieved from bibliography. Marine diet results from Peyroteo-Stjerna, 2016 correspond to Model 1. Conventional dates were calibrates using OxCal 4.4 (© Bronk Ramsey). Dates from terrestrial samples (charcoal and mammal bones) were calibrated using IntCal13 calibration curve (Reimer et al., 2013). Dates from marine samples (shells) were calibrated using Marine13 calibration curve (Reimer et al., 2013) using a ΔR value of 140±40 ^{14}C years (Martins et al., 2008) as determined for the Tagus valley Late Mesolithic. Dates from human remains were calibrated using a mixed curve, using the % of marine diet. To be continued.

Loc	Site	Material	Lab code	Conventional date BP	$\delta^{13}C$	$\delta^{15}N$	% marine diet	Date cal BP (95.4%)	Date cal BC (95.4%)	Reference
Ft Moça stream	Fonte da Moça 1	mammal bone	TO-11864	6890±140				7981-7502	6030-5551	Roksandic, 2006; Rolão et al., 2006
		mammal bone	TO-11863	6650±60				7611-7433	5660-5482	Roksandic, 2006; Rolão et al., 2006
Muge Stream	Cabeço da Arruda	*Homo*, bones	Beta-127451	7550±100	-19.0	-	24	8408-8029	6457-6078	Cunha and Cardoso, 2002-2003; Umbelino, 2006
		charcoal	TO-10215	7410±70				8375-8049	6357-6098	Roksandic, 2006
		Homo, bones	AA-101343	7351±70	-16.6	10.9	47	8130-7788	6179-5837	Jackes et al., 2014
		Homo, bones	Beta-447680	7260±30	-18.1	10.9	20	8020-7939	6069-5988	Peyroteo-Stjerna, 2020
		Homo, bones	Ua-46275	7263±46	-17.4	11.4	39	8130-7877	6179-5926	Peyroteo-Stjerna, 2016
		Homo, bones	Ua-47976	7261±40	-17.1	9.7	42	8052-7868	6101-5917	Peyroteo-Stjerna, 2016
		Homo, bones	Ua-46274	7200±41	-17.4	10.6	39	7937-7737	5986-5786	Peyroteo-Stjerna, 2016
		Homo, bones	Ua-46273	7198±46	-17.3	10.1	40	7935-7715	5984-5764	Peyroteo-Stjerna, 2016

Table 1.4 - Continuation and to be continued.

Loc	Site	Material	Lab code	Conventional date BP	$\delta^{13}C$	$\delta^{15}N$	% marine diet	Date cal BP (95.4%)	Date cal BC (95.4%)	Reference
Muge Stream	Cabeço da Arruda	*Homo*, bones	Ua-46272	7166±41	-16.6	11.2	47	7859-7668	5908-5717	Peyroteo-Stjerna, 2016
		Homo, bones	Ua-47975	7116±44	-16.7	9.5	46	7825-7620	5874-5669	Peyroteo-Stjerna, 2016
		Homo, bones	Beta-447681	7070±40	-17.0	11.3	31	7836-7670	5885-5719	Peyroteo-Stjerna, 2020
		Homo, bones	TO-10216	7040±60	-17.87	10.60	34	7833-7593	5882-5642	Roksandic, 2006
		Homo, bones	TO-360	6990±110	-17.7	11.2	36	7914-7468	5963-5517	Lubell and Jackes, 1988; Lubell et al., 1986; 1994
		Homo, bones	TO-354	6970±70	-19.0	12.2	24	7836-7577	5885-5626	Lubell and Jackes, 1988; Lubell et al., 1986; 1994
		Homo, bones	TO-359a	6960±60	-17.2	11.8	41	7707-7491	5756-5540	Lubell and Jackes, 1988; Lubell et al., 1986; 1994
		Homo, bones	TO-355	6780±80	-18.9	10.3	25	7659-7425	5708-5474	Lubell and Jackes, 1988; Lubell et al., 1986; 1994
		Homo, bones	TO-10217	6620±60	-18.1	10.46	32	7467-7262	5516-5311	Roksandic, 2006

Table 1.4 - Continuation and to be continued.

Loc	Site	Material	Lab code	Conventional date BP	$\delta^{13}C$	$\delta^{15}N$	% marine diet	Date cal BP (95.4%)	Date cal BC (95.4%)	Reference
Muge Stream	Cabeço da Arruda	charcoal	Sa-197	6430±300				7926-6669	5975-4718	Roche and Veiga Ferreira, 1972-1973
		Homo, bones	TO-356	6360±80	-15.3	12.5	59	7155-6725	5204-4774	Lubell and Jackes, 1988; Lubell et al., 1986; 1994
		charcoal	Sa-196	5150±300				6655-5145	4704-3194	Roche and Veiga Ferreira, 1972-1973
	Moita do Sebastião	*Homo*, bones	Ua-46264	7621±50	-17.0	10.8	42.9	8368-8132	6417-6181	Peyroteo-Stjerna, 2016
		Homo, bones	Ua-46263	7483±48	-17.0	10.5	42.9	8181-7982	6230-6031	Peyroteo-Stjerna, 2016
		charcoal	Sa-16	7350±350				9020-7520	7069-5569	Roche, 1972
		Homo, bones	Beta-447682	7280±40	-17.4	10.4	27	8034-7870	6083-5919	Peyroteo-Stjerna, 2020
		Homo, bones	Ua-46268	7243±45	-16.2	14.0	50.5	7933-7712	5982-5761	Peyroteo-Stjerna, 2016
		Homo, bones	TO-131	7240±70	-16.1	12.2	51	7950-7676	5999-5725	Lubell and Jackes, 1988; Lubell et al., 1986; 1994

Table 1.4 - Continuation and to be continued.

Loc	Site	Material	Lab code	Conventional date BP	$\delta^{13}C$	$\delta^{15}N$	% marine diet	Date cal BP (95.4%)	Date cal BC (95.4%)	Reference
Muge stream	Moita do Sebastião	*Homo*, bones	Ua-46271	7236±41	-16.3	11.9	49.5	7929-7713	5978-5762	Peyroteo-Stjerna, 2016
		Homo, bones	TO-133	7200±70	-16.9	10.4	44	7926-7706	5975-5755	Lubell and Jackes, 1988; Lubell et al., 1986; 1994
		Homo, bones	TO-132	7180±70	-16.8	11.9	45	7937-7661	5986-5710	Lubell and Jackes, 1988; Lubell et al., 1986; 1994
		Homo, bones	TO-134	7160±80	-16.7	11.2	46	7934-7625	5983-5674	Lubell and Jackes, 1988; Lubell et al., 1986; 1994
		Homo, bones	Ua-46269	7141±40	-17.4	10.6	39	7909-7678	5958-5727	Peyroteo-Stjerna, 2016
		Homo, bones	Ua-47977	7138±42	-16.9	9.3	43.8	7847-7663	5896-5712	Peyroteo-Stjerna, 2016
		Homo, bones	Ua-46267	7120±43	-16.9	12.8	43.8	7839-7645	5888-5694	Peyroteo-Stjerna, 2016
		Homo, bones	Beta-127449	7120±40	-16.8	-	45	7832-7648	5881-5697	Cunha and Cardoso, 2002-2003; Umbelino, 2006
		Homo, bones	Ua-47980	7105±42	-16.8	9.5	44.8	7817-7621	5866-5670	Peyroteo-Stjerna, 2016
		Homo, bones	Ua-46266	7095±45	-16.9	10.8	43.8	7816-7615	5965-5664	Peyroteo-Stjerna, 2016

Table 1.4 - Continuation and to be continued.

Loc	Site	Material	Lab code	Conventional date BP	$\delta^{13}C$	$\delta^{15}N$	% marine diet	Date cal BP (95.4%)	Date cal BC (95.4%)	Reference
Muge stream	Moita do Sebastião	unknown	H-2119/1546	7080±130				8170-7672	6219-5721	Roche and Veiga Ferreira, 1972-1973
		Homo, bones	Ua-47981	7058±44	-17.4	9.8	39	7794-7601	5843-5650	Peyroteo-Stjerna, 2016
		Homo, bones	Ua-46265	6986±40	-17.9	10.2	34.3	7720-7580	5769-5629	Peyroteo-Stjerna, 2016
		Homo, bones	TO-135	6810±70	-15.3	13.4	59	7551-7270	5600-5319	Lubell and Jackes, 1988; Lubell et al., 1986; 1994
		Homo, bones	Ua-47978	6753±46	-18.2	9	31.4	7565-7426	5614-5475	Peyroteo-Stjerna, 2016
		Homo, bones	Ua-46270	6743±44	-18.4	10.5	29.5	7562-7429	5611-5478	Peyroteo-Stjerna, 2016
	Cabeço da Amoreira	shell, *S. plana*	Wk-28033	7479±48				7930-7668	5979-5717	Bicho et al., 2011
		shell, *S. plana*	UGAMS-7197	7450±30				7899-7662	5948-5711	Bicho et al., 2011
		shell, *S. plana*	Wk-28048	7445±33				7900-7655	5949-5704	Bicho et al., 2011
		shell, *S. plana*	Wk-30671	7417±34				7860-7615	5909-5664	Bicho et al., 2011
		shell, *S. plana*	Wk-30673	7406±32				7844-7611	5893-5660	Bicho et al., 2011

Table 1.4 - Continuation and to be continued.

Loc	Site	Material	Lab code	Conventional date BP	$\delta^{13}C$	$\delta^{15}N$	% marine diet	Date cal BP (95.4%)	Date cal BC (95.4%)	Reference
Muge Stream	Cabeço da Amoreira	shell, *S. plana*	Wk-28035	7395±48				7855-7586	5904-5635	Bicho et al., 2011
		shell, *S. plana*	Wk-28039	7395±48				7855-7586	5904-5635	Bicho et al., 2011
		shell, *S. plana*	Wk-28041	7384±48				7840-7579	5889-5628	Bicho et al., 2011
		shell, *S. plana*	Wk-28050	7377±33				7818-7590	5867-5639	Bicho et al., 2011
		shell, *S. plana*	Wk-28047	7376±34				7818-7588	5967-5637	Bicho et al., 2011
		shell, *S. plana*	Wk-28034	7370±48				7829-7574	5878-5623	Bicho et al., 2011
		shell, *S. plana*	Wk-28038	7365±49				7827-7565	5876-5614	Bicho et al., 2011
		shell, *S. plana*	Wk-28046	7368±39				7815-7578	5864-5627	Bicho et al., 2011
		shell, *S. plana*	Wk-30672	7360±34				7803-7576	5852-5625	Bicho et al., 2011
		shell, *S. plana*	Wk-30674	7356±33				7795-7573	5844-5622	Bicho et al., 2011
		shell, *S. plana*	Wk-28042	7323±48				7792-7538	5841-5587	Bicho et al., 2011
		shell, *S. plana*	Wk-28045	7315±35				7765-7545	5814-5594	Bicho et al., 2011
		shell, *S. plana*	Wk-28044	7311±34				7759-7540	5808-5589	Bicho et al., 2011

Table 1.4 - Continuation and to be continued.

Loc	Site	Material	Lab code	Conventional date BP	$\delta^{13}C$	$\delta^{15}N$	% marine diet	Date cal BP (95.4%)	Date cal BC (95.4%)	Reference
Muge Stream	Cabeço da Amoreira	shell, *S. plana*	Wk-28037	7307±48				7771-7514	5820-5563	Bicho et al., 2011
		shell, *S. plana*	Wk-28040	7305±48				7771-7511	5820-5560	Bicho et al., 2011
		Homo, bones	TO-11819-R	7300±80	-16.3	-	50	8014-7692	6063-5741	Roksandic, 2006; Rolão et al., 2006
		shell, *C. edule*	Wk-26797	7291±35				7732-7514	5781-5563	Bicho et al., 2011
		shell, *S. plana*	Wk-28043	7273±34				7713-7499	5762-5548	Bicho et al., 2011
		shell, *S. plana*	Sac-2023	7260±60	-2.1			7742-7457	5791-5506	Martins et al., 2008
		shell, *S. plana*	Wk-28036	7251±48				7705-7465	5754-5514	Bicho et al., 2011
		shell, *S. plana*	Wk-28049	7193±33				7631-7435	5680-5484	Bicho et al., 2011
		Homo, bones	Beta-447684	7160±40	-16.3	11.9	39	7921-7689	5970-5738	Peyroteo-Stjerna, 2020
		shell, *C. edule*	Wk-26798	7145±37				7591-7410	5640-5459	Bicho et al., 2011
		charcoal	Hv-1349	7135±65				8155-7830	6204-5879	Monge Soares, 2008
		Homo, bones	Wk-32143	7132±41	-15.97	13.86	56	7785-7596	5834-5645	Bicho et al., 2013a
		shell, *S. plana*	Sac-2022	7120±50	-1.2			7590-7366	5639-5415	Martins et al., 2008
		Homo, bones	Beta-447687	7090±40	-15.9	12.4	43	7797-7615	5846-5664	Peyroteo-Stjerna, 2020
		shell, *S. plana*	Sac-2080	7080±80	-3.0			7592-7272	5641-5321	Martins et al., 2008

Table 1.4 - Continuation and to be continued.

Loc	Site	Material	Lab code	Conventional date BP	$\delta^{13}C$	$\delta^{15}N$	% marine diet	Date cal BP (95.4%)	Date cal BC (95.4%)	Reference
Muge Stream	Cabeço da Amoreira	shell, *C. edule*	Sac-2079	7050±45	-2.5			7543-7301	5592-5350	Martins et al., 2008
		Homo, bones	Beta-447688	7040±30	-15.3	13	50	7680-7575	5729-5624	Peyroteo-Stjerna, 2020
		charcoal	Sa-195	7030±350				8608-7247	6657-5296	Roche and Veiga Ferreira, 1972-1973
		mammal bones	TO-11862	6990±60				7938-7694	5987-5743	Roksandic, 2006; Rolão et al., 2006
		charcoal	UGAMS-7196	6990±30				7930-7735	5979-5784	Bicho et al., 2011
		Homo, bones	Beta-447685	6970±30	-16.4	11.9	37	7675-7579	5724-5628	Peyroteo-Stjerna, 2020
		Homo, bones	Wk-32142	6910±40	-15.78	12.86	58	7567-7429	5616-5478	Bicho et al., 2013a
		Homo, bones	Beta-447683	6890±30	-15.3	16.1	50	7572-7445	5621-5494	Peyroteo-Stjerna, 2020
		Homo, bones	Beta-127450	6850±40	-16.5	11.9	48	7564-7429	5613-5478	Cunha and Cardoso, 2002-2003; Umbelino, 2006; Meiklejohn et al., 2009
		Homo, bones	Beta-447686	6770±40	-15.7	13	46	7515-7330	5564-5379	Peyroteo-Stjerna, 2020
		Homo, bones	TO-10218	6630±60	-17.1	-	42	7437-7197	5486-5246	Roksandic, 2006; Rolão et al., 2006
		Homo, bones	TO-10225	6550±70	-20.1	8.2	0	7572-7324	5621-5373	Roksandic, 2006; Rolão et al., 2006
		fauna	Sac-2102	6520±120	-20.8			7616-7178	5665-5227	Martins et al., 2008

Table 1.4 - Continuation.

Loc	Site	Material	Lab code	Conventional date BP	$\delta^{13}C$	$\delta^{15}N$	% marine diet	Date cal BP (95.4%)	Date cal BC (95.4%)	Reference
		Homo, bones	Wk-26796	6329±40	-16.9	12.3	46	7145-6858	5194-4907	Bicho et al., 2011
		charcoal	Sa-194	6050±300				7555-6298	5604-4347	Roche and Veiga Ferreira, 1972-1973
		mammal bones	TO-11861	5970±70				6989-6655	5038-4704	Roksandic, 2006; Rolão et al., 2006
		mammal bones	TO-11860	5710±170				6951-6182	5000-4229	Roksandic, 2006; Rolão et al., 2006
		charcoal	Sac-2078	5170±40				5999-5760	4048-3809	Martins et al., 2008
Magos stream	Cova da Onça	*Homo*, bones	Beta-447676	7170±40	-16.1	11.9	41 ± 11	7936-7672	5985-5721	Peyroteo-Stjerna, 2020
		Homo, bones	Beta-127448	7140±40	-17.2	-	41 ± 10	7927-7655	5976-5704	Cunha and Cardoso, 2002-2003; Umbelino, 2006;
		Homo, bones	Beta-447674	6860±40	-14.9	13.6	55 ± 11	7582-7330	5631-5379	Peyroteo-Stjerna, 2020
		Homo, bones	Beta-447675	6830±40	-15.8	13.2	44 ± 11	7605-7342	5654-5391	Peyroteo-Stjerna, 2020
		Homo, bones	Beta-447677	6680±30	-15.7	13.5	46 ± 11	7476-7236	5525-5285	Peyroteo-Stjerna, 2020

During the time span of the Late Mesolithic occupation in the Tagus valley, the extension, environmental and morphological conditions of the estuary were substantially different from nowadays (Figure 1.3). The fluvial system that formed during the LGM (Figure 1.6; Vis et al., 2008) shaped deep fluvial valleys in pre-LGM sedimentary formations, reaching ca. 25 m depth at Benfica do Ribatejo (Vis et al., 2008; Figure 1.7). Due to the Holocene sea level rise, the valleys were flooded, forming an extensive estuarine area of ca. 1300 km^2 (Taborda et al., 2009; Figure 1.3). At ca. 7000 cal BP (5050 cal BC), during the maximum extension of the estuary (Vis et al., 2008), tidal areas (tidal flats and marshes) developed in the upstream margins of the Tagus, upstream Azambuja, and its tributaries (Vis et al., 2008; Figure 1.6), including the Magos, Muge (see also Figure 1.8 and 1.9; van der Schriek et al., 2007b) and Fonte da Moça streams. The steep and deep slopes of the Tagus valley, particularly in its right margin, and the high sea level rise rate certainly prevented the development of tidal environments along the margins of the central estuarine area.

According to García-Artola et al. (2018), the sea level in the Tagus and Estremadura area rose ca. 7.5 m during the Late Mesolithic occupation at a high rate of 0.81±0.07 cm yr^{-1} until 7500 cal BP (5550 cal BC) and at a rate of 0.34±0.01 cm yr^{-1} between 7500 and 6900 cal BP (5550 and 4950 cal BC; Figure 1.7). The tidal environments that formed by then in the shallow areas influenced by seawater, migrated upstream until the deceleration of the sea level that took place at ca. 7000 cal BP (e.g., Vis et al., 2008; Leorri et al., 2012; García-Artola et al., 2018).

From the Tagus tributaries with Late Mesolithic occupation, only Muge was studied for its environmental context and evolution (van der Schriek et al., 2007b). The rivulet has a 55 km length and a catchment area of ca. 620 km^2. The valley is embedded in Miocene, Pliocene and Pleistocene sediments from the Tagus basin (Figure 1.3) and has a maximum width of 1 km (Figure 1.8). At present the river is channelized and the flood plain intensively used for agriculture.

According to the multi-proxy analyses performed in several sediment cores collected in the Muge valley, estuarine intertidal environments established in the area at ca. 8200 cal BP (6250 cal BC) as evidenced by the presence of estuarine shells (*S. plana*), foraminifera assemblages from tidal flat and saltmarsh areas (*Haynesina germanica*, *Ammonia beccarii*, *Trochammina inflata* and *Jadammina macrescens*) and Chenopodiaceae pollen, a salt marsh indicator (van der Schriek et al., 2007b). The presence of *Isoetes* spores and *Alnus*, *Salix*, Cyperaceae, *Ranunculus* and *Equisetum* in the palynological sedimentary succession of the Muge cores point to the presence of freshwater environments in the upstream areas of the valley (van der Schriek et al., 2007b).

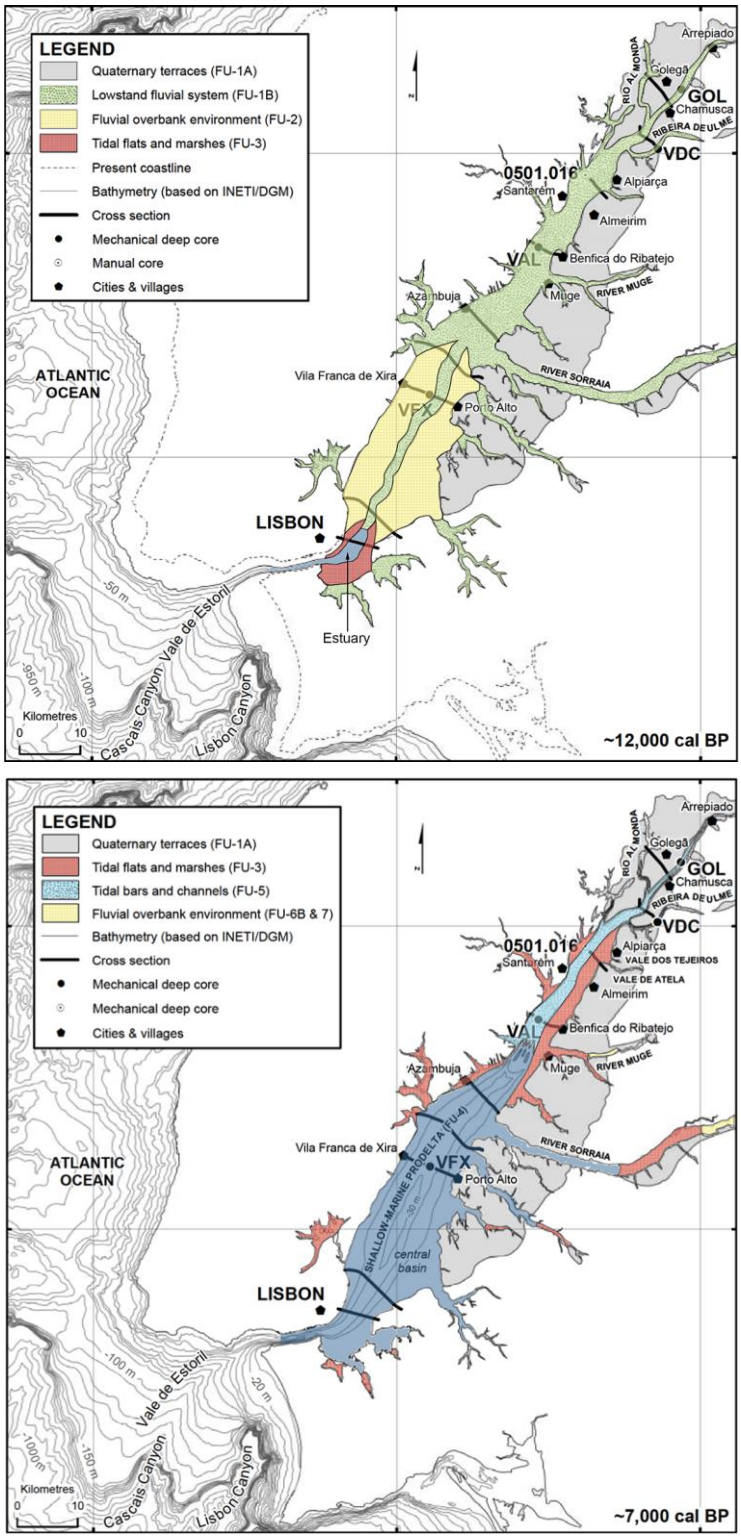

Figure 1.6 - Palaeoenvironmental characterization of the Tagus estuary at ca. 12000 (10050 cal BC) and ca. 7000 cal BP (5050 cal BC). Adapted from Vis et al., 2008.

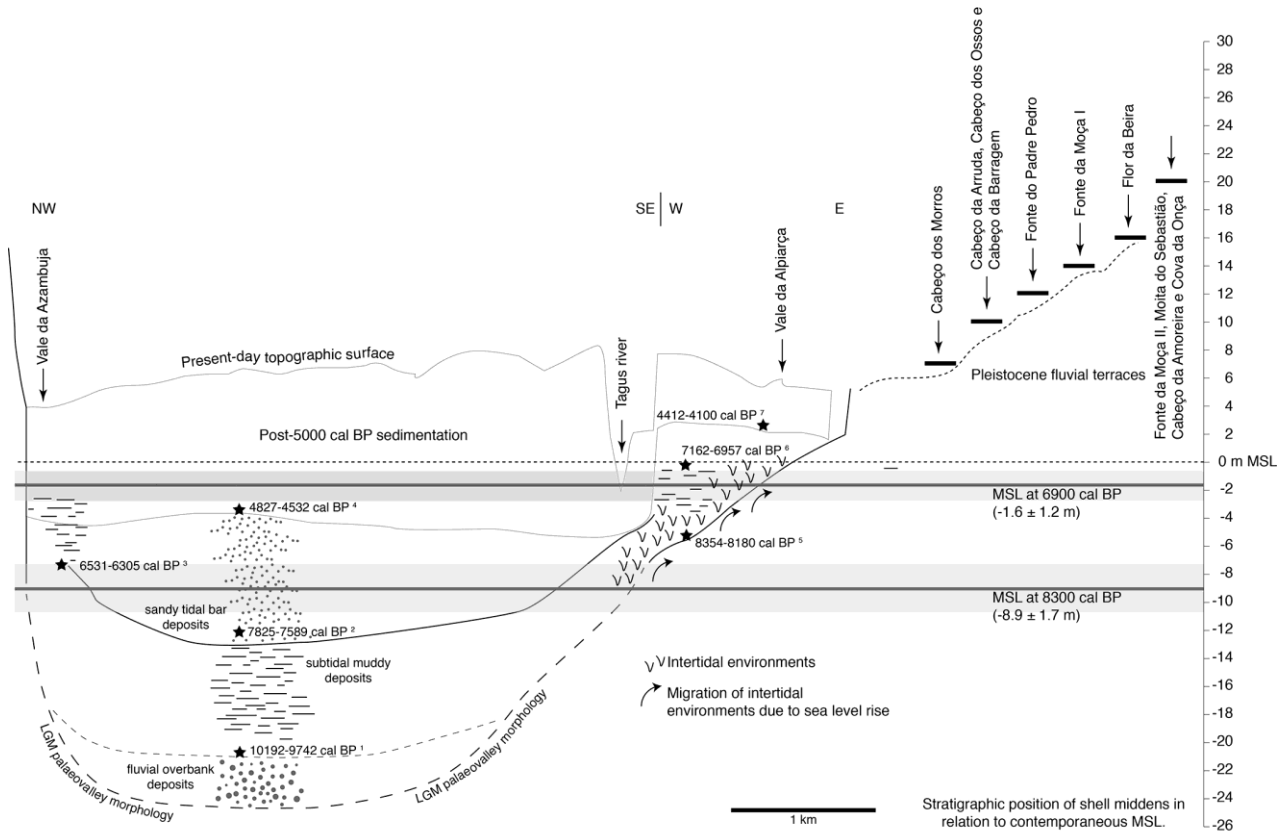

Figure 1.7 - Schematic environmental characterization of the Tagus valley at Benfica do Ribatejo, near the Muge tributary, with relevant information covering the Late Mesolithic occupation time-period and altimetric position of the Tagus shell middens (Gonçalves, 2014; Table 1.1). The scheme was produced based on Benfica do Ribatejo cross-section and the VAL sediment core published by Vis et al. (2008). The information from mean sea level at 8300 and 6900 cal BP (6350 and 4950 cal BC) was retrieved from García-Artola et al. (2018). The grey lines indicate the error associated to MSL. Black stars indicate radiocarbon dates published by Vis et al. (2008). Superscript numbers correspond to the dates presented in Table 1.5.

Table 1.5 - Radiocarbon dates for the Tagus (Benfica do Ribatejo, VAL core; Vis et al., 2008) and the Muge (cores 11 and 20; van der Schrieck et al., 2008) valleys sediment cores used in the schematic environmental characterization represented in Figures 1.7 and 1.9. Conventional dates were calibrated using OxCal 4.4 (© Bronk Ramsey). Dates from terrestrial samples were calibrated using IntCal20 calibration curve (Reimer et al., 2020). Dates from marine samples (shells) were calibrated using Marine13 calibration curve (Reimer et al., 2013) using a ΔR value of 140±40 ^{14}C years (Martins et al., 2008) as determined for the Late Mesolithic for the Tagus valley.

Loc	ID	Material	Lab code	Height m MSL	Conventional date BP	Date cal BP (95.4%)	Date cal BC (95.4%)	Reference
Tagus valley, Benfica do Ribatejo cross-section, VAL core	1	terrestrial botanical macrofossils	UtC-14911		8880±60	10192-9742	8241-7791	Vis et al., 2008
	2	terrestrial botanical macrofossils	UtC-14910		6860±50	7825-7589	5874-5638	Vis et al., 2008
	3	decidous leaf remains	GrA-33637		5640±45	6531-6305	4580-4354	Vis et al., 2008
	4	terrestrial botanical macrofossils	UtC-14909		4145±42	4827-4532	2876-2581	Vis et al., 2008
	5	terrestrial botanical macrofossils	GrA-32654		7440±40	8354-8180	6403-6229	Vis et al., 2008
	6	oxidized organic plant remains	GrA-32651		6165±35	7162-6957	5211-5006	Vis et al., 2008
	7	humic materials	UtC-14745		3849±47	4412-4100	2461-2149	Vis et al., 2008
Muge valley, core 11	8	selected shell fragments, *S. plana*	AA-49816	-6.8	7668±49	7974-7625	6023-5674	Van der Shrieck et al., 2007a
	9	selected plant fragments	AA-48977	-6.7	7263±46	8176-7979	6225-6028	Van der Shrieck et al., 2007a
Muge valley, core 20	10	selected plant fragments	AA-48979	-0.2	6626±44	7573-7430	5622-5479	Van der Shrieck et al., 2007a
	11	bulk organic samples	AA-48980	1.9	4985±73	5896-5596	3945-3645	Van der Shrieck et al., 2007a

The estuarine conditions prevailed in the occupied area of the valley until ca. 5800 cal BP (3850 cal BC; downstream locations), reaching a peak of marine influence between ca. 7800 and 7500 cal BP (between 5850 and 5550 cal BC; Figure 1.8; van der Schriek et al., 2007b). The valley has, at least, 11.5 m depth reaching a height of -7.5 m MSL at ca. 2 km from its confluence with the Tagus. It can be slightly deeper, but coarse (fluvial?) sediments occur below 11.5 m. Previously to 8200 cal BP (6250 cal BC) the MSL was below the valley bottom (ca. -8.9±1.7 m MSL; García-Artola et al., 2018) prevented it from being flooded by seawater, the first record of marine influence occurring between 8176-7979 cal BP (6226-6029 cal BC; Figure 1.9).

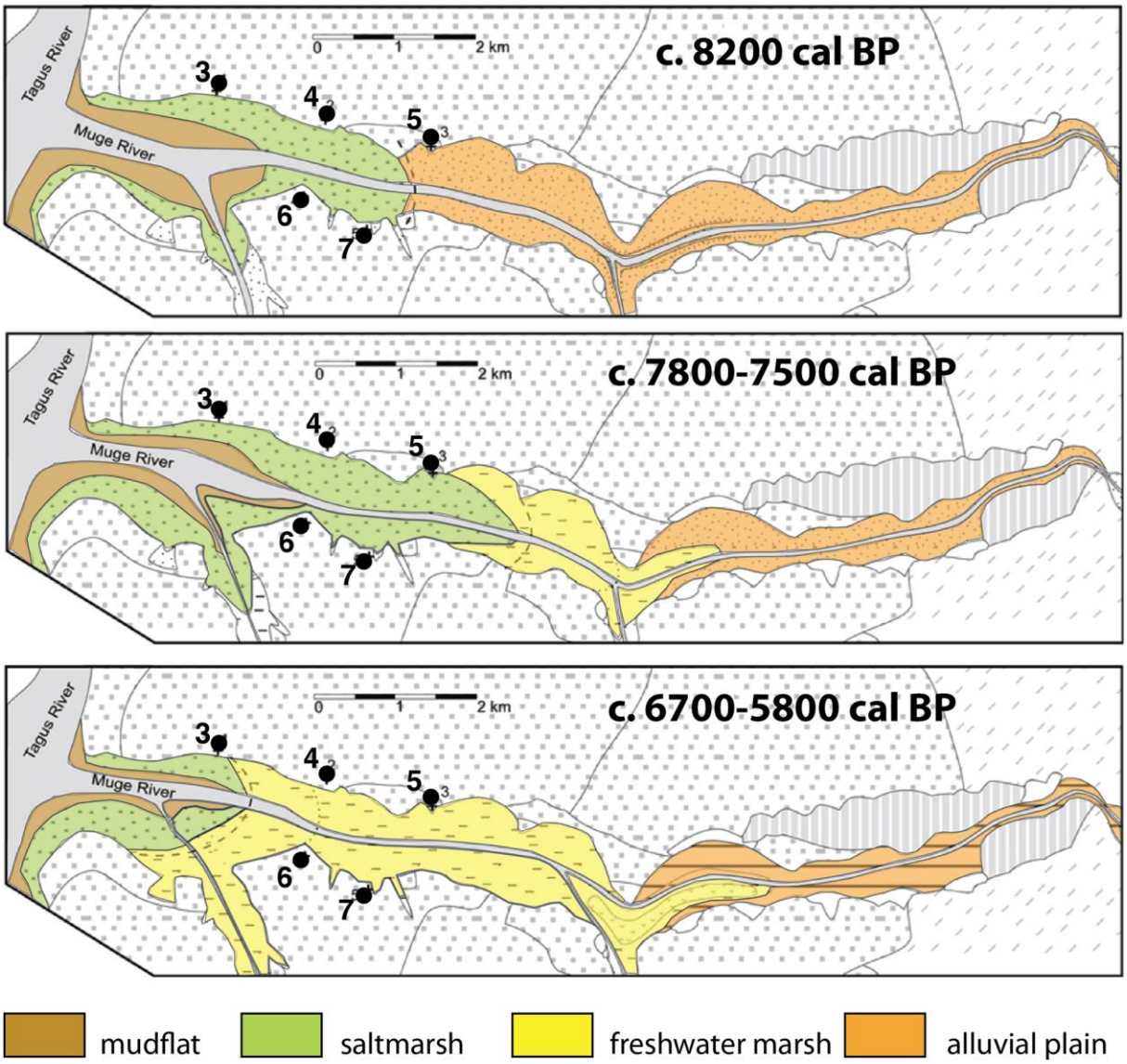

Figure 1.8 - Palaeogeographic evolution of the Muge stream covering the Late Mesolithic occupation. Adapted from van der Schriek et al., 2007b. 3 - Fonte do Padre Pedro; 4 - Flor da Beira; 4 - Cabeço da Arruda; 5 - Moita do Sebastião; 6 - Cabeço da Amoreira. Number follow the ones represented in Figure 1.4.

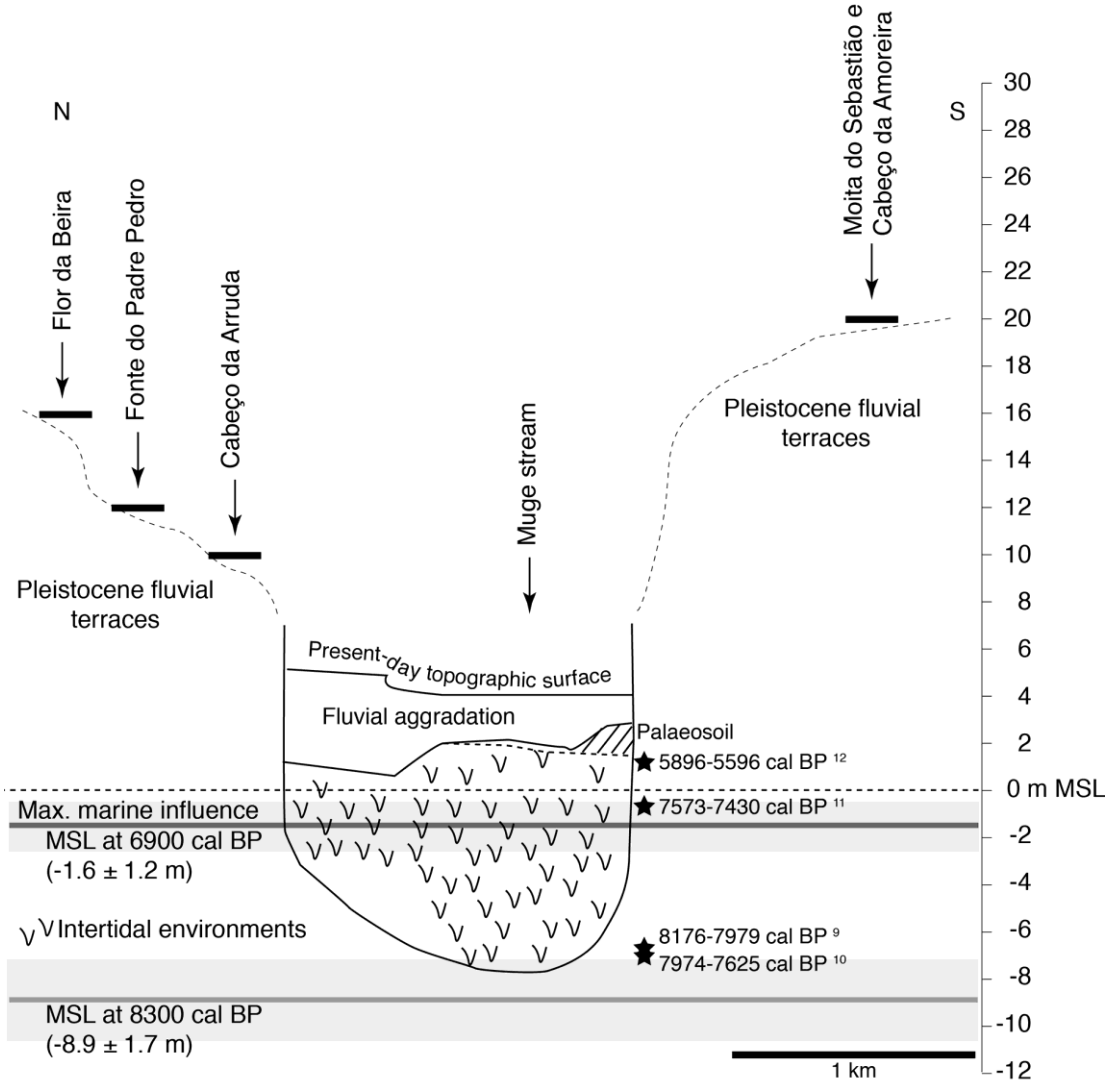

Figure 1.9 - Schematic environmental characterization of the Muge valley, with relevant information covering the Late Mesolithic occupation and the altimetric position of the Muge shell middens (Gonçalves, 2014; Table 1.1). The scheme was produced based on the N-S cross-section and the sediment core 11 published by van der Schriek et al. (2007b). The information from mean sea level at 8300 and 6900 cal BP (6350 and 4950 cal BC) was retrieved from García-Artola et al. (2018). Grey lines indicate the error associated to MSL. Black stars indicate radiocarbon dates published by van der Schriek et al. (2008). Superscript numbers correspond to the dates presented in Table 1.5.

According to these results, the Muge valley could still be under fluvial influence at the time of the first burials, identified at Moita do Sebastião site (8368-8132 cal BP; 6418-6182 cal BC; sample Ua-46264; Peyroteo-Stjerna, 2016), although estuarine tidal environments were already present in the near-by margins of the Tagus, ca. 4 km away from this shell midden (Figure 1.7). Notwithstanding, estuarine conditions abruptly established just after 8200 cal BP (6250 cal BC) in

the Muge valley and prevailed during the entire Late Mesolithic occupation (van der Schriek et al., 2007a).

The Sado valley

A detailed description of the Sado river and estuary is given in the Study Area section. Briefly, the Sado river is one of the greatest Portuguese rivers, with a maximum length of ca. 175 km and draining a wide watershed area ca. 7700 km^2. It runs northward until its confluence with the Odivelas stream and further downstream it bends to northwest to its mouth, near the city of Setúbal. The river has a Mediterranean flow regime with mean annual flows of ca. 7 $m^3 s^{-1}$ under irregular hydrological regime conditions (Bettencourt and Ramos, 2003). The terminal ribbon corresponds to a bar-built estuary occupying an area of about ca. 140-150 km^2 (Bettencourt and Ramos, 2003; Brito, 2009) protected by the Tróia sandspit. It reaches the Atlantic Ocean through a narrow inlet (ca. 2 km) between the northern tip of the sandy barrier and Setúbal. Sado is a well-mixed mesotidal estuary (e.g., Martins et al., 2000; Biguino et al., 2021), with estuarine semi-diurnal tides, the tidal range varying between 1.5 m and 3.9 m during neap and spring tides, respectively (Bettencourt and Ramos, 2003).

Presently, 12 shell middens are reported in the Sado valley. These sites are located on the lower course of the river, ~50 km upstream the present-day estuary inlet and are scattered through ~20 km river upstream, from Herdade de Arapouco to Quinta de D. Rodrigo (e.g., Diniz and Arias, 2012; Figure 1.10; Table 1.6).

The Late Mesolithic shell middens of the Sado valley are known since the 1930's (Barradas, 1936), but only two decades later they had got attention (Arnaud, 2000).

The first and largest excavations in the Sado valley Mesolithic shell middens took place between 1955 and 1964 under the responsibility of Manuel Heleno (Arias et al., 2021; Table 1.6), former director of the National Museum of Archaeology, but unfortunately scarce information was published concerning these archaeological works (e.g., Santos, 1967; Santos et al., 1972). A new and multidisciplinary research project directed by José Arnaud started in the 1980's aiming to study the collections and information from the previous Manuel Heleno works and performing new excavations in Poças de São Bento (in collaboration with Lars Larsson), Cabeço das Amoreiras and Cabeço do Pez (e.g., Arnaud, 1989, Larsson, 1996; 2010).

In 2010 the SADOMESO project was launched, led by Pablo Arias and Mariana Diniz, combining funding from the Spanish Ministry of Economy and Competitiveness through the project COASTTRAN - *Coastal transitions: A comparative approach to the processes of neolithization in Atlantic Europe* (HAR2011-29907-C03-00) and from the Portuguese Fundação para a Ciência e

Tecnologia with the project Back to Sado - *A case study between last hunter-gatherers and first agro-pastoralist societies in southern Portugal* (PTDC/HISARQ/121592/2010).

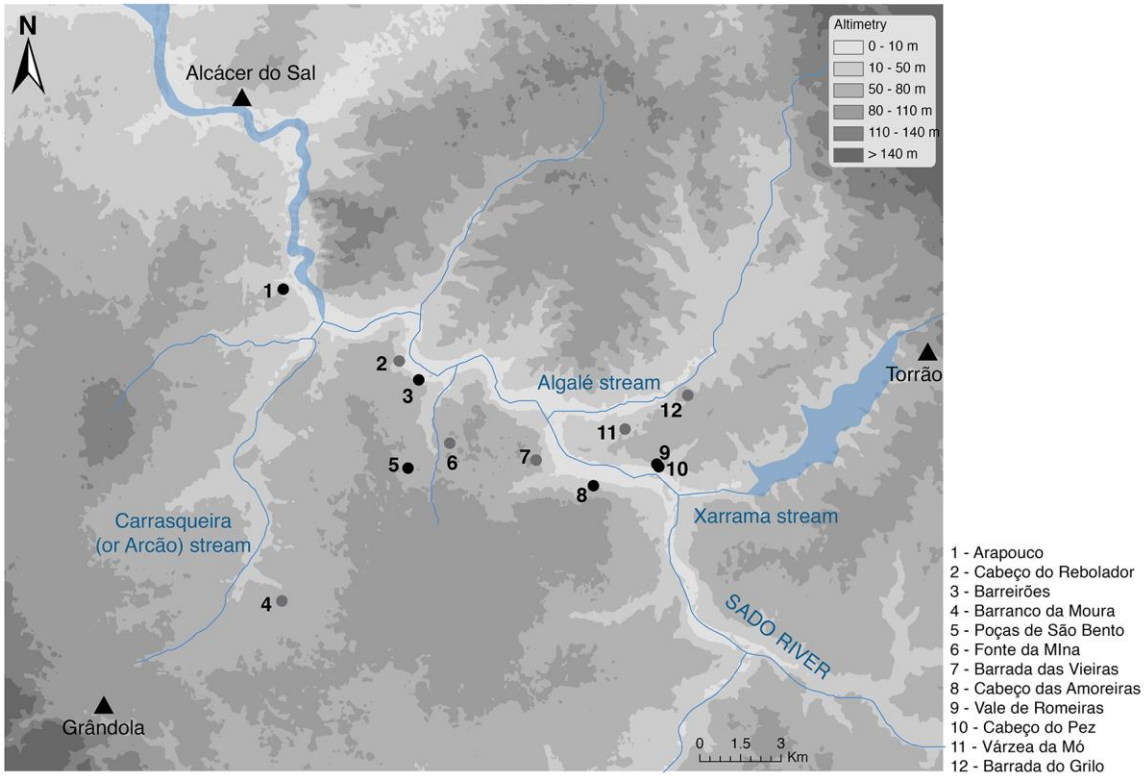

Figure 1.10 - Location of the Sado Late Mesolithic shell middens. Black circles correspond to the sell middens with known coordinates. Grey circles correspond to the shell middens whose location is uncertain. Coordinates and altimetry are presented in Table 1.6.

The present investigations were developed in the framework of the SADOMESO project and also funding by the following ones: CoChange - *Coastal societies in a changing world: A diachronic and comparative approach to the Prehistory of SW Europe from the late Palaeolithic to the Neolithic* (HAR2014-51830-P) and SimTIC - *Symbols below the ground: An approach to the thinking of late Glacial hunter-gatherers using information technology* (HAR2017-82557-P), both directed by Pablo Arias and funded by the Spanish Ministry of Economy and Competitiveness.

Most of the shell middens are positioned on the edge of very steep slopes at about 40 - 50 m above the valley, facing the river, with exception of Várzea da Mó (located at a low height), Barrada dos Grilos (located at a higher height) and Poças de São Bento, Barranco da Moura and Fonte da Mina (located at higher heights and more distant to the Sado) (e.g., Araújo, 1995-1997; Arnaud, 2000; Diniz and Arias, 2012; Table 1.6).

Table 1.6 - Coordinates, altimetry and area of the Sado Late Mesolithic shell middens. Coordinate system WGS84. Altimetry retrieved from Diniz and Arias, 2012, except when mentioned other source, and are reported in height in relation to MSL. ID corresponds to the identification of the sites in figure 1.10. Area retrieved from Arnaud, 1989. To be continued.

ID	Name	Latitude	Longitude	Altimetry (m)	Area (m^2)	Preservation state	Excavation years**	Responsible for the archaeological works
1	Arapouco	38.316882	-8.492417	47	1174	Partially destroyed	1961,1962, 1983, 2013, 2016 (test pit)	Manuel Heleno; José Arnaud; Mariana Diniz and Pablo Arias
2	Cabeço do Rebolador	38.283732	-8.442771	55	100	?	1955	Manuel Heleno
3	Barreirões	38.280731	-8.436824	55 (?)	-	Already destroyed when identified	2012 (test pit)	
4	Barranco da Moura	?	?	50 (?)***	300	Uncertain location	1967 (test pit)	Manuel Farinha dos Santos*
5	Poças de São Bento	38.252051	-8.439552	85	3570	Partially excavated	1960, 1964, 1986, 1987, 1988, 2010, 2011, 2012, 2013, 2014, 2015, 2016, 2017	Manuel Heleno, José Arnaud and Lars Larsson; Mariana Diniz and Pablo Arias
6	Fonte da Mina	38.253615	-8.436080	70 (?)***		Uncertain location	1968 (test pit)	Manuel Farinha dos Santos
7	Barrada das Vieiras	38.252750	-8.380009	20	100	Destroyed	-	
8	Cabeço das Amoreiras	38.246583	-8.362989	55	1270	Partially excavated? ****	1958, 1985, 1986, 2014, 2015, 2016	Manuel Heleno; José Arnaud; Mariana Diniz and Pablo Arias

Table 1.6 - Continuation.

ID	Name	Latitude	Longitude	Altimetry (m)	Area (m^2)	Preservation state	Excavation years**	Responsible for the archaeological works
9	Vale de Romeiras	38.251802	-8.331616	55	54	Partially excavated	1959, 1960	Manuel Heleno
10	Cabeço do Pez	38.251382	-8.330087	52	4000	Almost totally excavated	1956, 1958, 1959, 1983, 1984, 1985, 2010	Manuel Heleno; Silva and Soares; José Arnaud; Mariana Diniz and Pablo Arias
11	Várzea da Mó	38.269214	-8.359679	<20 (?)***	?	Destroyed	1959	Manuel Heleno
12	Barrada do Grilo	38.268373	-8.347598	69	5000 (?)**	Uncertain location	1960	Manuel Heleno

*Santos, 1967; **Santos et al., 1972; ***Gonçalves, 2014; Arias et al., 2017

Most of the shell middens are located in the left margin of the Sado valley, excepting the most upstream sites, Vale Romeiras and Cabeço do Pez that locate in the right river margin, and Várzea da Mó and Barrada do Grilo that occur in the left margin of Algalé stream (Figure 1.10).

Combining the altimetric data of the sites that were identified in the SADOMESO project (Table 1.6) and the local geological map information (Geological Map of Portugal, 1:50.000, 39-D Torrão; Antunes et al., 1991), the shell middens were accumulated above: i) Pleistocene dune sands (Ad); ii) Pliocene *Marateca* formation (Ma); iii) Miocene *Esbarrondadoiro* formation (Es); and iv) Eocene *Vale do Guizo* formation (VG) (Table 1.7). A more detailed description of these geological formations can be found in the Study Area section of this work. The age of the aeolian sand dunes below Poças de São Bento archaeological deposits was attested by OSL and dates to the Late Pleistocene (ca. 12±1 ky; GL14060; Duarte et al., 2019).

All geological formations comprise different lithologies (different *facies*; Table 1.6), but the documental analysis performed by Peyroteo-Stjerna (2016) concerning the stratigraphic position, the sedimentary description and the depth of the human burials, at least, from Arapouco, Poças de São Bento, Cabeço das Amoreiras, Vale de Romeiras and Cabeço do Pez all pointing to the presence of sandy layers at the base of the shell middens, that correspond to a sandy *facies* of each formation or to the presence of a aeolian thin sandy cover on the top of the Pre-Pleistocene formations.

Table 1.7 - Brief description of the geological formations where shell middens are located (based on the local geological maps 1:50000, 39-C Alcácer do Sal and 39-D Torrão; Antunes, 1983; Gonçalves and Antunes, 1992).

Geological formation	**Description**	**Shell middens**
Pleistocene aeolic sands (Ad)	rich-quartz aeolian sands, probably remnants of large dune formations	Arapouco Poças de São Bento Fonte da Mina Cabeço do Rebolador? Barreirões? Barranco da Moura?
Pliocene *Marateca* formation	conglomerates, feldspar sands and claystones	Vale de Romeiras Cabeço do Pez Barrada do Grilo
Miocene *Esbarrondadoiro* formation	sands, claystones, biocalcarenites and conglomerates	Várzea da Mó
Miocene *Vale do Guizo* formation	conglomerates, sands, marls, claystone and limestone	Barranco das Vieiras Cabeço das Amoreiras

The conglomerate *facies* of the *Vale do Guizo* formation is pointed out as the source of raw materials for the Sado lithic industries (Araújo, 1995-1997; Pimentel et al., 2015), knapped in siliceous slates, chert, jasper, quartz and quartzite (Araújo, 1995-1997; Marchand, 2001; Araújo et al., 2015).

Cabeço do Pez, Poças de São Bento, Arapouco and Cabeço das Amoreiras are the largest Sado shell middens. However, only Poças de São Bento and Cabeço das Amoreiras were excavated. The sites are thinner than the Tagus shell middens, with mean thickness of 60-80 cm (e.g., Arnaud, 1989). Poças de São Bento reach has a mean thickness of 100 cm (Arias et al., 2021). The difference in the shell midden thickness between the Tagus and the Sado areas have been interpreted as the result of different accumulation processes, with the Sado sites resulting essentially from a lateral accretion of materials (e.g., Arnaud, 1989). Indeed, the stratigraphic record of Poças de São Bento shows lateral and vertical variability (Arnaud, 1989; 2000; Larsson, 1996; 2010) that resulted from intra-site differential use of the space (e.g., Duarte et al., 2019). The microstratigraphic record reveals that the site also resulted from vertical accumulation of shell-rich deposits (Duarte et al., 2019), reflecting formation processes similar to the ones identified at Cabeço da Amoreira (Muge). Several anthropic structures such as storage and cooking pits, post-holes and hearths were reported in the site (e.g., Arnaud, 1989; 2000; Larsson, 1996; Arias et al., 2021) and different anthropic activities (e.g., tossing and dumping events) and occupational layers were also identified at a microscopic scale (Duarte et al., 2019).

The Sado shell middens correspond to anthropic accumulations of shells and shell fragments, mostly of peppery furrow shell (*Scrobicularia plana*) and cockle (*Cerastoderma edule*) revealing that both species were intensively exploited. Preliminary results of the shell assemblages from Poças de São Bento point to a predominance of peppery furrow shell (>95%) over cockle (Álvarez-Férnandez et al., 2012). Fish remains from coastal waters species such as meagre (*Argyrosomus regius*), tope shark (*Galeorhinus galeus*), European sea bass (*Dicentrarchus labrax*) and gilt-head sea bream (*Sparus aurata*), among other, were also identified, at least, in Arapouco, Poças de São Bento and Cabeço da Amoreira (Arnaud, 1989; Gabriel et al., 2012). Crabs (*Carcinus maenas*) are reported in several sites (e.g., Arnaud, 1989; Diniz and Arias, 2012; Rowley-Conwy, 2015). Despite the occurrence of fish remains in all the sites, their representation is sporadic in shell middens located more upstream, such as Cabeço das Amoreiras, Cabeço do Pez and Vale de Romeiras (Arnaud, 1989; 2000; Cunha et al., 2002). Among the mammal remains, red deer (*Cervus elaphus*), wild boar (*Sus scrofa ferus*), aurochs (*Bos primigenius*), roe deer (*Capreolus capreolus*), horse (*Equus caballus*), rabbit (*Oryctolagus cuniculus*) and hare (*Lepus capensis*) occur, being red deer, wild boar and rabbit the most frequent taxa (e.g., Arnaud, 1989; Rowley-Conwy, 2015). Mammal

remains are more abundant in the upstream shell midden sites (e.g., Arnaud, 1989; Cunha et al., 2002).

One hundred and thirteen burials were identified in six of the Sado shell middens: Arapouco, Cabeço das Amoreiras, Poças de São Bento, Vale de Romeiras, Cabeço do Pez and Várzea da Mó (Cunha and Umbelino, 1995-1997; Arias et al., 2015; Peyroteo-Stjerna, 2016; Table 1.8).

Table 1.8 - Late Mesolithic human remains in the Sado shell middens. Resumed by Peyroteo-Stjerna, 2016.

ID	Name	MNI	Reference
1	Arapouco	32	Cunha and Umbelino, 1995-1997
2	Cabeço do Rebolador	0	Peyroteo-Stjerna, 2016
3	Barreirões	-	Cunha and Umbelino, 1995-1997
4	Barranco da Moura	0	Santos,1968
5	Poças de São Bento	16	Cunha and Umbelino, 1995-1997; Arias et al., 2015
6	Fonte da Mina	0	Santos, 1967
7	Barrada das Vieiras	-	Peyroteo-Stjerna, 2016
8	Cabeço das Amoreiras	6	Cunha and Umbelino, 1995-1997
9	Vale de Romeiras	26	Cunha and Umbelino, 1995-1997
10	Cabeço do Pez	32/36	Cunha and Umbelino, 1995-1997
11	Várzea da Mó	1	Cunha and Umbelino, 1995-1997
12	Barrada do Grilo	0	Peyroteo-Stjerna, 2016

The first palaeodiet studies ($\delta^{13}C$ and $\delta^{15}N$) performed in the individuals buried in these shell middens pointed to a lower consumption of marine resources by these populations (Umbelino, 2006; Fontanals-Coll et al., 2014). Nevertheless, $\delta^{13}C$ and $\delta^{15}N$ isotopic results obtained by Guiry et al. (2015) and Peyroteo-Stjerna (2016) point to the co-existence of two different groups with distinctive dietary regimes: a group with a terrestrial oriented diet occupying the upstream shell middens (upstream Cabeço da Amoreira) and another group, with marine oriented diet regime that occupied the most downstream shell middens (Guiry et al., 2015; Peyroteo-Stjerna, 2016; Table 1.9). The results seem to be in line with the differences found in the percentages of mammals vs. fish remains identified in the archaeological record (e.g., Guiry et al., 2015).

Several models have been presented to explain the dietary differences found with-in the Sado shell middens Late Mesolithic groups: i) the upstream and downstream areas of the Sado valley were exploited by different Mesolithic groups; ii) the environmental context offered to the upstream and downstream groups was different with the different groups having easier vs. harder

access to marine resources (e.g., Diniz and Arias, 2012; Guiry et al., 2015; Peyroteo-Stjerna, 2016).

Table 1.9 - Average isotopic values ($\delta^{13}C$ and $\delta^{15}N$) for the human bone collagen samples from individuals buried in the Sado valley.

Site	Number of samples	$\delta^{13}C$	$\delta^{15}N$	Reference
Arapouco	12	-17.0±0.5	12.2±0.4	Guiry et al., 2015; Peyroteo-Stjerna, 2016
Poças de São Bento	8	-17.3±0.4	12.3±0.4	Guiry et al., 2015
	9	-17.4±0.3	12.3±0.4	Peyroteo-Stjerna, 2016
Cabeço das Amoreiras	4	-18.1±1.4*	10.5±2.0*	Guiry et al., 2015
	3	-18.8±0.3	9.6±0.4	
	10	-18.8±1.1	9.6±1.5	Peyroteo-Stjerna, 2016
Vale de Romeiras	7	-19.0±0.4	9.9±0.4	Guiry et al., 2015
	10/9**	-19.2±0.7	9.5±0.9**	Peyroteo-Stjerna, 2016
Cabeço do Pez	14	-19.1±0.7	9.4±1.1	Guiry et al., 2015
	13	-19.3±0.4*	9.2±0.7*	
	27	-19.3±0.7	9.8±1.5	Peyroteo-Stjerna, 2016
Várzea da Mó	1	-20.5±?	8.1±?	Peyroteo-Stjerna, 2016

* considering one outlier value

The radiocarbon dates for the Sado shell middens are presented in Table 1.10. Similarly, to the exercise done for the Tagus, the conventional dates were calibrated in a simple scientific dating mode using the InCatl13 and Marine13 calibration curves (Reimer et al., 2013) for terrestrial and marine samples, respectively, and OxCal 4.4 (© Bronk Ramsey). For the marine dates a ΔR value of -100±155 ^{14}C years. was applied (Martins et al., 2008) as determined for the Sado valley at ca. 7000 cal BP (5050 cal BC). For human dates, a mixed curve was used, drawn considering the % of marine diet for each and using the ΔR value previously mentioned.

The radiocarbon dating set derives from diverse samples, including human and mammal bones, charcoal, bulk organic sediment and shells, each of which can present issues that led to the determination of erroneous dates. Main problems are: i) lack of $\delta^{13}C$ isotopic results radiocarbon date results, ii) the dating of shells from low salinity environments and the application of the reservoir effect, iii) diets (when determined using or not using IRMS methods for the determination of C and N isotopic values); iv) dates on charcoal samples without prior identification of plant species (to avoid old wood effect), v) in bulk soil samples more recent humic organic materials can be dating and vi) the lack or poor preservation of collagen (in the

case of mammal bones) and carbon (in the case of samples of non-woody plants) prevented the dating, such as occurred in Poças de São Bento (López-Doriga et al., 2016).

According to Peyroteo-Stjerna (2020) and based on reliable radiocarbon dates performed in human bones and considering their diets, the first burial activity at the Sado valley took place between ca. 8540-8330 cal BP (6590-6380 cal BC; Vale de Romeiras; Peyroteo-Stjerna, 2020), previously than in the Tagus shell middens. The burial activity initiated then simultaneously between 8150-7860 cal BP (6200-5910 cal BC) at several sites, both in the Sado and Tagus valleys, becoming less frequent after ca. 7400 cal BP (5450 cal BC). The last known Meolithic burial event in the Sado valley occurred in Várzea da Mó at ca. 7314-7026 (5364-5076 cal BC; Peyroteo-Stjerna, 2020).

The environmental context of the Sado valley seems to be a key-element to the comprehension of the local settlement pattern of the Late Mesolithic populations. In the following chapters the palaeoenvironmental characterization of the Sado valley during the Late Mesolithic occupation period and is evolution through the Holocene is presented and discussed.

Table 1.10 - Radiocarbon dates for the Sado shell midden sites. Conventional dates, isotopic results and % of non-terrestrial carbon (% marine) for human samples retrieved from bibliography. Conventional dates were calibrated using OxCal 4.4 (© Bronk Ramsey). Dates from terrestrial samples (charcoal and mammal bones) were calibrated using IntCal13 calibration curve (Reimer et al., 2013). Dates from marine samples (shells) were calibrated using Marine13 calibration curve (Reimer et al., 2013) using a ΔR value of -100±155 ^{14}C years (Martins et al., 2008) as determined for the Late Mesolithic for the Tagus valley. Dates from human remains were calibrated using a mixed curve, using the % of marine diet.

Site	Material	Lab code	Conventional date BP	$\delta^{13}C$	$\delta^{15}N$	% marine diet	Date cal BP (95.4%)	Date cal BC (95.4%)	Reference
Arapouco	shell	Q-2492	7420±60				8320-7657	6371-5708	Arnaud, 1989
	Homo, bones	Beta-447689	7230±30	-17.0	12.5	31 ± 11	8150-7827	6201-5878	Peyroteo-Stjerna, 2020
	Homo, bones	Sac-1560	7200±130	-16.92; -17.2*	12.1*	44	8196-7615	6247-5666	Cunha and Umbelino, 2001; *Guiry et al., 2015
Cabeço do Rebolador	shell	ICEN-277	7140±70	-1.8			8033-7409	6084-5460	Arnaud, 2000
	shell	ICEN-278	7100±60	-3.3			7998-7385	6049-5436	Arnaud, 2000
Poças de São Bento	*Homo*, bones	OxA-29113	7238±35	-17.2	11.3	28 ± 11	8153-7851	6204-5902	López-Doriga et al., 2016
	shell	LU-2769	7150±70				8046-7417	6097-5468	Larsson, 2010
	shell	LU-2770	7050±60				7945-7323	5996-5374	Larsson, 2010
	shell (*S.plana*)	OxA-29114	7121±35				7977-7416	6028-5467	López-Doriga et al., 2016
	shell (*S.plana*)	OxA-24652	7107±37				7979-7406	6030-5457	López-Doriga et al., 2016
	shell (*C. edule*)	OxA-24648	7084±36				7971-7392	6022-5443	López-Doriga et al., 2016
	shell (*C. edule*)	OxA-24650	7070±35				7949-7372	6000-5423	López-Doriga et al., 2016
	shell (*C. edule*)	OxA-24651	7053±37				7936-7363	5987-5414	López-Doriga et al., 2016

Table 1.10 - Continuation.

Site	Material	Lab code	Conventional date BP	$\delta^{13}C$	$\delta^{15}N$	% marine diet	Date cal BP (95.4%)	Date cal BC (95.4%)	Reference
Poças de São Bento	shell (*C. edule*)	OxA-24649	7052±35				7937-7354	5988-5405	López-Doriga et al., 2016
	shell	Q-2493	7040±70				7942-7307	5993-5358	Arnaud, 1989
	bone (*Meles meles*)	OxA-29135	6962±37				7923-7693	5974-5744	López-Doriga et al., 2016
	bone (*Canis familiaris*)	OxA-26094	6866±33				7786-7623	5837-5674	López-Doriga et al., 2016
	charcoal	Q-2494	6780±65				7756-7510	5807-5561	Arnaud, 1989
	shell	Q-2495	6470±80				7421-6677	5472-4728	Arnaud, 1989
	soil	OxA-29169	6045±39				6997-6789	5048-4840	López-Doriga et al., 2016
	soil	OxA-29170	5511±34				6399-6220	4450-4271	López-Doriga et al., 2016
	Homo, bones	Ua-245	5390±110				-	-	Larsson, 2010
Cabeço das Amoreiras	*Homo*, bones	Beta-125110	7230±70	-20.8; -19.0*; -18.97**	9.5*; 9.53**	0; 14 ± 8*	8176-7860	6227-5911	Cunha and Umbelino, 2001; *Guiry et al., 2015; **Fontanals-Coll et al., 2014
	Homo, bones	Ua-47974	6645±42	-20.0	8.2	9 ± 7	7573-7434	5624-5485	Peyroteo-Stjerna, 2016
	Homo, bones	Ua-47973	6484±39	-20.0	7.6	9 ± 7	7435-7275	5486-5326	Peyroteo-Stjerna, 2016
	shell	Q-(AM85B2b)	5990±80				6947-6159	4998-4210	Arnaud, 2000
	charcoal	Q-(AM85B2a)	5990±75				7148-6656	5199-4707	Arnaud, 2000
Vale de Romeiras	*Homo*, bones	Ua-46972	7640±55	-20.2	8.7	8 ± 7	8545-8335	6596-6386	Peyroteo-Stjerna, 2016
	shell	ICEN-150	7390±80	-3.8			8311-7617	6362-5668	Arnaud, 2000
	shell	ICEN-146	7350±60	-4.3			8264-7593	6315-5644	Arnaud, 2000
	mammal bones	ICEN-144	7130±100	-17.4			8171-7751	6222-5802	Arnaud, 2000
	Homo, bones	Ua-47983	6625±51	-20.5	7.7	7 ± 6	7574-7427	5625-5478	Peyroteo-Stjerna, 2016

Table 1.10 - Continuation.

Site	Material	Lab code	Conventional date BP	$\delta^{13}C$	$\delta^{15}N$	% marine diet	Date cal BP (95.4%)	Date cal BC (95.4%)	Reference
Cabeço do Pez	*Homo*, bones	Beta-447690	6860±40	-18.3	11.4	18 ± 10	7760-7563	5811-5614	Peyroteo-Stjerna, 2020
	Homo, bones	Ua-46931	6791±43	-18.3	13	18 ± 10	7681-7496	5732-5547	Peyroteo-Stjerna, 2016
	Homo, bones	Ua-46933	6788±46	-20.7	6.7	7 ± 5	7691-7521	5742-5572	Peyroteo-Stjerna, 2016
Cabeço do Pez	*Homo*, bones	Ua-46932	6780±48	-19.8	10.4	10 ± 7	7684-7510	5735-5561	Peyroteo-Stjerna, 2016
	Homo, bones	Beta-125109	6760±40	-22.6		0 (?)	7675-7570	5726-5621	Cunha and Umbelino, 2001
	Homo, bones	Sac-1558	6740±110	-19.28			7786-7434	5837-5485	Cunha and Umbelino, 2001
	Homo, bones	Ua-46934	6734±51	-19.7	13.5	10 ± 7	7667-7475	5718-5526	Peyroteo-Stjerna, 2016
	shell	Q-2497	6350±80				7350-6527	5401-4578	Arnaud, 1989
	shell	Q-2496	6050±70				6994-6220	5045-4271	Arnaud, 1989
	Homo, bones	Ua-46930	5579±41	-19.1	11.5	16 ± 10	6435-6212	4486-4263	Peyroteo-Stjerna, 2016
	mammal bones	Q-2499	5535±130				6633-6003	4684-4054	Arnaud, 1989
	shells + charcoal	Q-2498	3565±50				3983-3703	2034-1754	Arnaud, 1989
Várzea da Mó	shell	ICEN-273	7110±50				7994-7411	6045-5462	Arnaud, 2000
	Homo, bones	Ua-46310	6305±44	-20.5	8.1	7 ± 6	7314-7026	5365-5077	Peyroteo-Stjerna, 2016

1.4 Dissertation structure

This work aims to reconstruct the environmental conditions of the Late Mesolithic populations that occupied the Sado valley, Portugal, through the analysis of sediment cores collected in the alluvial plain of the Sado river, near the area where the shell midden sites are located. The thesis is organized in 6 chapters, in addition to indexes and references.

Chapter 1, **Introduction**, is dedicated to the state of the art concerning the environmental context of Late Mesolithic communities. Several questions arise from the present-day knowledge that urge to solve in order to better comprehend the settlement of the last hunter-gatherer communities of SW Iberia. The Portuguese Mesolithic settlement and proposed environmental conditions are described, and particular attention is given to the Late Mesolithic communities of the Tagus and the Sado valley.

Chapter 2 relates to the description of the **Study Area**, combining the present-day characterization of the Sado river and estuary and the geological framework of the Sado basin.

In **Chapter 3, Methodology,** the materials are presented, i.e., the sediment cores used in this work, as well as the geophysical, sedimentological, geochemical and palaecological methods applied to the analyses of sediments with the description of the use and limitation of each method and proxy.

Chapter 4 concerns the **Results** with the geophysical characterization of sediments in depth as measured by Electric Resistivity Tomography (ERT) and the textural, geochemical and palaeontological data. Results are presented by core, from downstream (Arapouco) to upstream (Laxique), followed by the analyses of the Sado tributaries (Arez3).

Chapter 5 is dedicated to the **Discussion** of the palaeomorphology of the Sado valley, the reconstruction of the palaeoenvironmental conditions during the Early, Middle and Late Holocene. Finally, the environmental conditions and implications to the Sado Late Mesolithic communities are presented. This chapter also includes information concerning the influence of the palaeomorphology, climate, river hydrological characteristics and mean sea level rise in the extension of marine flooding.

Finally, **Chapter 6** concerns the main **Conclusions** achieved with the thesis.

In the **References** section all published sources cited in the manuscript text, figures, and tables are listed in alphabetical order.

The information presented in this thesis was submitted to publication as follows:

1) Costa AM, Freitas MC, Leira M, Costas S, Costa PJM, Andrade C, Bao R, Duarte J, Rodrigues A, Cachão M, Araújo AC, Diniz M, Arias P (2019). The role of climate, marine influence and sedimentation rates in Late Holocene estuarine evolution (SW Portugal). The Holocene 29, 622-632. https://doi.org/10.1177/0959683618824768.

2) Costa AM, Freitas MC, Mota R, Leira M, Andrade C, Pimentel N, Araújo AC, Bao R, Diniz M, Arias P (2020). Sado palaeovalley configuration: implications for the Mesolithic settlement during the Holocene sea level rise. In Roque, A, Brito, C, and Veracini, C (Eds.): People, Nature and Environments: Learning to live together. Part 4 - Landscape and Heritage, Chapter thirteen. Cambridge Scholars Publishing, 176-194.

3) Costa, A.M., Freitas, M.C., Leira, M., Fonseca R, Duarte J, Diniz M, Arias P. (2021). Late Holocene evolution of a Mediterranean incised river flowing to the Atlantic: sedimentary dynamics, fluvial activity and palaeoenvironmental reconstruction (SW Iberia), Quaternary International Special Issue Lost landscapes: reconstructing the evolution of coastal areas since the Late Pleistocene (PALEOCOASTS). https://doi.org/10.1016/j.quaint.2021.12.002.
Sedimentological and organic contents and chemistry data presented in above mentioned paper was made available in an open access database and can be find at: Costa, Ana Maria; Freitas, Maria da Conceição; Leira, Manel (2022), Sedimentology and organic content and chemistry data from the Sado estuary, Mendeley Data, V2, doi: 10.17632/wb73343r4v.2

4) Costa AM, Freitas MC, Jiménez-González MA, Jiménez-Morillo NT, Dias CB, Val-Péon C, Reicherter K, Araújo AC, Gabriel S, Leira M, Diniz M, Arias P (accepted for publication). Late Mesolithic lost environments: multidisciplinary approach to characterise the palaeoenvironmental conditions of the Sado valley during the Early-Middle Holocene transition (Portugal). Palaeogeography, Palaeoclimatology, Palaeoecology.

2. STUDY AREA

2. Study area

2.1 Characterization of the Sado river and estuary

The Sado river is located on southwest Portugal (Figure 2.1A). It is one of the greatest Portuguese rivers, with a maximum length of ca. 175 km and draining a ca. 7700 km^2 wide watershed (INE, 2007) (Figure 2.2). It runs northward until the confluence with Ribeira de Odivelas (Figures 2.1B and 2.2) and further downstream it bends to northwest until its mouth, near the city of Setúbal (Figures 2.1B and 2.2).

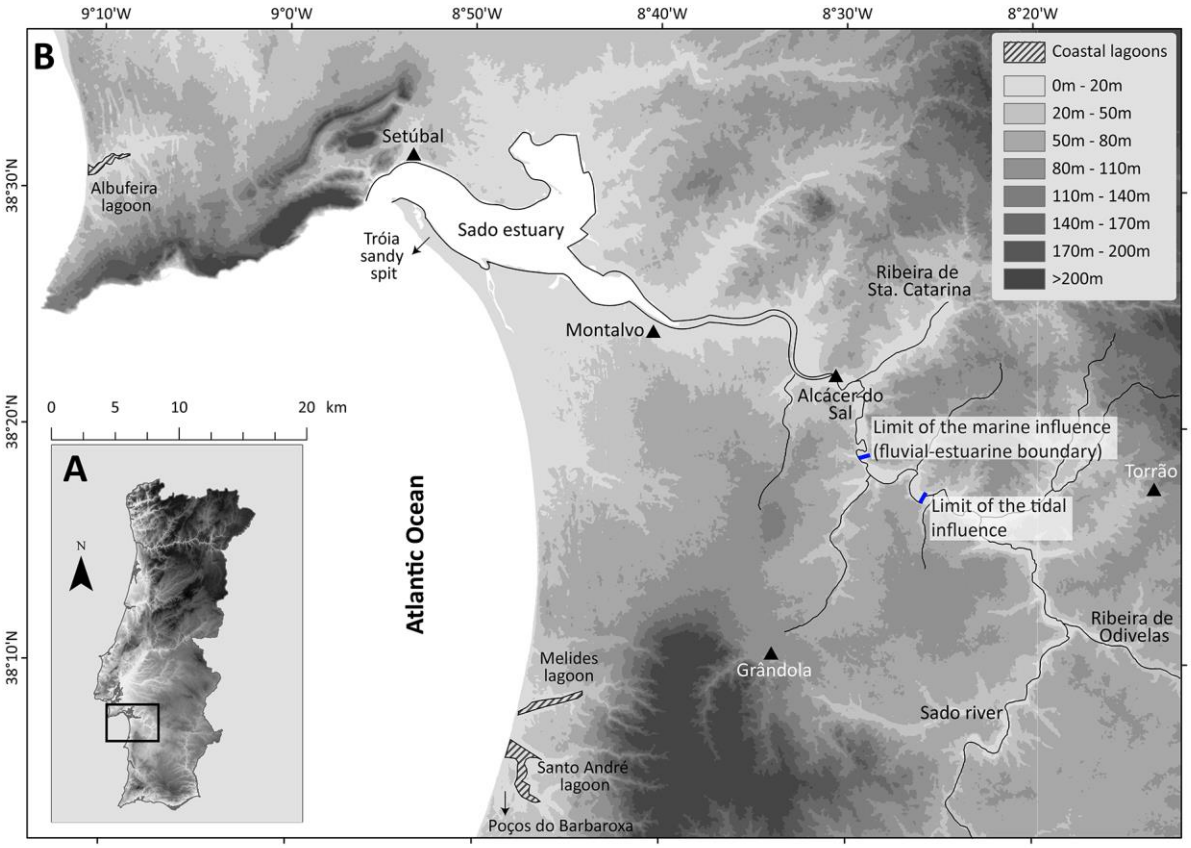

Figure 2.1 - A - Location of Sado river and estuary. B - Sado river and estuary morphology with location of maximum estuarine length.

The river has a Mediterranean flow regime, characterized by a torrential regime (e.g., Rodrigues, 1992), with instantaneous discharge of ca. 1 m^3 s^{-1} during the dry season (from May to September) and 50 to 80 m^3 s^{-1} during the rainy season (from October to April) that occasionally reaches 470 m^3 s^{-1} (Bettencourt and Ramos, 2003 and references therein), allowing for the flooding of alluvial plains margining the main channel (Figure 2.3). It is categorized as a perennial river considering its flow intermittency and variability, being characterized by low inter-annual

variability with very occasional zero-flow days (Oueslati et al., 2015). In natural conditions the mean annual flow was estimated to be 40 $m^3 s^{-1}$, but at present the river presents mean annual flows of ca. 7.7 $m^3 s^{-1}$ under irregular hydrological regime conditions (Bettencourt and Ramos, 2003). Nowadays the river discharge is mostly controlled by 14 dams built-in during the 20th century, distributed through the hydrographic basin (Psuty and Moreira, 2000, Brito, 2009) (Figure 2.2). Since the dam construction, Magalhães (1999 *in* Brito, 2009) estimated a loss of sediment load to the estuary higher than 50% (Brito, 2009).

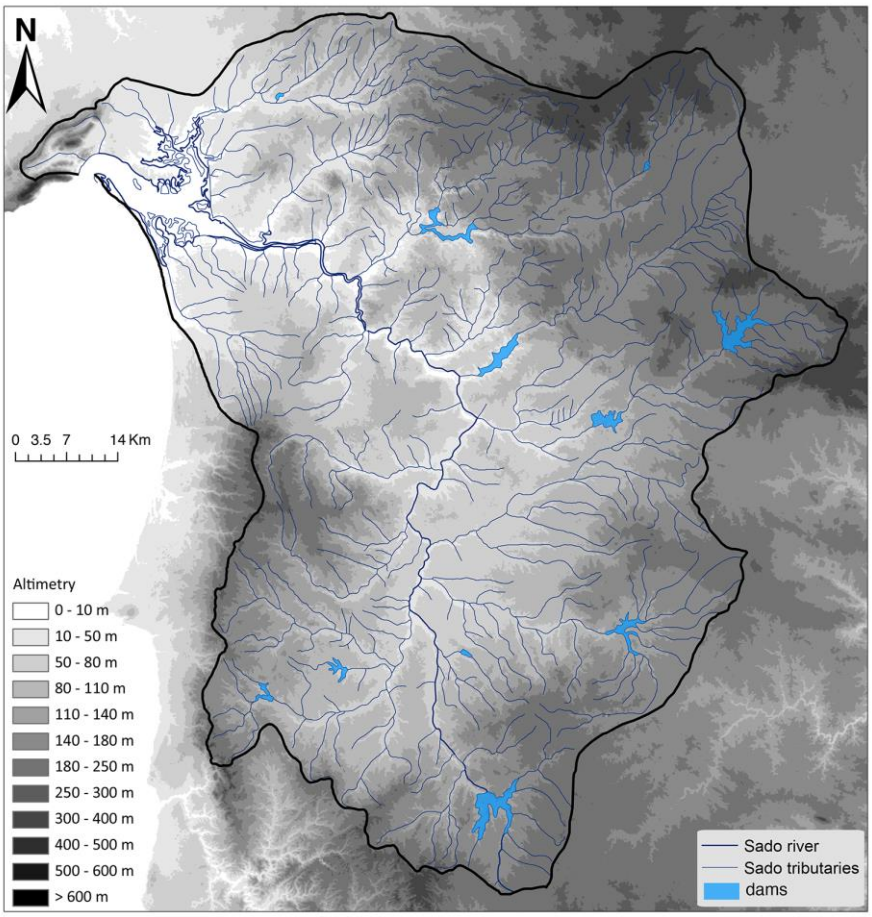

Figure 2.2 - Sado hydrographic basin and location of the dams built during the 20th century plotted in an altimetric base map.

The terminal ribbon corresponds to a bar-built estuary occupying about ca. 140 km^2 (Bettencourt and Ramos, 2003; Brito, 2009) with a mean depth of ca. 8 m, reaching 44 m near the inlet (Brito, 2009). The estuary is protected by the Tróia sandspit (Figure 2.1B), a sandy barrier ca. 25 km long that started to growth northwards since ca. 6500 cal BP (4550 cal BC; Costas et al., 2015) progressively inhibiting exchanges between the estuary and the sea. The estuary reaches the

Atlantic Ocean through a narrow inlet (ca. 2 km) between the north of the sandy barrier and Setúbal.

Figure 2.3 - Flooding of the Sado alluvial plain in the 12th march 2013. Photo © Maria da Conceição Freitas.

According to Bettencourt and Ramos (2003), the estuary extends for a maximum length of 50 km considering the maximum marine intrusion (herein considered as the fluvial-estuarine boundary) reaching the downstream limit of the studied area near Arapouco, or 57 km if the upper limit of tidal rise and fall is considered, reaching São Bento (Figure 2.1B) (Bettencourt and Ramos, 2003). Estuarine tides are semi-diurnal, the tidal range varying between 1.5 m and 3.9 m during neap and spring tides, respectively (Bettencourt and Ramos, 2003). However, the tidal range is amplified within the estuary reaching heights of ca. 4.1 m at Montalvo decreasing upstream to ca. 3.6 m at Alcácer do Sal during spring tides (Vale and Sundby, 1982) (Figure 2.1B).

The water within the estuary is well mixed considering river flow conditions although in periods with high fluvial discharge moderate stratification in some areas can occur (Ferreira et al., 2003). According to Ferreira et al. (2003), three homogeneous zones were defined for the estuary based on salinity available values (Figure 2.4): i) Zone 1, between the estuary inlet and Monte Novo do Sul, at the entrance to the Alcácer do Sal channel with salinity values higher than 25 ‰; ii) Zone 2, between Monte Novo do Sul and Alcácer do Sal, with salinity values between 25 and 0.5 ‰;

and iii) Zone 3, on this classification, the marine influence would reach areas of the river that are usually under prevalent fluvial condition (e.g., Bettencourt and Ramos, 2003; Figure 2.1), but the limits of the third zone were defined based on modelled salinity values (Ferreira et al., 2003) and can be overestimated. In the present work, the maximum saline influence and maximum tidal influence limits determined by Bettencourt and Ramos (2003) will be used (Figure 2.1 and 2.4).

Considering the sedimentological component, the sediments deposited in the estuarine central basin correspond essentially to sand and muddy-sand materials, coarsening at the estuary mouth and in the main estuarine channels (e.g., Rodrigues, 1992; Figure 2.6). Finer sediments occur particularly in the marginal intertidal areas, where saltmarshes and tidal flats develop (e.g., Andrade et al., 2006a). River upstream the occurrence of muddy sediments increases performing in total more than 75% of total sediment (Figure 2.6).

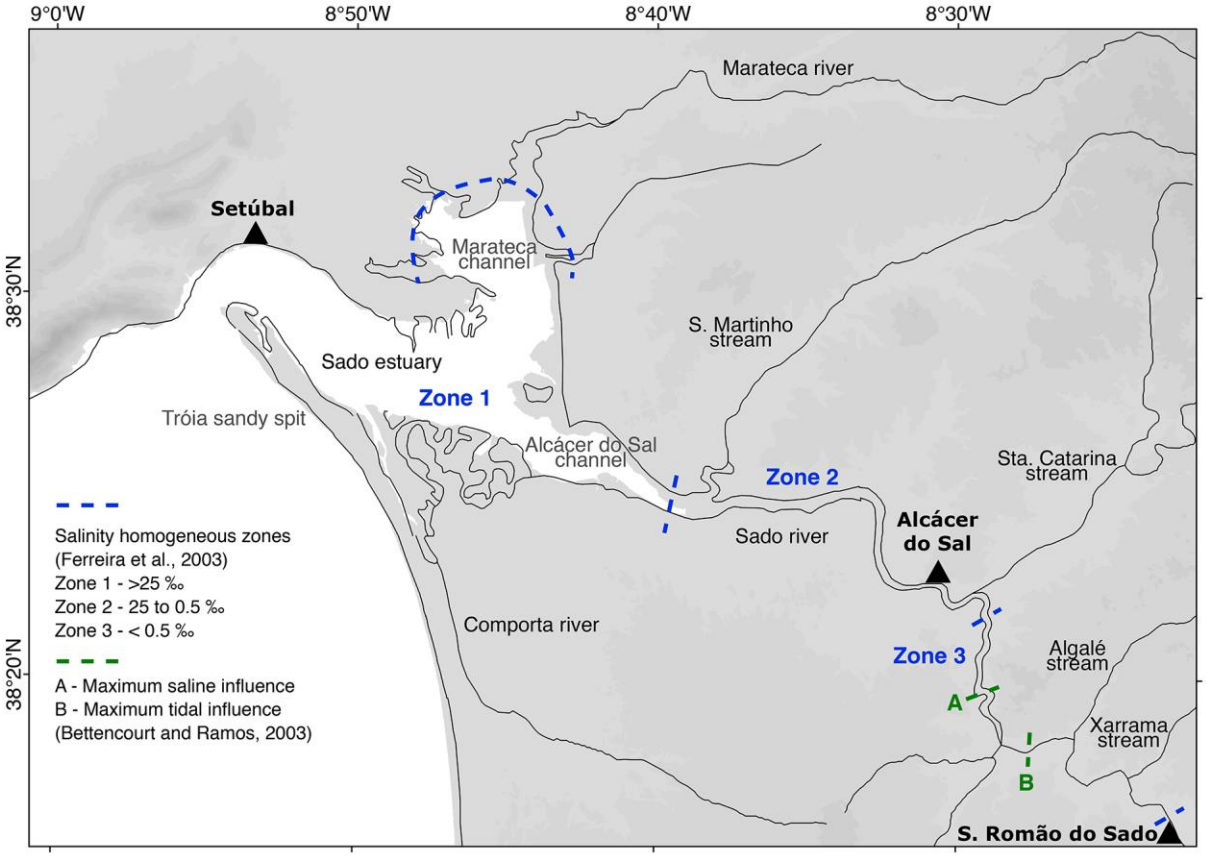

Figure 2.4 - Sado estuary salinity zones and maximum saline and tidal influence limits. Adapted from Ferreira et al. (2003) and Bettencourt and Ramos (2003), respectively.

According to Rodrigues (1992), the distribution of superficial sediments is probably sourced in three different environments: tide-related coarse marine sediments that accumulate in the south estuarine channel; fluvial coarse and fine sediments that accumulate at the mouth of the Alcácer

do Sal channel and in the central estuarine basin; and materials sourced in the industrialized northern margin of the estuary that increase the fine component of the total sediment, but that also contribute with other pollutants to the estuary (e.g., Quevauviller et al., 1989; Cortesão e Vale, 1995; Caeiro et al., 2005; Freitas et al., 2008).

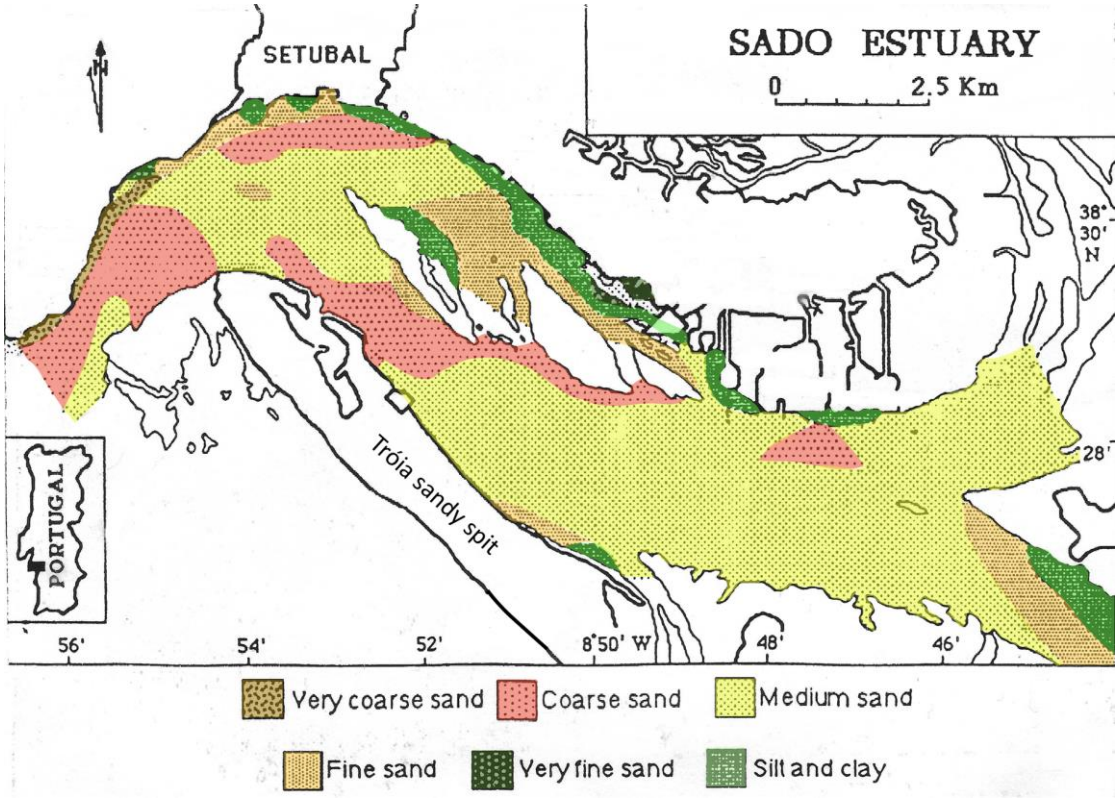

Figure 2.5 - Classification and distribution of subtidal surface sediments in the Sado estuary. Adapted from Rodrigues, 1992.

Considering the present-day spatial distribution of bivalves in the estuary, a high diversity of species was identified (Santos, 2019). Although not being the most abundant species, *Scrobicularia plana* and *Cerastoderma* spp. are still present in the estuarine area. *S. plana* was mostly identified in the Alcácer do Sal channel, in an area affected by lower salinity contents and with mud to fine sand sediments. *Cerastoderma* spp. was identified in the Alcácer do Sal channel and in the central estuarine basin. The most important factors for the distribution of *Cerastoderma* in the Sado estuary are salinity (values between 17 and 30 ‰), grain-size (fine sediments), organic matter content and water depth (shallower areas), similar to other European estuarine areas (Santos, 2019).

The northwards elongation of the Tróia spit since ca. 6500 cal BP (4550 cal BC) onwards reduced water exchange between the sea and the river promoting the onset of low energy

conditions allowing sediment deposition within the estuary (Costas et al., 2015) and favouring the aggradation of the alluvial plain at upstream areas.

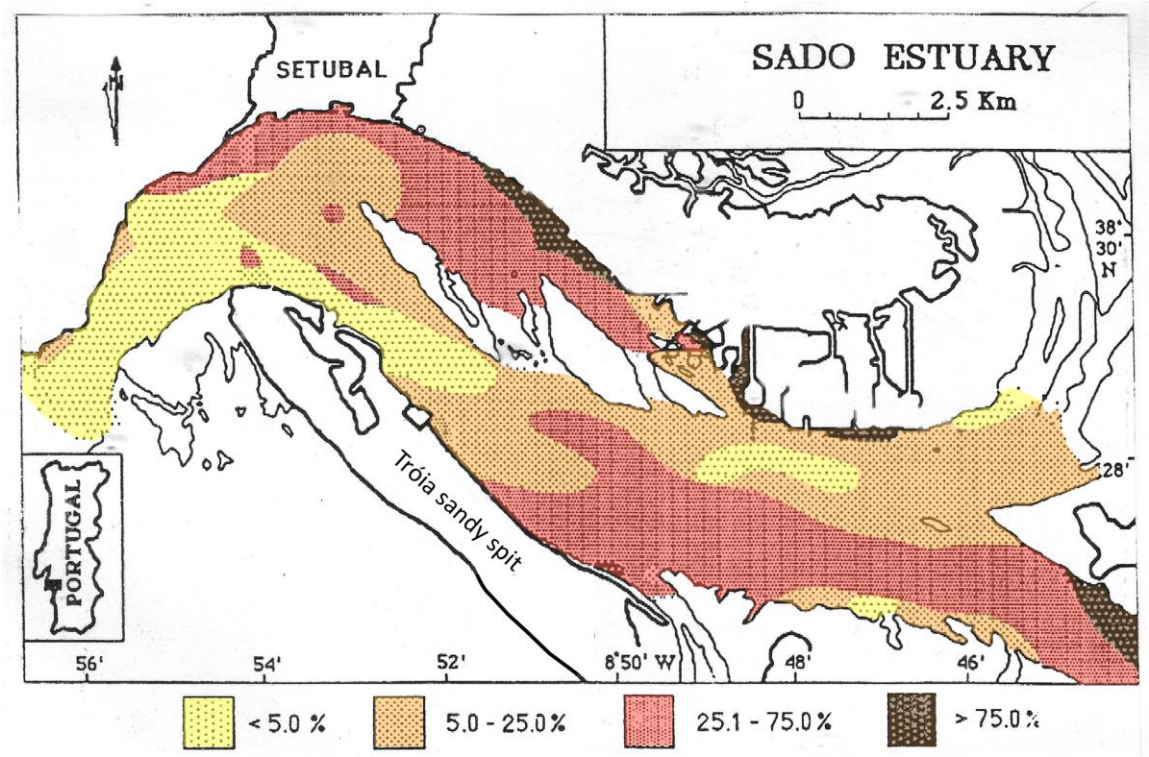

Figure 2.6 - Spatial distribution of fine particles (<63 μm) in the subtidal superficial sediments. Adapted from Rodrigues, 1992.

Limited research has been addressed considering the environmental evolution of the Sado estuary through the Holocene (e.g., Moreira, 1992, Psuty and Moreira, 2000; Andrade et al., 2006b; Freitas and Andrade, 2008). According to available data, sediment aggradation took place, at least, since ca. 7200 cal BP (5250 cal BC) in the Marateca channel margins (Zambujal; Figure 2.7) considering the radiocarbon dates published by Psuty and Moreira (2000) (Table 2.1). Notwithstanding, the older dates determined at the Alcácer do Sal channel date back to ca. 2700 cal BP (750 cal BC) at Murta (Psuty and Moreira, 2000), closer to the present-day main estuarine area (Figure 2.7) reflecting certainly the general lack of information concerning the evolution of the estuarine area but also, the influence of the valley morphology, the accommodation space and the sea level rise. Saltmarshes occur and develop nowadays in the margins of the estuary (see Table 2.1 for radiocarbon dates). However, rice plant crops, fish-farming and salt evaporation ponds occupy, nowadays, extensive marginal areas of the estuary (e.g., Andrade et al., 2006a; Figure 2.7).

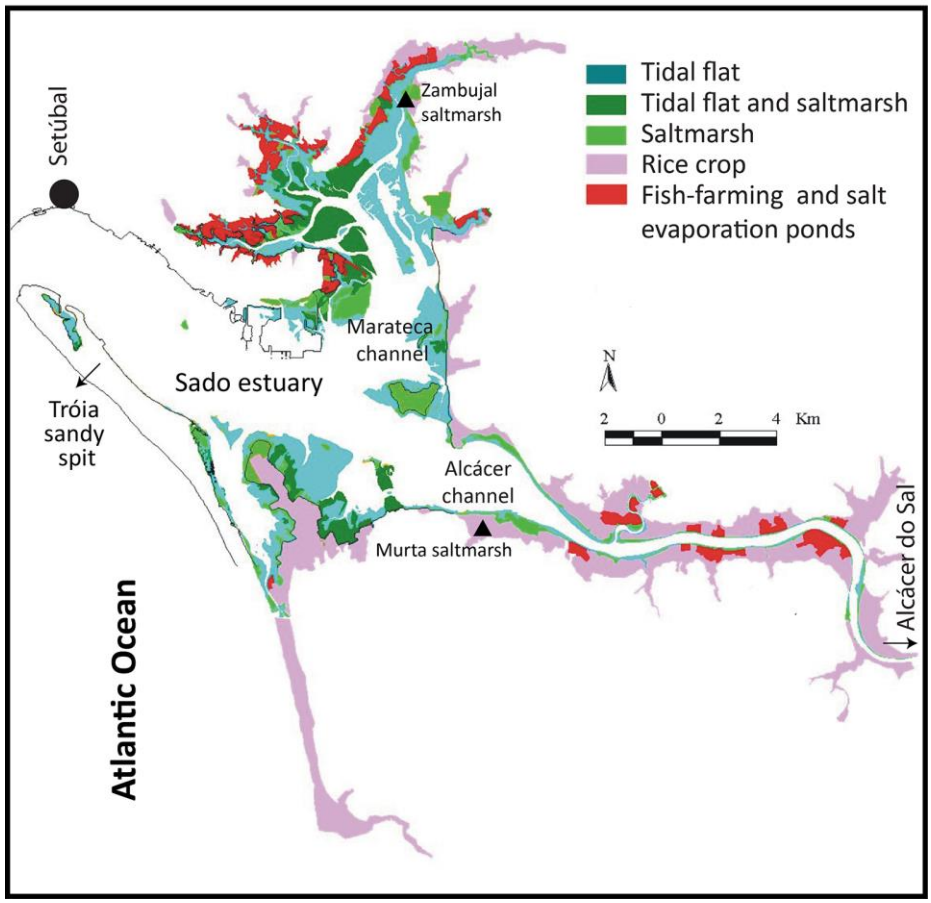

Figure 2.7 - Morphosedimentary characterization of the Sado marginal occupied areas (adapted from Andrade et al., 2006a), with location of the Murta and Zambujal saltmarshes.

In the studied area, located ca. 45 km upstream the estuarine inlet - upstream Alcácer do Sal (Figure 2.8A and 2.8B) - the fluvial channel feeds the alluvial plain that ranges between 50 and 100 m in width. The river channel with a mean depth of 1 m (Rodrigues, 1992; Bettencourt and Ramos, 2003; Brito, 2009) corresponds to a meander incised in a flat alluvial plain (Figure 2.8C) that reaches ca. 2 m mean sea level (MSL) near the downstream limit of the studied area, at Arapouco and ca. 6 m MSL at the more upstream study area, at Laxique (altimetry collected using Global Navigation Satellite Systems (GNSS) roving receiver units (Leica Geosystems models GPS 900 and NetRover) operating in real-time, connected to Portuguese internet-based correction services during field work). At present, and as mentioned before, the river thalweg is anthropically-controlled and the alluvial plain of Sado river is intensely used for rice production among other agricultural practices since, at least, the 18th century (Figure 2.9).

The coastal area southwest of the estuary is characterized as a sandy coast with a continuous beach that extends over more than 65 km from the north limit of the Tróia spit until Sines (Figure 2.1B). Several coastal lagoons and wet dune slacks occur in this area: Melides, Santo André, Poços do Barbaroxa (Figure 2.8A), Poço do Pinheirinho e Sancha (not represented in the figure) nowadays separated from the ocean by the presence of a sandy barrier. Andrade and Freitas (2001) point these lowland areas as remnants of older estuaries formed during the Holocene transgression, silted-up after the deceleration of the sea level rise.

2.2 Geology and geomorphology settings

Sado river basin drains diverse rock formations (Figure 2.10) from the Precambrian and Palaeozoic Ages of the South Portuguese (SPZ - greenish and reddish colours in Figure 2.11) and Ossa Morena (OMZ - pinkish colours in Figure 2.11) Zones and Caenozoic deposits from Sado Basin (SB - yellowish colours in 2.11). In addition, Mesozoic sandstones, conglomerates, limestones and marls, outcropping at the Arrábida Mountain, occur north of the Sado estuary inlet (Zbyszewski et al., 1972; Antunes et al., 1983, 1991; Schermerhorn et al., 1984; Inverno et al., 1986; Oliveira, 2006; Dias, 2011; Geological Map of Portugal 1:500000, SGP, 1992 synthetized by Brito, 2009; Figure 2.10 and 2.11).

In its initial course the Sado river crosses Palaeozoic, essentially turbidites (shales and greywackes; e.g., Pimentel, 2002). At a lesser extended it also drains limestones, quartzites, amphibolites and conglomerates (Geological Map of Portugal 1:500000, SGP, 1992) from the SPZ, and metavolcanic rocks from the Iberian Pyrite Belt bearing massive sulphide polymetallic deposits rich in magnetic particles (Pimentel et al., 2001; Matos and Oliveira, 2003) (Figure 2.10 and 2.11). To northeast, crossed essentially by the right margin Sado tributaries, quartzite, quartzdiorites, shales and greywackes constitute the main lithologies outcropping from the OMZ, but dolerites, gabbros, metavolcanic and carbonated rocks are also present (Geological Map of Portugal 1:500000, SGP, 1992; Figure 2.10 and 2.11).

In the study area, located between Arapouco (upstream Alcácer do Sal) and Laxique (downstream São Romão do Sado) (Figure 2.8), the Sado channel runs essentially through Caenozoic sediments from the Palaeogene *Vale do Guizo* and the *Alcácer do Sal* formations (Antunes, 1983; Antunes et al., 1983, 1991; Gonçalves and Antunes, 1992) (Figure 2.12). The Eocene *Vale do Guizo* formation is composed of alluvial pinkish to brownish sandy conglomerates and marly clays (Antunes, 1983; Gonçalves and Antunes, 1992; Pimentel, 2002; Pais et al., 2013) with the presence of some limestone outcropping at the top.

Table 2.1 - Radiocarbon dates published for sediment cores collected in the Sado estuary saltmarshes. ^{14}C BP dates were calibrated using the IntCal20 curve (Reimer et al., 2020) using the OxCal 4.4 (© Bronk Ramsey). Calibrated dates presented in cal BP (BP = 1950) and cal BC/AD. Calibrated dates from Psuty and Moreira (2000) should be taken cautiously once the dated organic materials can be contaminated by carbonate from microorganism shells affected by reservoir effect. To be continued.

Loc	Sample reference	Lab code	Material	Core depth (cm)	Height (cm MSL)	Conventional ^{14}C age BP	Calibrated age BP (95.4%)	Calibrated age BC/AD (95.4%)	References
Marateca channel	Zambujal 1	Beta-56159	Bulk organic sediment	210	-10	3920±100	4796-4761 (1.5%) 4692-4679 (0.4%) 4642-4637 (0.1%) 4625-4082 (92.5 %) 4033-4005 (1.0%)	2847-2812 BC (1.5%) 2743-2730 BC (0.4%) 2693-2688 BC (0.1%) 2676-2133 BC (92.5%) 2084-2056 (1.0%)	Psuty and Moreira, 2000
	Zambujal 3a	Beta-30217	Bulk organic sediment	690	-490	5190±170	6291-5600	4342-3651 BC	Psuty and Moreira, 2000
	Zambujal 3b	Beta-30990	Bulk organic sediment	695	-495	4750±130	5846-5829 (0.5%) 5749-5213 (88.5%) 5194-5051 (6.4%)	3897-3880 BC (0.5%) 3800-3264 BC (88.5%) 3245-3102 (6.4%)	Psuty and Moreira, 2000
	Zambujal 4a	Beta-30220	Bulk organic sediment	840	-640	6320±150	7560-7542 (0.7%) 7510-6885 (94.7%)	5611-5593 BC (0.7%) 5561-4936 BC (94.7%)	Psuty and Moreira, 2000
	Zambujal 4b	Beta-30989	Bulk organic sediment	790	-590	5770±130	6665-6170 (89.6%) 6150-6112 (2.4%) 6080-6007 (3.4%)	4716-4221 BC (89.6%) 4201-4163 BC (2.4%) 4131-4058 (3.4%)	Psuty and Moreira, 2000
	Zambujal 5	Beta-30988	Bulk organic sediment	475	-275	3970±120	4823-4745 (6.8%) 4734-4145 (87.1%) 4122-4093 (1.5%)	2874-2796 BC (6.8%) 2785-2196 BC (87.1%) 2173-2146 (1.5%)	Psuty and Moreira, 2000

Table 2.1 - Continuation.

Loc	Sample reference	Lab code	Material	Core depth (cm)	Height (cm MSL)	Conventional ^{14}C age BP	Calibrated age BP (95.4%)	Calibrated age BC/AD (95.4%)	References
Marateca channel	Zambujal 6	Beta-30218	Bulk organic sediment	530	-330	4210±90	4972-4516 (93.7%) 4477-4446 (1.7%)	3023-2567 BC (93.7%) 2528-2497 (1.7%)	Psuty and Moreira, 2000
	Gâmbia I	Beta-30991	Bulk organic sediment	440	-290	3970±80	4798-4760 (2.6%) 4694-4678 (0.8%) 4645-4224 (88.5%) 4206-4155 (3.5%)	2849-2811 BC (2.6%) 2745-2729 (0.8%) 2696-2275 (88.5%) 2257-2206 (3.5%)	Psuty and Moreira, 2000
	Gâmbia II	Beta-56157	Bulk organic sediment	505	-355	4200±100	4974-4504 (91.6%) 4493-4437 (3.7%) 4431-4425 (0.2%)	3025-2555 BC (91.6%) 2544-2488 (3.7%) 2482-2476 (0.2%)	Psuty and Moreira, 2000
	Gâmbia III	Beta-55389	Bulk organic sediment	560	-410	4560±70	5465-5027 (92.5%) 5013-4976 (3.0%)	3516-3071 BC (92.5%) 3064-3027 BC (3.0%)	Psuty and Moreira, 2000
	Gâmbia IV	Beta-56158	Bulk organic sediment	480	-320	4090±140	4960-4226 (94.0%) 4204-4156 (1.5%)	3011-2277 BC (94.0%) 2255-2207 (1.5%)	Psuty and Moreira, 2000
Alcácer do Sal channel	Murta 3	Beta-30218	Bulk organic sediment	310	-110	2640±110	2996-2978 (0.9%) 2969-2405 (93.2%) 2393-2366 (1.3%)	1047-1029 BC (0.9%) 1020-456 BC (93.2%) 444-417 (1.3%)	Psuty and Moreira, 2000
	ALC-S S1 0.78-0.79	Beta-417791	Bulk organic sediment	78.5	72	610±30	651-546	1299-1404 AD	Moreira, 2016
	ALC-S S1 2.68-2.69	Beta-417792	Bulk organic sediment	268.5	-118	740±30	725-652	1225-1299 AD	Moreira, 2016

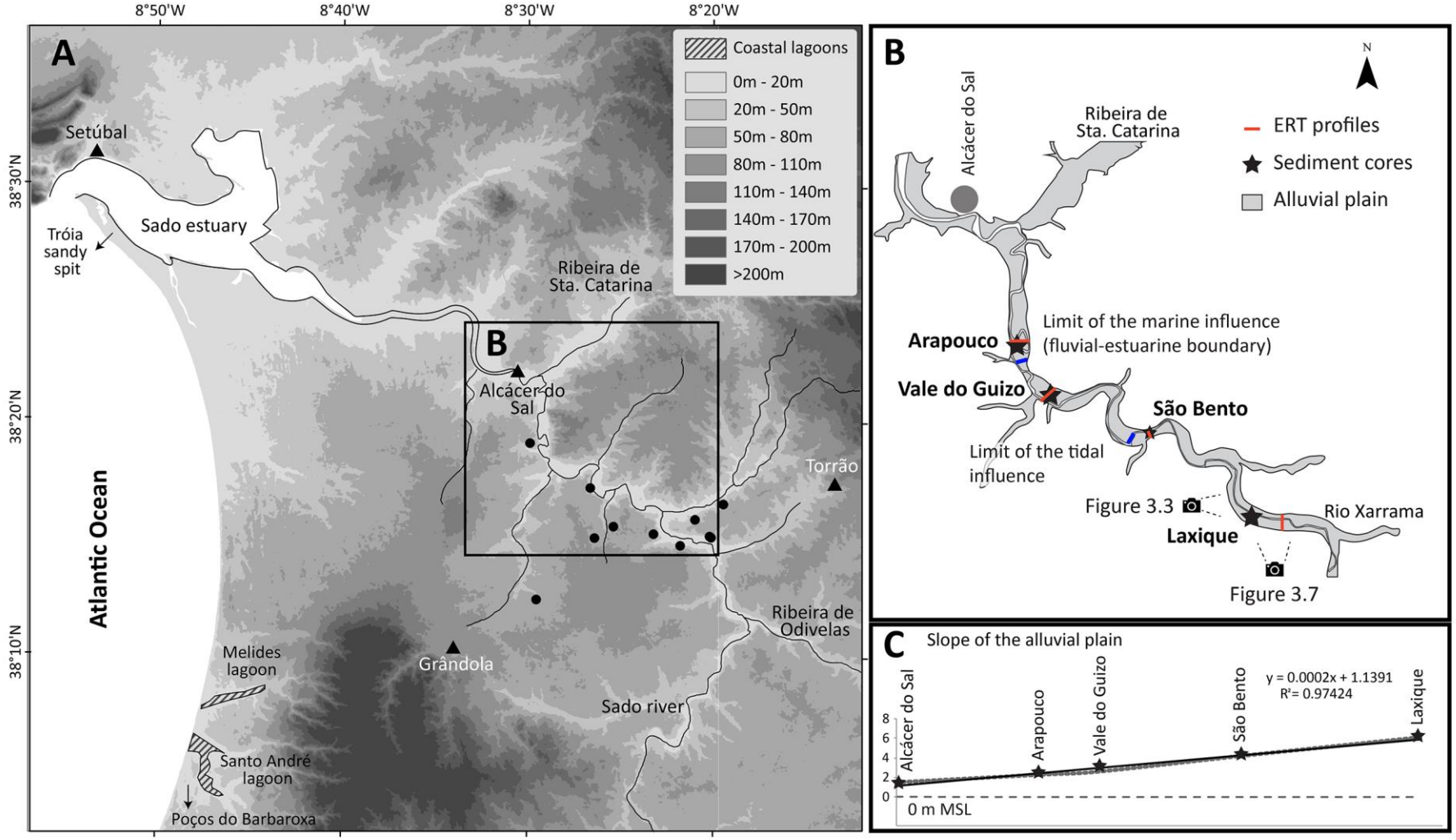

Figure 2.8 - A - Identification of the studied area, with location of the Mesolithic shell middens (black circles); B - Sado valley studied section with location of the ERT profiles (red lines), sediment cores collected from the alluvial plain (black stars) and of the point of view of Figures 2.3 and 2.8. C - alluvial plain surface profile between Laxique (upstream) and Arapouco (downstream).

Figure 2.9 - Rice planting in the Sado alluvial plain. Photo © Ana Cristina Araújo, 2015.

The first meter of the base of the *Vale do Guizo* formation that outcrops near Xarrama river dam (Figure 2.12) is composed by a heterogeneous and heterometric conglomerate with carbonated cement (Gonçalves and Antunes, 1992). The formation corresponds to an incipient fluvial to fluvial deposit on the top of Palaeozoic formations (e.g., Gonçalves and Antunes, 1992). These rather consolidated rocks are the basement of the Late Quaternary alluvial infill of the Sado river, upstream of Arapouco. Rare outcrops of the Miocene *Esbarrondadoiro* formation occur at upstream Sado areas and in the margins of Algalé stream (Figure 2.12). These outcrops are worth to mention once Várzea da Mó shell midden was accumulated on the top of this sedimentary formation. The *Esbarrondadoiro* formation is a marine deposit composed by a yellowish sand with mica and frequent fossils (Antunes et al., 1991; Gonçalves and Antunes, 1992; Pais et al., 2013). Downstream of Arapouco, the Miocene *Alcácer do Sal* formation, with coastal yellowish biocalcarenites and marly sandstones, outcrops in the left margin of the river, corresponding to the basement of the recent alluvial infill (Antunes, 1983; Antunes et al., 1983, 1991; Gonçalves and Antunes, 1992).

The Pliocene *Marateca* formation is represented all over the study area. It is composed by conglomerates, coarse to medium sand, occasionally rich in feldspars, and clay deriving from fluvial channels and flooding plains, respectively (e.g., Gonçalves and Antunes, 1992). According

to Gonçaves and Antunes (1992), the source of materials are essentially the granitic rocks of the OMZ (Figures 2.10 and 2.11).

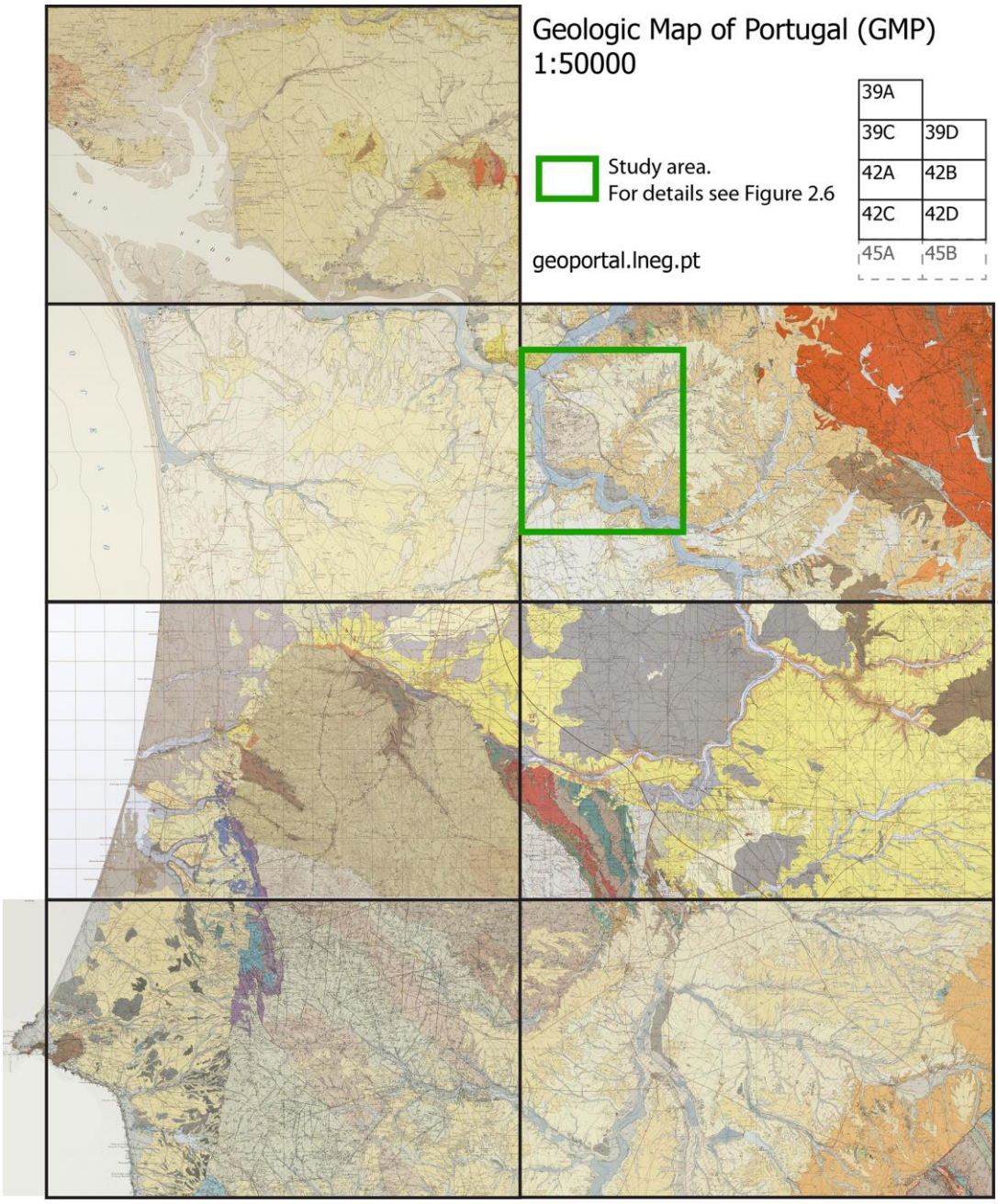

Figure 2.10 - Mosaic with the different sheets of the Geologic Map of Portugal (GMP) 1.50000. The number of each sheet is represented in the upright grid. GMP 39A from Zbyszewski et al. (1972), 39C from Antunes et al., 1983, 39D from Antunes et al., 1991, 42A from Dias, 2011, 42B from Oliveira, 2006, 42C from Inverno et al., 1986, 42D from Schermerhorn et al., 1984. Images available from geoportal.lneg.pt.

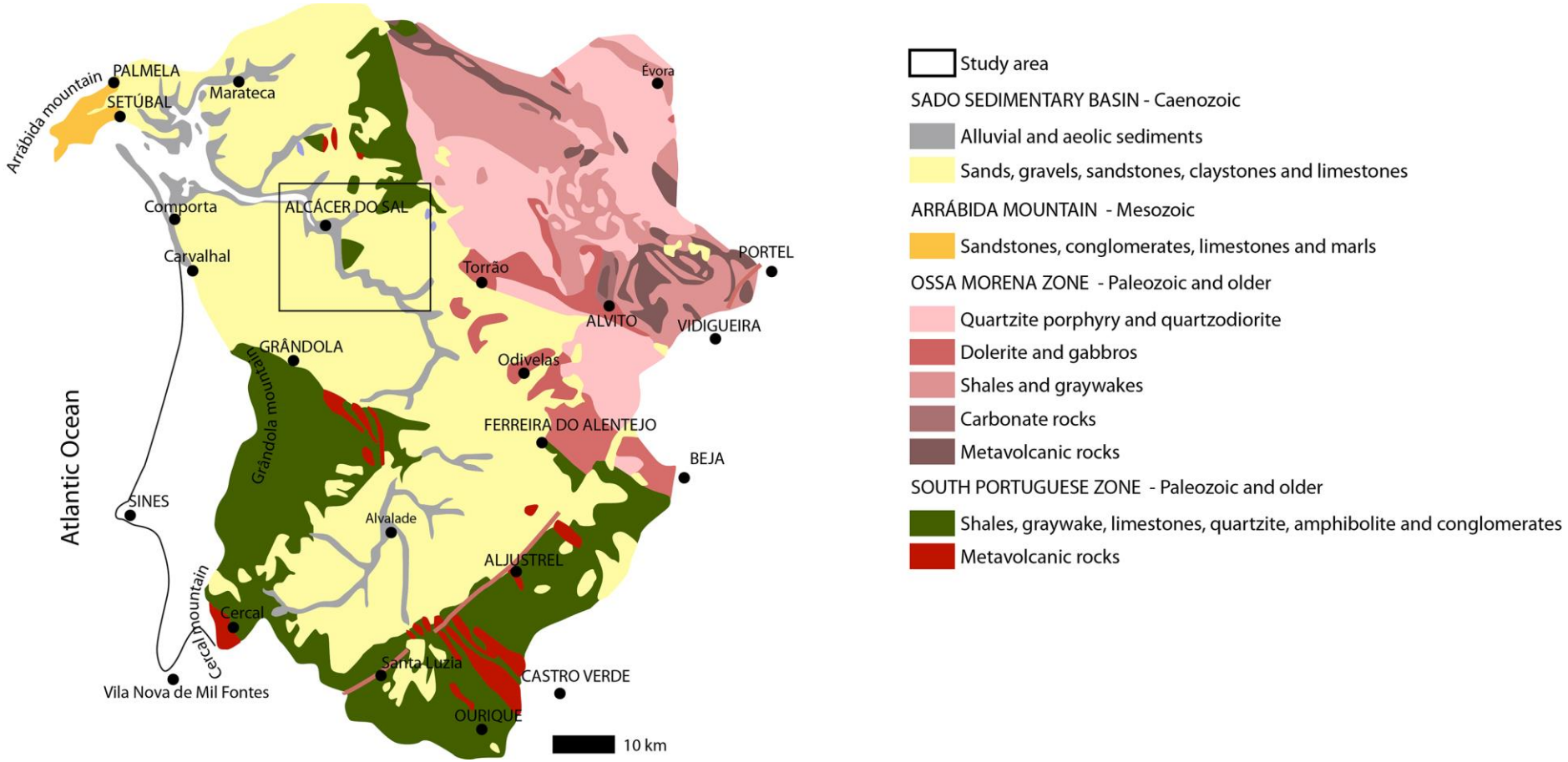

Figure 2.11 - Simplified lithological map of the Sado hydrographic basin. Adapted from Brito, 2009 that used the lithological units defined by Zbyszewski (1939).

On the convex margins of the Sado valley, Pleistocene terraces constituted by sand and gravel with abundant e.g., quartz, porphyry, greywacke clasts were identified. Aeolian quartz-rich sands dated from Plistocene/Holocene extend over the study area (Gonçalves and Antunes, 1992).

Near Arapouco and along the right margin, just before the confluence with Sta. Catarina stream, slaty pelitic rocks, siltites and greywackes of the *Mértola* formation outcrop reaching a height of 132 m at the Sra. da Conceição vertex point (Antunes et al., 1991; Gonçalves and Antunes, 1992; Figure 2.12). At the left margin, the Caenozoic sediments also form a steep slope achieving heights ca. 50 m. The plateaux surrounding the Sado valley, and its tributaries is occupied by a decametric cover of fluvial orange sands and clays of the Pliocene *Marateca* formation (Antunes et al., 1991, Gonçalves and Antunes, 1992). Aeolian quartz-rich sands dated from the Pleistocene-Holocene, resulting from the remobilization of the Pliocene sands, extend over the plateaux and some slopes of the study area (mostly to the south), while Quaternary sandy terraces are present at both margins (Gonçalves and Antunes, 1992).

Claystones and sandstones from the Pulo do Lobo formation (SPZ) and granites, diorites and gabbros (OMZ) are crossed by the Xarrama tributary, at the proximity of its mouth, near Laxique (Antunes et al., 1991, Gonçalves and Antunes, 1992; Figure 2.12).

All the Plio-Quaternary sediments, as well as the Palaeogene sandy clays, are probably the main source for the Late Quaternary alluvial infill of the Sado river, but the SPZ and OMZ have certainly a contribute to the composition of sediments and its geochemical signature (e.g., Freitas et al., 2008; Moreira, 2016).

From the geomorphological point of view, to the West, the region has a low relief, except for the structural relief that uplifts the deposits of *Alcácer do Sal* and *Vale do Guizo* formations at Alcácer do Sal (Antunes, 1983). To NE, the highest locations correspond to OMZ outcrops that form a flattened platform at heights between 200 and 240 m (Beja Complex; Gonçalves and Antunes, 1992). Tectonic is the main factor controlling the relief and the Sado basin pattern, that develops in a rectangular geometry, mainly controlled by fractures (Gonçalves and Antunes, 1992). Geomorphological characterization of the Sado valley Late Quaternary incision resulted from the reports on the geotechnical cores performed at Alcácer do Sal (GRID, 1989; ENGIVIA, 1995; Figure 2.13). Here, a deep incised valley reaching ca. 38 m is interpreted from alluvial sediments deposited above Palaeogene and Neogene materials.

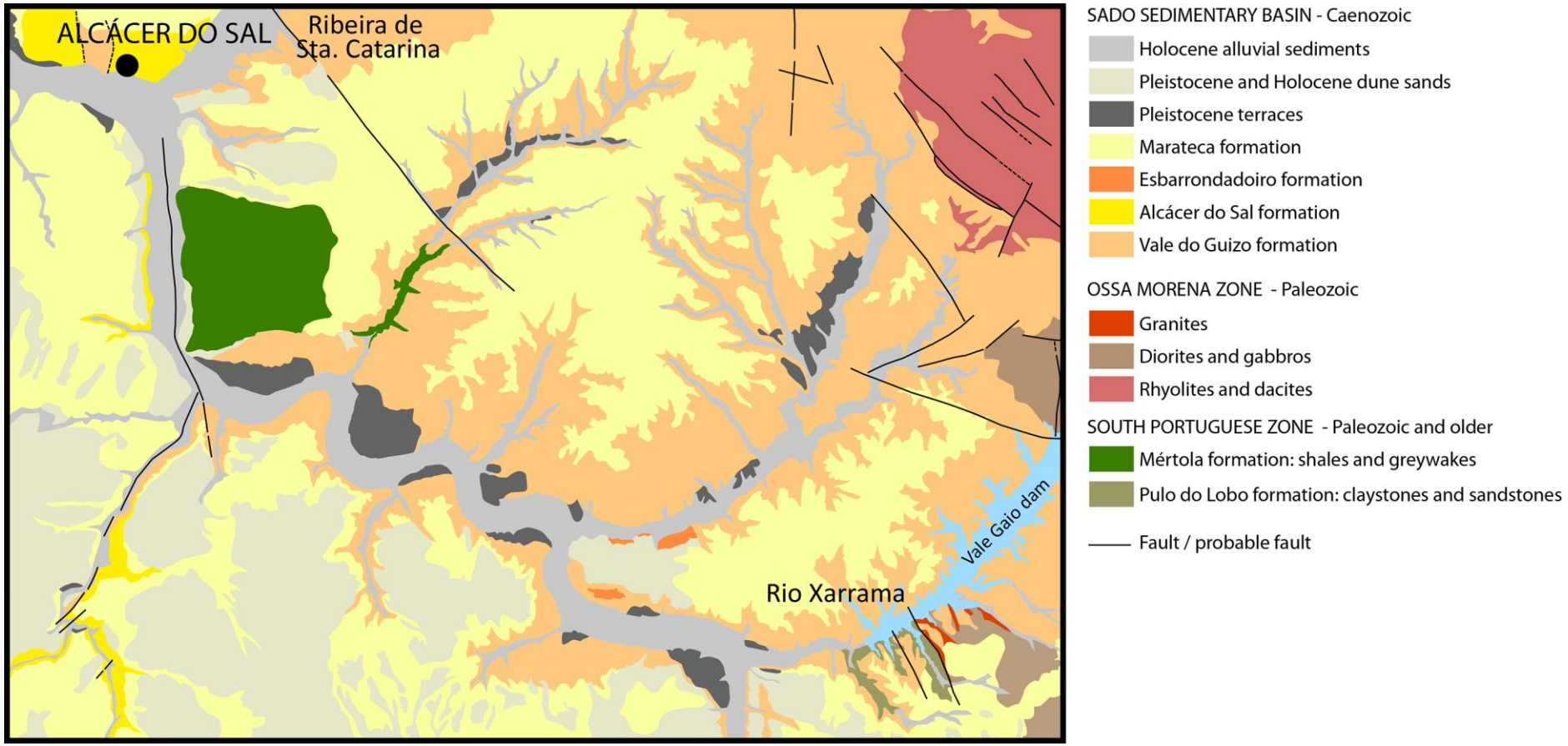

Figure 2.12 - Geological map of the studied area adapted from Geological Map of Portugal 1:50000 39-C, Alcácer do Sal (Antunes et al., 1983), and Geological Map of Portugal 1:50000 39-D, Torrão (Antunes et al., 1991)

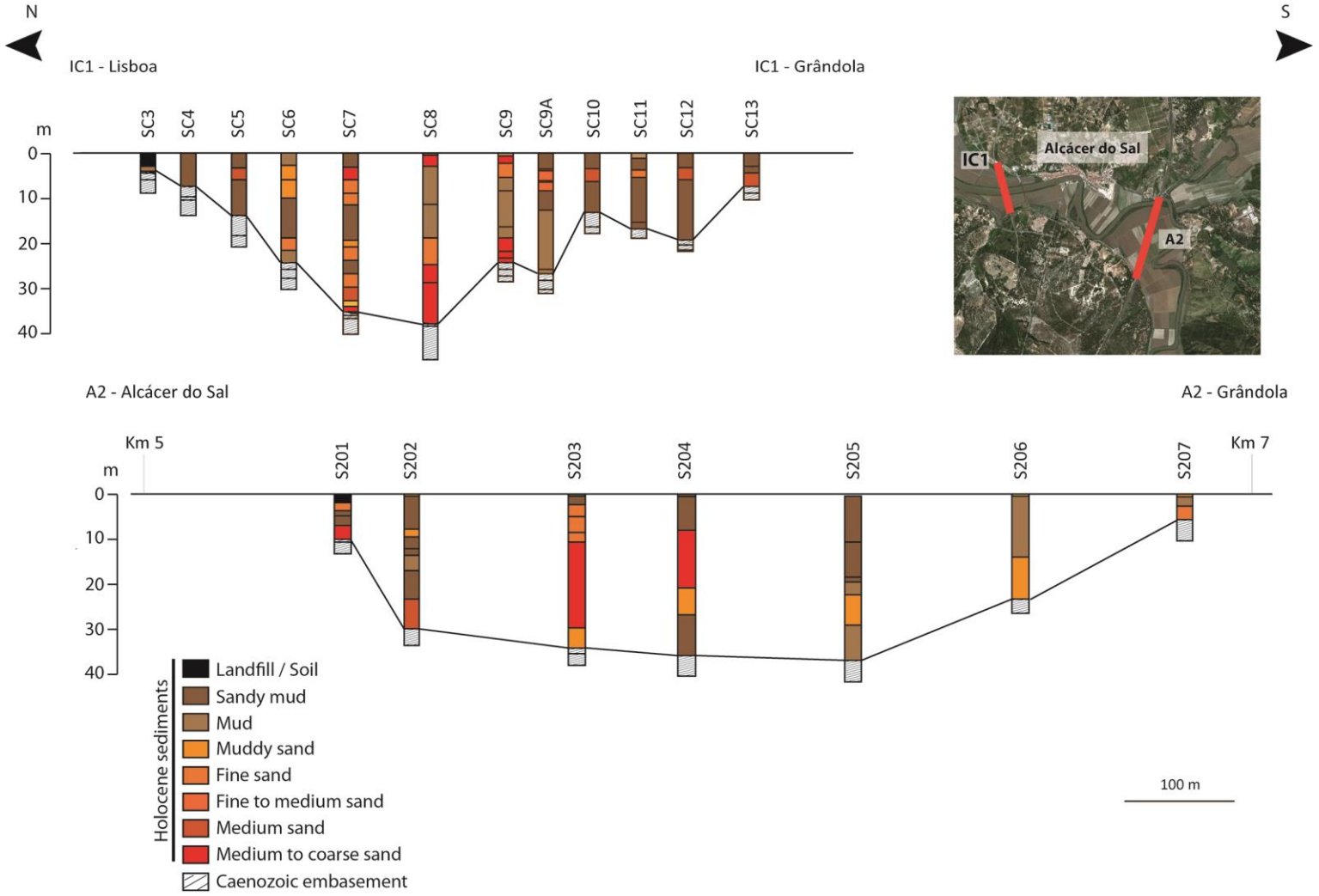

Figure 2.13 - Sado palaeovalley morphology and characterization of the alluvial sediment at Alcácer do Sal (adapted from GRID, 1989; ENGIVIA, 1995).

2.3 Holocene sea level rise

Several curves have been drawn to modulate the sea level rise in the Portuguese margin during the Late Glacial (Dias et al., 2000) and the Holocene (Teixeira et al., 2005; Vis et al., 2008; Leorri et al., 2012; Costas et al., 2016a; García-Artola et al., 2018; Figure 2.14). According to these curves, the MSL rose at a high rate since the beginning of the Holocene until ca. 7000 cal BP (5050 cal BC) and decelerated from 7000 cal BP onwards. According to the model built by García-Artola et al. (2018) for the Estremadura and Tagus area, based on 17 index points and 4 marine limiting dates, the MSL rose ca. 34 m (± 1.2 to 1.7 m) between 11500 and 7500 cal BP (9550 and 5550 cal BC) at a rate of ca. 0.81±0.07 cm yr^{-1}; ca. 0.8 m (± 1.7 to 1.2 m) between 7500 and 6900 cal BP (5550 and 4950 cal BC) at a rate of ca. 0.34±0.10 cm yr^{-1}; and finally the index points indicate a MSL rise from -160±160 cm at ca. 4100 cal BP (2150 cal BC) to -150±150 cm at ca. 1500 cal BP (450 cal AD) at a rate of 0.0±0.05 cm yr^{-1}.

The model drawn by Costas et al. (2016a) for the Sado area, derived from berm sea level index points identified at the Tróia spit, and OSL dated, estimated a low but continuous sea level rise rate of ca. 0.31±0.02 mm yr^{-1} for the last 6000 years.

In the present work, the value estimated by Costas et al. (2016a) was used for the interpretations of Middle and Late Holocene sedimentary successions (e.g., Arapouco and Laxique sediment cores, collected in the Sado channel; see location, description and age-model below). However, the interpretations done in the sedimentary successions covering the Early Holocene (e.g., Arez3, collected in a Sado tributary; see location, description and age-model below) was done based on the sea level rise rate model draw by García-Artola et al. (2018) once it covers the time period being analysed.

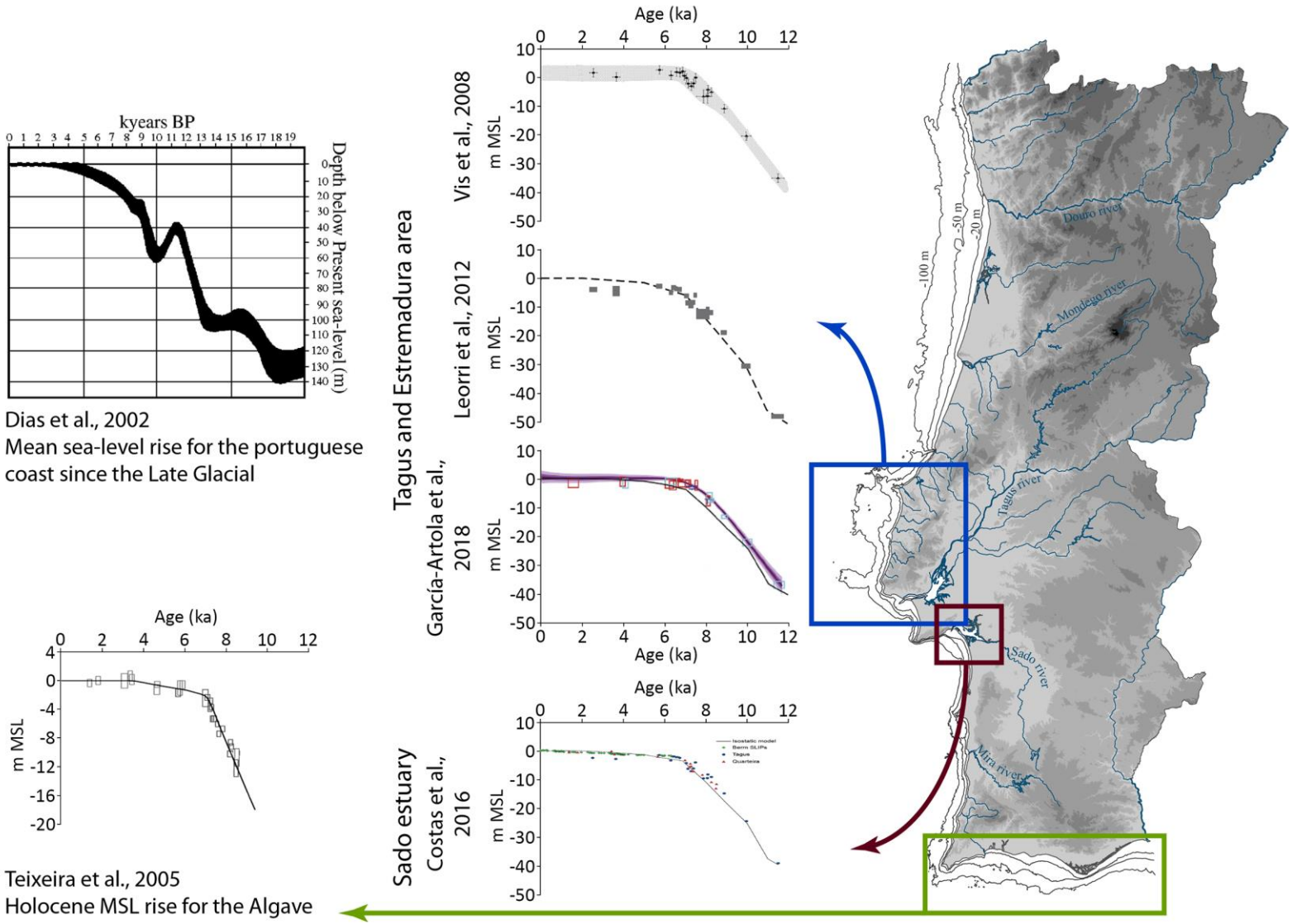

Figure 2.14 - Mean sea level (MSL) rise curves drawn for the Portuguese Atlantic margin.

3. METHODOLOGY

3. Methodology

3.1 Electrical Resistivity Tomography profiles

The electrical character of the materials differs from each other, and the electrical resistivity measures the degree to which a material resists to the electrical current flow (e.g., Smith and Sjogren, 2006; GeoSci Developers, 2015-2018; Figure 3.1 - please note that the scheme present opposite colours comparing to that of Sado ERT profiles). Electrical Resistivity Tomography (ERT) consists in introducing an electrical current into the ground with two electrodes and measuring the voltage drop across the surface with two other electrodes, a procedure that yields information about the distribution of electrical resistivity below the surface. The different behaviour of the material to electrical input allows identifying different types of materials. Such a continuous procedure along a line with several dozens of electrodes materializes an ERT profile.

One of the most important characteristics of ERT is the ability to accurately identify and distinguish sand and gravel deposits from silt and clayey sediments (Baines et al., 2002), being widely used to reconstruct the geometry of fluvial channels and river valleys infillings (e.g., Baines et al., 2002; Maillet et al., 2005; Chambers et al., 2012). In similar environmental conditions, silts and clays present low electrical resistivity while sands and gravels show high electrical resistivity (e.g., Gourry et al., 2003).

A total of eight ERT profiles were performed in the study area (Figure 3.2; Table 3.1), six on the Sado channel and two in the Carrasqueira (Arez) (Figure 3.3) and Vale dos Açudes tributaries. All ERT profiles were oriented perpendicular to the present-day channels. Three profiles were performed at Arapouco in order to test different dipole configurations, dipole-dipole and Wenner arrays, and dipole distance, that will result in different ERT resolutions (Table 3.1). The ERT profiles at this location are superimposed and only one is represented in figure 3.2.

ERT profiles can be performed using different electrodes arrays and different dipolar distances. In the studied area, two ERT profiles were performed using the Wenner array and six using the dipole-dipole array (Figure 3.4; Table 3.1). In the Wenner electrode array four dipoles are placed in line and equidistant from each other producing higher vertical resolution: the outer electrodes are current electrodes, and the inner electrodes are potential electrodes. The dipole-dipole array places the current electrode pair and the potential electrode pair in opposite positions reflecting a measurement value, the apparent resistivity value, that results from the weighted average of the resistivity values of sediment below the electrodes used for the measurement. This electrode array produces results with high vertical resolution, despite lower than Wenner configuration, but it yields the highest horizontal resolution and was applied more often in the presented work.

Resolution of ERT profiles depends on the distance between electrodes (e.g., Baines et al., 2002) and different electrode distances between profiles were used due to the extension of the surveyed area (Table 3.1). At Arapouco, an ERT profile with 2-m dipolar distance was performed in order to test the coarseness of the sediments at ca. 10 m depth (maximum depth of the ERT profile; Table 3.1), as characterized by the sediment core granulometry.

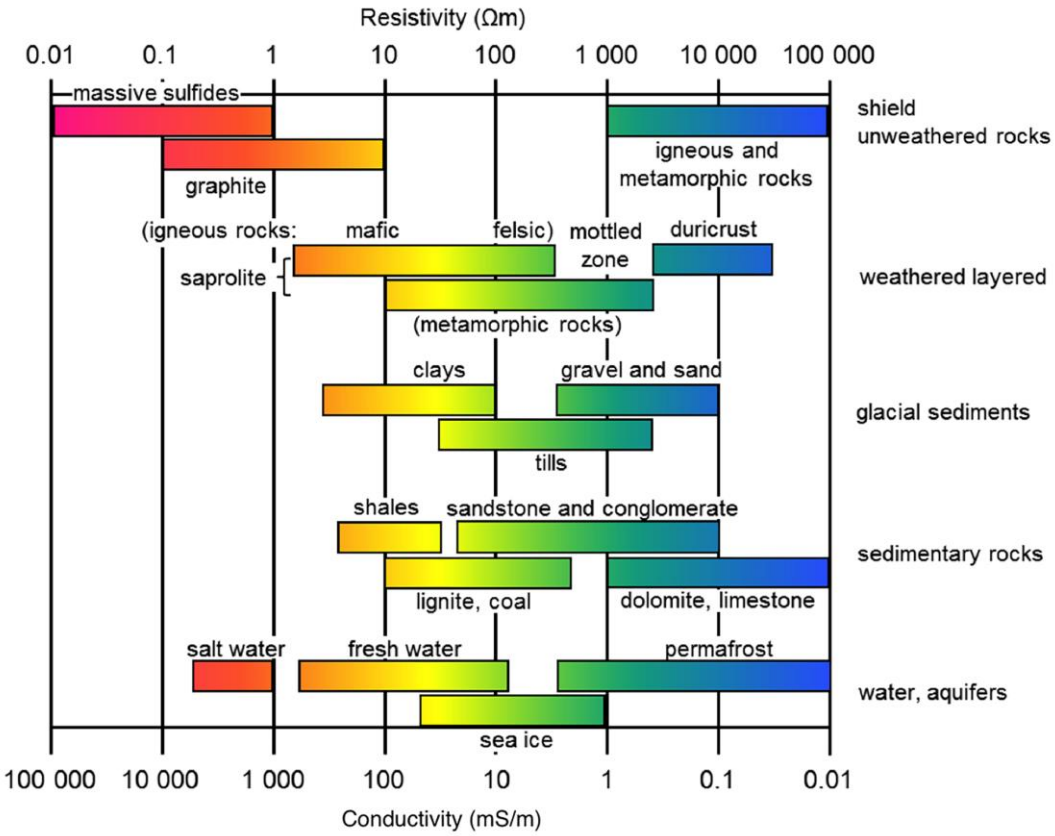

Figure 3.1 - Electric resistivity and conductivity of common rocks. CC by GeoSci Developers, 2015-2018. Please note that the scheme present opposite colours comparing to that of Sado ERT profiles.

A ABEM resistivity meter equipped with a Lund system was used to collect resistivity data. Data was processed with the Res2Dinv software. Topographic data (coordinates and altimetry), collected using a Global Navigation Satellite Systems (Topcon Geosystem with field controller FC-25) operating in real-time, was incorporated in resistivity data processing.

ERT profiles were done in collaboration with Laboratório Nacional de Engenharia Civil (LNEC) and coordinated by Rogério Mota. Data and preliminary results were reported in Mota (2013; 2017).

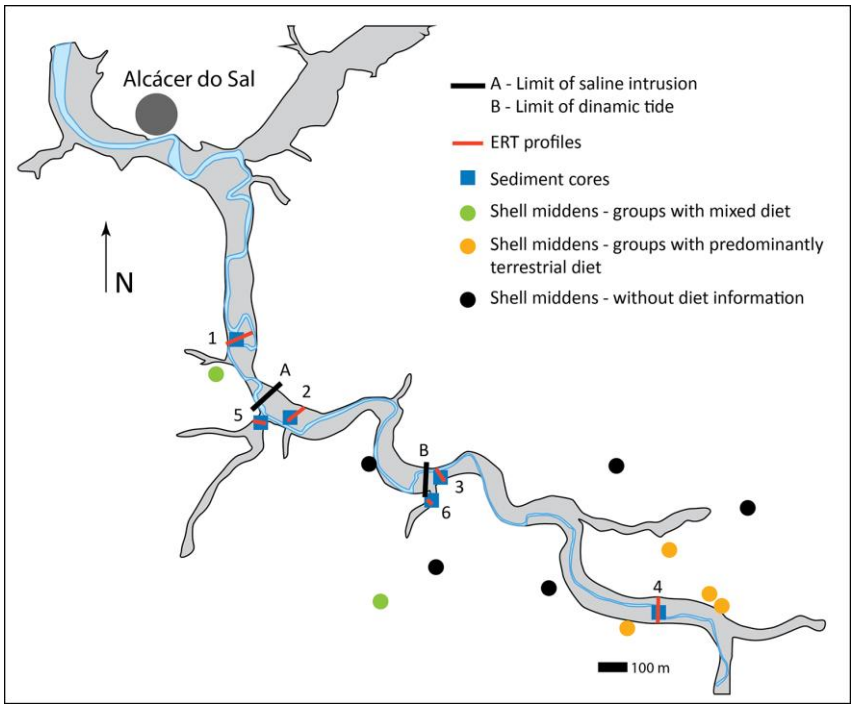

Figure 3.2 - Location of shell middens (green, yellow and black circles), ERT profiles (red line) and the sediment cores used for proxy analyses (blue squares). 1 - ERTs Arapouco D-D, Arapouco W and Arapouco 2 and Arapouco sediment core; 2 - Vale do Guizo ERT and sediment core; 3 - São Bento ERT and sediment core; 4 - Laxique ERT and sediment core; 5 - Arez ERT and sediment core; 6 - Vale dos Açudes ERT and sediment core.

Figure 3.3 - Fieldwork for measurement of electrical resistivity tomography (ERT) in the Carrasqueira (Arez) tributary. The orange cable connects all the electrodes in the ground to perform the ERT profile. October 2017.

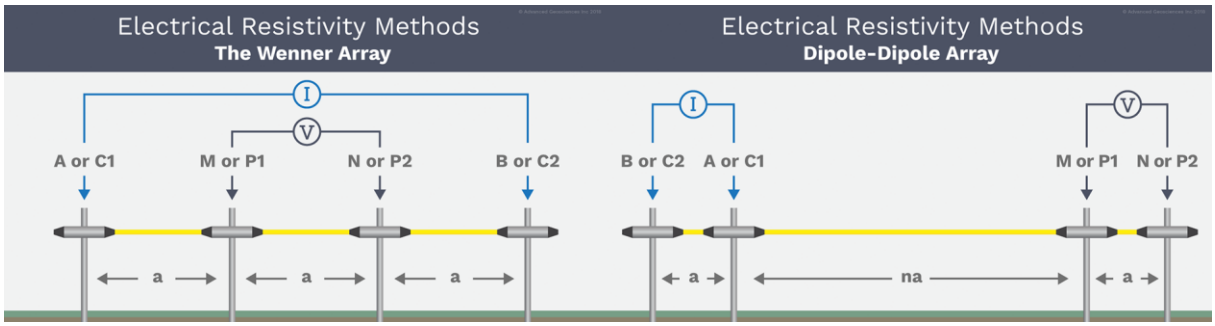

Figure 3.4 - The Wenner and dipole-dipole arrays used for the ERT profiles. Images © AGI - Advanced Geosciences Inc. (@ www.agiusa.com).

Table 3.1 - Location of the ERT profiles and their main characteristics. * - Refers to the transect number in Figure 2.1.

Location	Transect number*	Reference	Electrode configuration	Dipolar distance (m)	Maximum depth (m)	Profile extension (m)	Date
Sado channel	1	Arapouco D-D	dipole-dipole	20	102	800	October 2017
		Arapouco W	wenner	20	131	800	October 2017
		Arapouco 2	dipole-dipole	2	10.2	80	October 2017
	2	Vale do Guizo	dipole-dipole	20	102	800	May 2013
	3	São Bento	dipole-dipole	10	51	400	May 2013
	4	Laxique	dipole-dipole	10	65,6	650	May 2013
Sado tributaries	5	Arez	wenner	4	26.2	160	October 2017
	6	Vale dos Açudes	dipole-dipole	6	30	240	May 2013

3.2 Sediment cores and sampling

A total of 12 sediment cores were collected in the study area (Figure 3.2; Table 3.2): eight from the Sado channel and four from two different tributaries, all at the proximity of the ERT profiles. Cores Arapouco 1, VG1 (Vale do Guizo), Sado 3A (São Bento) collected in the Sado channel and Sado 3AC1 (Vale do Açudes) and Arez1 collected in two Sado tributaries were done as prospecting cores (Table 3.2).

In total, 5 cores were collected at Arapouco performing a transect perpendicular to the Sado channel (Figures 3.2 and 3.5), close to Arapouco archaeological site, the most downstream shell midden identified in the area. Cores were performed in the Sado alluvial plain (Figures 3.5 and 3.6), adjacent to the left margin of the channel and close to the present-day fluvial-estuarine boundary within the inner estuary.

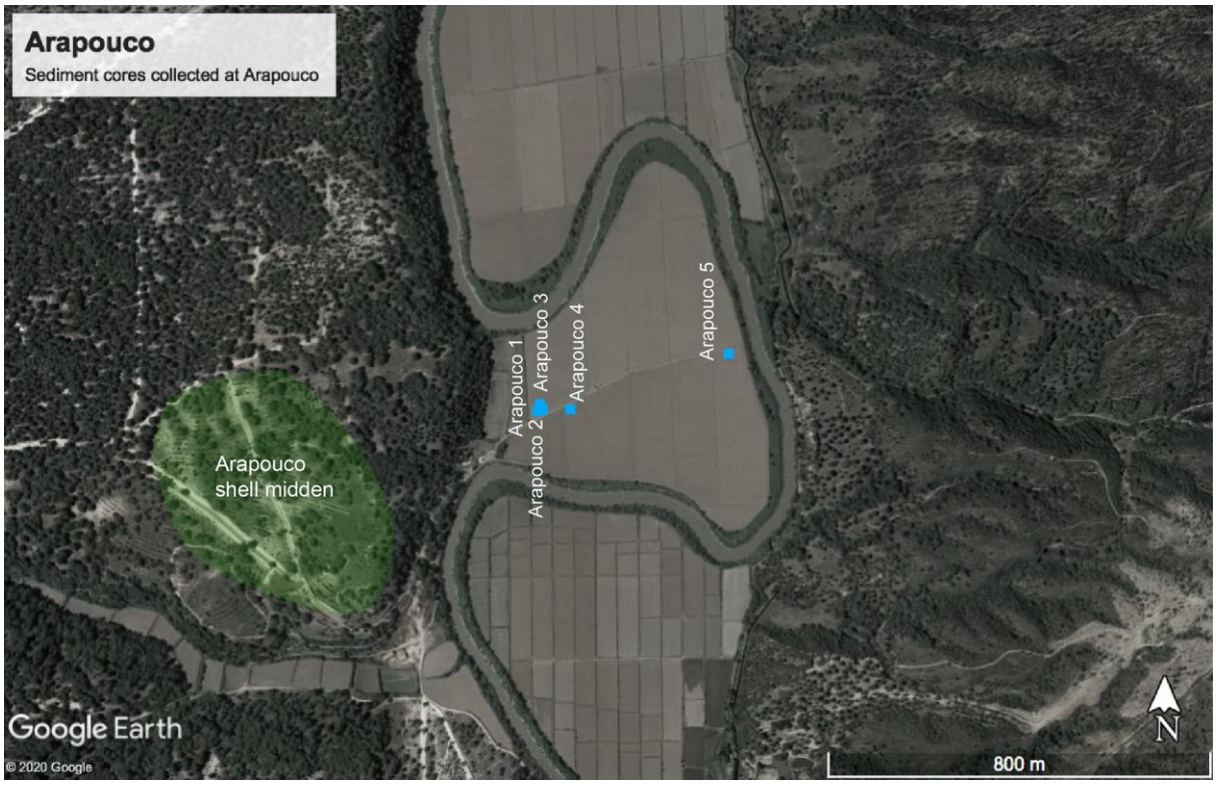

Figure 3.5 - Location of the sediment cores collected at Arapouco performing a transect perpendicular to the Sado channel and schematic location of the Arapouco shell midden. Satellite image from Google Earth Pro 7.3.4.8248, 2019, Arapouco, Sado valley (Portugal).

Sediment samples from Arapouco 1 and Arapouco 5 cores were not preserved, but macroscopic description was performed while coring in order to characterize the sediment and identify possible collection areas.

Figure 3.6 - Collection of the sediment core Arapouco 5 in the Sado alluvial plain.

Sediment from Arapouco 4 was collected and sampled between 600 and 730 cm depth to complement the information recovered from Arapouco 2/3, but analyses were not performed once it locates only few meters apart from Arapouco 2 and 3 and is macroscopically similar to both. The macroscopic description of the 3 cores was used in the interpretation of the ERT profiles.

Arapouco 2 and 3 are partially overlapping (overlap of 68 cm) sediment cores (located few meters apart) performing a total length of ca. 690 cm (Figure 3.7). The two sections were later combined to yield a composite core. At the base of the core the sediment became coarser and few materials were recovered between ca. 645 cm and 690 cm. From now on both cores are referred to as by Arapouco 2/3.

Three other sediment cores were collected in the Sado channel alluvial plain (Figure 3.2; Table 3.2): Vale do Guizo (VG1), São Bento (Sado 3A) and Laxique 1. From two of those cores, VG1 and Sado 3A (Figure 3.2), only the basal section was collected (Table 3.2). Macroscopic description was done, and bulk organic material was radiocarbon dated in selected samples from the base of the cores. For the sediment samples collected, texture and chemical organic analyses

were performed. The results were used to improve the knowledge of the studied area and helped in the ERT profiles interpretation.

Figure 3.7 - Arapouco 2/3 after field collection in November 2013.

Laxique 1 was collected on the left bank of the Sado river, near São Romão do Sado and at the confluence of Xarrama with the Sado (Figures 3.1 and 3.8). It locates at the proximity of the most upstream shell middens identified in the Sado valley: Cabeço da Amoreira, Vale de Romeiras and Cabeço do Pez (Figure 3.8).

Sado 3AC1 was collected in an upstream tributary of the Sado river, Vale dos Açudes, whose source is located at the proximity of the Poças de São Bento shell midden (Figure 3.1; Table 3.2). Following the same procedure of other prospecting cores, only the basal sediment was collected, but texture and chemical organic analyses were performed in the collected samples combined with radiocarbon dating.

Three sediment cores (Arez1, Arez2 and Arez3) were collected at the mouth of Ribeira da Carrasqueira, a tributary of the Sado that flows close to Arapouco shell midden (Figures 3.1; Table 3.2). From Arez1 only the basal section between -745 and -798 cm MSL was collected. Samples were analysed for texture and organic chemistry, and the most basal sample ^{14}C dated. Arez2 and Arez3 are replicas reaching -1030 and -1080 cm MSL, respectively. Once Arez3

reaches deeper sediments it was analysed for several proxies. Arez2 was maintained intact and preserved at ProCost laboratory at FCUL for future analysis.

Cores Arapouco 2, 3 and 5, VG1, Sado 3A and Sado 3AC1 were collected manually using *Van der Horst* and *Livingstone* core samplers (Figure 3.9).

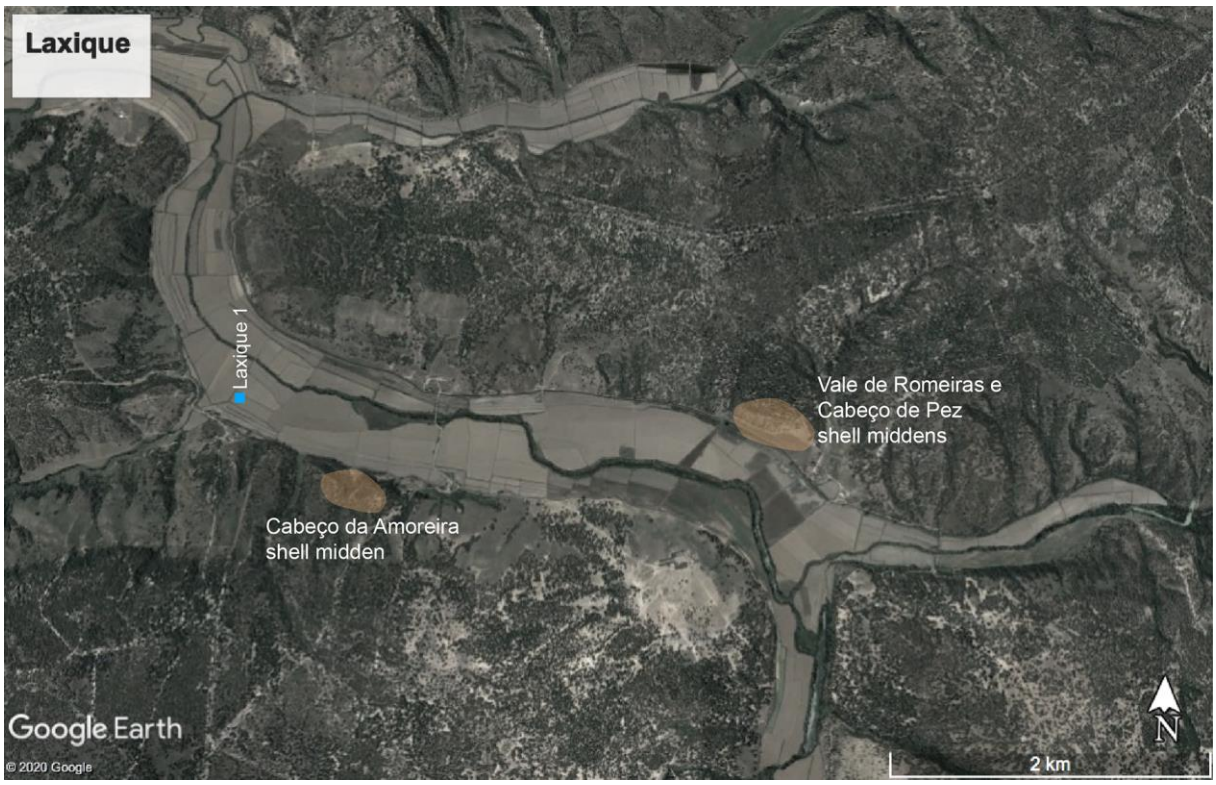

Figure 3.8 - Location of the sediment core collected at Laxique and schematic location of the Cabeço da Amoreira, Vale de Romeiras e Cabeço do Pez shell middens. Satellite image from Google Earth Pro 7.3.4.8248, 2019, Laxique, Sado valley (Portugal).

Topographic data (coordinates and altimetry) was collected using Global Navigation Satellite Systems (GNSS) roving receiver units (Leica Geosystems models GPS 900 and NetRover) that operated in real-time, connected to Portuguese internet-based correction services.

Arapouco 1 was collected with an Eijkelkamp bi-partite gouge auger (Table 3.2). Arapouco 4 and Laxique 1 were collected by Geocontrole - Geotecnia e Estruturas de Fundação, S.A. using a mechanical CASABRANCA M3D sampler (Figure 3.10).

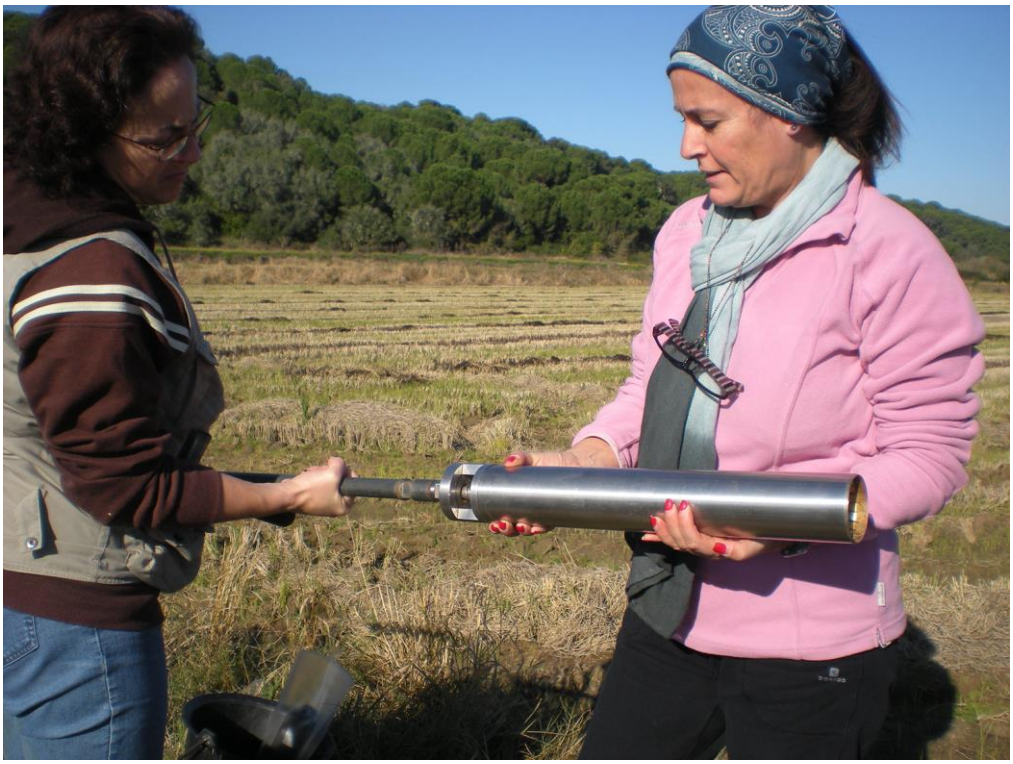

Figure 3.9 - Collection of the sediment core Arapouco 2 in the Sado alluvial plain using a *Van der Horst* core sampler. Photo © Randi Danielsen.

Figure 3.10 - Collection of the sediment core Laxique 1 in the Sado alluvial plain using a CASABRANCA M3D sampler.

Arez2 and Arez3 were collected using a Cobra TT of Atlas Copco coring device and a hydraulic lifting unit using closed PVC tubes. This work was done in collaboration with the RWTH Aachen University (Figure 3.11).

Sediment was stored at 4 °C until sub-sampling and then described and sampled every 2 centimetres. After sampling, sub-samples were freeze-dried, split and a representative quantity was grinded for posterior analyses using a: i) Retsch planetary ball-mill with agate jars; ii) or by using an agate mortar and pestle.

Figure 3.11 - Collection of the sediment core Arez2 in the Sado alluvial plain with the team from RWTH Aachen University. At the moment of photo capture 13 m depth were reached. Photo © Hannes Laermanns.

Table 3.2 – Location and altimetry of the analysed sediment cores. Coordinates are referenced to PT-TM06/ETRS89 coordinate system. Elevations given relatively to mean sea level (msl). To be continued.

Location	Core reference	Easting	Northing	Elevation of ground surface at core location (m msl)	Start collection point (m msl)	End collection point (m msl)	Collected core length (cm)	Collection equipment	Collection date
Sado Channel	**Arapouco1**	-31026.1743	-149671.94	2.2	No sediment collection			Eijkelkamp bi-partite gouge auger	November 2013
	Arapouco2	-31026.1743	-149671.94	2.2	2.20	-0.48	268	Van der Horst	November 2013
	Arapouco3	-31030.6767	-149673.241	2.2	0.20	-4.70	490	Livingstone	November 2013
	Arapouco4	-30988.830	-149676.072	2.4	2.40			CASABRANCA M3D	November 2015
	Arapouco5	-30580,3148	-149534,356	2.7	No sediment collection			Van der Horst	October 2016
	VG1	-29665,2468	-152173,473	0.7	-6.31	-9.54	328	Van der Horst and Livingstone	July 2012
	Sado 3A	-25457,145	-153829,555	4.2	-0.68	-3.01	235	Van der Horst	July 2012
	Laxique1	-21174.326	-157053.121	6.1	6.10	-2.00	810	CASABRANCA M3D	November 2015

Table 3.2 - Continuation.

Location	Core reference	Easting	Northing	Elevation of ground surface at core location (m msl)	Start collection point (m msl)	End collection point (m msl)	Collected core length (cm)	Collection equipment	Collection date
Sado tributaries	**Arez1**	-30449,923	-152111,168	2.7	-7.75	-7.98	23	Van der Horst and Livingstone	July 2012
	Arez2	-30470,6	-152175	2.9	2.90	-10.1	1300	Cobra TT of Atlas Copco; hydraulic lifting unit	March 2018
	Arez3	-30473,2	-152179	2.9	2.90	-10.6	1350	Cobra TT of Atlas Copco; hydraulic lifting unit	March 2018
	Sado3AC1	-25410,0282	-154087,357	6.3	1.13	-1.37	252	Van der Horst	July 2012

3.3 Sediment analyses

Radiocarbon dating and calibration

In order the characterise the chronological framework of the studied sediments and determine mean sedimentation rates, 24 bulk organic sediment samples and 1 *Scrobicularia plana* shell were selected from the different cores for AMS radiocarbon dating and processed at Beta Analytic Radiocarbon Dating (USA) and A.E. Lalonde AMS (Canada) laboratories following each laboratories treatment and analysis procedures. Samples pretreatment and AMS measurement procedures used at Beta Analytic laboratories are described at https://www.radiocarbon.com/beta-lab.htm (consulted in January 2021). Bulk organic sediments are submitted to the acid washes pretreatment where acid (HCl) is applied to a grind and homogenized sample repeatedly to ensure the absence of carbonates.

The AMS measurement is done on graphite produced by hydrogen reduction of the CO_2 sample over a cobalt catalyst. The CO_2 is obtained from the combustion of the sample at 800°C+ under a 100% oxygen atmosphere. The CO_2 is first dried with methanol/dry ice then collected in liquid nitrogen for the subsequent graphitization reaction. The identical reaction is performed on reference standards, internal QA samples, and backgrounds to ensure systematic chemistry.

The analytical result is obtained by measuring sample $^{14}C/^{13}C$ relative to the $^{14}C/^{13}C$ in Oxalic Acid II (NIST-4990C) in a particle accelerator using SNICS ion source. Quality assurance samples are measured along with the unknowns and reported separately.

The AMS result is corrected for total fractionation using machine graphite $\delta^{13}C$. For solid organics, the $\delta^{13}C$ reported is obtained by converting a sub-sample to CO_2 with an elemental analyser (EA) connected directly to an isotope-ratio mass spectrometer (IRMS). The IRMS performs the separation and measurement of the CO_2 masses (44, 45, and 46) and calculation of the sample $\delta^{13}C$.

For bulk organic samples ^{14}C dating results reflect the total organic content of the analysed material (https://www.radiocarbon.com/beta-lab.htm, consulted in January 2021).

At A.E. Lalonde laboratories sample preparation and processing are described in Crann et al. (2017). Samples were treated using the standard acid-alkali-acid (AAA) pre-treatment following protocol outlined in Brock et al. (2010). Using the mentioned protocol, carbonates are removed during the first acid wash using HCl (1N) at 80°C for 30 min, then humics are removed by rinsing the sample in an alkali solution (NaOH, 0.2N, 80°C, 30 min) and finally a second acid wash (HCl, 1N, 80°C, 30 min) is done to remove any CO_2 absorbed during the alkali step (Crann

et al., 2017). Each step is followed by three rinses in Milli-Q water. Clean samples are freeze-dried overnight.

After sample preparation, ^{14}C analyses are performed on a 3MV tandem accelerator mass spectrometer built by High Voltage Engineering (HVE). $^{12,13,14}C^{+3}$ ions are measured at 2.5MV terminal voltage with Ar stripping. The F14C is calculated according to Reimer et al. (2004) as the ratio of the sample $^{14}C/^{12}C$ ratio to the standard $^{14}C/^{12}C$ ratio (Ox-II) measured in the same data block. Both $^{14}C/^{12}C$ ratios are background-corrected and the result is corrected for spectrometer and preparation fractionation using the AMS-measured $^{13}C/^{12}C$ ratio and is normalized to $\delta^{13}C$ (PDB). ^{14}C ages are calculated as $-8033\ln(F^{14}C)$ and reported in ^{14}C yr BP (BP=AD1950) as described by Stuiver and Polach (1977). The errors on ^{14}C ages (1σ) are based on counting statistics and $^{14}C/^{12}C$ and $^{13}C/^{12}C$ variation between data blocks. As $^{12,13,14}C$ isotopes are measured online and corrections done during the procedure, $\delta^{13}C$ measurements are not reported.

Radiocarbon ages were calibrated using Oxcal 4.4 (© Bronk Ramsey) and the IntCal20 (Reimer et al., 2020) and Marine13 (Reimer et al., 2013) calibration curves. Post-bomb dates were calibrated using the NH zone 2 curve (Hua et al., 2013), CLAM 2.3.2 software and the IntCal20 calibration curve (Reimer et al., 2020). Sedimentation rates were determined using the CLAM 2.3.2 software (Blaauw, 2010), also using the IntCal20 (Reimer et al., 2020) (for sedimentation rate purposes, marine dated samples were excluded. See Results chapter). Calibrated dates are presented in cal BP and cal BC/AD to better relate data with both environmental and archaeological information. Best-fit ages determined based on sedimentation rate curves were used as chronological indicators.

Magnetic susceptibility

Magnetic Susceptibility (MS) is a dimensionless measure that reflects the degree to which a material can be magnetized when applying an external magnetic field (Blum, 1997). MS is frequently used as a relative indicator for changes in sediment composition related to changes in palaeoclimatic controlled depositional processes (Blum, 1997) or changes in the sediment source (e.g., Rowntree et al., 2017). In addition, the high precision and sensitivity of magnetic susceptibility equipment's make this analysis extremely useful for core-to-core and in-depth core correlation (Blum, 1997).

Volume MS was measured in SI units directly over the core using a Bartington® MS2 instrument equipped with:

i) a MS2C Core Logging Sensor with a 100 mm diameter ring in cores Arapouco 2/3 and Laxique where measurements were done at every 2 cm. Measured values were corrected for drift and diameter following the method from Bartington's operation manual OM1131;
ii) a MS2E Surface Scanner Sensor in Arez where measurements were performed at each 1 cm. Measured values were corrected for drift using the Bartington´s equipment drift correction.
Measurements using the MS2C Core Logging Sensor took place at the Marine Geology Department from Instituto Hidrográfico (Portugal) and MS measurements done using the MS2E Surface Scanner Sensor were performed both at the Marine Geology Department from Instituto Hidrográfico and at the Geology Department from Faculdade de Ciências, Lisbon University (FCUL).

Grain-size and morphoscopic and compositional analysis of coarse fraction

In order to characterise the sedimentological *facies* of the Sado alluvial sediments in the studies area, texture analyses were performed.
In Arapouco 2/3 total sediment grain-size distribution was measured in essentially muddy sediment by laser diffraction using a Malvern Mastersizer 2000 equipment. Samples were previously washed with tap water and passed through a 1 mm-mesh sieve. The fraction >1 mm was determined, and total grain-size distribution recalculated. Coarse sediment samples were washed through a 63 μm-mesh sieve and the <63 μm fraction was measured by laser diffraction. The fraction >63 μm was weighted and total grain-size distribution recalculated. Sediment was classified according to Flemming (2000). The coarse fraction was described using a Leica MZ12 binocular stereomicroscope to characterize composition and morphoscopic characteristics. Coarse fraction description was done by Maria da Conceição Freitas.
In Laxique and Arez sediment cores, texture was characterized by analysing the contents of coarse (CF; >63 μm) and fine fractions (FF; <63 μm) by wet sieving using a standard 63 μm mesh. In samples where the CF was dominant, the coarse samples were additionally sieved in a normalized series of ASTM screens between -2 ϕ and 4 ϕ with an interval of 0.5 ϕ. In these cases, samples were characterized following Folk (1954) using the software GRADISTAT (Blott, 2000). Analyses were performed at the Geology Department from FCUL.
In addition, Micro Fourier-transformed infrared spectroscopy (μ-FTIR) comprised of a Bruker Hyperion 3000 IR microscope with a mercury-cadmium-telluride detector (MCT) for MIR measurements, controlled by OPUS 7.2 software © Bruker Optik GmbH 2012 was carried out at Hércules Laboratory on a plastic fragment found at ca. 25 cm core depth in order to identify the material. Transmission measurements were performed using a 15x magnification objective and a

micro compression diamond cell EX'Press 1.6 mm, STJ-0169. Spectre was recorded with 4 cm^{-1} resolution using 64 co-added scans.

Organic matter and organic C and N chemistry

Sediments are characterised by its contents in inorganic and organic materials. The organic materials are frequently used as palaeoenvironmental and relative mean sea level proxies (e.g., Wilson et al., 2005b; Lamb et al., 2006; Castro et al., 2010; Zhan et al., 2011; Khan et al., 2015). In the sediment samples from the cores collected in the studied area, total organic matter (OM) content was determined following Kristensen (1990) adapted method *Loss on ignition* (LOI): samples were heated in a muffle furnace at 520ºC for 6h and OM determined by weight difference.

To infer the organic materials source, several sediment samples from all the collected cores were used to determine the total organic carbon (%C_{org}), total nitrogen (%N), $\delta^{13}C_{VPDB}$ and $\delta^{15}N_{AIR}$. The analyses were performed in grounded sub-samples after removing inorganic carbon using HCl 10% and processed at: i) Servizos de Apoio a Investigación, University of A Coruña (UDC), Spain; and ii) the Stable Isotopes and Instrumental Analysis Facility from FCUL. Samples were homogenized and weighed in tin capsules. $\delta^{13}C$ and $\delta^{15}N$ of capsulated samples were analysed by continuous flow isotope mass spectrometry (CF-IRMS) (Preston and Owens, 1983) with a FlashEA1112 combustion elemental analyser (ThermoFinnigan) coupled on−line with a Delta Plus Finnigan MAT Isotope Ratio Mass Spectrometer (UDC) and a Sercon Hydra 20-22 (Sercon, UK) stable isotope ratio mass spectrometer, coupled to a EuroEA (EuroVector, Italy) elemental analyser for online sample preparation by Dumas-combustion (UL). Delta calculation was performed according to $\delta = [(R_{sample}–R_{standard})/R_{standard}]x1000$, where R is the ratio between the heavier isotope and the lighter one. $\delta\ ^{15}N_{Air}$ values are referred to air and $\delta^{13}C_{VPDB}$ values are referred to PDB (Pee Dee Belemnite). Quality assurance in UDC is made by the measure of duplicates samples.

At UL the reference materials USGS-25, USGS-35, BCR-657 and IAEA-CH7 (Coleman and Meier-Augenstein, 2014) were used for quality assurance. The laboratory standard used was Protein Standard OAS/Isotope (Elemental Microanalysis, UK). Uncertainty of the isotope ratio analysis, calculated using values from 6 to 9 replicates of laboratory standard, interspersed among samples in every batch of analysis, was ≤0.1‰. The major mass signals of N and C were used to calculate total N and C abundances, using Protein Standard OAS (Elemental Microanalysis, UK, with 13.32% N, 46.5% C) as elemental composition reference material.

In addition, to differentiate the proportion of particulate organic materials derived from marine and freshwater algae and from terrestrial vascular plants in the sediment samples from Laxique 1, the formula (a) was applied, following Alonso-Hernandez et al. (2017):

(a) $\left(C_{org} / N\right)_S = P_A * \left(C_{org}/N\right)_A + (1 - P_A) * \left(C_{org} / N\right)_{TP}$

where $\left(C_{org} / N\right)_S$, $\left(C_{org}/N\right)_A$ and $\left(C_{org} / N\right)_{TP}$ correspond to the C_{org}/N ratios of total bulk sediment, algae and terrestrial plants, respectively, being the values of $\left(C_{org}/N\right)_A$ = 6 and $\left(C_{org} / N\right)_{TP}$ = 32, according to e.g., Meyers (1994) and Lamb et al. (2006).

In order to distinguish organic carbon from freshwater and marine sources the equation (b) was applied (Schultz e Calder, 1976):

(b) $\partial^{13}C = X_T * \partial^{13}C_T + X_M * \partial^{13}C_M$

where $\delta^{13}C$, $\delta^{13}C_T$ and $\delta^{13}C_M$ correspond to the $\delta^{13}C$ values of the sediment, marine phytoplankton and freshwater phytoplankton, respectively. Values of -21‰ ($\delta^{13}C_T$) and -27‰ ($\delta^{13}C_M$) according to published references (e.g., Meyers, 1994; Lamb et al., 2006). X_T and X_M are the relative percentages of freshwater and marine phytoplankton and $X_T + X_M = 1$.

The equation was only applied in Laxique, once $\delta^{13}C$ values for this sediment core are >25‰, pointing essentially to terrestrial sources (see Results section).

Molecular characterization of lipid fraction

The alkane composition of the sediment organic matter was analysed by analytical pyrolysis technique (Py-GC/MS) applied directly to bulk sediment samples grinded to fine powder (<0.01 mm). The samples (15-20 mg) were pyrolyzed using single shot at 500 °C for 1 min. In the case of interface, a temperature of 280ºC was used. The analytical instrument consisted of a micro-furnace type double-shot pyrolizer (Frontier Lab PY-3030D) coupled to a gas chromatograph (Shimadzu GC2010) fitted with a low polar-fused silica capillary column (Phenomenex Zebron-ZB-5HT Inferno, 30 m length, 0.25 mm internal diameter, 0.50 μm film thickness). The splitless injector operated at a temperature of 250°C. The GC oven temperature was set at 50°C for 1 min, then increased to 100°C at a rate of 30°C min^{-1}, from 100 to 300°C at a rate of 10°C min^{-1}, and finally isothermal at 300°C for 10 min. The total analysis time was of 32 min. Helium was used as carrier gas at a flow rate of 1 cm^3 min^{-1}.

The mass spectra were acquired using a quadrupole mass spectrometer (Shimadzu GCMS-QP2010) working at negative electronic ionisation mode. In the mass spectrometer, the acquisition of data ranged between 45 and 700 m/z. The ion 85 trace was used to identify and quantify the homologous series of alkanes by comparison with the Libraries NIST and Wiley. The peak areas (total ion 85 area counts) in the chromatogram were integrated and expressed as percentage (%) of total abundances. Analytical pyrolysis analyses were done in samples from the transitions between the defined sedimentary units within the core to help better identify the transition.

Different sources of natural organic matter are frequently distinguished by changes in specific n-alkane ratios (e.g., Li et al., 2020). In the present study the Carbon preference index (CPI), P_{aq}, Terrigenous/aquatic ratio (TAR), Terrestrial-marine discriminate index (TMD), Pr/Ph, Pr/C_{17} and Ph/C_{18} ratios were applied (Table 3.3).

A discriminant analysis was carried out to check how the distribution of the *n*-alkanes could be reflecting information about the different sedimentary units. For the analysis, the abundance of the alkanes detected by analytical pyrolysis was normalized by equalling the sum of the peak of areas of the alkanes to 100 in Microsoft Excel. In this treatment, the relative abundances of the different alkanes were used as descriptors (independent variables). On the other hand, the dependent variables (sedimentary units) consisted of the different layers selected according to the previous textural and chemical analysis. The software Statgraphics Centurion XVI.II was used for this analysis.

Nicasio T. Jiménez-Morillo, Marco A. Jiménez-González and Cristina Barroca Dias were responsible for the n-alkanes analyses. Analyses were performed at HERCULES laboratory, Évora.

Table 3.3 - *n*-Alkane ratios used in this work as proxies to distinguish the different sources of natural organic matter. To be continued.

Name	*n*-alkane ratios	description	diagnostic values	references
Carbon preference index (CPI)	$CPI^{*} = \frac{\sum_{odd} C_n}{\sum_{even} C_n}$	estimates the relative abundance of odd to even C chain numbers and allows discerning different sources of organic matter	<1: bacterial, algal and degraded OM input to the soil/sediments ~1: petrogenic or marine 5-10: terrestrial	Bray and Evans, 1961
P_{aq}	$P_{aq} = \frac{(C_{23} + C_{25})}{(C_{23} + C_{25} + C_{29} + C_{31})}$	distinguishes terrestrial and aquatic plants with mid-length *n*-alkane chains in terrestrial lacustrine environments or coastal environments with freshwater inputs	0.01-0.25: terrestrial plants 0.4-0.6: emergent aquatic plants (including mangroves) >0.6: submerged aquatic plants (including marine macrophytes)	Ficken et al., 2000 Sikes et al., 2009
Terrigenous/aquatic ratio (TAR)	$TAR = \frac{(C_{27} + C_{29} + C_{31})}{(C_{15} + C_{17} + C_{19})}$	distinguishes the relative contributions between land plants (represented by C_{27}, C_{29} and C_{31} *n*-alkanes) and algal inputs (represented by C_{15}, C_{17} and C_{19} *n*-alkanes)	>4: terrigenous <1: aquatic	Silliman et al., 1996; Meyers, 2003
Terrestrial-marine discriminate index (TMD)	$TMD = \frac{(C_{25} + C_{27} + C_{29} + C_{31} + C_{33}^{*})}{(C_{15} + C_{17} + C_{19} + C_{21} + C_{23})}$	distinguishes organic matter from terrestrial (represented by C_{25}, C_{27}, C_{29}, C_{31} and C_{33} n-alkanes) and marine (represented by C_{15}, C_{17}, C_{19}, C_{21} and C_{23}) sources * not measured in the analysed samples	>1: dominant terrestrial input 1: equal inputs from terrestrial and marine sources 0.5: dominant marine contribution 0.5-1: mixed contribution between marine and terrestrial sources	Elfadly et al., 2017

Table 3.3 - Continuation.

Name	*n*-alkane ratios	description	diagnostic values	references
		estimates the origin of the organic matter and its maturity	<1: anoxic environments 1: alternated oxic and anoxic conditions >1: oxic conditions	Hughes et al., 1995
Pristane/Phitane (Pr/Ph)	Pr/Ph		0.8-2.5: most organic-rich marine sediments <1-3: marine oils and sediments >3: input from terrestrial organic matter 5-10: higher plants	Powell, 1988 Mita and Shimoyama, 1999
Pristane/n-alkane C_{17} and Phitane/n-alkane C_{18}	Pr/C_{17}; Ph/C_{18}	often used to indicate the extent of biodegradation of n-alkanes; significant depletion of n-alkanes leads to an increase in these two ratios	higher values point to higher organic matter degradation	e.g., Wang et al., 2008

* $\sum_{odd} C_n$ and $\sum_{even} C_n$ correspond to the total carbon numbers of odd-carbon-chain and even-carbon-chain alkanes in the sediment samples, respectively.

Nutrients as palaeoecological indicators

Nutrient contents in shallow coastal areas rely on allochthonous fluvial loads and on autochthonous nutrient cycling (e.g., Slomp, 2011; Scanes et al., 2017). Nutrient cycling is highly dependent on diverse physical forcing factors such as temperature, salinity, light, tidal currents, biological activity, among others (e.g., Henriksen and Kemp, 1988; Herbert, 1999; Scanes et al., 2017) and thus its influence on the palaeoecological record is difficult to access and should be taken with care (e.g., Scanes et al., 2017). Estuarine water nutrients, particularly nitrogen (N) and phosphorus (P), are limiting factors for biological productivity. Its contents are mostly dependent on inputs from the catchment area and its availability sustained by internal nutrient recycling where nutrient remineralisation in the sediment-water interface plays a major role (e.g., Henriksen and Kemp, 1988; Scanes et al., 2017). Nutrients and nutrient cycling are also affected by anthropic landscape manipulation (e.g., Slomp, 2011), so nutrient variations with depth can improve our knowledge on the anthropogenic influence in riverine/estuarine systems (e.g., Scanes et al., 2017)

In the present work, sulphate was used as a proxy for the influence of marine water since it is a conservative element in sea and estuarine water and its concentration varies depending on salinity (e.g., Marino and Howarth, 2009).

Nitrate, total sulphate, phosphate and total phosphorus are nutrients that, depending on their concentration, can lead to the eutrophication of water bodies. At Laxique 1, their concentration was determined. Analyses were performed at the AmbiTerra laboratory from the University of Évora, under the responsibility of Rita Fonseca.

Nitrate (NO_3^-; mg kg^{-1}) content was carried out in 2 g of sample to which 10 ml of extracting solution (20 ml ISA solution $(NH_4)_2SO_4$ 2M) was added. Samples were stirred on an orbital shaker for 1 hour and the NO_3^- content in the supernatant was measured using a Consort multi-parameter analyser (model C863) with a nitrate selective electrode (model ISE 31B), pre-calibrated with standard solutions. The method followed the Phoenix Electrode Company Instructions adapted for this specific electrode.

Total Sulphate (SO_4^{-2}; mg kg^{-1}) determination followed the method described by Singh et al. (2011): sulphate was extracted by stirring 5 g of bulk sample for 30 min, with an acidified ammonium acetate solution, with the subsequent conversion to a $BaSO_4$ suspension. 10 ml of this suspension was filtered into a 50 ml volumetric flask, 1 ml of the acidic "seed" solution + 0.25 g of barium chloride were added and stirred again to dissolve barium chloride crystals. The resulting turbidity was analysed by molecular absorption spectrophotometry at 420 nm on a Thermo Scientific (Evolution 201) spectrophotometer, using a K_2SO_4 solution as a standard.

Total Content of Phosphorus (P; mg kg^{-1}) was calculated adding 0.25 g of grounded and dried sample to a porcelain crucible to which 0.75 g of Spectroflux 100B (tetraborate and lithium metaborate) was added. After homogenization, the mixture was transferred to a graphite crucible heated at 1000 °C for 30 min in a muffle in order to melt the sample. The molten material was transferred to plastic cups with 4 ml of 65% HNO_3 and 40 ml of ultra-pure water and stirred until being completely dissolved. After dissolution, the sample was filtered into a 100 ml volumetric flask with ultra-pure water and finally transferred to an analysis tube. The phosphorus was analysed by optical emission spectroscopy with inductive plasma source (ICP-OES, Perkin-Elmer OPTIMA 8300), operated under the following conditions: plasma gas flow - 10 L/min; auxiliary gas flow - 0.2 L/min; nebulizer gas flow - 0.70 L/min; sample flow - 1.50 mL/min; RF Power - 1450 watts; viewing modes - radial and axial; reading time - 2-5 min; read delay - 80 sec; normal resolution; internal standard – yttrium. For quality control, this analytical procedure was tested with analytical replicates, two blanks prepared using the same analytical methods and Certified Reference Materials (CRMs) with an accuracy of R <5%: NIM-L (MINTEK, South Africa), JR-3 and JA-2 (GSJ, Japan), GSR-1 and GSR-5 (IGGE IRMA, China). Multi-element Quality Control (QC) solution accounted for less than 2% and CRMs were run every 10 samples.
Total phosphates (PO_4^{3-}) were determined on ignited samples in a furnace at 550°C for 2 hours, followed by acid extraction with 1 N H_2SO_4 (50 mL g^{-1} of sample) supplemented by shaking of the samples on an orbital shaker for 16 h and centrifugation (Pansu and Gautheyrou, 2006). Phosphate was determinate by UV visible spectrophotometry on a Thermo Scientific (Evolution 201) spectrophotometer, following the ascorbic acid – ammonium molybdate method (Murphy and Riley, 1962). The accuracy and analytical precision of all the analysis have been checked by the analyses of duplicate samples in each analytical set.
Nutrient analyses were done at Laboratório de Biogeoquímica Ambiental, from Évora University by Rita Fonseca.

Diatom identification

Diatoms are extremely sensitive to salinity, sediment availability and hydrodynamic conditions, factors that control the evolution of coastal water bodies (e.g., Cooper, 1999; Denys and De Wolf, 1999) providing evidence of process-response thresholds controlled by local factors. Several sediment samples were analysed for diatom identification, analyses that were performed by Manel Leira from IDL and La Coruña University.
At Arapouco 2/3, for diatom analyses, sediment samples (0.01 g dry weight) were processed according to standard techniques (Renberg, 1990). Cleaned subsamples were dried onto

coverslips and mounted onto microscope slides with Naphrax (RI = 1.74). Identification was performed with a magnification of 1000 x using a Nikon Eclipse 600 microscope with Nomarski differential interference contrast optics. A minimum of 300 valves was counted per sample. Interpretation was based on the diatom species (with relative abundances equal to or higher than 5% in at least one sample), environmental preferences (salt, brackish or fresh water), habitat and lifeform (benthic, thycoplanktonic or planktonic), following Vos and De Wolf (1993).

For diatom identification in the VG1, SADO3A (Sado channel), Arez1 and SADO3AC1 (Sado tributaries), smear slides were prepared by placing 15 - 20 mg of sediment in distilled water, stirring, and letting it settle for approximately 10 s. A pipette was placed just above the bottom of the vial and the suspension removed. Naphrax in toluene (refractive index: 1.73) was used as a mounting medium. A light microscope at magnifications of 1000x was used to identify randomly encountered diatom valves in at least three transects across the slide. Partial valves were counted according to the method of Schrader and Gersonde (1978). Diatoms were identified following the published taxonomic descriptions of Witkowski et al. (2000) and Álvarez-Blanco and Blanco (2014). Diatom-based reconstruction of sedimentary environments was based on Vos and De Wolf (1993) methodology. Salinity trends were constructed specifically to capture potential palaeoenvironmental information from sediments from using autoecological information by summarizing the relative frequencies of occurrence in all *salinity* classes described in Vos and De Wolf (1993).

Palynological analyses

Eight sub-samples concentrated at the base of the Laxique sedimentary sequence (collected at -1027, -957, -927, -837 and -817 cm MSL from Unit 1, -597 and -417 cm MSL from Sub-unit 2A and -135.5 cm MSL from Sub-unit 2B) were analysed for its palynological content in order to characterize Late Mesolithic landscape. All samples were chemically treated with HCl (10%) to remove carbonates, KOH (10%) to remove humic acids, and Sodium Polytungstate (SPT: $3Na_2WO_4 \cdot 9WO_3 \cdot H_2O$) at 2.0-2.1 $cm^3\ g^{-1}$ for densimetric separation. The final residue obtained after the treatment was mounted on slides with the use of glycerol mixed with phenol. Palynomorphs were counted using an optical microscope at 400x and 1000x to a minimum pollen sum of 300 terrestrial pollen grains. Fossil pollen grains, spores, and non-pollen palynomorphs were identified using published keys (van Geel, 1978, 1986, 1992, 2006; van Geel et al., 1981, 1989, 2003; Pals et al., 1980; Jarzen and Elsik, 1986; Moore et al., 1991; Reille, 1992, 1995; Scott, 1992; López-Sáez et al., 2000; Miola, 2012). Microcharcoal particles ≥ 120 μm and

<120 μm were counted alongside the identification of pollen grains and interpreted as indicators of local and regional fires, respectively (Whitlock and Larsen, 2001). Pollen and microcharcoal concentrations (grains gr^{-1} and particles gr^{-1} of dry sediment, respectively) were estimated by adding two *Lycopodium clavatum* tablet to each sample (Stockmarr, 1971). Palynological diagrams were plotted against age using TiliaIT software (version 2.1.1, Illinois State Museum, Research and Collection Center, Springfield USA). Pollen percentages for terrestrial taxa were calculated against the main sum of terrestrial grains, while percentages for aquatics and spores were calculated against the total sum of all pollen and spores.

Cristina Val-Péon from the Institute of Neotectonics and Natural Hazards, RWTH Aachen University performed palynological analyses, under the responsability of Klaus Reicherter.

Foraminifera, calcareous nannoplankton and calcium carbonate content

Benthic foraminifera are an important proxy to build palaeoenvironmental reconstructions and may function as sea level indicators (e.g., Fatela et al., 2009a, 2009b). In order to analyse the foraminiferal content and determine the foraminiferal assemblages in sediment and assess the maximum extension of marine influence in the Sado palaeovalley sediment sub-samples from the prospecting cores were washed through a 63 μm sieve to collect foraminifera with help of a binocular microscope. Foraminifera analyses were performed by Francisco Fatela.

Mainly produced by marine Coccolithophore algae, calcareous nannoplankton is a proxy of marine influence inside estuaries. Rippled smear slides for calcareous nannoplankton were prepared for some samples and permanently mounted with optical cement (Entellan) following the procedure described in Johnson et al. (2012). Slides were observed using the optical petrographic microscope Ortholux II-Pol under 1250 magnification. The work was performed by Mário Cachão.

In addition, calcium carbonate ($CaCO_3$ contents in sediment were determined using an Eijkelkamp calcimeter that measures the CO_2 produced by the reaction of calcium carbonate in the sample with HCl 4 mol in a known sample mass. Nevertheless, carbonated forms and calcium carbonate contents are almost absent in all the studied sediments cores (except for Arez3 where foraminifera were identified) and do not provide results to be discussed in the present work.

4. RESULTS

4. Results

4.1 Electrical Resistivity Tomography

At Arapouco 3 ERT profiles were done with different measurement characteristics (Table 3.1). Arapouco D-D and Arapouco W were performed using different electrode configurations, dipole-dipole (D-D) and wenner dipole (W) configuration, respectively (Figure 4.1). The dipole-dipole configuration is more apt to delimitate vertical and sub-vertical changes in electric resistivity, and usually helps to define a better transition in geological formations with different characteristics (Mota, 2017). However, the ERT profile Arapouco D-D presented an error superior to the expected during measurement (Figure 4.1; error RMS = 37.1%) and by this reason an ERT profile using the wenner configuration was also implemented (Figure 4.1; error RMS = 6.4%). Results are similar concerning resistivity values (Figure 4.1), but the Arapouco W ERT profile presents a smaller area in what respect to resistivity low values (Figure 4.1A) than Arapouco D-D ERT profile, where low resistivity values reach ca. 60 m depth (Figure 4.1). The wenner dipole configuration tends to smooth resistivity values in the interface between formations with different resistivity values, and by that the area presenting lower resistivity values is smaller (Mota, 2017). Considering the pros and cons of the different dipole configurations, a mean value of ca. 40 m was considered for the depth of the area until where low resistivity values occur.

Concerning resistivity, lower values (<10 ohm.m; dark blue colours) occur at the top of the profiles and higher resistivity was measured at the base of the profiles (>10 ohm.m and <400 ohm.m, represented from green to red colours) until ca. 40 m, considering the mean depth values found for the interface between both ERT profiles (Figure 4.1). Low values of resistivity were interpreted as the Holocene infilling (composed by fine sediments, such as mud and fine sand) and higher values (>100 ohm.m) as the older Caenozoic sediments from *Vale do Guizo* and *Alcácer do Sal* formations (Figure 2.11; see geological description of the sediments where the Sado is embedded in section 2) where the Sado valley in embedded.

For Arapouco, a third ERT profile with 2 m dipole distance (Table 3.1) was performed in order to identify small differences in the resistivity of the infilling in depth (Figure 4.2). The sediment infilling until ca. 10 m presented low resistivity values (<5 ohm.m), but slightly increases at ca. 8 m depth to values >5 ohm.m, probably in response to a slighter coarse texture. As the Arapouco 2 ERT profile has a better resolution in depth due to the small distance between dipoles, slightly changes in the resistivity of the materials were registered while the same do not occur in the

lengthy profiles that have lower resolution in depth due to higher dipole distances. It is important to keep this fact in mind while interpreting the ERT results.

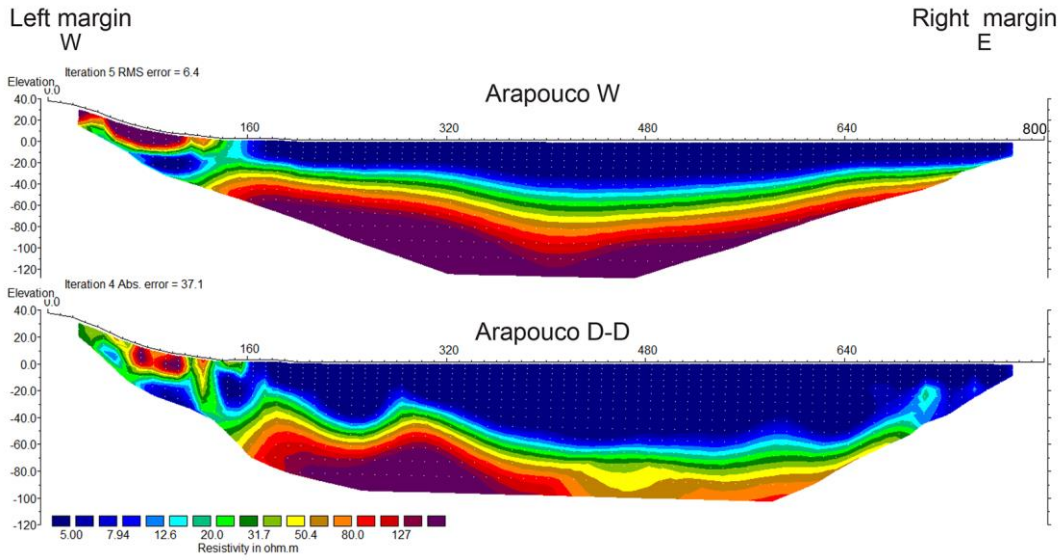

Figure 4.1 - Arapouco W (above) and Arapouco D-D (below) ERT profiles presenting resistivity values changes in depth.

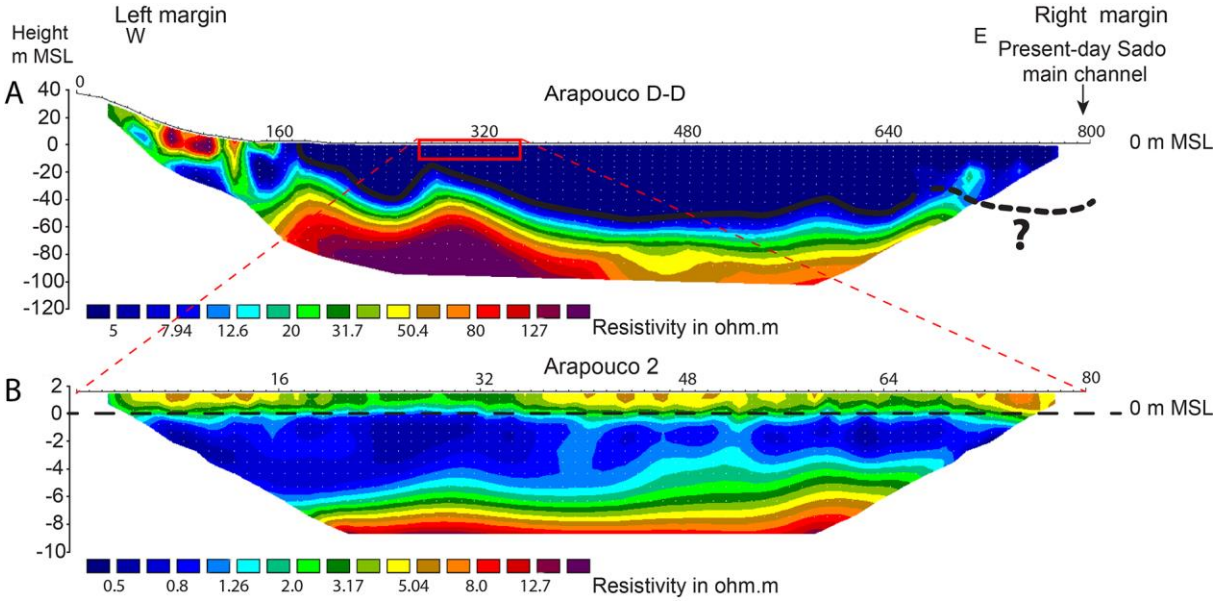

Figure 4.2 - Arapouco D-D and Arapouco 2 ERT profiles presenting resistivity values changing with depth. Please note the different scales for the different profiles (Arapouco D-D >127 ohm.m; Arapouco 2 >12.7 ohm.m).

For the comparison of Arapouco with the other ERT profiles, the Arapouco D-D ERT was used once all the other profiles were performed using the dipole-dipole configuration, except for Arez that was done using the wenner configuration (Table 3.1).

Considering the 5 ERT profiles performed in the downstream section of the studied area, between Arapouco and São Bento, resistivity values both for the Sado channel (Arapouco D-D, Vale do Guizo and São Bento) and tributaries (Arez and Vale dos Açudes), were always lower than 400 ohm.m, with many values as low as 5 ohm.m on the top layers (Figure 4.3). Results are consistent with the other Arapouco profiles.

In the Sado channel lower resistivity values are present until depths ca. -40 m MSL in Arapouco and Vale do Guizo, and until ca. -38 m MSL at São Bento, while in the tributaries resistivity values increase ca. -15 m MSL at Arez and are very superficially at Vale dos Açudes (Figure 4.3).

Resistivity values seem to increase upstream, from Arapouco to São Bento (Figure 4.3). In Arapouco, low resistivity values were measured in all the profiles in depth, only increasing at ca. 40 m depth, while in Vale do Guizo and São Bento higher resistivity layers occur within the area fulfilled with sediments with lower resistivity values (Figure 4.3). At Vale do Guizo, higher resistivity values occur in the right margin, above sediments with lower resistivity values, but also as isolated areas with resistivity values >80 ohm.m in what corresponds to the right margin of the valley. At São Bento, the higher resistivity values (resistivity values between ca. 20 and 50 ohm.m) appear as an extensive area that occupies almost the entire valley in length, between ca. 20 and 5 m depth (Figure 4.3). Changes in the resistivity values are must probably related with the existence of sediments with coarser grain-size (Figure 4.5).

For the Arez tributary, despite shallower than Arapouco, the ERT profile has a similar pattern, with low resistivity values from the top layers to ca. 15 m depth where resistivity increases.

The Vale dos Açudes ERT profile have no pattern regarding the distribution of resistivity values, presenting mixed values between ca. 10 and ca. 40 ohm.m from the top to the base (Figure 4.3).

The Laxique ERT profile was done near the most upstream studied area. It presented an opposite pattern in relation to the ERT profiles done downstream concerning resistivity, with higher resistivity values at the top of the profile (varying between 15 and 50 ohm.m), excepting the very top where lower resistivity values also occur (<15 ohm.m). In depth, from ca. 30 m downward, low resistivity values were measured, lower than 15 ohm.m (Figure 4.4). The higher resistivity values are probably reflecting coarser sediments for the Holocene infilling until ca. 30 m depth following the interpretation done for the profiles located at downstream areas. Given this, lower resistivity values would reflect fine sediments that could correspond to the *Vale do Guizo* formation or a different lithology that could be related with shales of the *Mértola* formation that occur below the Palaoegene deposits. According to the local geological map the base of the *Vale do Guizo* formation outcrops near the Vale do Gaio dam in the Xarrama stream (Figure 2.12) and the contact between the two formations can be at shallow depths at Laxique. Both shales (in

the case of the *Mértola* formation) and clays (in the case of *Vale do Guizo* formation) should have lower resistivity values than sand and gravel (Figure 3.1). Given this, according to our interpretations, the contact between different resistivities found at ca. 30 m depth corresponds, most probably, to the LGM valley bottom.

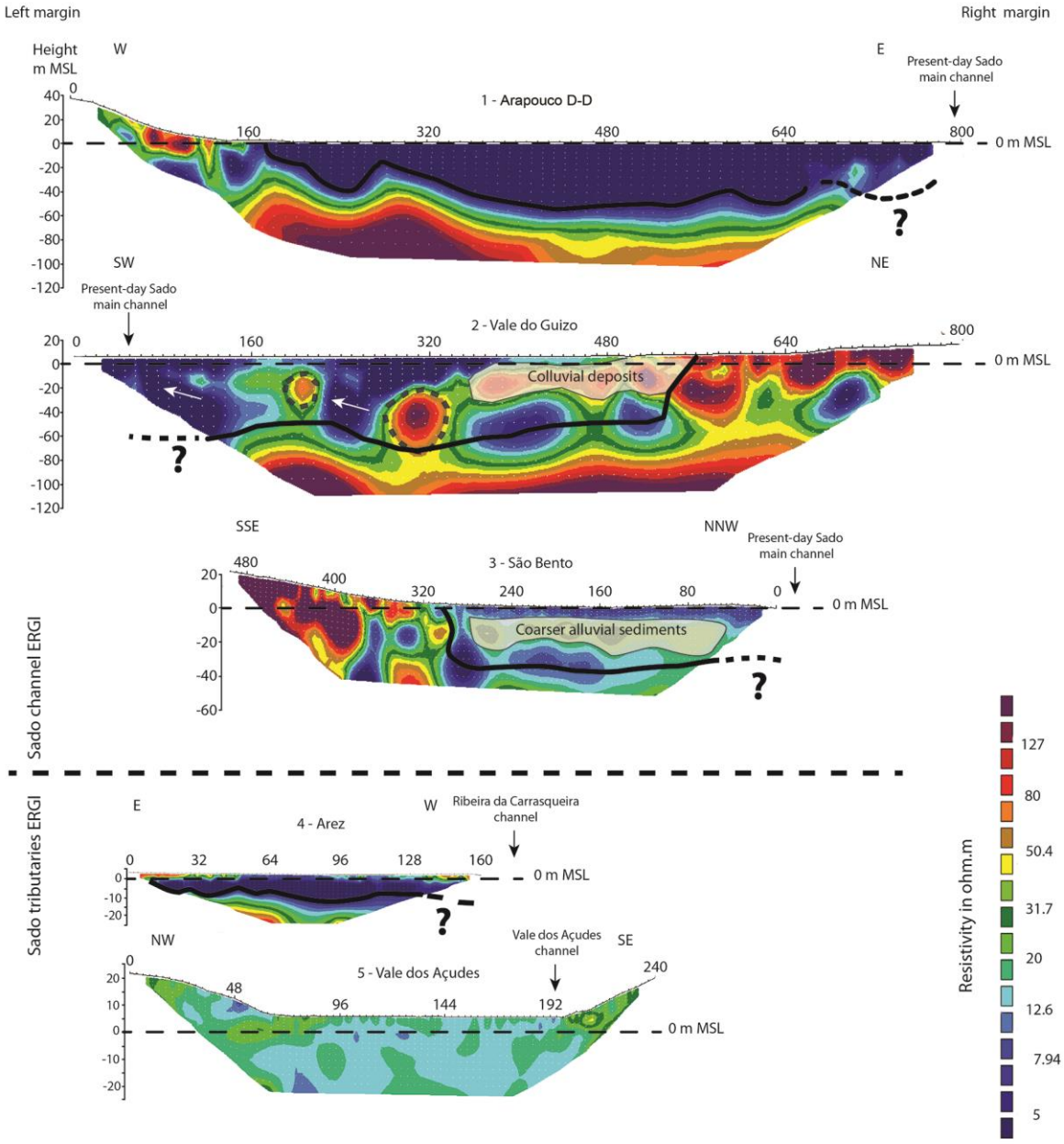

Figure 4.3 - ETR profiles of the Sado channel (Arapouco D-D, Vale do Guizo and São Bento) and tributaries (Arez and Vale dos Açudes) and interpretation. The white arrow in Vale do Guizo profile indicates the channel migration SW. Black-line indicates the proposed palaeomorphology for the valleys.

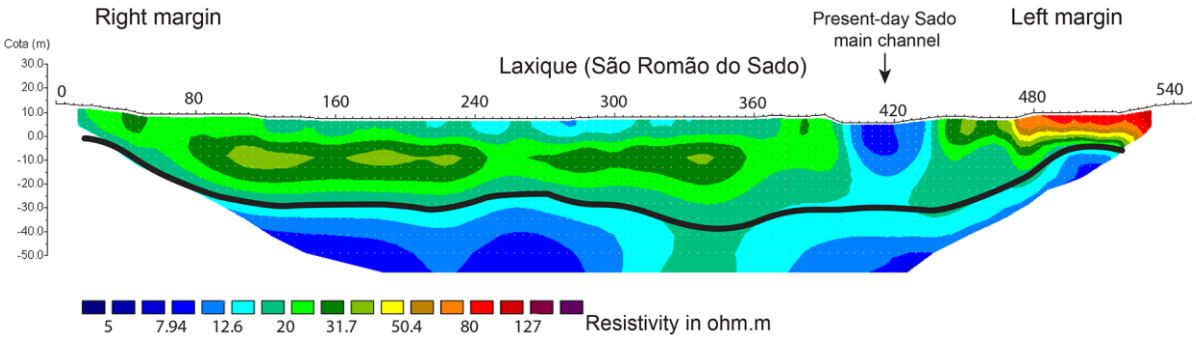

Figure 4.4 - ERT profile of the Sado channel at Laxique and interpretation.

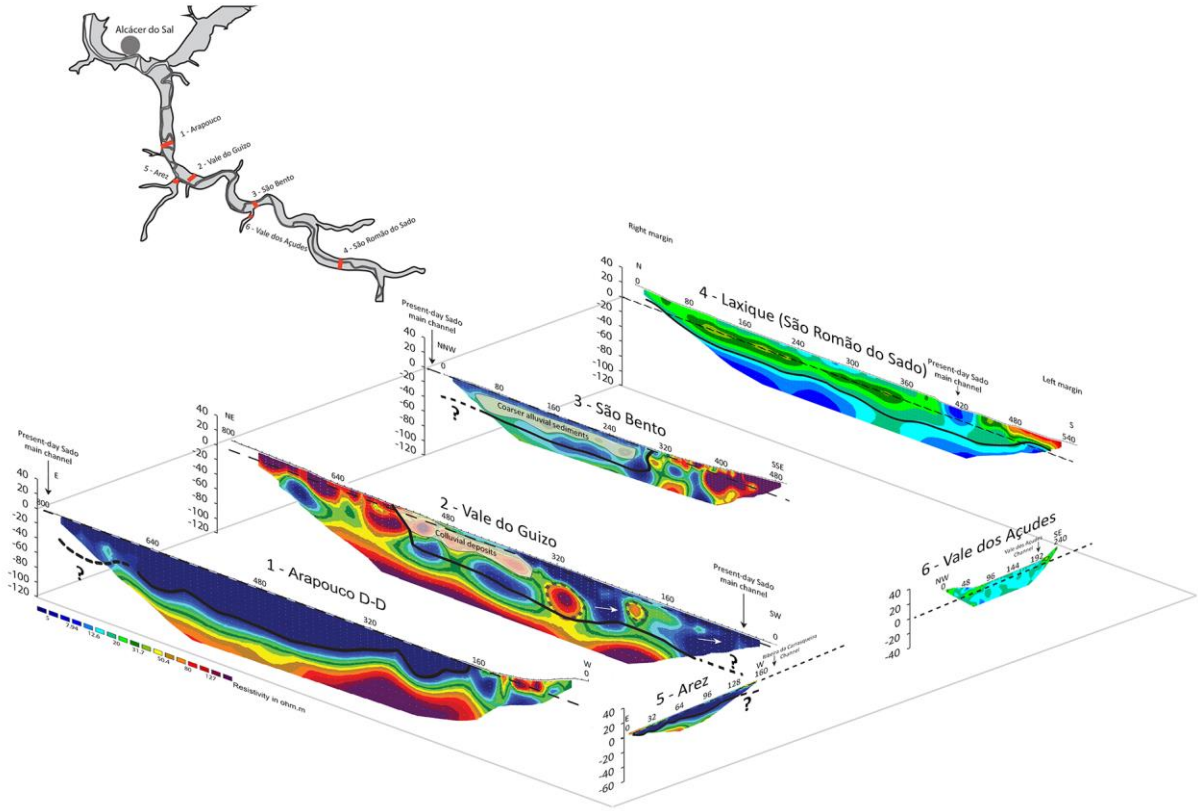

Figure 4.5 - ERT profiles from the Sado channel with indication of the palaeovalleys morphology and Holocene infilling, based on interpretation of the resistivity values.

4.2 Chronology

Results of radiocarbon dates and calibrated ages are presented in Table 4.1. Radiocarbon ages at the base of the Sado cores are younger than the ages for the base of the tributaries cores. In the Sado, calibrated ages are all younger than ca. 4400 cal BP (2450 cal BC; median calibrated age

value for the sample Laxique1 801-803; -191 cm MSL; Table 4.1) and sediments represent the infilling of the valley during the Middle-Late Holocene transition and Late Holocene. Median calibrated ages for the base of the cores collected on the tributaries are older and the sequences represent the sedimentation occurring since the Early-Middle Holocene transition and Middle Holocene. At base of Arez1 (-10.6 m MSL) median calibrated age is ca. 8590 cal BP (6640 cal BC) and at the base of Arez3 (-10.8 m MSL) median calibrated age is 8800 cal BP (6850 cal BC) while in Vale dos Açudes median calibrated age is ca. 7300 cal BP (5350 cal BC; Table 4.1).

Carbon in the sediments of estuarine reservoirs is the result of a mixture between different sources and so determined dates should be considered cautiously (e.g., Kristensen, 1990; Colman et al., 2002; Lamb et al., 2006; Loh et al., 2008). Both marine reservoir effect (ΔR) and/or freshwater reservoir effect (e.g., Philippsen, 2013) can play a role on ^{14}C dating procedures. Freshwater reservoir effect in the studied area can be neglected once the studied section of the Sado valley is mostly embedded in detrital quartzic caenozoic sediments despite the existence of limestone at the top of the *Vale do Guizo* formation sequence (Gonçalves and Antunes, 1992).

For the correction of the marine reservoir effect of the shell sample dated from Arapouco 2/3, two ΔR values are published for the studied area which have been determined using estuarine shell/carbon pair recovered from the Mesolithic site of Vale de Romeiras for ages of ca. 8000 cal BP (6050 cal BC; Sado; Figure 1.10): -170±60 ^{14}C years (Monge Soares and Dias, 2006) and -100±155 ^{14}C years (Martins et al., 2008). Both values have been used for calibration purposes and results reported in Table 4.1. The determined date for the inorganic carbon from the shell is younger than all the other radiocarbon dates below 2 m depth estimated for Arapouco 2/3.

The bivalve *Scrobicularia plana* is mainly a deposit feeder (Riera et al., 1999; Santos et al., 2012), but also behaves as a suspension feeder (Riera et al., 1999). It is frequently found in upper intertidal muddy areas (Santos et al., 2012; Pizzolla, 2002), burrows up to 20 cm in the sediment and tolerates low salinities (Pizzolla, 2002).

Table 4.1 – Radiocarbon determinations for the sediment cores used in this chapter. The dates have been calibrated with the IntCal20 curve (Reimer et al., 2020) using the Oxcal v.4.4 program (© Bronk Ramsey). * $\delta^{13}C$ values were not made available by the lab due to radiocarbon method procedures measure (Crann et al., 2017; see Section 4. for the description of the methods). Dated samples of *Scrobicularia plana* were calibrated using the marine radiocarbon age calibration curve Marine13 (Reimer et al., 2013) ** for calibration ΔR = -170±60 ^{14}C years (Monge Soares and Dias, 2006). *** for calibration ΔR = -100±155 ^{14}C years (Martins et al., 2008). ****calibrated using the Post-bomb curve NH Zone 2 (Hua et al., 2013). To be continued.

Loc	Sample reference	Lab code	Material	Core depth (cm)	Height (cm MSL)	$\delta^{13}C$ (‰)	Conventional ^{14}C age BP	Calibrated age BP (95%)	Calibrated age BC (95%)
Sado channel	Arapouco2#9 152-154	Beta-436176	Bulk organic sediment	153	67	-25.4	2620±30	2776-2721 (95.4%)	827-772 BC (95.4%)
	Arapouco2#10 200-202	Beta-408535	Bulk organic sediment	201	19	-25.4	3170±30	3454-3346 (95.4%)	1505-1397 BC (95.4%)
	Arapouco3#2 354-356	Beta-393523	Bulk organic sediment	355	-135	-22.7	3100±30	3383-3227 (95.4%)	1434-1278 BC (95.4%)
	Arapouco3#4 552-554	Beta-408534	Bulk organic sediment	553	-333	-23.5	3400±30	3815-3801 (2.0%) 3718-3564 (93.4%)	1866-1852 BC (2.0%) 1769-1615 BC (93.4%)
	Arapouco3#4 571-574**	Beta-436175	*Scrobicularia plana* shell	572.5	-352.5	-6.01	3000±30	3035-2614 (95.4%)	1086-665 BC (95.4%)
	Arapouco3#4 571-574***	Beta-436175	*Scrobicularia plana* shell	572.5	-352.5	-6.01	3000±30	3142-2315 (95.4%)	1193-366 BC (95.4%)
	Arapouco3#5 624-627	Beta-431370	Bulk organic sediment	625.5	-405,5	-23.4	3210±30	3468-3371 (95.4%)	1519-1422 BC (95.4%)
	Arapouco3#5 635-637	Beta-431371	Bulk organic sediment	636	-416	-23.5	3330±30	3636-3466 (95.4%)	1687-1517 BC (95.4%)
	VG1 1010-1011	Beta-457795	Bulk organic sediment	1010.5	-299	-24.2	2750±30	2930-2897 (7.8%) 2889-2766 (87.7%)	981-948 BC (7.8%) 940-817 BC (87.7%)

Table 4.1 - Continuation and to be continued.

Loc	Sample reference	Lab code	Material	Core depth (cm)	Height (cm MSL)	$\delta^{13}C$ (‰)	Conventional ^{14}C age BP	Calibrated age BP (95%)	Calibrated age BC (95%)
Sado channel	Sado3A 719-720	Beta-457793	Bulk organic sediment	719.5	-940,5	-24.3	2110±30	2288-2275 (2.7%) 2148-1995 (92.7%)	339-326 BC (2.7%) 199-46 BC (92.7%)
	Laxique1 150-152	Beta-510626	Bulk organic sediment	151	459	-24.9	101± 0.38pMC****	-6 to -7	1955-1956 AD
	Laxique1 320-322	Beta-482231	Bulk organic sediment	321	289	-25.8	1060±30	1056-1024 (16.8%) 1007-926 (78.6%)	895-926 AD (16.8%) 948-1030 AD (78.6%)
	Laxique1 521-523	Beta-51062	Bulk organic sediment	522	88	-26.0	3670±30	4090-3900 (95.4%)	2141-1951 BC (95.4%)
	Laxique1 801-803	Beta-476962	Bulk organic sediment	802	-191	-25.9	3940±30	4515-4480 (10.2%) 4445-4289 (82.8%) 4270-4254 (2.5%)	2566-2531 BC (10.2%) 2496-2340 BC (82.8%) 2321-2305 BC (2.5%)
	ALC-S S1 0.78-0.79	Beta-417791	Bulk organic sediment	78.5		-23.2	610±30	651-546 (95.4%)	1299-1404 AD (95.4%)
	ALC-S S1 2.68-2.69	Beta-417792	Bulk organic sediment	268.5		-25.6	740±30	725-652 (95.4%)	1225-1299 AD (95.4%)

Table 4.1 - Continuation.

Loc	Sample reference	Lab code	Material	Core depth (cm)	Height (cm MSL)	$\delta^{13}C$ (‰)	Conventional ^{14}C age BP	Calibrated age BP (95%)	Calibrated age BC (95%)
Sado tributaries	Arez1 1062-1063	Beta-343145	Bulk organic sediment	1062.5	-792.5	-25.9	7810±30	8645-8517 (93.5%) 8497-8472 (2.0%)	6696-6568 BC (93.5%) 6548-6523 BC (2.0%)
	Arez3#3 176-178	UOC-13332	Bulk organic sediment	177.5	92.5	*	1239±33	1273-1201 (38.1%) 1193-1069 (57.4%)	678-749 AD (38.1%) 758-882 AD (57.4%)
	Arez3#4 300-302		Bulk organic sediment	301.5	-31.5		On going		
	Arez3#5 360-362	UOC-13333	Bulk organic sediment	361.5	-91.5	*	5965±33	6893-6726 (90.6%) 6707-6676 (4.9%)	4944-4777 BC (90.6%) 4758-4727 BC (4.9%)
	Arez3#8 746-748	UOC-10286	Bulk organic sediment	747	-477.5	*	6231±79	7319-6938 (95.4%)	5370-4989 BC (95.4%)
	Arez3#9 786-788	UOC-13334	Bulk organic sediment	787.5	-517.5	*	6011±30	6944-6781 (92.1%) 6765-6749 (3.3%)	4995-4832 BC (92.1%) 4816-4800 BC (3.3%)
	Arez3#11 966-968	Beta - 582890	Bulk organic sediment	967.5	-697.5	-25.7	6550±30	7561-7541 (6.8%) 7511-7422 (88.7%)	5612-5592 BC (6.6%) 5562-5473 BC (88.7%)
	Arez3#13 1216-1218	UOC-13335	Bulk organic sediment	1217.5	-947.5	*	7787±33	8636-8614 (5.3%) 8608-8512 (77.3%) 8503-8455 (12.8%)	6687-6665 BC (5.3%) 6659-6563 BC (77.3%) 6554-6506 BC (12.8%)
	Arez3 1348-1349	Beta-510624	Bulk organic sediment	1348.5	-1078.5	-25.2	7970±30	8992-8716 (89.8%) 8709-8699 (1.5%) 8671-8650 (4.1%)	7043-6767 BC (89.8%) 6760-6750 BC (1.5%) 6722-6701 BC (4.1%)
	Sado3AC1 766-769	Beta-457794	Bulk organic sediment	767.5		-26.0	6360±30	7417-7393 (5.9%) 7332-7246 (74.0%) 7209-7169 (15.6%)	5468-5444 BC (5.9%) 5383-5297 BC (74.0%) 5260-5220 BC (15.6%)

Nowadays, as mentioned before (Chapter 3. Study area), *Scrobicularia plana* is present in the Sado estuary in an area with low salinities, in the Alcácer do Sal channel (Santos, 2019) confirming the environmental conditions where the bivalve usually occurs. The $\delta^{13}C$ determined for this shell (-6.01 ‰; Table 4.1) indicates a clear estuarine origin (Keith and Anderson, 1963; McConnaughey and Gillikin, 2008) reflecting the inclusion of both fluvial and marine dissolved inorganic carbon on its shell. However, despite the shell carbon of several aquatic organisms derive mainly from ambient dissolved organic carbon (McConnaughey and Gillikin, 2008), studies performed in shells from *Scrobicularia plana* concluded that it also reflects the incorporation of metabolic and/or kinetic carbon altering the $\delta^{13}C$ values (Santos et al., 2012) and the ^{14}C content and thus the radiocarbon date. For this reason, the inorganic carbon date was excluded from the Arapouco dating model (Figure 4.6) despite the proximity to the results obtained with organic samples.

Age-models were produced for Arapouco 2/3, Laxique and Arez3 from where several radiocarbon dates were done in depth (Table 4.1). Dates for Vale do Guizo (VG1), São Bento (Sado 3A), Arez1 and Vale dos Açudes (Sado 3AC1), where only one sample was dated at the base of the core, were used in the analyses and interpretation of the ERT profiles but helped to confirm the results achieved in the other sediment cores.

At Arapouco 2/3 mean sedimentation rate (SR) of 2.2 cm yr^{-1} was determined using CLAM (Blaauw, 2010), representing a high sedimentation rate in a short time interval (Figure 4.6). A mean SR of 0.06 cm yr^{-1} was determined for the last 3232 years (Figure 4.6). The date obtained for the sample Arapouco3#4 552-554 (Table 4.1) was not used on the SR model once it presents an older date considering the value obtained for the samples on the base of the core (samples Arapouco3#5 635-637 and Arapouco3#5 624-627). The stratigraphic inversion at 553 cm is possibly the result of the presence of old organic material brought to the area by the fluvial network during intense fluvial episodes.

At Laxique lower SR were determined when comparing the values with the ones determined for Arapouco, but also high SR of 0.75 cm yr^{-1} were determined for the interval between the core base (4400 cal BP; 2450 cal BC) and ca. 90 cm MSL (4000 cal BP; 2050 cal BC) and lower sedimentation rates of ca. 0.07 cm yr^{-1} were calculated for the sedimentary column between 90 cm and 290 cm MSL (between 970 cal BP and the present; between 980 cal AD and the present; Figure 4.7). From that depth upwards SR increases to values of 0.2 cm yr^{-1} (between 290 cm and 460 cm MSL) and then returns to high values of 0.74 cm yr^{-1} (between 460 cm and the top of the core, at 610 cm MSL). According to the model settings, the goodness of fit was 3.62 despite the short number of dates available (4) and the model was accepted.

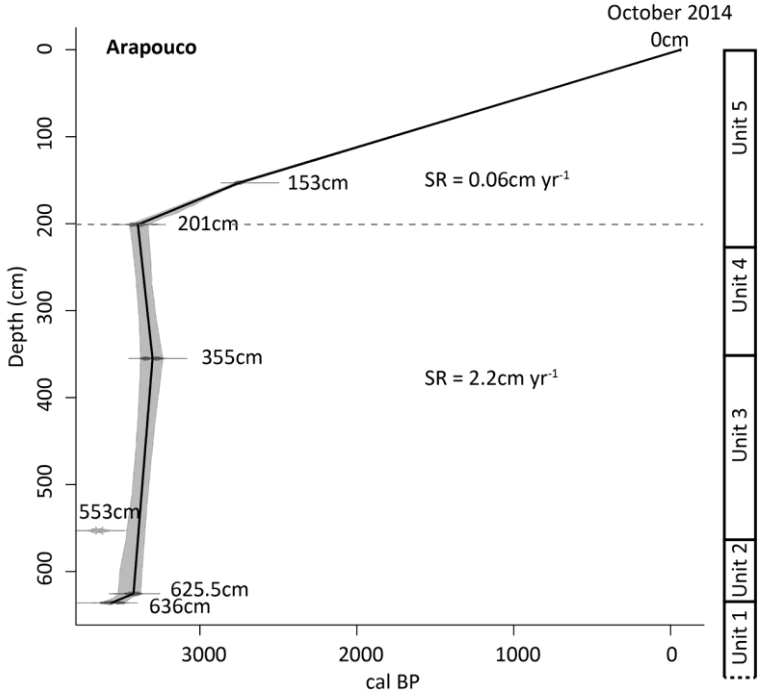

Figure 4.6 - ^{14}C BP dates and age model for Arapouco 2/3 with representation of the samples used for ^{14}C dating. For unit's description, see Section 5.3.

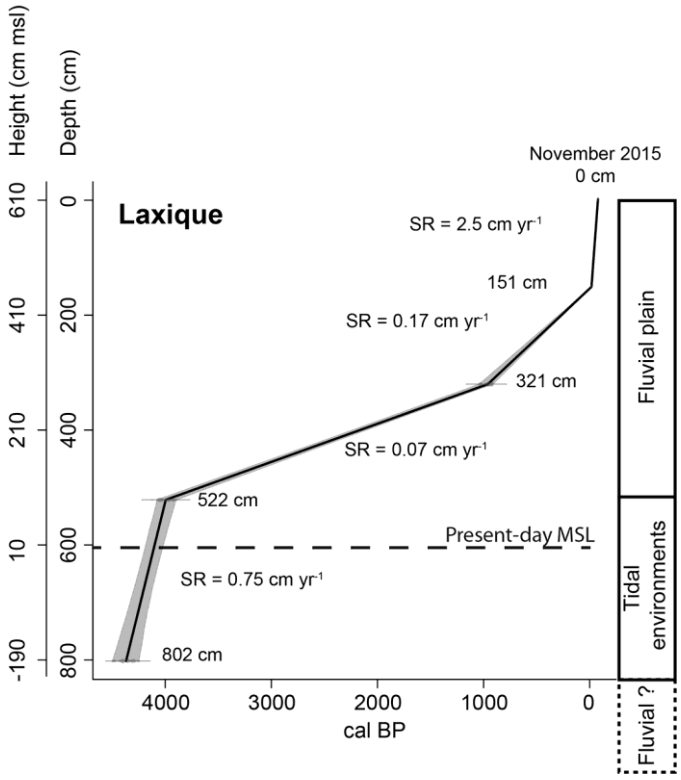

Figure 4.7 - ^{14}C BP dates and age model for Laxique with representation of the samples used for ^{14}C dating.

Figure 4.8 displays the age-model draw for Arez3 sediment core. Older samples presented dates of ca. 8800 cal BP (6850 cal BC) covering a 13-m long Holocene sedimentary sequence. Almost all dates are consecutive revealing a coherent age-model (Figure 4.8). The dates obtained for samples Arez3#4 300-302 and Arez3#8 786-788 present small inversions in relation to the samples collected just below. However, the error associated with the dates is within the limits of the age-model. Even so, the dating of the sample Arez3#8 786-788 was considered an outlier and was not used for the age-model (red mark in Figure 4.8). According to the model settings, the goodness of fit was 8.6 considering all dates used (7) and the model was accepted. Ages and uncertainty ranges for each date were calculated for each cm and best-fit dates were used for the presentation of the results and interpretations.

Variable and high sedimentation rates (SR) were determined for Arez3 between the base of the core, at -1060 cm MSL and the present-day MSL, following the SR pattern achieved in other cores collected in the Sado valley (Figure 4.8). The highest SR of 1.2 cm yr^{-1} was determined for the section between -456.5 and -10 cm MSL corresponding to the interval between 7120 and 6800 cal BP (5170 and 4850 cal BC). The lowest SR of 0.02 cm yr^{-1} was determined above present-day MSL and 177 cm MSL, corresponding to the interval between 6800 and 1170 cal BP (4850 cal BC and 780 cal AD). SR increases in the top 180 cm to values of 0.14 cm yr^{-1}, i.e., for the last ca. 780 years. SR in the top of the core can be affected by agriculture procedures (see discussion).

For all age models, ages and uncertainty ranges for each date were calculated for each cm and best-fit dates were used for the presentation of the results and interpretations.

4.3 Sediment cores description

Prospecting sediment cores: VG1, Sado3A, Arez1 and Sado3AC1

The sediment cores Vale do Guizo (VG1), São Bento (Sado3A), Arez1 and Vale dos Açudes (Sado3AC1) (Table 3.2) correspond to the first prospecting sediment cores retrieved from the studied area and only the basal section of the cores was collected. Even so, the collected sediments were analysed for several proxies and radiocarbon dated.

All sediment cores are essentially constituted by mud with occasional intercalations of sandy mud, with exception of the Vale dos Açudes core where intercalations of fine to coarse sand were identified (Figure 4.9). At the base of most of these sedimentary successions, coarser sediments, constituted essentially by sand, occur (Figure 4.9 and 4.10).

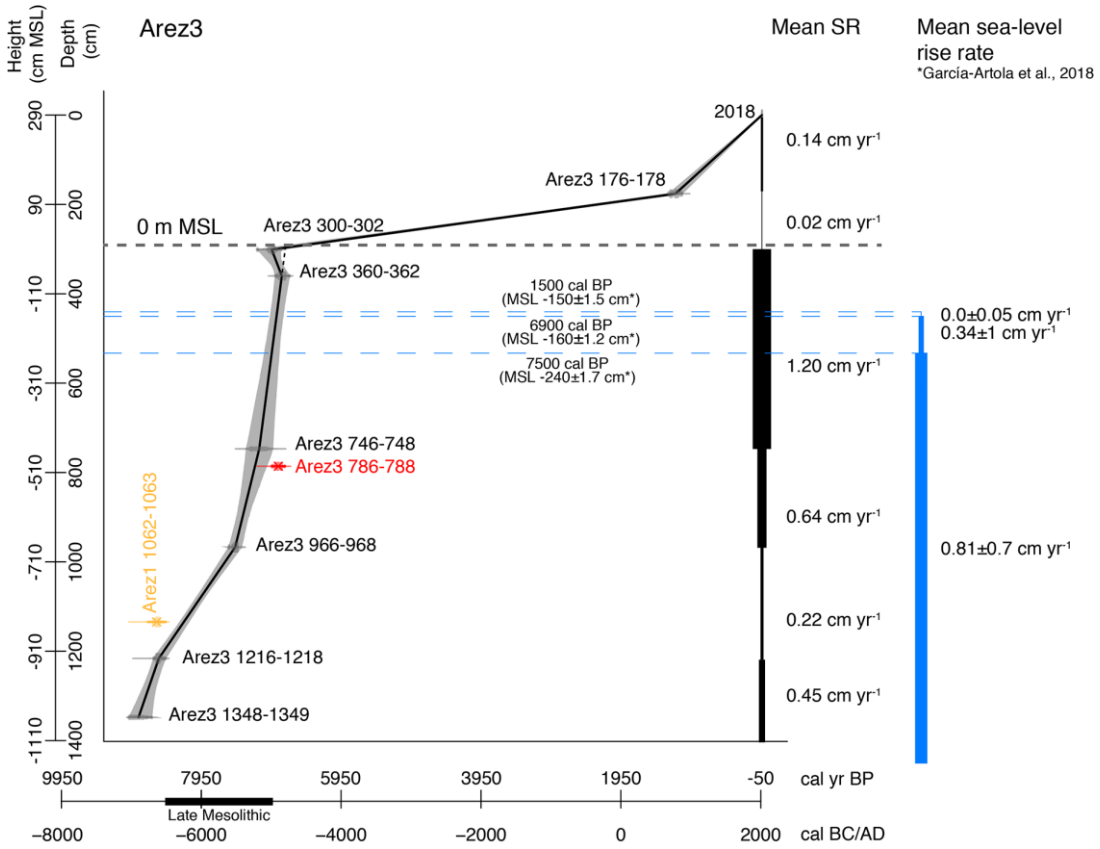

Figure 4.8 - ^{14}C BP dates and age model for Arez3 with representation of the samples used for ^{14}C dating.

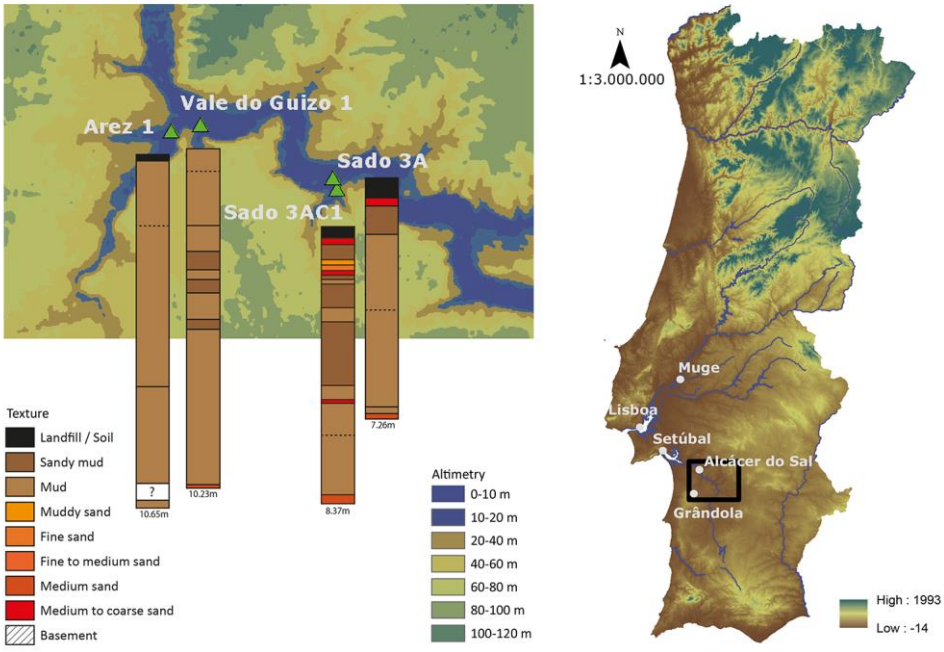

Figure 4.9 - Location and representation by texture of the sediment cores Vale do Guizo 1 (VG1), São Bento (Sado3A), Arez1 and Vale dos Açudes (Sado3AC1). The texture represented in the image was done by macroscopic description during field sampling.

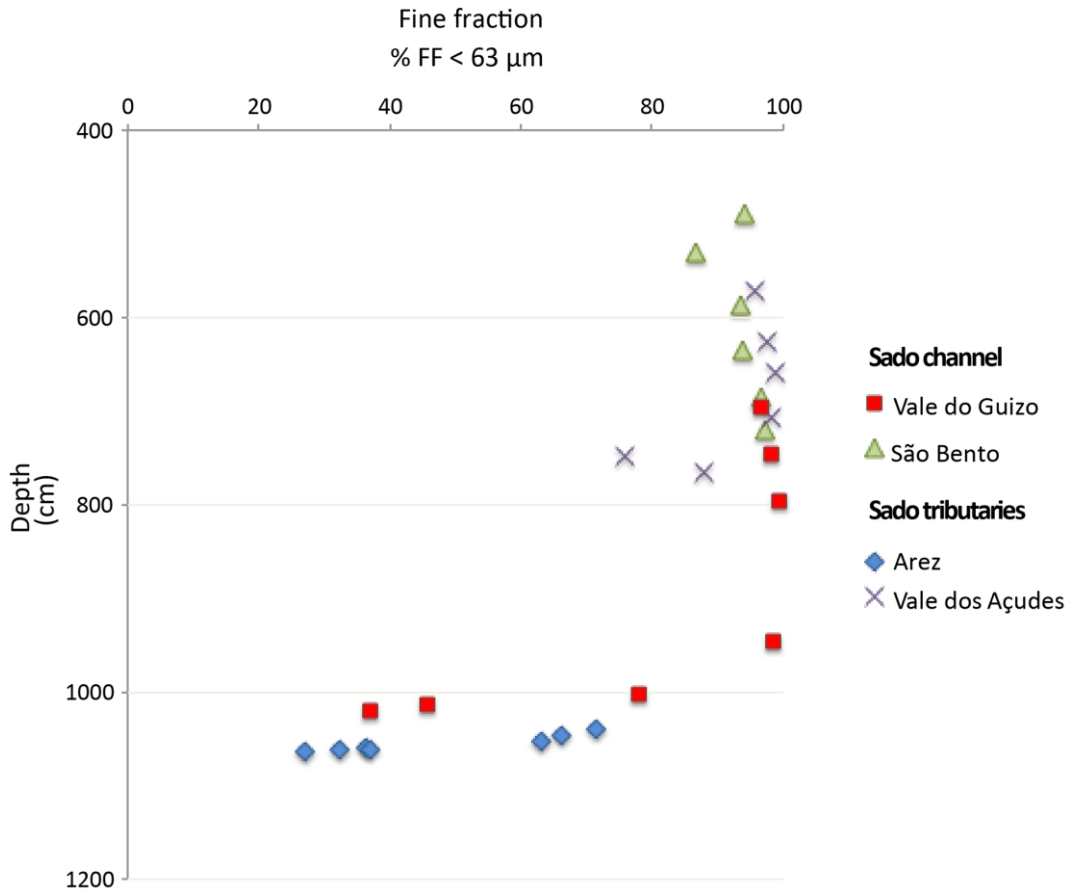

Figure 4.10 - Fine fraction contents (%<63 µm) for the sediment cores Vale do Guizo (VG1), São Bento (Sado3A), Arez1 and Vale dos Açudes (Sado3AC1).

The cores collected at Vale do Guizo (VG1) and São Bento (Sado3A), located in the Sado valley, present mean values of $\delta^{13}C$ of ca. -24.7‰, while in the samples collected in Arez1 and Vale dos Açudes (Sado3AC1) tributaries, mean $\delta^{13}C$ values of -26.3‰ were determined (Figure 5.11). In the top samples, $\delta^{13}C$ determined in Vale do Guizo also decrease, presenting mean values of ca. -25.5‰ for the samples located at -600 cm MSL (Figure 4.11).

Diatom assemblages in Vale do Guizo are dominated by the marine tychoplanktonic *Cymatosira belgica,* while an epipsammic diatom, *Opephora mutabilis* is the most frequent taxon in the Arez record (Figures 4.12 and 4.13).

In São Bento sediments, diatom assemblages are composed by planktonic species common in fresh and brackish waters (Figure 4.12). The marine tychoplanktonic *C. belgica* is also present. This is also a cosmopolitan species found both in plankton and in the benthos, frequently found in sandy beaches but also very abundant in silty sediments. Upper core São Bento diatom assemblages are dominated by planktonic estuarine species.

At Vale dos Açudes all samples above -98 cm MSL depth are almost barren of diatoms (Figure 4.12). Whole valves were rare. Epipelic diatoms are the most frequent taxa. The diatom content at the core base shows the highest abundances of cosmopolitan epipelic species, common in marine to brackish waters.

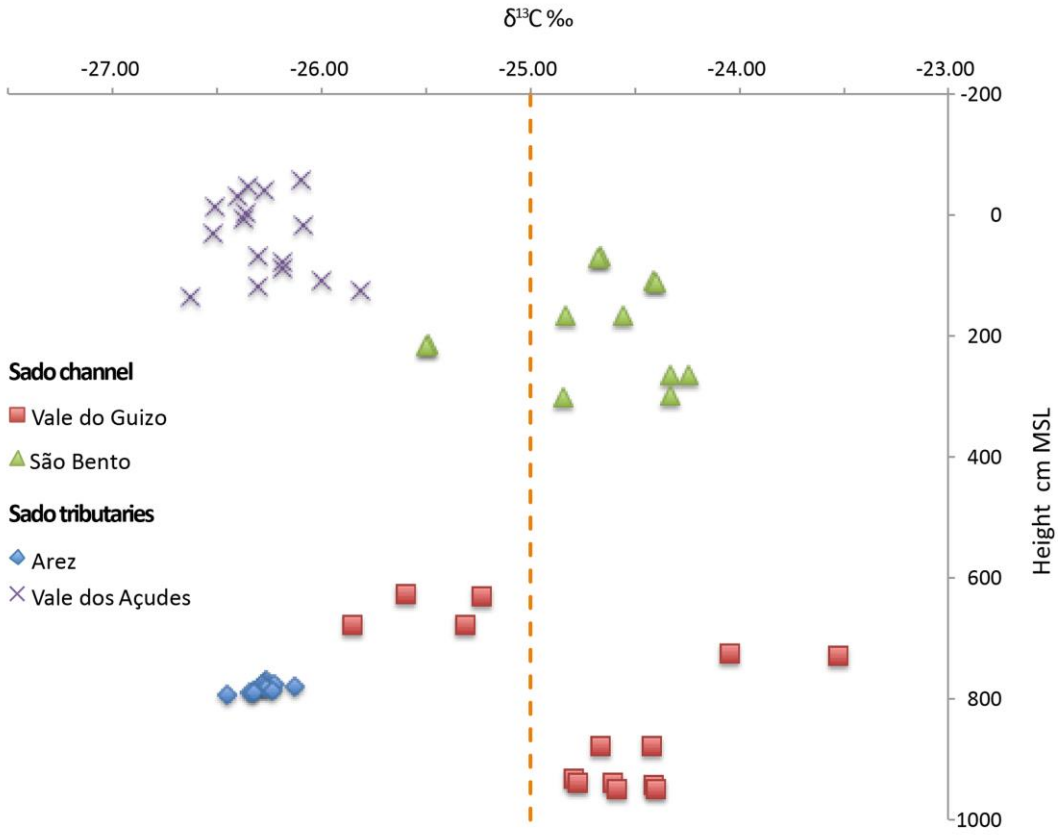

Figure 4.11 - Variation of $\delta^{13}C$ with height in the sediment cores Vale do Guizo (VG1), São Bento (Sado3A), Arez1 and Vale dos Açudes (Sado3AC1).

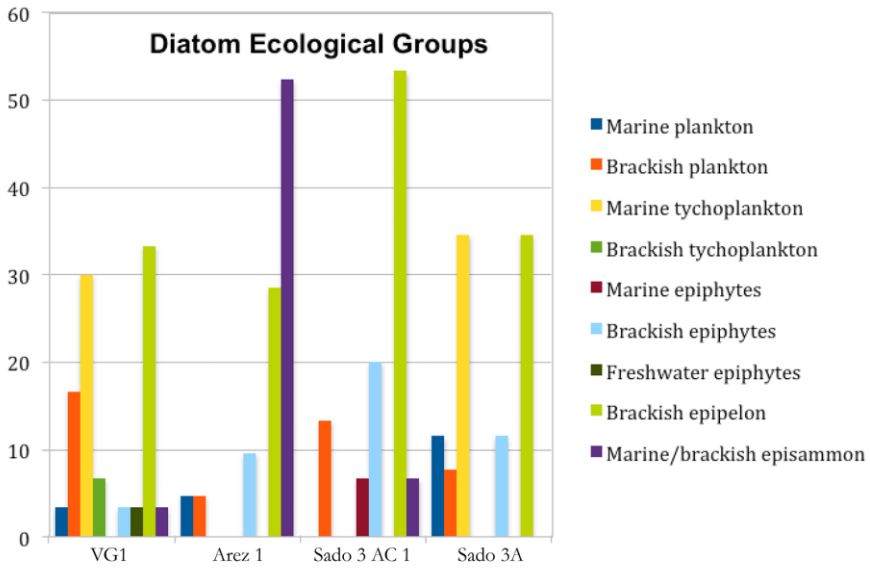

Figure 4.12 - Diatoms ecological groups identified in the basal samples of the sediment cores Vale do Guizo (VG1), São Bento (Sado3A), Arez1 and Vale dos Açudes (Sado3AC1).

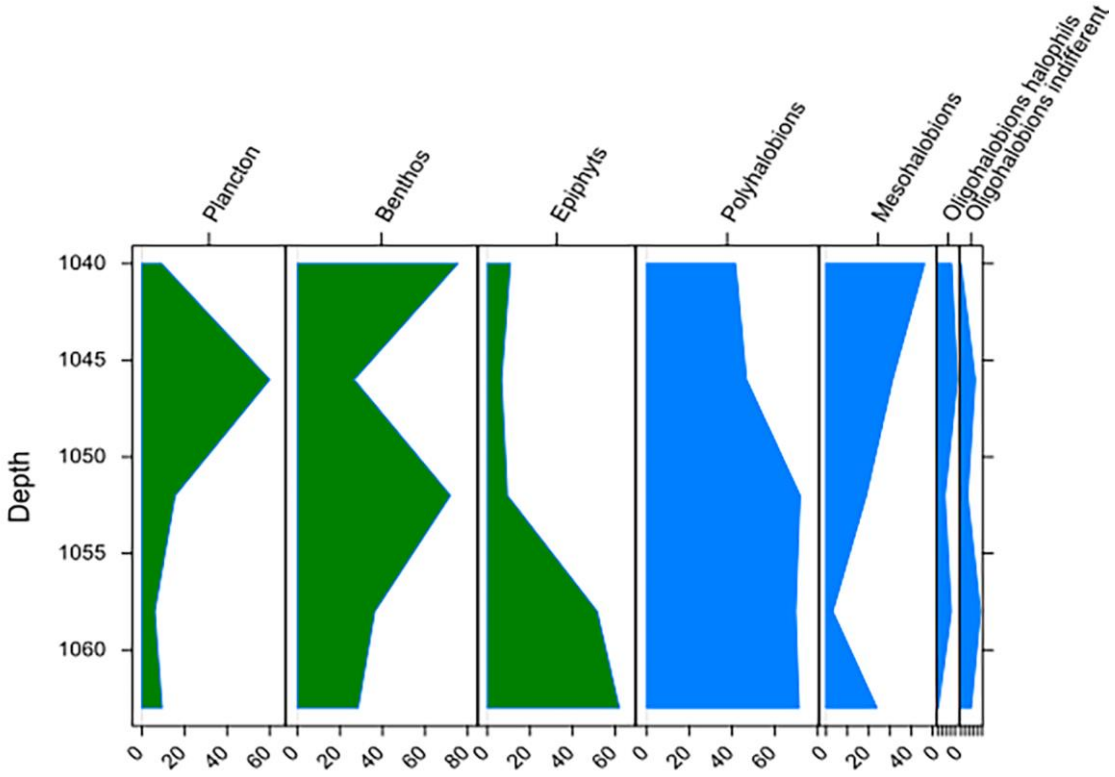

Figure 4.13 - Down-core distribution of selected diatom ecological groups in the sediment record of Arez1 plotted against core depth.

Arapouco transect

Five sediment cores were collected in Arapouco performing a transect perpendicular to the Sado channel. Only Arapouco 2 and 3 were analysed for multi-proxy analyses and the results are presented below. According to the macroscopic description, the sediment is essentially composed by mud (Figure 4.14). In the top 1-2 meters, the sediment presents a brownish colour, probably due to oxidation, and frequent macro-plant remains were described. Below, the sediment presents a greyish colour. Bioturbation and macro-plant remains are rare. At the base of Arapouco 3 and Arapouco 4, a coarse layer, composed by sand, was found preventing the collection of sediment at higher depths. The sandy layer was identified in the ERT profile Arapouco 2 (Figure 4.2), but it was not recognized in Arapouco D-D and Arapouco W (Figure 4.1) due to the resolution of the longer resistivity profiles.

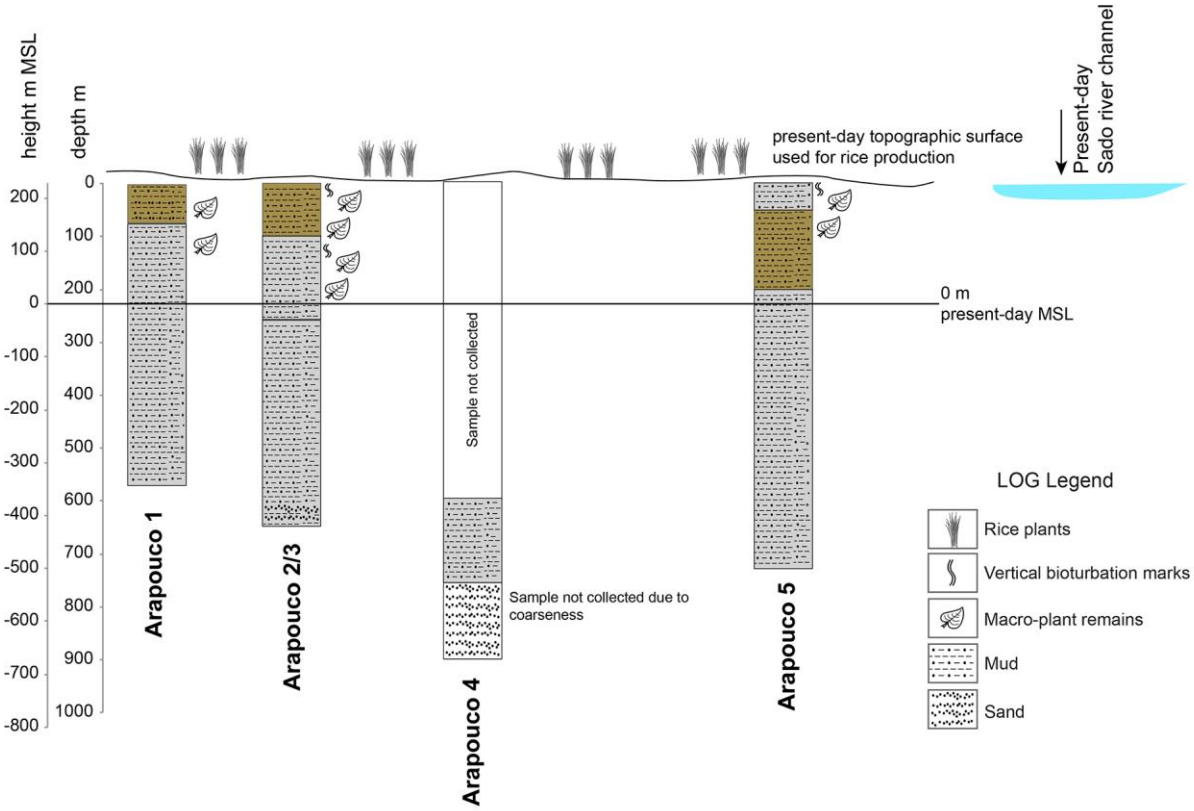

Figure 4.14 - Representation by texture of the sediment cores collected in the Arapouco transect. The texture represented in the image was done by macroscopic description during field sampling.

Arapouco 2/3

At Arapouco 2/3, five sediment units were identified considering changes in the analysed proxies (Figure 4.15 and Table 4.2). The interval of deposition was determined considering the proposed

age-model. All samples prepared for calcareous nannofossils were completely barren. Calcium carbonate results indicate null or negligible amounts (<1% on the analysed samples).

Unit 1 (at the bottom, below -425 cm MSL; deposited before ca. 3570 cal BP; ca 1620 cal BC) consists essentially of heterometric sand, mainly composed by angular to sub-angular hyaline and milky quartz (ca. 99%) and mica grains. Rare lithoclasts occur.

Unit 2 (-425 cm to -350 cm MSL; deposited between ca. 3570 and 3400 cal BP; ca. 1620 and 1450 cal BC) is characterized by MS values between $13x10^{-5}$ (SI) and $34x10^{-5}$ (SI) with the highest values corresponding to two peaks (at 415 and 407 cm MSL; Figure 4.15 and 4.16) and related to two sand lenses observed between 407-409 cm and 413-415 cm MSL. The sand (sediment >63 μm) from these two layers is composed of ca. 99% of hyaline and milky quartz grains and in the fraction >1.4 mm charcoal fragments were observed. Apart from these two coarser samples, the sediment is essentially muddy (mean values of 91%; 64% silt and 27% clay; 9% sand; Figure 4.15) with OM values of 8% (min. 7%; max. 9%) with a single exception collected between the sandy lenses (-411 cm MSL) where OM shows values of ca. 5%. The sand from the muddy samples is also composed by heterometric hyaline quartz (ca. 99%) and mica. Vegetal and charcoal fragments were observed. Rare forms of *Actinoptychus* spp were also observed. Organic carbon presents mean values of 2%, C/N ratio varies between 11 and 12.5 (mean value of 11.5) and $\delta^{13}C$ shows mean values of -24‰ (Figure 4.15).

The bottom of the Arapouco record shows the development of brackish diatom assemblages (Figure 4.17), dominated by *Cyclotella meneghiniana*, a brackish/freshwater planktonic species. In the mid-core section diatoms show an assemblage almost exclusively composed by marine planktonic *Thalassiossira* species, similar to those found today in the Sado estuary, along with some brackish forms. In the uppermost part of the record, diatom assemblages show a return to brackish conditions, characterised by marine, marine/brackish and brackish/freshwater diatoms, with *Cocconeis* spp. and *Nitzschia* spp. as dominant taxa.

At the top of this Unit (-354 to -351 cm MSL) a whole shell of *Scrobicularia plana* was found (Figure 4.18). The diatom record is mainly composed by marine to marine/brackish planktonic taxa such as *Paralia sulcata* and/or *Actinoptychus senarius*, although some epiphytic and epipelic diatoms of brackish character (as *Cocconeis placentula* and *Epithemia adnata*) also occur (Diatom Association Zone (DAZ) 1; Figure 4.17).

Table 4.2 - Sedimentological and chemical statistic parameters of the defined units for the Arapouco sediment core.

		MS $x10^{-5}$ (SI)	Texture Clay (%)	Silt (%)	Sand (%)	Total organic matter (%)	Organic carbon (%)	Total nitrogen (%)	C/N	$\delta^{13}C$ (‰)	$\delta^{15}N$ (‰)
Unit 5	average	20.87	29	58	13	4.74	0.76	0.08	8.88	-25.93	6.00
	max.	38.56	37	68	47	7.41	2.39	0.22	12.35	-25.45	7.97
	min.	4.58	15	38	2	2.68	0.38	0.06	4.79	-26.94	3.40
Unit 4	average	17.08	30	60	10	8.4	2.36	0.19	12.40	-25.08	5.05
	max.	36.74	27	63	27	10.12	2.69	0.22	13.76	-24.50	5.42
	min.	10.42	18	54	4	6.06	1.53	0.11	11.62	-25.95	4.45
Unit 3	average	12.11	25	60	15	7.77	2.25	0.18	12.36	-24.36	4.81
	max.	15.26	33	65	28	9.10	2.68	0.21	13.75	-23.93	5.14
	min.	9.70	16	55	8	6.62	1.77	0.14	11.35	-24.83	4.36
Unit 2	average	18.85	27	64	9	8.24	2.33	0.20	11.48	-24.01	4.96
	max.	34.21	32	71	19	9.60	2.55	0.24	12.48	-23.43	5.06
	min.	12.77	21	59	3	7.34	1.93	0.17	10.77	-24.71	4.69

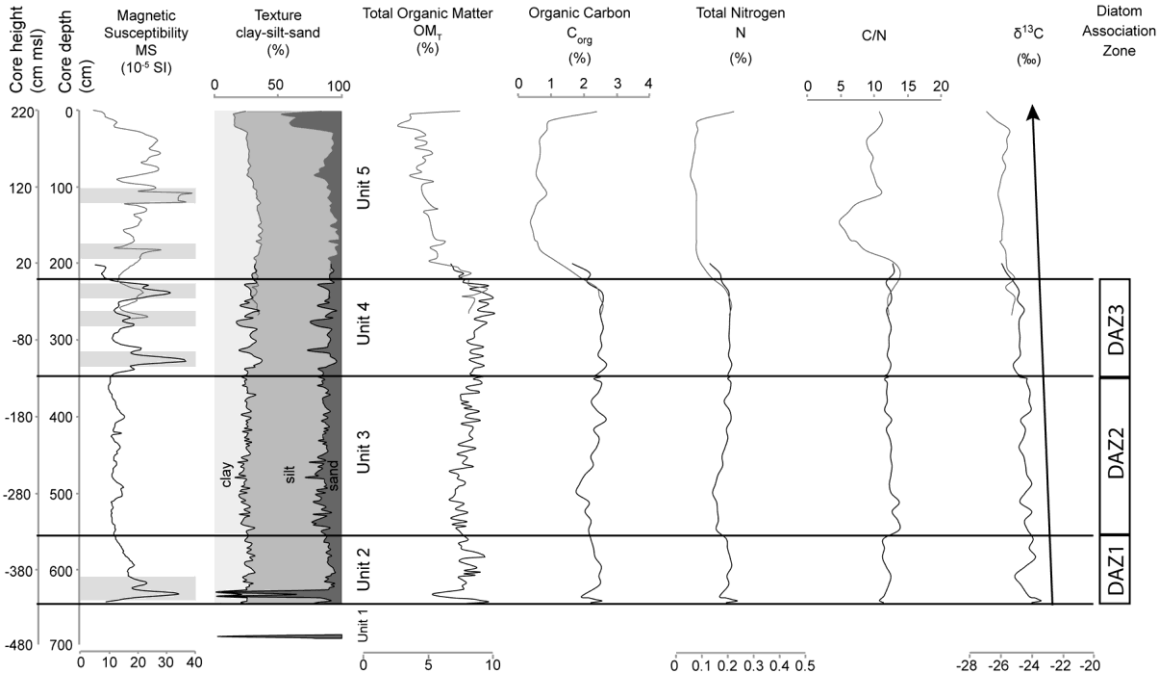

Figure 4.15 - Representation of sedimentological and organic proxies against depth below surface and height: magnetic susceptibility (MS), texture, total organic matter (OM), organic carbon (C_{org}), total nitrogen (N), C/N and $\delta^{13}C$. The black line represents results obtained in Arapouco3 and the grey line results from Arapouco2 sections. Both present the same behaviour on the overlapping region. Grey bars in MS profile represent higher inputs of terrestrial material (see discussion below). Black arrow indicates the decreasing trend of $\delta^{13}C$ upcore.

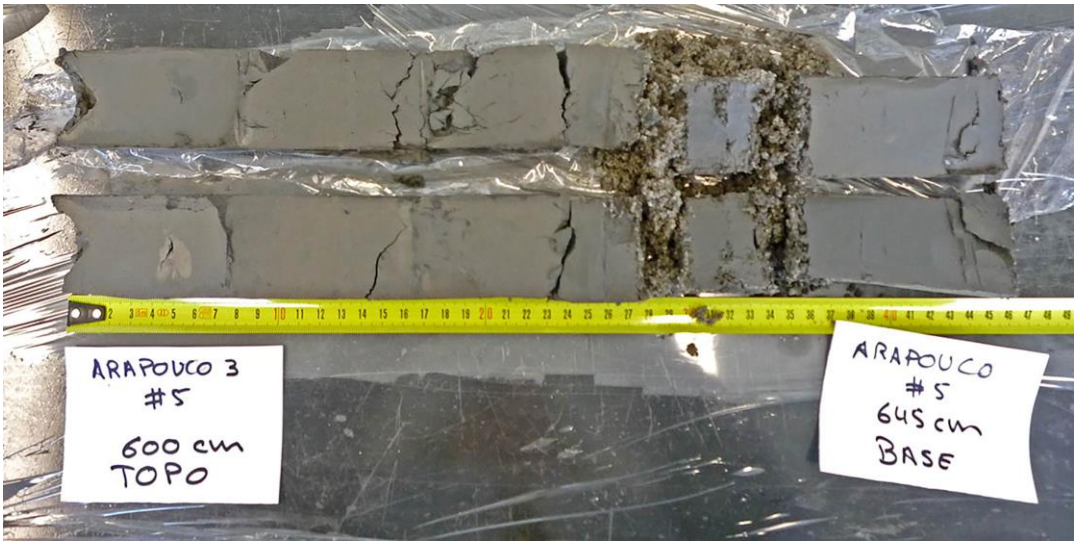

Figure 4.16 - Photo of the base of the Arapouco sediment core during sampling showing the sandy lenses between -407 - -409 cm and -413 - -415 cm MSL.

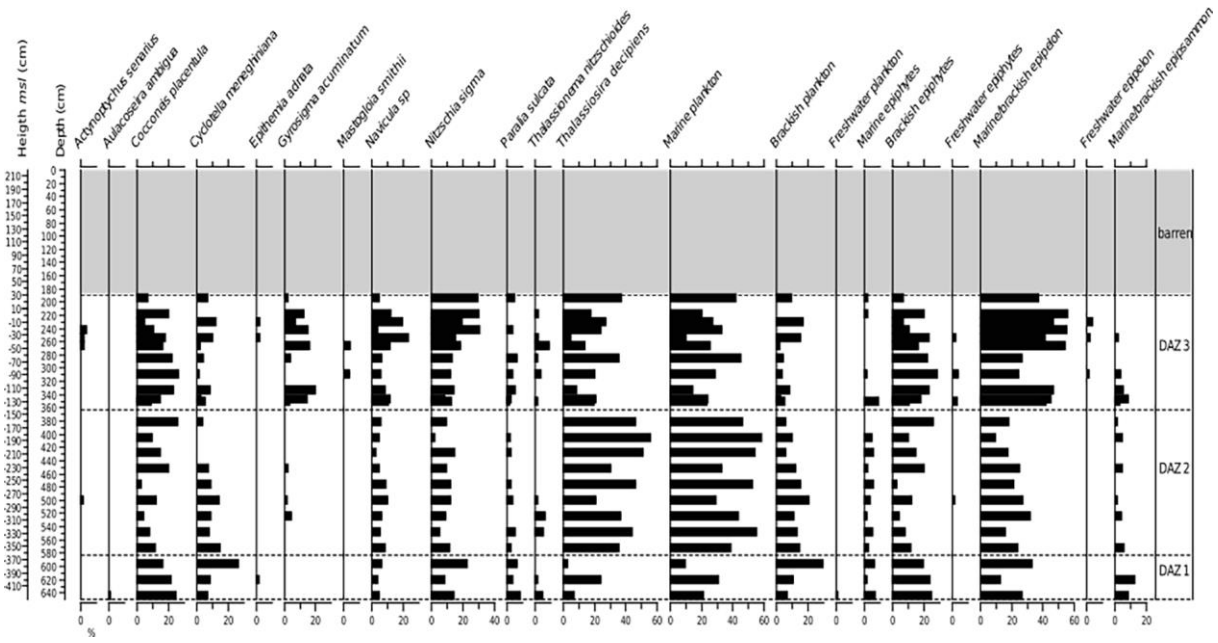

Figure 4.17 – Down-core distribution of selected diatom taxa and diatom-assemblages' zones (DAZ) in the sediment record plotted against core depth and MSL height.

Unit 3 (-350 cm to -130 cm MSL; deposited between ca. 3400 and 3300 cal BP; 1450 and 1350 cal BC) shows the lowest MS values in Arapouco core (average MS of $12x10^{-5}$ (SI), min. of $10x10^{-5}$ (SI) and max. of $15x10^{-5}$ (SI); Figure 4.15). Sediment mostly consists of mud (average 85%; 60% silt and 25% clay) with ca. 15% of sand. The sand is composed by very fine, slightly heterometric, hyaline quartz grains (ca. 99%) and mica. Similarly with Unit 2, vegetal and charcoal fragments were observed and rare *Actinoptychus* spp specimens were identified. Total OM is ca. 8% (Figure 4.15; min. 6.6%, max. 9.1%). Organic carbon presents mean values of 2%, mean C/N ratio of ca. 12, with higher values at the base of the unit (ca. 13.7%). Values for $\delta^{13}C$ are virtually invariant in this unit, averaging -24‰. A whole shell of *S. plana* was found at -295 cm MSL and the diatom assemblage contains almost exclusively the marine planktonic diatoms (DAZ 2; Figure 4.17) *Thalassiosira* species associated with other brackish epipelic and epiphytic taxa such as *Gyrosigma* spp and *Mastogloia* spp. The presence of the also marine planktonic *Thalassionem nitzschioides* is noticeable.

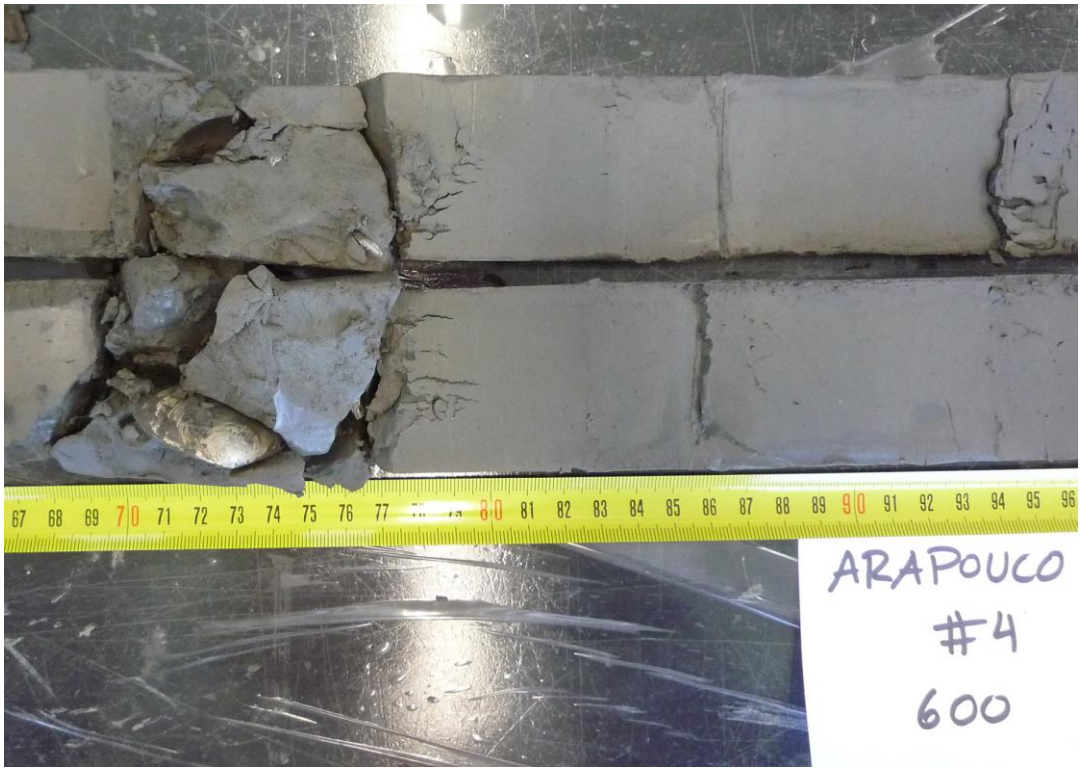

Figure 4.18 - Photo of a whole shell of *Scrobicularia plana* found in the Arapouco sediment core at -354 to -351 cm MSL (574-571 cm depth).

Unit 4 (-130 cm MSL to MSL; deposited between ca. 3300 and 3240 cal BP; 1350 and 1290 cal BC) is characterized by an increase in MS, the susceptibility profile showing regularly spaced MS peaks (MS average $17x10^{-5}$ (SI) and MS maxima at -108 cm MSL ($37x10^{-5}$ (SI)) and -18 cm MSL ($31x10^{-5}$ (SI), min. $9x10^{-5}$ (SI)); Figure 4.15). The sediment is essentially muddy (average 90%; 60% silt and 30% clay; 10% sand). The particles with sand dimension (>63 μm) correspond to coarse vegetal fragments. Rare quartz grains were observed. Total OM presents mean values of 8.4%, C_{org} is of 2.4% and C/N ratio increases from 12 at the base of the unit to 14 at MSL. $\delta^{13}C$ varies between -24.5 and -26‰ decreasing upwards (Figure 4.15).

In what concerns diatom content, the most significant feature in this unit is the reduction of the previously dominant marine planktonic diatoms and the increase in the proportion of brackish/freshwater to freshwater taxa (DAZ 3; Figure 4.17). The transition is mainly characterized by marine, marine/brackish and brackish/freshwater diatoms, with *Cocconeis* spp and *Nitzschia* spp as dominant species. The dominance of epiphytic diatoms suggests shallow water with abundant macrophytes. Similarly, the dominance of *Cocconeis* spp and *Nitzschia* spp associated with *Cyclotella* sp. aff. *meneghiniana* suggests brackish conditions. Marine/brackish to

brackish epipelic diatom assemblages associated with species such as *C. placentula* also occur in this unit.

Unit 5 (MSL to 220 cm MSL; after 3240 cal BP; after 1290 cal BC) represents the 2 uppermost meters of Arapouco core. It is characterized by MS values between $4.5x10^{-5}$ (SI) and $38x10^{-5}$ (SI) with the lower values ($4.5x10^{-5}$ and $10x10^{-5}$ (SI)) measured in the top 10 cm (Figure 4.15). MS peaks occur between 112 cm and 100 cm MSL (maximum value of $38x10^{-5}$ (SI)) and between 146 cm and 182 cm with values of ca. $27x10^{-5}$ (SI). The sediment is mostly composed by mud (averaging 87%; 58% silt and 29% clay; 13% sand; Figure 4.15). However, above 100 cm the content in sand increases: a peak in sand proportion was found at ca. 80 cm (ca. 22% of sand) and in the topmost 30 cm and constitutes ca. 50% of the total sediment. The coarse fraction (>63 μm) corresponds to sand <1 mm and is mainly composed by quartz grains. Iron oxides are frequent among the sand. Total OM gradually decreases upwards, presenting mean values of ca. 5% (min. of 2.7 and max. of 6.3%; Figure 4.15). Organic carbon shows the lowest values found in the core with mean values of 0.8%. The three upmost samples show an increase in C_{org} from 1% to 2.4% at the very top sample. Between 0 m MSL and 110 cm MSL a marked decrease in the C/N ratio (mean value of. 6.6) is observed, related with the decrease in the proportion of C_{org} (N_{Tot} is almost constant). From 110 cm MSL to the top of the core C/N ratios show values around 10. $\delta^{13}C$ values vary between -25 and -27‰ with lower values at the top. In this unit the diatom record is mostly composed by fragments, making impossible the identification of correspondent species.

Laxique 1

Laxique 1 is the most upstream core studied in the present work. The sediment core is mostly constituted by grey to brown sandy mud (Coarse fraction (CF) between 20% and 40%), slightly sandy mud and mud (CF lower than 20%; Figure 4.19A) excepting the most basal sample (-195 to -200 cm MSL), characterized as sandy gravel (63% gravel, 37% sand and negligible amounts of mud; Figure 4.19A). The coarse fraction is essentially constituted by quartz, with very rare to slightly abundant heavy minerals, micas (biotite and muscovite). Very rare to rare macroplant remains (e.g., wood fragments, seed, fibres, spores) are present in all samples. The gravel and sand components of the basal sample are constituted by angular centimetric clasts containing essentially quartz and quartzite and, at a lesser extent, by shale, granite, greywacke and sandstone, among other less representative rock materials. Despite only the top 5 cm sediment of this coarse unit were sampled and no other analyses were performed, a basal Unit 0 was established, at least

between -440 m and -195 m MSL, until where the corer sample drilled (Figure 4.19). The ERT profile performed near Laxique is consistent with the existence of coarse material in depth (Mota, 2017). However, deep boreholes crossing the infilling are needed to confirm this hypothesis.

Above -195 m, changes in depth in all the analysed proxies were identified and based on these changes Laxique 1 was divided in 6 main sedimentary units, which were subdivided in smaller sub-units, when necessary, due to profile changes in one or more proxies (Figure 4.19, 4.20 and 4.21). In general, organic materials seem to be enriched in terrestrial and/or fluvial compounds, at least, according to the $\delta^{13}C$, C/N and POC values (Figure 4.20; e.g., Meyers, 1994; Lamb et al., 2006; Alonso-Hernandez et al., 2017). Sedimentary statistic parameters are presented in Table 4.3.

Unit 1 (between -195 cm and -160 cm MSL; ca. 4400 and 4350 cal BP; 2450 and 2400 cal BC) is constituted by brown slightly sandy mud coarsening upwards to a sandy mud associated with a peak in the MS between -187 and -161 cm MSL reaching values of $86x10^{-5}$ (SI) (Figure 4.19A; Table 4.3). The sand content may, in part, be associated with bioturbation (described while sampling). Most quartz grains present clean surface, but some show orange colours related to Fe coating. The OM content is low which is consistent with the low contents of C_{org} and N and the C/N ratio presents constant values around 10 (Figures 4.20 and 4.21). The $\delta^{13}C$ and the $\delta^{15}N$ reflect a freshwater/terrestrial source for the organic material (Figures 4.20 and 4.21; Lamb et al., 2006; Khan et al., 2015).

Unit 2, only 30 cm thick (between -160 and -130 cm MSL; ca. 4350 and 4300 cal BP; 2400 and 2350 cal BC), is marked by abrupt changes in several analysed proxies. Similarly to Unit 1, it is characterized as a slightly sandy mud with low contents of coarse materials. In the coarse fraction, very rare to rare fibrous gypsum occur. Magnetic susceptibility is low (Figure 4.19A) with the maximum MS values recorded at the top of the unit, reaching $27x10^{-5}$ (SI) at -130 cm MSL. Total OM, C_{org} and N increase in relation to Unit 1, as well as the C/N ratio (Figure 4.20; Table 4.3). Notwithstanding, $\delta^{13}C$, $\delta^{15}N$ and nutrients have similar values to Unit 1, with the NO_3^- presenting the highest values of the sedimentary succession, above 90 mg kg^{-1}.

Table 4.3 - Sedimentological and chemical statistic parameters of the defined units for the Laxique sediment core. CF - Coarse fraction (>63 μm); MS - Magnetic susceptibility; OM - Total organic matter; N - Total nitrogen; C_{org} - Organic carbon; NO_3^- - Nitrates; PO_4^{-3} - Phosphates; P - Total phosphorus; SO_4^{-2} - Sulphates. To be continued.

			CF (%)	**MS x 10^{-5} SI**	**OM (%)**	**N (%)**	**$\delta^{15}N$ (‰)**	**C_{org} (%)**	**$\delta^{13}C$ (‰)**	**C/N**	**NO_3^- (mg kg^{-1})**	**PO_4^{-3} (mg kg^{-1})**	**P (mg kg^{-1})**	**SO_4^{-2} (mg kg^{-1})**
UNIT 6	SU-6C	average	14.8	35.6	4.2	0.10	6.4	0.90	-25.6	9.3	19.5	1101.3	366.5	70.8
		max.	21.8	60.5	6.7	0.18	7.5	1.89	-24.6	10.3	37.3	1731.6	480.4	106.6
		min.	10.1	13.7	3.1	0.05	5.7	0.43	-26.3	8.0	11.7	624.3	279.6	32.4
	SU-6B	average	17.1	38.2	4.5	0.11	6.3	1.09	-25.4	9.8	29.2	1145.0	406.2	111.6
		max.	19.2	61.3	5.6	0.14	6.7	1.46	-25.0	10.8	35.7	1354.4	460.4	141.8
		min.	13.2	28.2	3.1	0.07	5.9	0.59	-25.7	7.9	25.3	828.3	342.6	73.4
	SU-6A	average	11.1	62.0	3.7	0.06	7.2	0.55	-25.2	8.9	23.9	1072.6	350.2	65.6
		max.	17.9	76.7	4.8	0.09	8.3	0.93	-24.8	9.8	38.7	1249.5	505.5	103.6
		min.	3.6	30.6	2.9	0.05	6.4	0.45	-25.7	8.1	14.8	590.6	250.4	19.8
UNIT 5		average	5.0	22.9	4.7	0.07	6.0	0.78	-26.5	10.8	22.9	692.5	295.4	252.1
		max.	12.5	32.7	5.8	0.09	7.4	1.08	-26.2	12.0	32.8	1261.9	428.1	535.8
		min.	1.9	6.6	3.8	0.05	5.2	0.54	-26.8	9.9	13.6	46.3	173.1	59.6
UNIT 4		average	21.4	30.4	5.3	0.05	5.7	0.50	-26.2	9.6	42.1	1472.2	304.4	218.4
		max.	43.2	37.9	5.4	0.07	6.4	0.74	-25.8	11.0	63.2	2404.3	362.0	431.7
		min.	5.9	17.5	3.4	0.04	4.6	0.32	-26.5	7.8	7.7	181.4	225.2	28.6

Table 4.3 - Continuation.

			CF (%)	MS x 10^{-5} SI	OM (%)	N (%)	$\delta^{15}N$ (‰)	C_{org} (%)	$\delta^{13}C$ (‰)	C/N	NO_3^- (mg kg^{-1})	PO_4^{-3} (mg kg^{-1})	P (mg kg^{-1})	SO_4^{-2} (mg kg^{-1})
UNIT 3	SU-3B	average	11.8	15.2	5.3	0.06	5.1	0.62	-26.1	9.9	49.0	1569.6	245.5	64.9
		max.	34.0	21.1	6.3	0.07	5.7	0.84	-26.0	11.5	51.4	1798.8	379.3	66.5
		min.	3.6	12.6	4.3	0.04	4.7	0.36	-26.2	8.1	46.6	1340.5	111.7	63.2
	SU-3A	average	13.6	13.2	6.0	0.10	5.0	1.16	-25.9	11.9	10.6	101.4	146.8	3885.7
		max.	40.5	8.8	7.3	0.12	5.2	1.46	-25.6	12.8	31.4	193.3	311.2	22430.6
		min.	1.9	28.2	4.8	0.07	4.9	0.80	-26.2	11.3	0.8	69.0	107.2	215.8
UNIT 2		average	15.2	15.1	6.9	0.14	5.0	1.82	-25.9	13.0	117.8	1332.2	257.5	403.9
		max.	25.35	26.6	7.6	0.15	5.1	1.86	-25.9	13.2	117.8	1332.2	257.5	403.9
		min.	7.2	7.7	5.6	0.14	4.9	1.79	-26.0	12.6	117.8	1332.2	257.5	403,90
UNIT 1		average	23.5	49.8	4.1	0.05	6.0	0.46	-26.1	9.8	108.6	1644.0	380.8	488.5
		max.	31.2	85.8	4.9	0.05	6.4	0.55	-26.0	10.2	126.9	1685.6	404.3	541.2
		min.	15.4	32.4	3.5	0.04	5.7	0.41	-26.2	9.5	90.3	1602.4	357.3	435.9

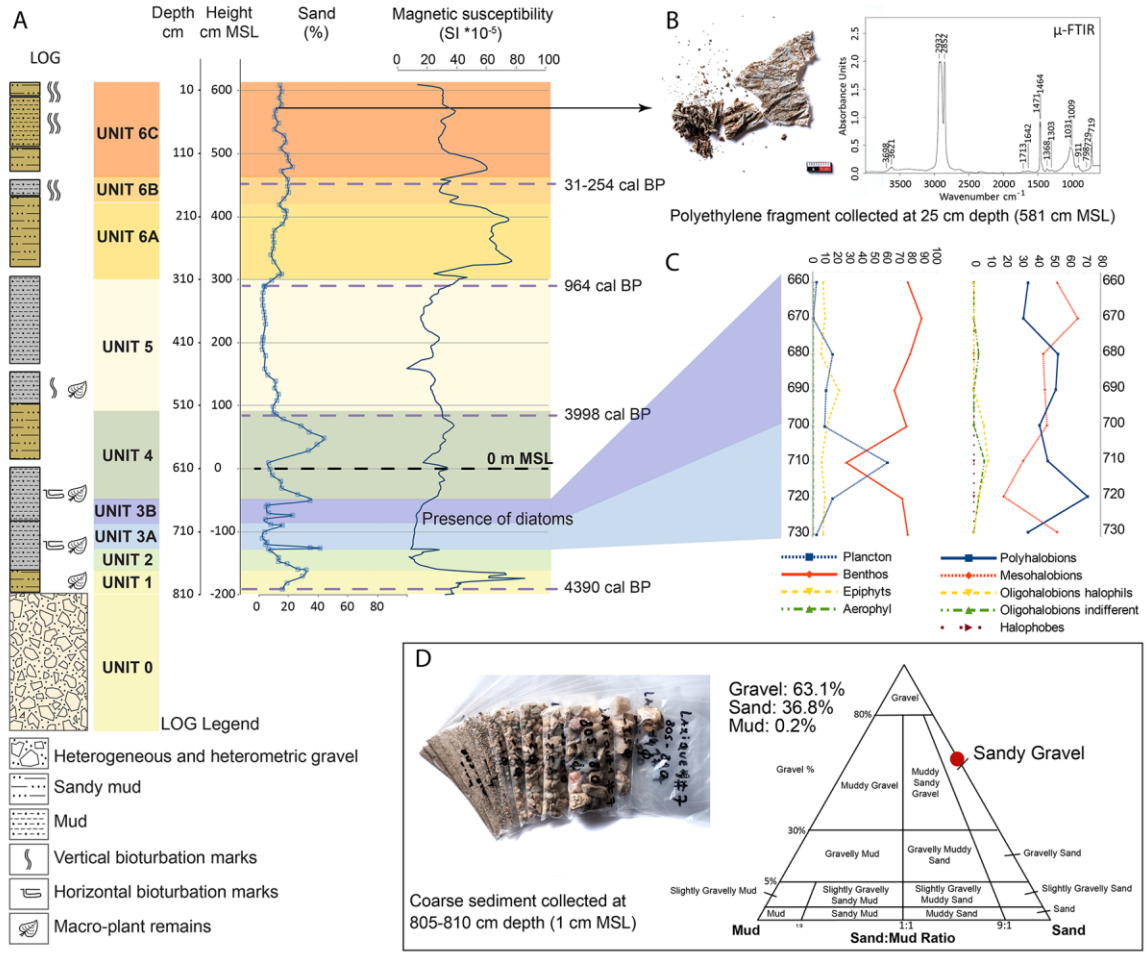

Figure 4.19 - Representation of the different sedimentological units identified in Laxique. A - LOG and representation of sand and magnetic susceptibility (MS) against depth below surface and height, with identification of the depth where the plastic fragment was collected (25 cm core depth). B - Plastic fragment photo and μ-FTIR analyses graph reflecting its components (polyethylene); C - Down-core distribution (between -50 and -120 cm MSL; 660 and 730 cm core depth) of diatom life forms and salinity preferences. D - Photo of the sample collected between -200 and -195 cm MSL separated by ϕ and ternary-plot gravel-sand-mud with representation and classification of the sample collected at the core base, following Folk, 1954. Photos © José Vicente | Agência Calipo.

Unit 3 (between -130 and -50 cm MSL; ca. 4300 and 4200 cal BP; ca. 2350 and 2250 cal BC) was primarily identified due to the presence of diatoms (Figure 4.19C) and higher contribution of marine compounds to the particulate organic carbon (Figure 4.20). It presents low MS response (Figure 4.19A), low $\delta^{13}C$ and $\delta^{15}N$ values and C/N ratio ca. 12. $\delta^{13}C$, C/N and OM decrease progressively upwards, whereas $\delta^{15}N$ content is almost constant (Figure 4.20).

However, the results of the subsequent analyses made possible to distinguish two different sub-units. **Sub-unit 3A** (between -130 and -90 cm MSL; ca. 4300 and 4250 cal BP; ca. 2350 and 2300

cal BC) is constituted by sandy mud at the base and mud to the top (the content of the CF increasing to ca. 15% in the top sample) with low content in particles susceptible to magnetize (Figure 4.19A). Rare quartz grain surfaces present iron oxide coating (FeO) and iron oxide minerals were identified in the base samples as well as gypsum crystals and fibrous and nacreous gypsum grains. Heavy minerals increase to the top. Charcoal fragments only occur in the top samples. The Sub-unit is marked at the base by a sharp peak in the concentration of SO_4^{-2} that reaches values of 22430 mg kg^{-1} at -128 cm MSL (Figure 4.21), being the concentration of SO_4^{-2} always high within this sub-unit despite decreasing progressively upwards (Figure 4.21), similarly to other compounds. The high contents of SO_4^{-2} are probably related to the presence of gypsum crystals. Conversely, the contents of NO_3^-, PO_4^{-3} and P present the lower contents of all the entire sedimentary succession, with the lower concentration of NO_3^- and PO_4^{-3} coincident with the peak of sulphates (Figure 4.21). Despite the low contents of P, a peak occurs at -120 cm MSL with values of 310 mg kg^{-1}. **Sub-unit 3B** (between -90 and -50 cm MSL; ca. 4250 and 4200 cal BP; ca. 2300 and 2250 cal BC) is characterized as slightly sandy and mud, and sandy mud at the very top, according to its contents in coarse sediments (Figure 4.19A). In coarse fraction quartz grains present clean surfaces. Iron oxide minerals occur at the top samples. SO_4^{-2} decreases one order of magnitude to mean values of 66 mg kg^{-1}. Phosphorus has low values at the base of the Sub-unit but increases to values of 330 mg kg^{-1} at the top of the Sub-Unit.

The dominant diatoms at the base of this Unit are polyhalobious diatoms mostly with a planktonic life form such as *Cymatosira belgica*, *Thalassionema nitzschioides*, *Thalassiosira eccentrica* which are later replaced in Sub-unit 3B by benthic species like *Tryblionella navicularis* and *Navicula incerta* with lower salinity preferences (Figure 4.22).

Unit 4 (between -50 and 88 cm MSL; ca. 4200 and 4000 cal BP; ca. 2250 and 2050 cal BC) has variable contents in the CF being characterized as mud until ca. 9 cm MSL, and as slightly sandy mud and sandy mud to the top where MS presents slightly higher values. Unit 4 is characterized by the presence of very rare to rare calcite grains in the coarse fraction at the base and abundant calcite grains at the top near the transition to Unit 5. In addition, FeO minerals are slightly abundant to abundant. Total OM has a decreasing trend to the top and the maximum values of C_{org} and N (0.7% and 0.07%, respectively at 4 and 9 cm MSL) are coincident with the higher contents of OM (Figure 4.20). Similarly to the Units below, $\delta^{13}C$ has values of -26‰ while $\delta^{15}N$ varies between 6.4 and 4.6‰. C/N ratio ranges between 11 and 7.8 (Figure 4.20). The concentration of NO_3^-, PO_4^{-3} and P are similar to Sub-unit 3B but decrease at the top of the Unit (Figure 4.21). However, the transition to Unit 5 is marked by an increase in the PO_4^{-3} and P

contents that reach concentrations of 2400 mg kg^{-1} and 360 mg kg^{-1}, respectively. Sulphates decrease to very low values of 28 mg kg^{-1} at the top of the Unit (Figure 4.21).

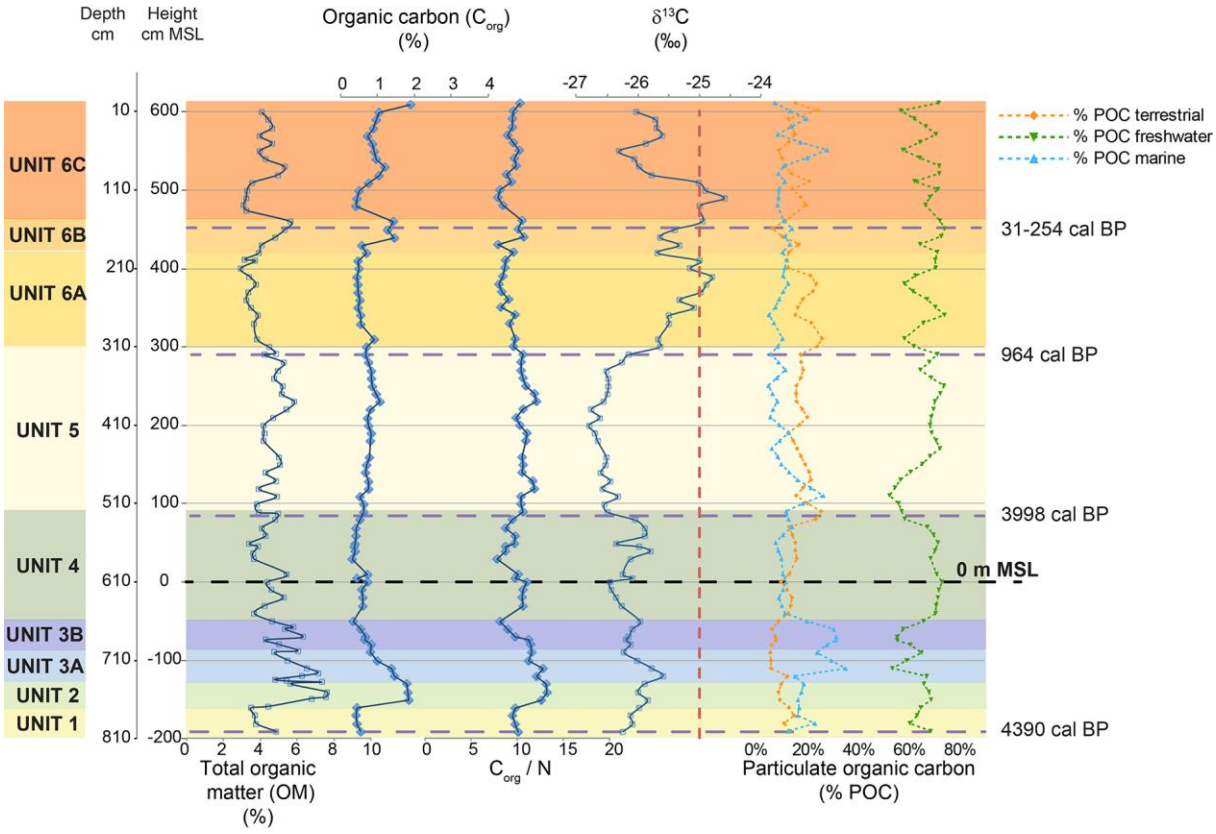

Figure 4.20 - Representation of the organic analysed proxies against depth below surface and height: total organic matter (OM), organic carbon (C_{org}), C/N, $\delta^{13}C$ and particulate organic carbon (POC) with terrestrial, freshwater and marine origin (Alonso-Hernandez et al., 2017).

Unit 5 (between 88 and 289 cm MSL; ca. 4000 and 960 cal BP; ca. 2050 cal BC and 980 cal AD) is composed by very fine sediments (mud) with low contents of CF and low MS values despite the slightly coarser sediments at the base between 88 and 148 cm MSL with CF mean values of 10% (sandy mud) (Figure 4.19A). In coarse fraction quartz grains are coarser than in the units below. Some grains present orange surface due to Fe coating. Iron oxides and orange sandstone fragments were identified above 400 cm (i.e., 210 cm MSL) and slightly abundant ore slag fragments were also identified in the samples above 362 cm (i.e., 250 cm MSL). The OM content has mean values of 4.7%, C_{org} presents mean contents of 0.8% with a maximum value of 1.1% at 230 cm MSL and N shows mean values of 0.07%. The C/N ratio varies between 12 and 9.9, presenting slightly higher values than the Unit 4. $\delta^{13}C$ has the lower values of all the sedimentary succession, always lower the -26‰ and $\delta^{15}N$ varies between 7.4 and 5.2‰, with the higher value measured at 160 cm MSL.

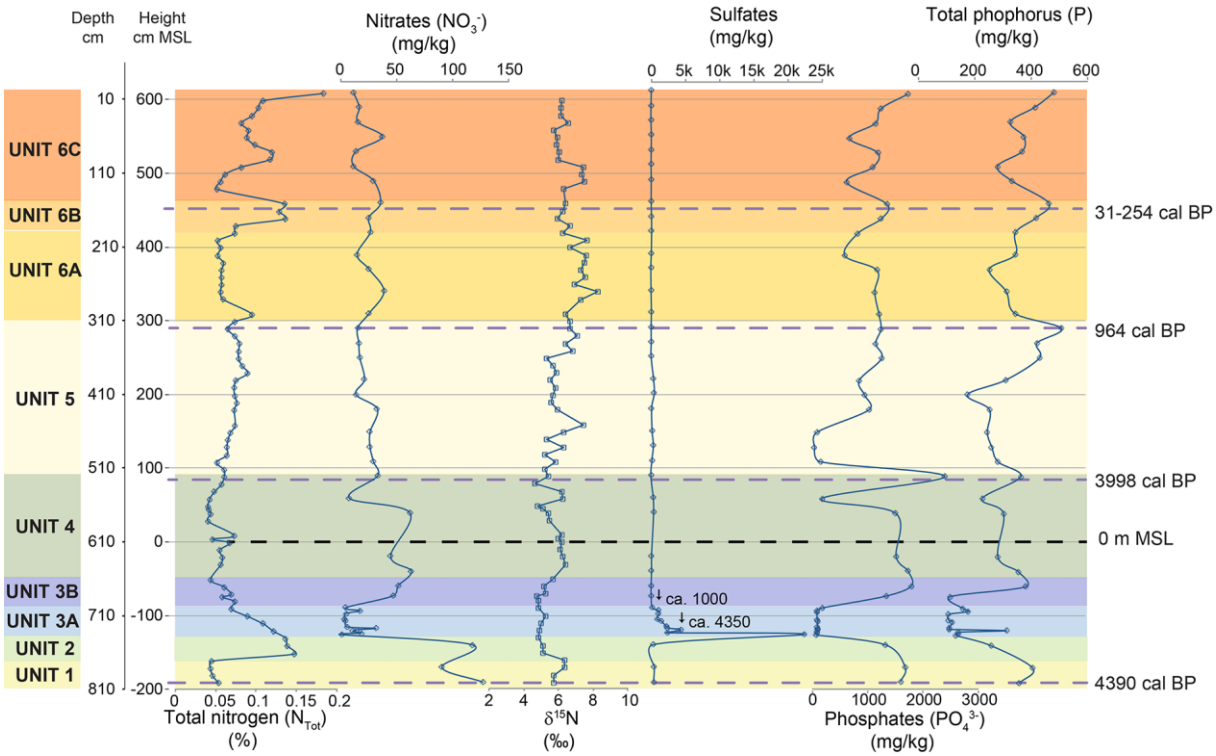

Figure 4.21 - Representation of the nutrients against depth below surface and height: Total nitrogen (N), nitrates (NO_3^-), $\delta^{15}N$, sulphates (SO_4^{-2}), phosphates (PO_4^{-3}) and phosphorus (P).

Sulphates vary between 150 mg kg^{-1} at 180 cm MSL and 536 mg kg^{-1} at 200 cm MSL, decreasing to the top of the Unit to values lower than 80 mg kg^{-1}. The concentration of NO_3^- is low, below 33 mg kg^{-1}. Phosphate's concentration range between 150 and 46 mg kg^{-1} from the base of the Unit until ca. 150 cm MSL, increasing to high values of 1261 mg kg^{-1} upwards. Phosphorus has a diminishing tendency until 200 cm MSL, from where it starts to increase reaching values of 430 mg kg^{-1} at the top of the Unit. No signs of bioturbation were identified while sampling.

Unit 6 corresponds to the top 3 meters of the core deposited during the last ca. 1000 years (between 289 and 610 cm MSL; Figure 4.19A). The Unit was divided in three sub-units based on changes in several proxies, particularly MS, C_{org}, N and $\delta^{13}C$ (Figure 4.20 and 4.21). In general, OM decreases in relation to the Units below and nitrates are almost constant over the Unit presenting low values resumed in Table 3. Sulphates present values lower than 140 mg kg^{-1}.

Sub-Unit 6A (between 289 and 410 cm MSL) is composed by a slightly sandy mud with relative high values of MS ranging between 30-40x10^{-5} (SI) at the base (ca. 289 to 310 cm MSL) and between 50 and 77x10^{-5} (SI) between 310 and 410 cm MSL. The C_{org} and N contents decrease

from maximum values of 0.9% and 0.09% at the base and minimum values of 0.5% and 0.05% at the top, respectively (Figures 4.19A and 4.20) with C/N ranging between 9.8 and 8.1. $\delta^{13}C$ reaches high values of -24.8‰ at ca. 390 cm MSL, one of the higher $\delta^{13}C$ values of the entire sedimentary succession (Figure 4.20). Phosphates decrease upwards from 1250 to 1175 mg kg^{-1}, reaching a low concentration value of 590 mg kg^{-1} at ca. 390 cm MSL and P decrease from ca. 500 mg kg^{-1} to 250 mg kg^{-1} at ca. 370 cm MSL, slightly increasing upwards to ca. 350 mg kg^{-1} (Figure 4.21; Table 3).

Sub-Unit 6B (between 410 and 460 cm MSL) is only 50 cm thick, but it is characterized by increases in the OM (increasing from 3.1% to 5.6%), C_{org} (minimum values of 0.6% at the base, reaching 1.5% at 440 cm MSL), N (increasing from 0.07 at the base to 0.14 at the top), PO_4^{-3} (increasing upwards from ca. 830 to ca. 1350 mg kg^{-1}) and P (also increasing upwards from concentration of 340 to 460 mg kg^{-1}) contents. By opposition, MS values decrease to minimum values of ca. $30x10^{-5}$ (SI). $\delta^{13}C$ is in general lower than Sub-Unit 6A (Figures 4.19A, 4.20 and 4.21).

Sub-unit 6C corresponds to the top 150 cm of the core, deposited during the last 50 years. It is composed by slightly sandy mud, with CF contents always higher than 10%. Among the sediment, a plastic fragment of polyethylene was recovered at ca. 580 cm MSL (Figure 4.19B). It is characterized by a new increase in the MS values with a maximum peak of $61x10^{-5}$ (SI) at the base of the Sub-unit (Figure 4.19A). The OM content decrease, C_{org} has lower values but with two peaks at 520-530 and 600-610 cm MSL exceeding 1% (Figure 4.20). Nitrogen increases from 0.05% at the base to 0.18% at the very top, but two values of 0.12% were measured between 520 and 530 cm MSL (Figure 6). Phosphates and P have similar behaviours varying between 624 and 1731 mg kg^{-1} and 280 and 480 mg kg^{-1}, respectively (Figure 4.21) with the higher values at the very top of the core.

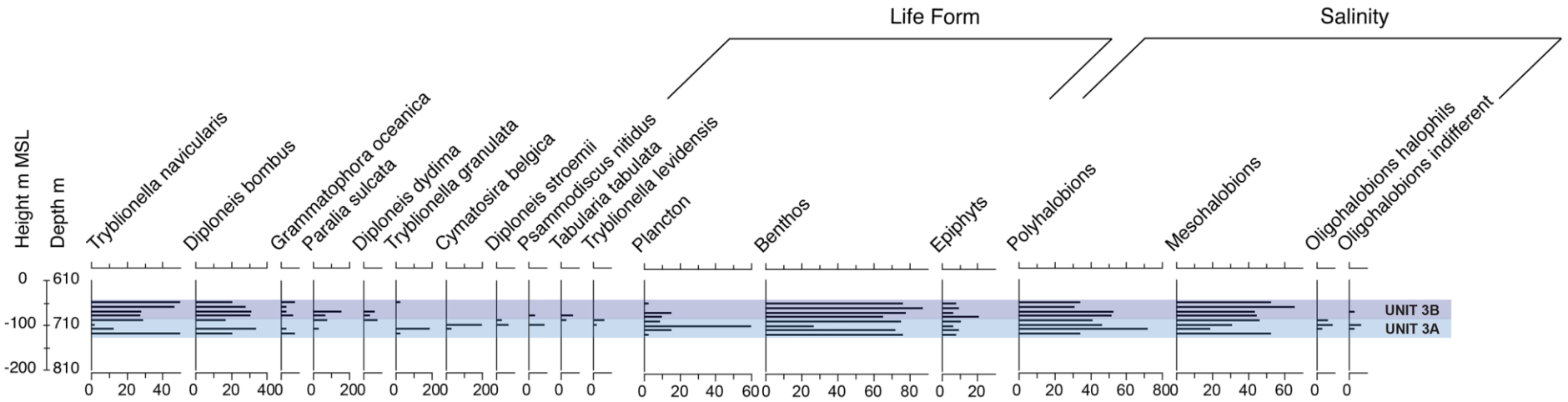

Figure 4.22 - Diatom taxa, life form and salinity preferences in Sub-units 3A and 3B, from Laxique.

Arez3

In the Arez3 core, three sedimentary units were identified considering changes in the analysed proxies (Figures 4.23 and 4.24). The interval of deposition for each unit was determined considering the proposed age-model (Figure 4.8). Sedimentological statistic parameters are presented in Table 4.4. and organic geochemistry results are resumed in Table 4.5. Following the pattern of the other sediment cores, calcium carbonate results indicate null or negligible amounts (<1.5% on the analysed samples), even in the samples where foraminifera shells were identified (Figure 4.23).

Table 4.4 - Sedimentological statistic parameters from the Arez3 core. MS - Magnetic susceptibility; Mud (fraction <63 μm); Sand (fraction >63 μm).

			MS $x10^{-5}$ (SI)	Texture		Total organic matter (%)
				Mud (%)	Sand (%)	
Unit 3		average	21.1	77.5	22.5	5.2
		max.	107.8	96.6	76.5	11.2
		min.	3.3	23.5	3.4	1.1
Unit 2	Sub-unit 2C	average	40.3	99.2	0.8	5.7
		max.	130.4	99.8	5.9	6.3
		min.	14.6	94.1	0.2	4.2
	Sub-unit 2B	average	35.7	98.8	1.6	7.3
		max.	192.8	99.8	2.6	9.8
		min.	11.3	97.4	0.2	6.2
	Sub-unit 2A	average	20.3	98.2	1.8	7.8
		max.	157.5	99.7	3.8	9.7
		min.	9.8	96.2	0.4	6.3
Unit 1		average	28.2	97.2	2.8	8.1
		max.	562.2	99.7	13.1	10.5
		min.	3.0	86.9	3	6.5

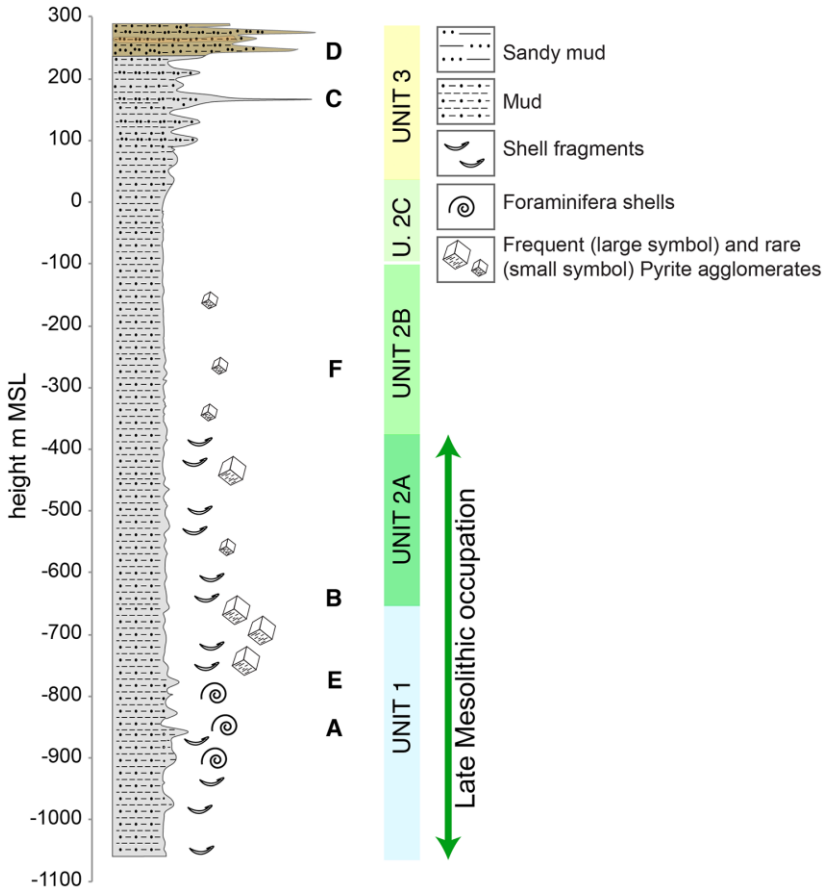

Figure 4.23 - Arez3 LOG and representation of coarse fraction principal constituents. Letters in the profile correspond to the CF photos presented in Figure 4.25.

Table 4.5 - Statistic parameters (mean values) considering the organic geochemistry results: organic carbon (C_{org}), total nitrogen (N), C/N, $\delta^{13}C$ and $\delta^{15}N$; and diagnostic *n*-alkane ratios: Carbon Preference Index (CPI), Terrigenous/aquatic ratio (TAR), Terrestrial-marine discriminate index (TMD), Pristane (Pr) over Phytane (Ph) ratio (Pr/Ph), Pristane to *n*-alkane C_{17} (Pr/C_{17}) and Phytane to *n*-alkane C_{18} (Ph/C_{18}).

		UNIT 1	SUB-UNIT 2A	SUB-UNIT 2B	SUB-UNIT 2C	UNIT 3
Quantification and isotopic characterization of organic matter	C_{org} (%)	1,90	1,32	1,25	1,01	1,37
	N (%)	0,14	0,12	0,12	0,10	0,12
	C/N	13,83	10,84	10,38	10,38	11,30
	$\delta^{13}C$ (‰)	-24,95	-25,35	-25,74	-26,01	-25,92
	$\delta^{15}N$ (‰)	4,37	4,15	4,11	3,90	5,36
Diagnostic *n*-alkanes ratios	CPI	1,08	1,13	0,99	1,05	0,97
	P_{aq}	0,78	0,80	0,75	0,72	0,72
	TAR	0,11	0,09	0,04	0,13	0,33
	TMD	1,31	1,39	1,37	1,26	1,17
	Pr/Ph	0,44	0,55	0,52	1,04	0,87
	Ph/C_{18}	0,47	0,57	0,81	0,21	0,32
	Pr/C_{17}	0,29	0,42	0,48	0,29	0,15

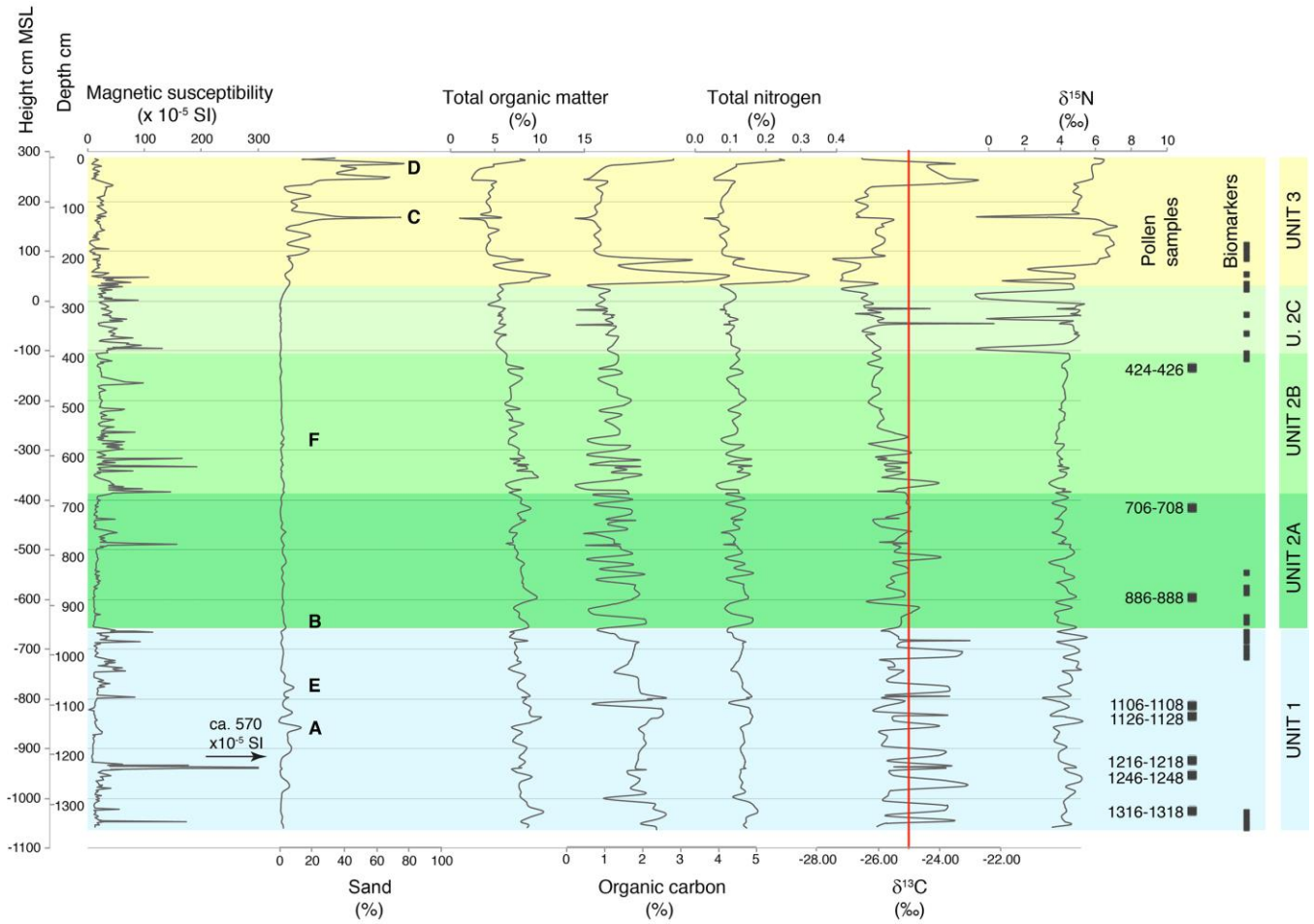

Figure 4.24 - Representation of sedimentological and organic proxies against height cm MSL and depth cm: magnetic susceptibility (MS), sand, total organic matter (OM), organic carbon (C_{org}), total nitrogen (N), $\delta^{13}C$ and $\delta^{15}N$. The red line in the $\delta^{13}C$ profile represents the -25‰ value, the limit that usually is used to distinguish between terrestrial/freshwater and marine organic materials (e.g., Lamb et al., 2006; Khan et al., 2015). Letters in texture in-depth profile correspond to the CF photos presented in Figure 4.25.

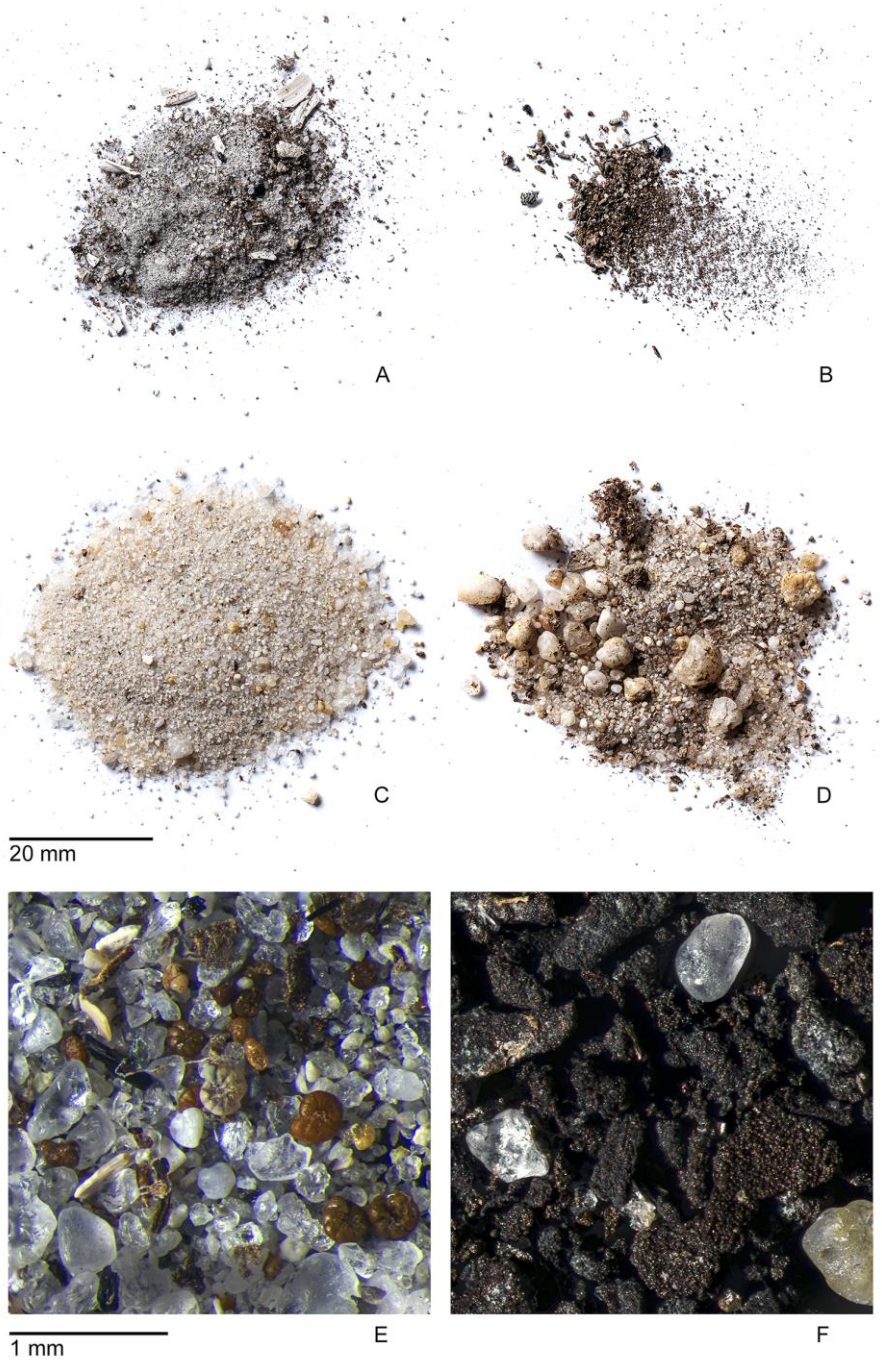

Figure 4.25 - Total coarse fraction content from: A - Unit 1, sample Arez3#12 1146-1148, located at -857 cm MSL; B - Unit 1, transition Unit 1/2, sample Arez3#11 966-968, located at -677 cm MSL; C - Unit 3, samples Arez3#2 121-123, located at 168 cm MSL; D - Arez3#1 14-16, located at 275 cm MSL. E - Detail of coarse material showing several foraminifera shells, from Unit 1, sample Arez3#12 1066-1068, located at -777 cm MSL; F - Detail of coarse material showing pyritized plant remains, from Sub-Unit 2B, sample Arez3#7 566-568, located at -277 cm MSL. Photos © José Vicente | Agência Calipo | 2020-2021.

Unit 1 (-1060 to -677 cm MSL; 8850 to 7450 cal BP; 6900 to 5500 cal BC) is constituted by mud and slightly sandy mud with high contents of OM (>5%; Table 4.4), organic carbon (>1.2% with

exception of 2 values lower than 1%) and nitrogen (>0.1%; Figure 4.24). The CF is low (mostly <10%; Table 4.4). The coarse material is essentially composed by heterometric, fine to medium, quartz grains, shell (gastropods) and shell fragments (e.g., *S. plana*?, *Cerastoderma* sp?, gastropods) and macro plant remains (Figure 4.25A). Usually, quartz grains predominate when the sediment is coarser and plant remains are dominant when the CF has lower %. Frequent foraminifera and rare ostracod valves were identified between -958 and -776 cm MSL (Figure 4.25E). The foraminifera assemblage is constituted essentially by *Haynesina germanica*, *Ammonia tepida*, *Elphidium gunteri oceanensis*. *Anomalinoides cf. globosus* specimens are also common and *Ammonia aoteana* occurs in low percentages. Above -746 cm MSL pyrite is frequent together with quartz and pyritized macro plant remains (similar to Sub-unit 2B; Figure 4.25F). Magnetic susceptibility is low, but several peaks with higher MS values were measured, including a peak ca. -940 cm MSL that reaches values of $570x10^{-5}$ (SI), the highest value of all the sedimentary column (Figure 4.24). $\delta^{13}C$ is quite variable in this unit, varying constantly between maximum values of -23‰ and minimum values of -26‰.

Unit 2 (-677 to 33 cm MSL; 7450 to 4910 cal BP; 5500 to 2960 cal BC) is constituted by mud with the CF always <1%. Total organic matter, C_{org} and N are slightly lower than Unit 1 and vary between 9.8 and 6.2%, 2.1 and 0.3% and 0.17 and 0.06%, respectively, with an upward decreasing tendency (Figure 4.24). Taking into consideration in-depth changes in MS, $\delta^{13}C$ and $\delta^{15}N$, three Sub-Units were defined. **Sub-Unit 2A** (-677 and -390 cm MSL; 7450 to 7040 cal BP; 5500 to 5090 cal BC) has a low MS response, $\delta^{13}C$ is quite constant with mean values of -25‰ and $\delta^{15}N$ has mean values of 4.1% (Figure 4.24). The CF is essentially composed by quartz, with the top samples (above -440 cm MSL) mostly composed by pyritized macro plant remains. Pyrite was identified in this Sub-unit, more frequent in the base. Foraminifera shells also occur at the base of the Sub-Unit, mostly represented by *H. germanica*, *A. tepida* and *E. gunteri oceanensis*. **Sub-Unit 2B** (-390 to -107 cm MSL; 7040 to 6530 cal BP; 5090 to 4580 cal BC) is characterised by a higher frequency in the MS peaks, the $\delta^{13}C$ decreases upwards to lower values of -26‰, while $\delta^{15}N$ has mean values of 4.2% similar to the Sub-Unit below (Figure 4.24). The Sub-Unit´s CF is similar to the top samples of Sub-Unit 2A, essentially constituted by pyritized macro plant remains with occasional pyrite agglomerates (Figure 4.25F). **Sub-Unit 2C** (-107 to 33 cm MSL; 6530 to 4910 cal BP; 4580 to 2960 cal BC) is characterised essentially by changes in the $\delta^{13}C$ and $\delta^{15}N$ values. $\delta^{13}C$ reaches the highest value of -22‰ of the entire sedimentary column at -47 cm MSL. $\delta^{15}N$ has several negative peaks with values <1‰ (Figure 4.24). The transition between Unit 2 and Unit 3 is marked by peaks in the organic material (OM, C_{org} and N) that reach maximum values of 11, 4.2 and 0.3%, respectively at 53 cm MSL (Figure 4.24). The CF is composed by Fe

concretions (more abundant in the base of the Sub-unit) and quartz grains with Fe coating (more abundant at the top).

Unit 3 (33 to 290 cm MSL; 4910 cal BP to present; 2960 cal BC to present) is essentially characterized as slightly sandy mud and sandy mud, with muddy sand intercalations at 167 cm and between 245 and 250 cm MSL where the CF is >60% (Figure 4.24). The coarse material is mostly composed by quartz grains, some presenting Fe coating, and Fe concretions (Figure 4.25C and 4.25D). The sample collected at 275 cm MSL differs from the other samples being essentially composed by very heterometric quartz grains. Between the base of the Unit (33 cm MSL) and 53 cm MSL, $\delta^{13}C$ values have minimum values of -27‰, the lowest of the sequence (Figure 4.24), increasing after to mean values of -26‰. The top 50 cm present high mean $\delta^{13}C$ values of 23‰, decreasing in the very top to values of -26‰. In Unit 3, very low $\delta^{15}N$ values were also measured at the base and at 168 cm MSL, but between 83 and 163 cm MSL values are high with mean values of 6.5‰. In the top 115 cm, $\delta^{15}N$ values present an increasing tendency, growing from values of 4.7 to values of 6.4‰ (Figure 4.24).

Considering biomarkers, in total, 30 samples were analysed for *n*-alkane content (C_{12} to C_{32}), all with enough material for *n*-alkane analysis. The concentration of *n*-alkanes ranges between 0.06 and 28.1% of total abundance (with exception of C_{30} that was not identified in sample Arez3#4 266-268). In general, short-chain *n*-alkanes are more abundant in samples from all the Units (Figure 4.26). Despite scarcer, long-chain *n*-alkanes presented higher concentrations in samples from Unit 3 (Figure 4.26). The *n*-alkane C_{15} is the most abundant in all samples with mean values of 16.3% of total abundance (max = 25.0% of total abundance, Arez3#4 356-358, Unit 2C; min = 5.4% of total abundance, Arez3#3 236-238, Unit 1), with exception in samples Arez3#3 204-206 (most abundant *n*-alkane C_{25}; 7.8% of total abundance), Arez3#3 236-238 (most abundant *n*-alkane C_{23}; 8.1% of total abundance; both from Unit 3) and Arez3#11 1006-1008 (Unit 1; most abundant *n*-alkane C_{14}; 28.1% of total abundance) (Figure 4.26).

The discriminant analysis performed to check the distribution of all *n*-alkanes by the different sedimentary units resulted in an outstanding prediction potential with 100% of the cases grouped in five different clusters corresponding to the Units and Sub-units previously defined (Figure 4.27). The result indicates that Units/Sub-units were well separated considering the *n*-alkane concentration and that the source of organic materials differs between each Unit/Sub-unit.

Pristane (Pr) and Phytane (Ph) acyclic isoprenoids were also identified in all samples. Pristane maximum values (4.2% of total abundance) occur at -117 and -577 cm MSL (Sub-unit 2B and 2A) and the minimum value (0.5% of total abundance) was measured at -697 cm MSL (Unit 1).

Phytane presents maximum values of 8.8% of total abundance at -667 cm MSL (Sub-unit 2C) and minimum values of 0.3% of total abundance at 85 cm MSL (Unit 3).

In-depth variations of *n*-alkanes proxy ratios are presented in figure 4.28, reflecting differences in the depositional environment and organic matter source. CPI values vary between 1.4 and 0.6, with maximum values at the base of Unit 1 and minimum values at the top of Unit 1. P_{aq} ratio is always higher than 0.6, excepting the sample at -667 cm MSL (Sub-unit 2C). TAR is always below 1 with two small peaks in the top of Unit 1 (at -697 and -667 cm MSL; Figure 4.28) and two peaks at the base of Unit 3 (at 53 and 85 cm MSL; Figure 4.28). TMD varies between 0.9 at 85 cm MSL and 1.5 at -587 cm MSL and Ph/Pr ratio has values lower or equal to 0.8 with some values higher than 0.9 in Sub-unit 2C and Unit 3 (Figure 4.28). Ph/C_{17} and Pr/C_{18} present always low values, with maximum mean values of 0.81 and 0.48 represented in Sub-unit 2B (Table 3.3) pointing to low degradation of *n*-alkanes (e.g., Wang et al., 2008).

Considering the Arez3 core pollen analyses, most of the samples display high values of non-arboreal pollen grains, with exception of the samples collected at -1027 (Unit 1) and -417 cm MSL (Sub-unit 2A; Figure 4.29). However, it must be considered that the main herb represented in this set of samples is Asteraceae Cichorioideae, a taxa with ambiguous significance that may act as indicator of open-ground environments, anthropogenic activities, or marsh flora (Fletcher et al., 2007). Its local character could imply an overrepresentation of the taxa depending on the scenario, so their values should be carefully taken into consideration.

The vegetation in Unit 1 is mainly composed of mixed forests of evergreen and deciduous *Quercus* accompanied by Mediterranean pines (*Pinus halepensis-pinea* type and *Pinus pinaster*) (Figure 4.29). Riparian communities are primarily composed by *Alnus* (alder) and they experience a progressive rise from the bottom to the top of the sequence. Unit 1 displays high values of Asteraceae Cichorioideae and the highest percentages of Chenopodiaceae, typical from salt marshes, also appear in this section of the core. The presence of *Isoetes* (freshwater marsh), although permanent and abundant throughout the sequence, seems to be slightly lower in this Unit. It is noteworthy to highlight a slight but progressive increase of heaths since -717 cm MSL (Figure 4.30).

Foraminiferal linings (sample -1027 cm MSL), dinoflagellates (sample -817 cm MSL), and some specific types of diatoms, such as *Paralia sulcata*, *Triceratium* and *Diploneis* were punctually identified (Figure 4.30).

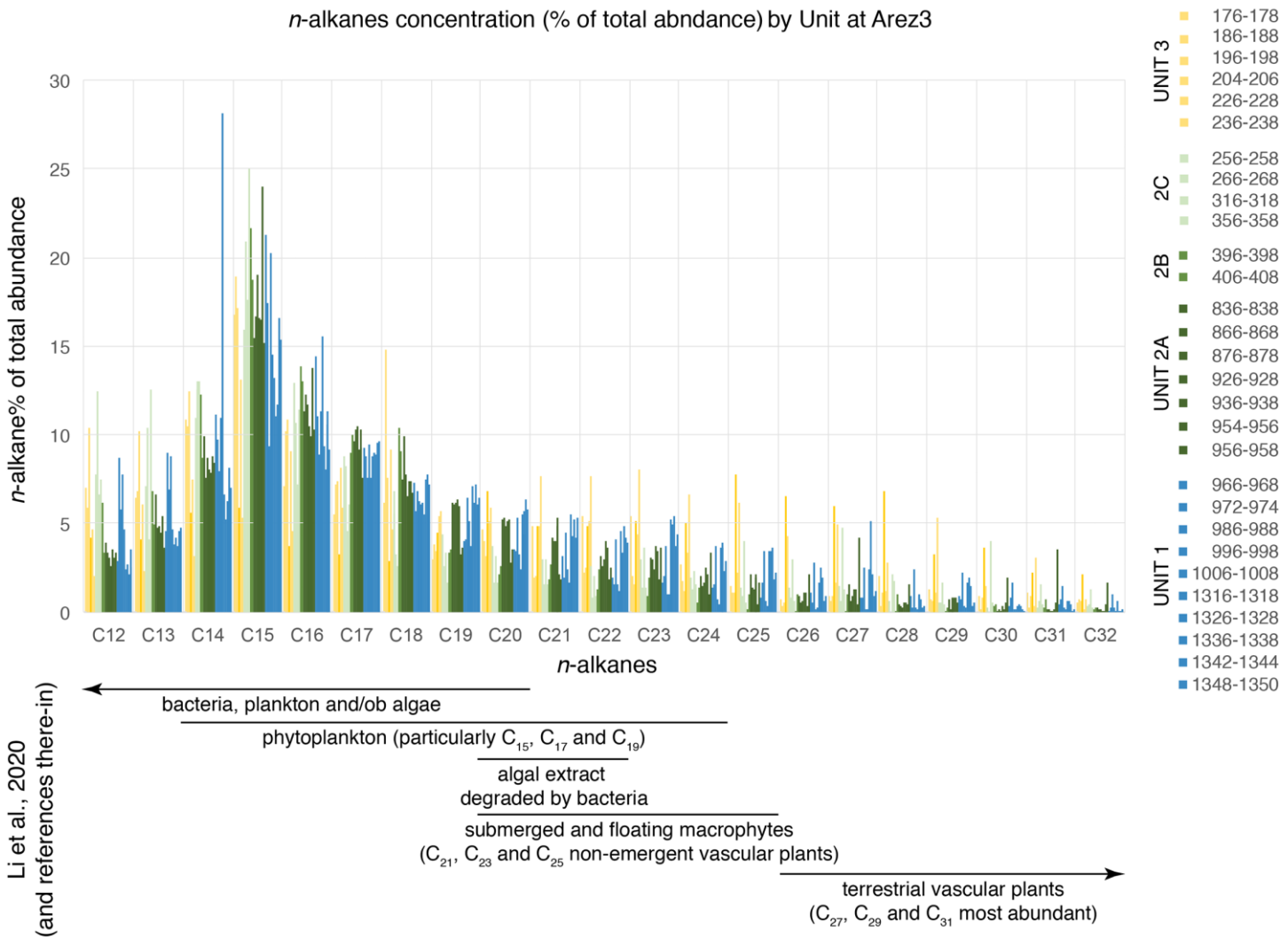

Figure 4.26 - *n*-alkane % of abundance in Arez3 core and organic carbon source information derived from *n*-alkanes retrieved from Li et al. (2020) and references there-in. Colours correspond to the defined Units.

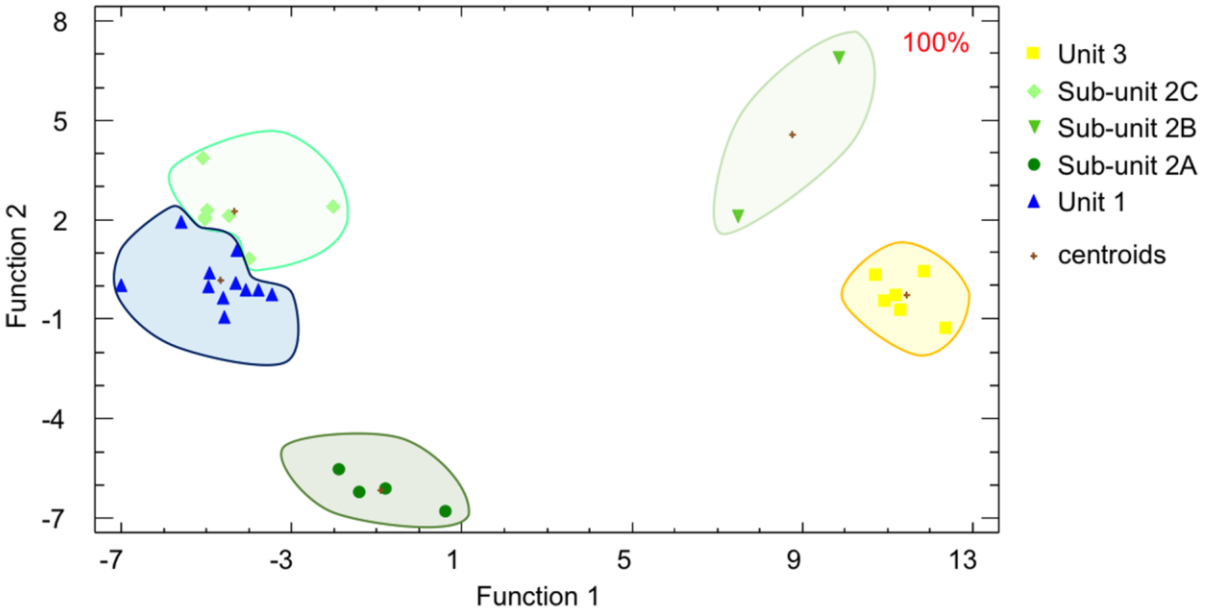

Figure 4.27 - Discriminant analysis using the *n*-alkanes series (C_{12} to C_{32} alkanes) as variables and the sedimentary units (Units 3, 2C, 2B, 2A, 1) as classification factor.

Sub-unit 2A share similar characteristics with the previous Unit 1, with a slight decrease of Asteraceae Cichorioideae and the presence of mixed forest, with a slight rise of Mediterranean trees in their components. *Isoetes* slightly increases, while Chenopodiaceae decreases. Notwithstanding, diatoms were also identified in this unit reflecting marine influence.

Sub-unit 2B is dominated by the presence of Asteraceae Cichorioideae and an abrupt decline of forest and shrublands. *Isoetes* reaches maximum values in this sample (Figure 4.30). Some Poaceae bigger than 40 µm were identified in samples from Sub-unit 2A and 2B (Figure 4.29).

In the whole analysed sequence (between -1027 and -135.5 cm MSL), coprophilous fungi, indicative of anthropogenic activities, and palynomorphs related to erosive processes displayed low values (Figures 4.29 and 4.30).

Regarding the microcharcoal percentages, particles bigger than 120 µm and related to local fires, appear in low values, especially in the bottom of the core (Figure 4.29). Those particles smaller than 120 µm were present in high values through the analysed sequence, with peaks in samples collected at -1027, -817 and -597 cm MSL, indicating the possible existence of regional fires (Figure 4.29).

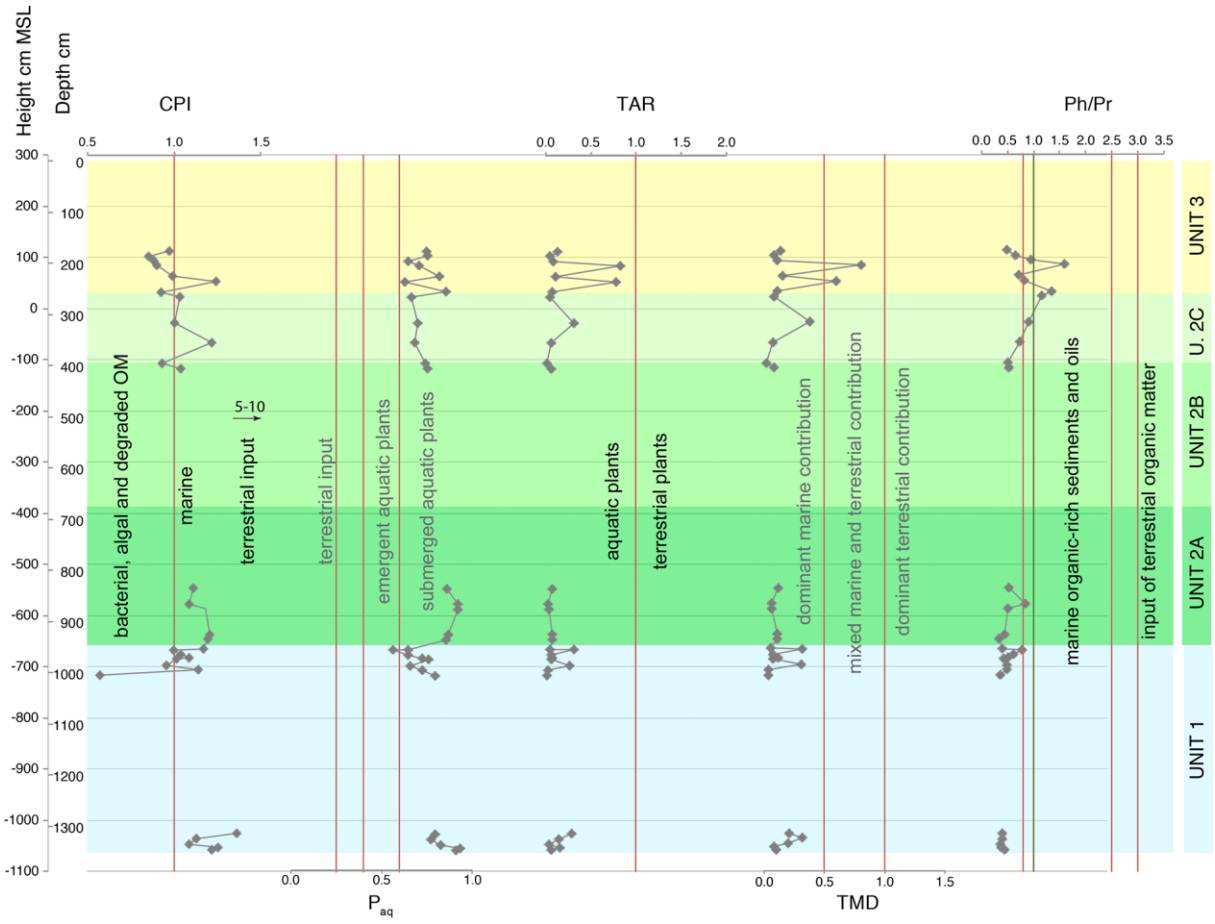

Figure 4.28 - In-depth variation of n-alkane and acyclic isoprenoid ratios against height cm MSL and depth cm: CPI, P_{aq}, TAR, TMD and Ph/Pr. Diagnostic values and references described in Table 1. Green vertical line in Ph/Pr indicates anoxic (<1) / oxic (>1) environments (e.g., Powell, 1988; Hughes et al., 1995).

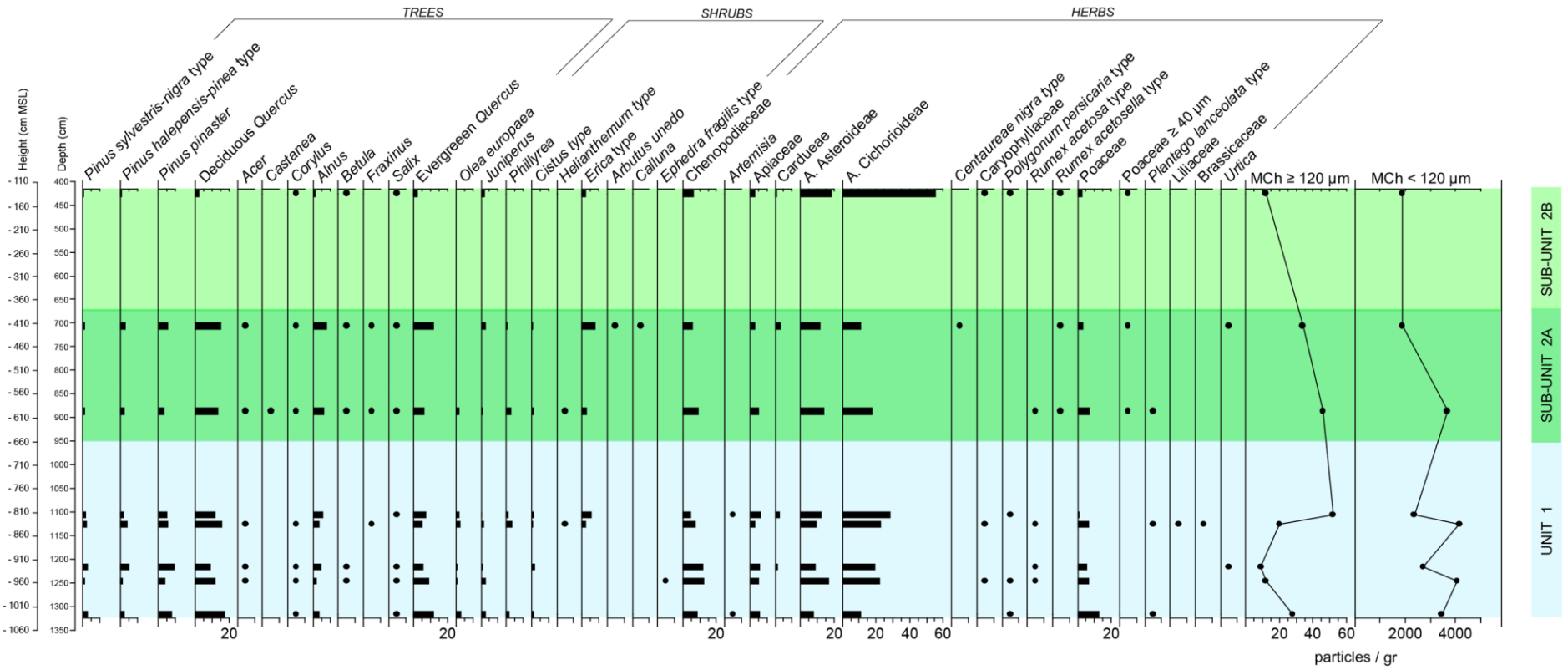

Figure 4.29 - Percentage pollen diagram for trees, shrubs, and herbs. Black dots represent percentages below 3%. Microcharcoal particles (MCh) are expressed in particles gr^{-1} of dry sediment (concentrations).

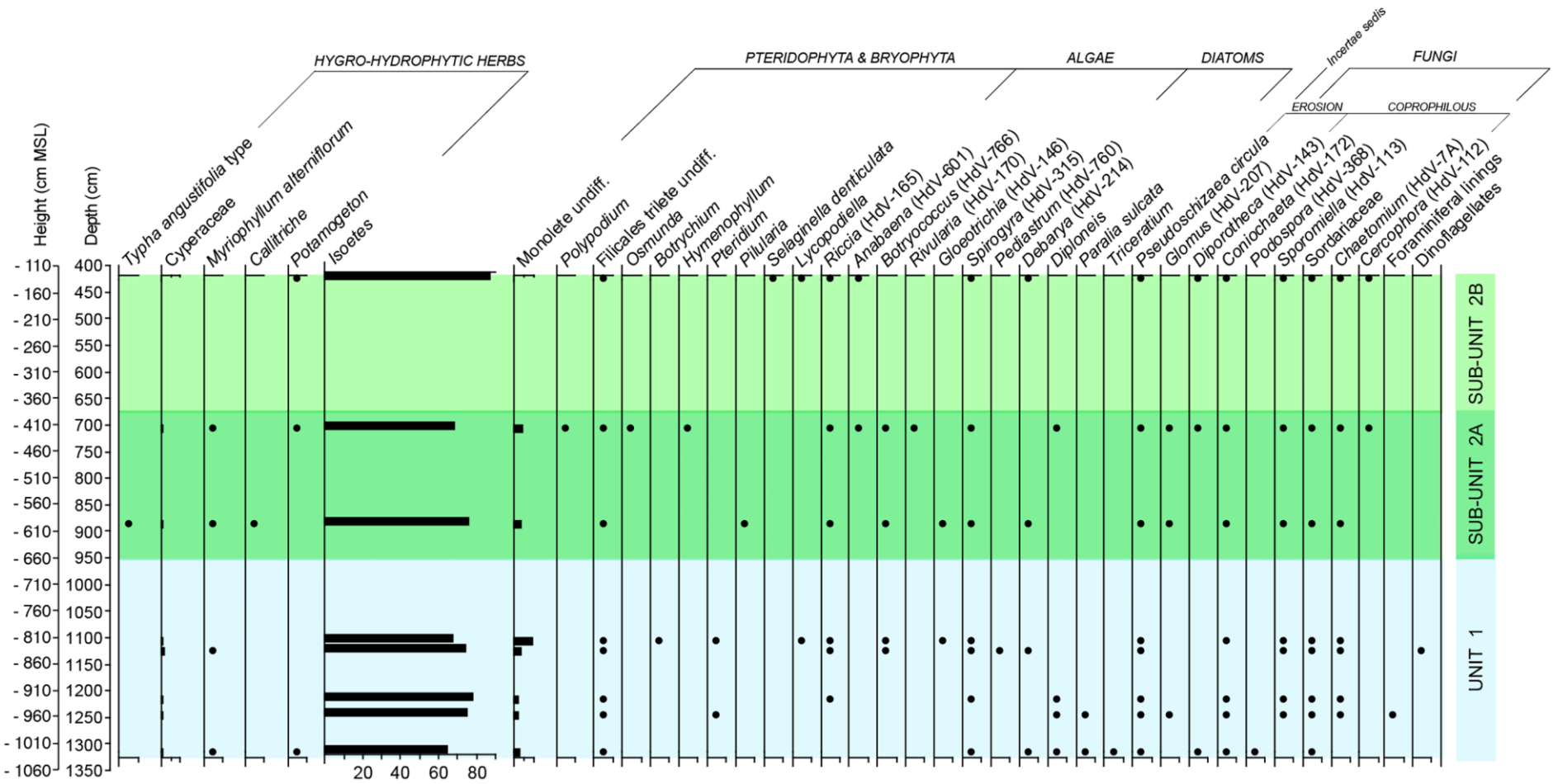

Figure 4.30 - Percentage pollen diagram for aquatic herbs, ferns and mosses, diatoms, and Non-Pollen Palynomorphs (NPPs). Black dots represent percentages below 3%.

5. DISCUSSION

5. Discussion

5.1 Sado and tributaries palaeovalleys configuration

During the Last Glacial Maximum (LGM; ca. 26.9 to 19 ky; e.g., Clark et al., 2009; Lambeck et al., 2014) the mean sea level drop in response to the formation of extensive ice sheets, exposing the coastal shelf and shaping the Iberian coastal morphology (Figure 5.1). According to Dias et al. (2000) the MSL in the Portuguese Atlantic margin has dropped by about 130 m from its present-day position (Figure 2.14), promoting the incision of the fluvial network and forming deep valleys that could reach, such as the case of the Tagus, to more than 80 m depth (Vis et al., 2008).

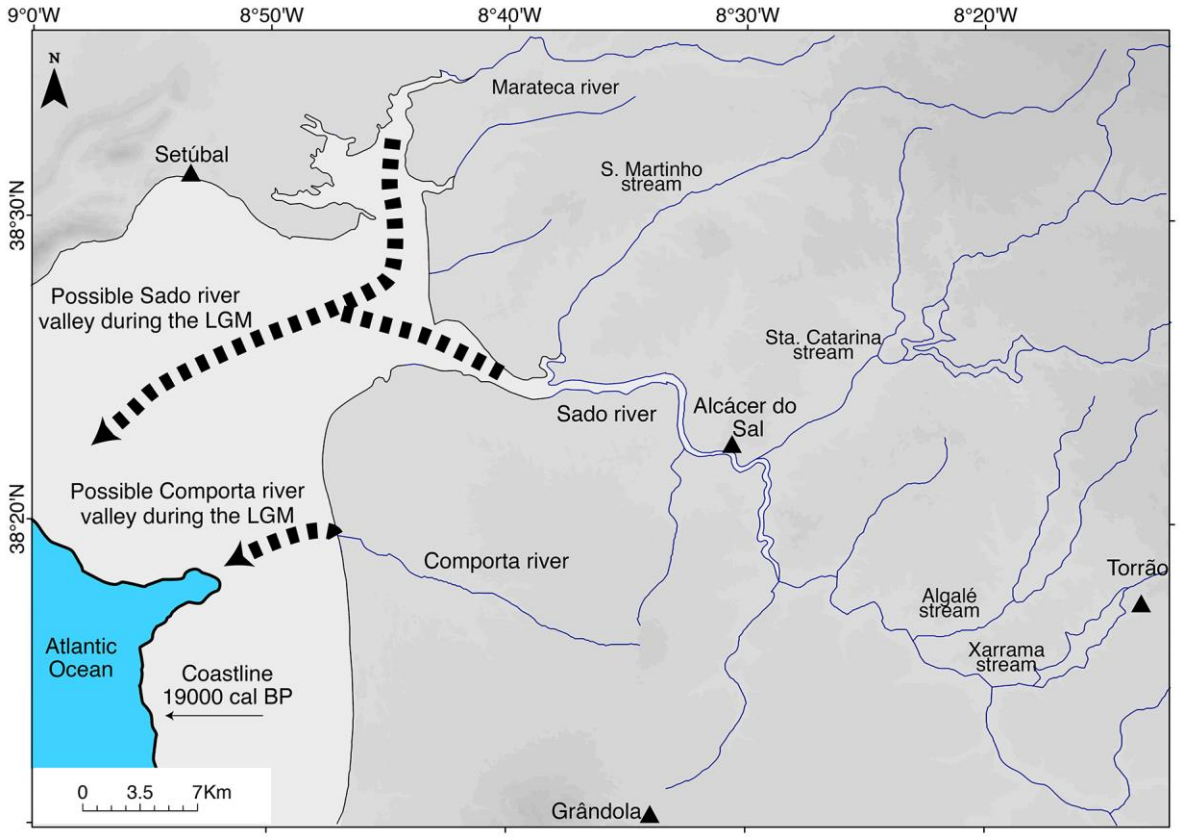

Figure 5.1 - Coastal palaeomorphology during the Last Glacial Maximum (LGM) in the Sado area. Coastline in the LGM (black line) defined at -130 m MSL bathymetric contourline (Dias et al., 2000). Grey line - schematic coastline at 7000 cal BP. Greyish colours - emersed areas.

Despite the morphology of rivers bottom is of extreme importance during transgression periods, being one of the main factors controlling the flooding of inland areas, the palaeomorphology of the Sado valley and its tributaries shaped during the LGM (and previous low stands) is still barely

known. To our knowledge, the only geomorphologic data on the Sado valley Late Quaternary incision resulted from the interpretation of geotechnical cores performed at Alcácer do Sal (GRID, 1989; ENGIVIA, 1995; Figure 2.13) that crossed the Palaeogene and Neogene formations where the river is embedded (Figure 5.2). Here, a deep incised valley reaching ca. 38 m is interpreted from alluvial sediments deposited above encasing sediments (Figure 5.2), ca. 50 km upstream the present-day estuary inlet.

The valley infilling presents a fining upward sequence until ca. -10 m depth, varying from coarse sand and rounded pebbles to silty mud sediments. The top 10 m are fulfilled with (muddy) medium to coarse sand over with a silty mud deposit (Figure 5.2). However, the sedimentary deposits lack in dating preventing to infer about the palaeoenvironmental evolution of the basin through time.

The ERT profiles performed in the studied area, located between ca. 7 (Arapouco) and 22 km (Laxique) upstream Alcácer do Sal, revealed contrasts in the electrical resistivity signal pointing to different geological formations and lithologies (Figure 4.3 and 4.4) that reflect the geological variability of the bedrock and the valley infilling.

The Sado palaeovalley is embedded in Palaeogene and Neogene sediments constituted mainly by conglomerates, sands and pelites (Antunes et al., 1991; Gonçalves and Antunes, 1992; Figures 2.11) and the surrounding Caenozoic formations are, certainly, the ones that mostly provide sediments to the fluvial area. In this context, similar resistivity values can be achieved for the encasing sediments and for the coarser accumulations of the fluvial/estuarine area that can difficult the interpretation of ERT profiles. Nevertheless, between Arapouco and São Bento it was possible to identify a strong contrast between the Caenozoic basement, with higher resistivity values, and the Sado recent alluvial infilling, with lower resistivity signal (Figure 4.3). These ERT profiles allowed therefore distinguishing different incision depths in the Sado main channel and in its tributaries (Figure 5.3).

Arapouco ERT profile reflects a palaeovalley ca. 40 m deep (-38 m MSL) filled with mud (low resistivity) embedded in sediments with higher resistivity corresponding to the Caenozoic basement (Figure 4.3). This profile was performed in a straight section of the valley (Figures 3.2 and 5.5), probably controlled by the occurrence of a fault that raised the Palaeozoic block of *Mértola* formation (Antunes et al., 1991; Figure 2.12). Slightly coarser sediments seem to occur near the river right margin where the Sado thalweg is at present. The mud sediments correspond to the infilling of the valley (whose composition will be discussed below) and the slightly coarser sediments reflect the proximity of the thalweg that, in this section and due to old tectonic constraints, could always have been located near the right margin of the river.

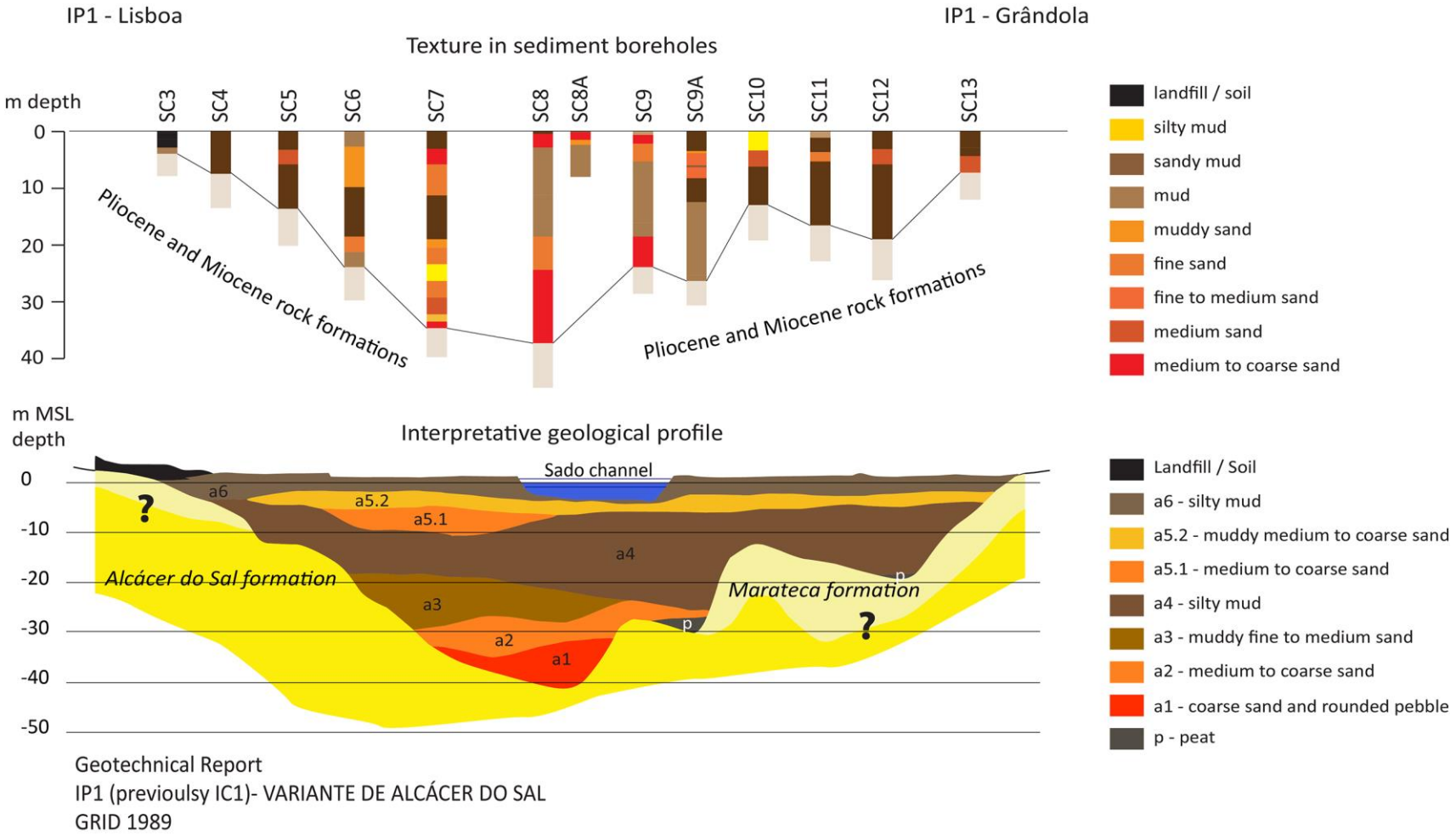

Figure 5.2 - Sado palaeovalley morphology and characterization of the alluvial sediments and Palaeogene and Neogene formation where the valley is embedded, at Alcácer do Sal (adapted from GRID, 1989).

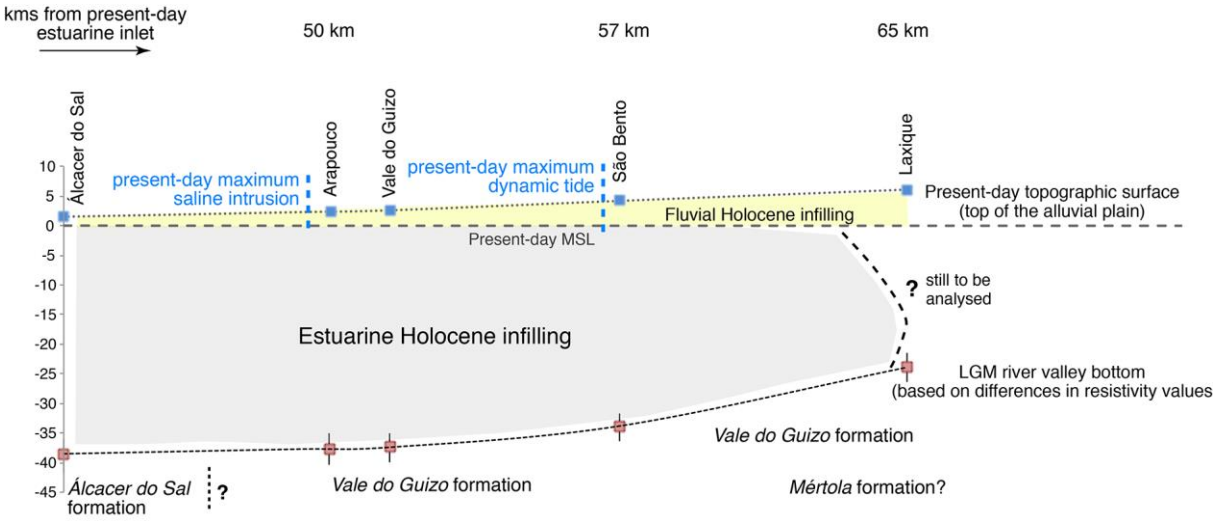

Figure 5.3 - Schematic representation of the palaeomorphology of the Sado valley based on the depths where abrupt changes in the electric resistivity values occur. Present-day maximum saline and dynamic tide influence from Bettencourt and Ramos, 2003. Grey area - estuarine Holocene infilling; Yellow area - fluvial Holocene infilling.

At Vale do Guizo, the depth of the valley was assumed to reach ca. 40 m deep (-38 m MSL) considering the above discussion, however high resistivity areas (Figure 4.3 - dashed dark grey lines) were detected above that depth and within the fine sediment valley infilling. Those areas are interpreted as old active channels that changed position due to meander migration by extension to southwest and as a result of accumulation of sediments derived from colluvial processes at northeast (Figure 4.3). Meander migration in meandering systems is the most common type of channel change (Brown, 1997). However, those high electrical resistive areas could also be the consequence of avulsion processes, that resulted from the rapid abandonment of a channel and the adoption of a new course, generally at lower areas of the floodplain (Brown, 1997). Both hypotheses favour the accumulation of sediments eroded from the opposite margin. In addition, the hypothesis of the higher resistivity values being derived from a Palaeogene residual relief cannot be discarded.

At São Bento, ca. 7 km upstream Arapouco, the valley reaches depths of ca. 38 m (ca. -34 m MSL) reflecting the slope profile of the fluvial valley. A high electrical resistivity area was found on the ERT profile (Figure 4.3), reflecting the accumulation of coarser sediments that are probably related with fluvial coarser accumulations.

Upstream, the Laxique ERT profile revealed an opposite pattern then the previous ones (Figure 4.4). Notwithstanding, abrupt changes in the resistivity values occur at ca. 30 m depth (-24 m MSL) that are interpreted as the contact between the valley infilling (coarse materials) and the

valley bottom (fine materials from the *Vale do Guizo* formation or shales from the *Mértola* formation) (Figure 5.3). The coarse materials at the top, by its turn, could be the result of alluvial fan accumulations, occurring near the area where the Xarrama stream meets the Sado river, or deposits resulting from a bay-head delta that formed at the maximum marine influence area after the deceleration of the sea level rise rate. The coarse character of the sediment prevented us to collect samples for analyses and dating, and to support the proposed hypotheses. Further research is needed in order to estimate the maximum estuarine area and the limit of maximum marine influence.

Considering the Sado tributaries, at Arez, the ERT profile reproduces a valley filled with fine sediments (reflecting the low dynamic of the small Carrasqueira stream), corresponding the higher resistivity values below -15 m MSL to the encasing Caenozoic formations (Figure 4.3).

It was not possible to draw the palaeomorphology of the Vale dos Açudes valley as ERT data provide similar electrical values in all the profile (Figure 4.3). That is interpreted as being the result of a proximal source contribution to the sediment valley infilling in a very shallow valley rise. The different ERT resolution achieved in the Sado channel and in the tributaries leads to anomalies in the profiles that can be misleading. For example, at Arapouco and Vale do Guizo, where the resolution is lower, resistivity low values (valley sediment infilling) are positioned ca. -50/-60 m MSL at some points (Figure 4.3), particularly when considering the Wenner configuration profile (W-W). It is very unlikely that the valley presents higher depths at upstream areas, unless tectonics had played a role in the area. There is no clear evidence of recent tectonic in the Sado valley and so the deeper low resistivity values are considered anomalous.

Despite the different resolution of ERT, resistivity values show that the Sado palaeovalley is deeper than the Sado tributaries. It reaches ca. -38 m MSL (assuming the depth considered at Alcácer do Sal) while at Arez it only reaches ca. -15 m MSL (Figure 4.3 and 5.4). At Vale dos Açudes, despite not being possible to draw the palaeomorphology of the valley due to the similarity in the electrical resistivity response, a shallow valley is expected.

Combining (only) the information concerning the depth of the Sado and tributaries palaeovalleys through the area occupied by Late Mesolithic communities and the MSL stipulated for the Early and Middle Holocene (ca. -36.7±1.2 m MSL at 11500 cal BP; 9550 cal BC; ca. -9.7 m MSL at 8400 cal BP; 6450 cal BC and -1.6±1.2 m MSL at 6900 cal BP; 4950 cal BC; García-Artola et al., 2018) it appears that there were suitable conditions for the flooding of the valley by marine waters at the onset of the Holocene (Figure 5.4). Nevertheless, other environmental and morphological constraints could have prevented the inundation of the valley and the establishment of estuarine conditions and are discussed below.

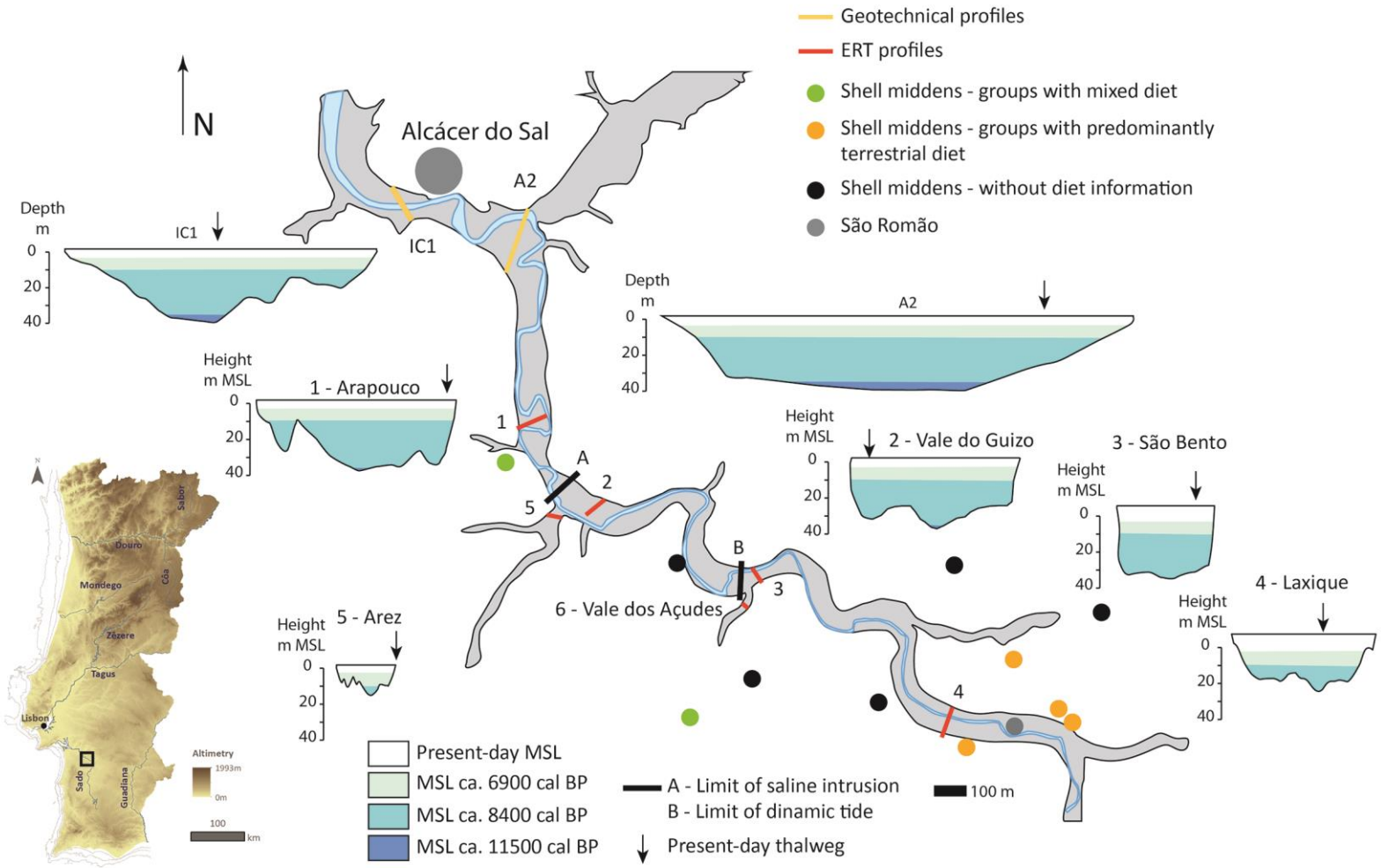

Figure 5.4 - Location of shell middens, geotechnical profiles and ERT profiles. Palaeovalleys morphology derived from ERT with representation of mean sea level at ca. 11500 cal BP, ca. 8400 cal BP and ca. 6900 cal BP according to García-Artola et al. (2018). The Vale dos Açudes palaeovalley was not possible to drawn using the ERT profile.

5.2 Sado valley infilling: marine vs. fluvial influence

During post-glacial sea level rise deeply incised coastal valleys and lowlands in Atlantic Europe (and elsewhere) were flooded by marine water forming extensive estuarine areas and open bays (e.g., Freitas et al., 2002; Boski et al., 2008; Vis et al., 2008; Hijma et al., 2009; Chaumillon et al., 2010). In such conditions new boundary spaces were created at the interface between the land and the sea.

According to the sedimentary record of the Tagus basin, located ca. 80 km north of the studied area, tidal deposits were dated near Vila Franca de Xira, located ca. 48 km upstream from the estuarine inlet, shortly after 11800-11200 cal BP (9850-9250 cal BC) and north of Santarém, ca. 90 km distant from the sea, at 9030-8750 cal BP (7080-6900 cal BC; Vis et al., 2008). The maximum marine flooding in the Tagus basin occurred ca. 7000 cal BP (5050 cal BC; Vis et al., 2008), forming a large estuarine area of nearly 1300 km^2 (Taborda et al., 2009). From that date onwards, a bay-head delta formed and started to prograde downstream until present (Vis et al., 2008).

The most recent studies concerning the Holocene sea level rise on the Portuguese coast, estimate a rise rate of 0.81±0.07 cm yr^{-1} between 11500 and 7500 cal BP (9550 and 5550 cal BC) and a rate of ca. 0.34±0.10 cm yr^{-1} between 7500 and 6900 cal BP (5550 and 4950 cal BC), as mentioned previously. During that period, the sandy spit that protects the Sado estuary at present was not yet formed (Costas et al., 2015; Figure 5.5) allowing for the formation of an open bay and transitional estuarine area in the Sado valley (also in the Marateca valley - not studied in the present work) (Freitas and Andrade, 2008; Brito, 2009). The sea level rise rate abruptly decreased at ca. 7000-6900 cal BP (e.g., Vis et al., 2008; Leorri et al., 2012; García-Artola et al, 2018) and a continuous mean sea level rise rate of 0.31 mm yr^{-1} was stipulated for the Sado valley since then (Costas et al., 2016a). The Tróia sand spit started to develop to north at ca. 6500 cal BP (4550 cal BC; Costas et al., 2015) protecting the Sado estuary and limiting the exchanges between the estuary and the sea (Figure 5.6).

The discussion presented in this section will contribute to the palaeoenvironmental characterization of the Sado estuary through the Holocene based on the interpretation of the source of the materials, palaeoecological indicators and sedimentation rates.

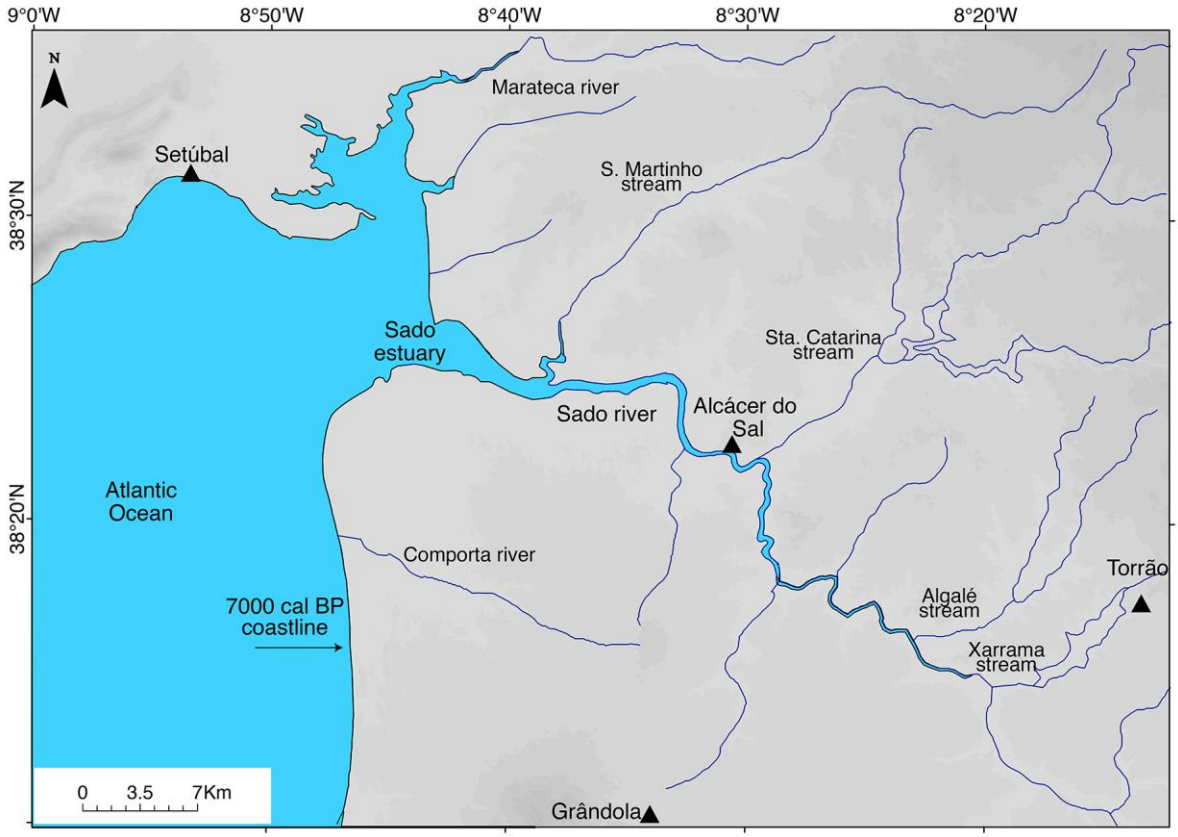

Figure 5.5 - Schematic representation of the coastal palaeomorphology and inland flooded area at ca. 7000 cal BP in the Sado valley.

The sediment core Arez3, collected in a tributary of the Sado with a shallower palaeovalley (see discussion above) covers a higher portion of the Holocene (since ca. 8850 cal BP, i.e., 6900 cal BC, until present), while in the sediment cores collected in the Sado channel, with a deeper palaeovalley, only the top sedimentary infilling was recovered, just representing the Middle to Late and Late Holocene (Figure 5.7). This discussion will follow a chronological order, and by this reason, interpretations done for the Arez3 sedimentary record will be presented first, followed by Laxique and Arapouco.

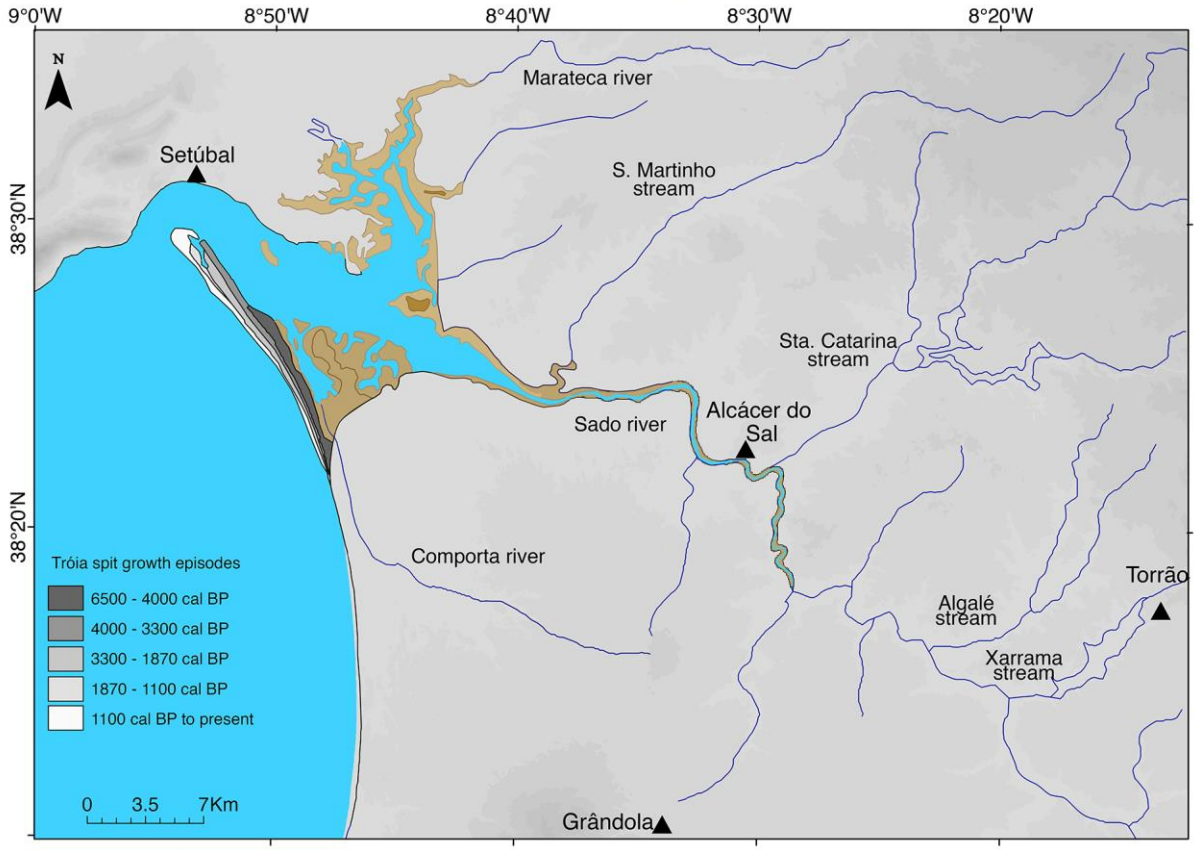

Figure 5.6 - Present-day coastal morphology with indication of the Tróia spit growth time episodes, as referred to by Costas et al., 2015. Brownish colours represent saltmarsh environments.

Sources of materials and characterization of depositional environments

Estuaries are transitional areas between fluvial and marine environments and sediment sinks for material brought downstream by the fluvial network, material transported landward from the sea (allochthonous material) and organic material produced in the estuarine basin (autochthonous material) (e.g., Schubel, 1982; Meyers, 1994; Khan et al., 2015; Scanes et al., 2017). Organic proxies, such as $\delta^{13}C$, $\delta^{15}N$ and C/N are widely used to distinguish between the organic matter sources, helping to characterize past environments (e.g., Meyers, 1994, 1997; Wilson et al., 2005a, 2005b; Lamb et al., 2006; Castro et al., 2010; Khan et al., 2015) since, even after early degradation processes, palaeoenvironmental and source information remains preserved in the molecular and isotopic composition of the organic materials (e.g., Meyers, 1994). Particular attention should be given to $\delta^{15}N$ since its degradation could lead to either depletion or enrichment in ^{15}N (e.g., Meyers, 1997) and it can result from the introduction of terrestrial derived inorganic N.

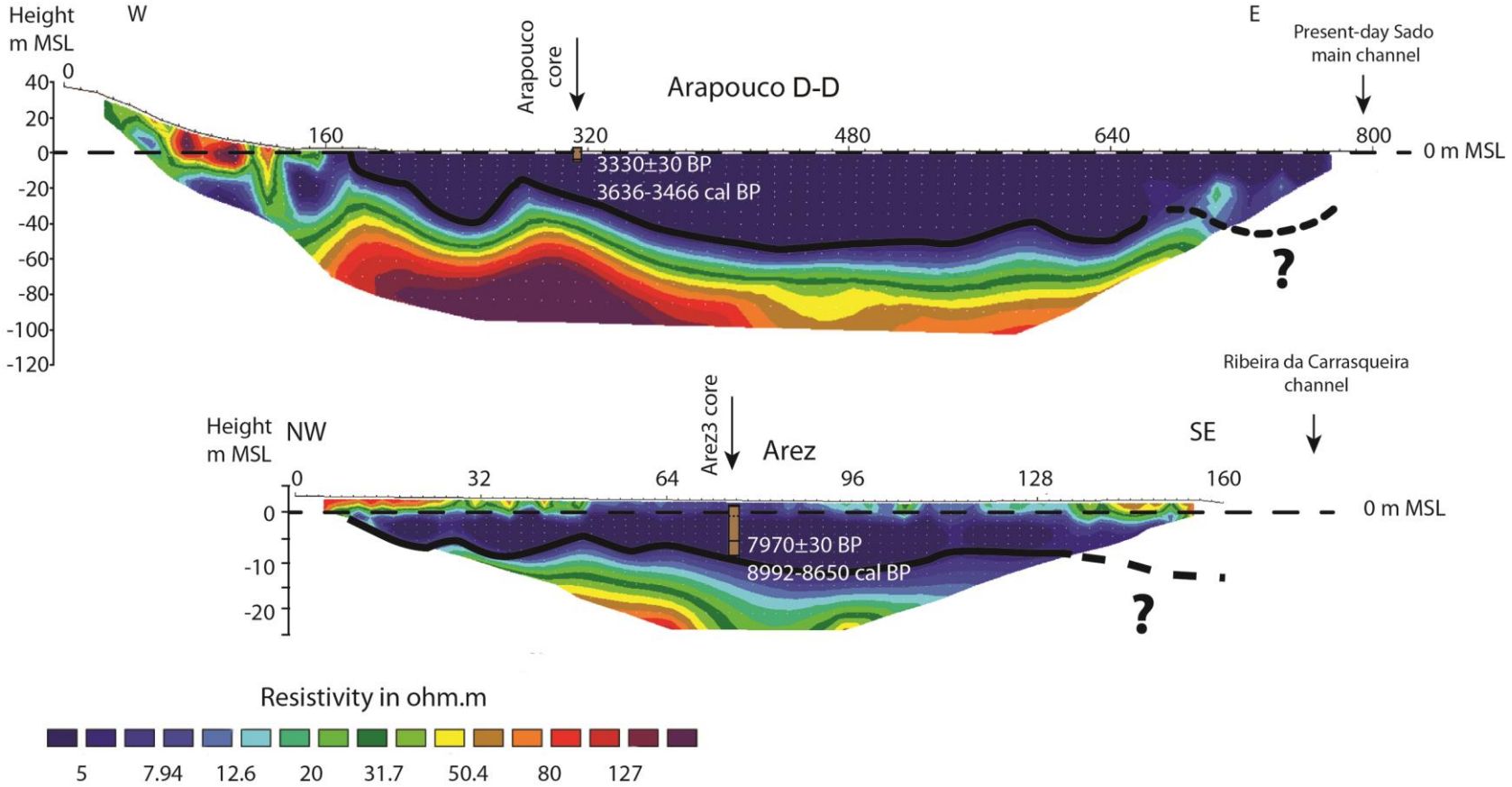

Figure 5.7 - ERT profiles and interpretation for Arapouco (above) and Arez (below) with the sedimentary cores Arapouco 2/3 and Arez3, respectively, represented in the location where they were collected. Indication of the date achieved for the base of each core (Table 4.1).

Geochemical results from Arez3, Arapouco and Laxique (Figures 5.8, 5.9, 5.10) were plotted in diverse charts draw by Lamb et al. (2006), Castro et al., 2010 and Khan et al. (2015) that compile information concerning the source of organic matter in intertidal wetland areas using $\delta^{13}C$, $\delta^{15}N$ and C/N values measured in sediments and were used in our interpretations. In Arez3, the analyses of such geochemical indicators were interpreted together with the results of lipid biomarkers and indices, also pertinent indicators of palaeoenvironmental conditions and organic matter source (e.g., Meyers, 2003; Ouyang et al., 2015; Li et al., 2020). In Laxique, in addition to organic chemistry, the environments were also characterized based on nutrient (PO_4^{-3}, P, NO_3^- and SO_4^{-2}) changes.

The characterization of past environments relies on available data and environmental characteristics of present-day intertidal environments (present-day analogues). By this reason, the results from Arez3, Laxique and Arapouco were, when necessary, compared with palaeoenvironmental (and chronological - see below) information from a sediment core, ALC-S, collected further downstream, in a saltmarsh that develops in the left margin of the Sado estuary near Alcácer do Sal, in intertidal estuarine conditions (Moreira, 2016). ALC-S (Lat: -33471.69; Long: -143995.7; ERTS89 TM06 Portugal coordinate system) has 270 cm, and the elevation ground surface at the core location is 1.5 m MSL. Sediments are mainly constituted by grey mud to slightly sandy mud, with brownish colours at the top 70 cm (Moreira, 2016). The base of the core represents accumulation in a tidal flat environment that evolved at the top to a saltmarsh that continues to grow at present in the area (Moreira, 2016). In addition, one surface sediment sample (composed mostly of mud) was collected from the margin of the Sado main channel at Arapouco, to characterize the organic material accumulating at present in this location.

In Arez3, $\delta^{15}N$ only present significant changes in the top unit (Sub-unit 2C and Unit 3), while $\delta^{13}C$ seems to reflect different organic sources considering depth (Figure 4.24).

According to Lamb´s chart (Figure 5.8), Unit 1 (8850 to 7450 cal BP; 6900 to 5500 cal BC), characterized by strong variations in the $\delta^{13}C$ values, seems to reflect constant changes in the source of organic materials from marine (higher values; -23‰; Marine Dissolved Organic Carbon (DOC)) and freshwater/terrestrial environments (lower values; -26‰; Freshwater DOC and Macroalgae/C3 Terrestrial plants) (Lamb et al., 2006 and references there-in). Values are quite similar to the ones determined for Units 2 to 4 from Arapouco (Figure 5.10).

In addition, *n*-alkanes total abundance exhibits higher values in short chain *n*-alkanes C_{12} to C_{19} pointing to the existence of an aquatic environment, with a gradual decreasing tendency to the top if considering mid- and long-chain *n*-alkanes (Figure 4.26). Maximum values in C_{15} are usually related to phytoplankton (Figure 4.26; e.g., Li et al., 2020). Carbon preference index (CPI; values

near 1 and slightly higher) and TMD (values lower than 0.5) ratios seem to reflect a dominance of marine OM in Unit 1 with occasional terrestrial inputs (Figure 4.28). Ph/Pr ratios values in Unit 1 also fell within the marine organic-rich sediments values deposited in an anoxic environment (e.g., Powell, 1988; Hughes et al., 1995; Meyers, 2003), i.e., presenting less environmental conditions for the degradation of organic matter (e.g., Meyers, 2003).

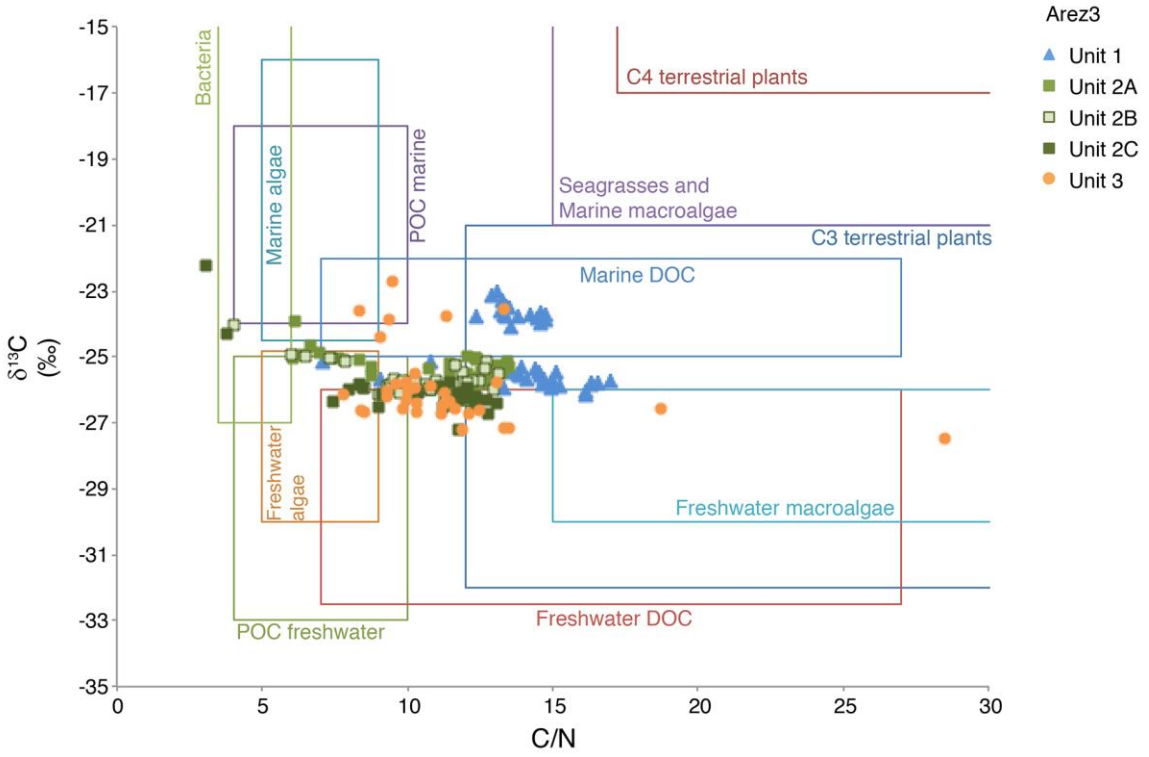

Figure 5.8 - C/N vs. $\delta^{13}C$ results from Arez3 plotted in the adapted graph from Lamb et al.'s (2006), updated by Khan et al. (2015).

Anoxic conditions are also attested by the presence of pyrite agglomerates and the precipitation of pyrite on the macro-plant remains (Figures 4.23 and 4.25). Mid-chain *n*-alkane (C_{21} to C_{25}), usually attributed to submerged and floating aquatic plants including marine macrophytes (Sikes et al., 2009), with higher abundance than long-chain *n*-alkanes (Figure 4.26) and a P_{aq} value ca. 0.9 in the base of Unit 1 and Sub-unit 2A (Figure 4.28; Mean values of 0.8; Table 3.3; Ficken et al., 2000; Sikes et al., 2009) point to the importance of aquatic plants contributing to the OM content during this period. The foraminifera assemblages identified in Unit 1 are dominated by species (*Haynesina germanica*, *Ammonia tepida* and *Elphidium gunteri oceanensis*) that usually occur in brackish conditions giving evidence of the marine influence in the area. Such assemblage is today found in the Sado estuary in subtidal to tidal flat environments (Fatela et al., 2009a). In addition, the absence of agglutinated species such as *Jadammina macrescens* and *Trochamina inflata,* frequently

found in the estuarine areas with low salinities (low to high marsh) is indicative of low fluvial influence (Fatela et al., 2009a). The presence of planktonic juvenile forms results, most probably, from the proximity to the open sea. The presence of Chenopodiaceae together with the punctual appearance of foraminiferal linings, dinoflagellates, and some specific types of diatoms (e.g., *Paralia sulcata*, *Triceratium*, and *Diploneis*; Figures 4.29 and 4.30) identified during pollen analyses is yet another evidence to the existence of a brackish environment. Indeed, assemblages characterized by epipsammic diatoms, with *Opephora mutabilis* being the most frequent taxon, and sponge spicules were also attested at the base of Arez1 core (between -775 and -798 cm MSL; dated to ca. 8500 cal BP; 6550 cal BC), collected few meters from Arez3, corroborating the presence of a brackish environment in the Carrasqueira stream during this time-period. In addition, the foraminiferal linings leave evidence of an undersaturated $CaCO_3$ environment, as identified in other Atlantic estuaries (e.g., Moreno et al., 2007; Valente et al., 2009).

Assuming the MSL rise rate estimated by García-Artola et al. (2018), during the time-interval of deposition of Unit 1 and Sub-unit 2A, the sea level rose from a depth of ca. -1330 cm at ca. 8850 cal BP (6900 cal BC) to -240 cm MSL at ca. 7500 cal BP (5550 cal BC). The sediments corresponding to this chronology are represented approximately between -1060 and -390 cm MSL (Unit 1 and Sub-unit 2A), pointing to the occurrence of an extensive drowned area. This fact is consistent with the existence of an aquatic environment as revealed by the contribution of aquatic plants to the OM source.

Taking into consideration that a date of 8850 cal BP (6900 cal BC; best-fit date) was determined for the base of Arez3 core, at -1060 m MSL, the sea level at that time must be higher than -1330 cm, but an error between ±120 (error estimated by the authors for the MSL at 11500 cal BP; 9550 cal BC) and ±170 cm (error estimated by the authors for the MSL at 7500 cal BP, i.e., 5550 cal BC; García-Artola et al., 2018) must be assumed. In this case, the maximum error of + 170 cm was used and a MSL of -1185 cm MSL was considered. By these values the base of the core was approximately at the limit of tidal influence, if tidal parameters similar to present-day are assumed, but due to the high rate of sea level rise, the area was rapidly flooded. In addition, the error associated to the radiocarbon date should also be considered.

In Units 2 (7450 to 4910 cal BP; 5500 to 2960 cal BC) and 3 (4910 cal BP to present; 2960 cal BC to present), the $\delta^{13}C$ presents an upward decreasing tendency (from -25‰ to -27‰; Figure 4.24) reflecting an increase in the contribution of OM from terrestrial plants and freshwater phytoplankton (Freshwater DOC, Particulate Organic Carbon (POC) and algae) to the sediment through time (Figure 5.8). Values are within the range of the $\delta^{13}C$ determined for Unit 5 in Arapouco (Figure 5.10), interpreted (see below) as corresponding to the aggradation of the

alluvial plain. The relative total abundance of long-chain *n*-alkanes, particularly in Unit 3, also points to higher inputs of terrestrial organic materials (Figure 4.28). The MSL rose to -160 cm MSL at ca. 6900 cal BP, but contemporary sediments occur at -10 cm MSL also reflecting a change in the environmental conditions with intertidal areas occupying previous drowned areas from that date onwards.

In Sub-unit 2A (7450 to 7040 cal BP; 5500 to 5090 cal BC) C/N and $\delta^{13}C$ point to the presence of freshwater POC and freshwater algae, confirming the increased influence of freshwater environments (Figure 5.8). In addition, Chenopodiaceae decrease, Asteraceae Cichorioideae slightly declines while *Isoetes* slightly increases reflecting the development of freshwater marshes (Figures 4.29 and 4.30). In Sub-units 2B and 2C (7040 to 4910 cal BP; 5090 to 2960 cal BC), the increase in the contribution of OM from terrestrial plants and freshwater phytoplankton (Figure 5.8) suggest higher influence of the river(s) in the area and the expansion of freshwater wetlands in detriment of brackish environments. This is also corroborated by the decrease of Chenopodiaceae and the high values of *Isoestes* (Figures 4.29 and 4.30).

In Sub-unit 2C and Unit 3, $\delta^{13}C$ presents sharp peaks with values ≥-24‰ (Figure 4.26). These values can result from higher marine influence, with contributions from marine algae and/marine POC, from the presence of bacteria, at least considering the lower values from Sub-Unit 2C (Figure 5.8) or from runoff inputs enriched in N-fertilizers (e.g., Bogaard et al., 2013). $\delta^{15}N$ also presents several negative peaks in Sub-unit 2C and Unit 3, reaching values of 0‰ (Figure 4.24). $\delta^{15}N$ values are related with nitrogen cycle processes and with nitrogen source (e.g., Yamamuro et al., 2003; Torres et al., 2012; Golubkov et al., 2020). At present, high $\delta^{15}N$ isotopic values in aquatic environments are usually related to polluted areas due to e.g., sewage inputs and fertilizers runoff and are frequently used as a tracer for human activities (e.g., Meyers, 2003; Yamamuro et al., 2003; Lepoint et al., 2004; Senbayram et al., 2008; Laussaque et al., 2010; Connolly et al., 2013; Fiorentino et al., 2015; Treasure et al., 2016). Recent studies showed that depletion in ^{15}N (0‰ or lower $\delta^{15}N$ values) could also be related to ammonium peaks in highly polluted aquatic systems (e.g., Kopprio et al., 2018). In pristine aquatic systems, $\delta^{15}N$ isotopic values are usually lower than in systems with anthropic influence and most related to the source of organic matter (e.g., Meyers, 2003), microbial processes of nitrification, denitrification and N-fixation (e.g., Scanes et al., 2017). In general, $\delta^{15}N$ isotopic ratio increases from oligotrophic to eutrophic systems, but decreases in hypereuthophic and anoxic conditions due to the presence of cyanobacteria (e.g., Meyers, 2003; Gu, 2009; Golubkov et al., 2020). In diverse aquatic systems $\delta^{15}N$ values ~0‰were related to N-fixation processes and the dominance of N-fixing cyanobacteria in the

phytoplankton community (e.g., Yamamuro et al., 2003; Torres et al., 2012; Bardhan et al., 2017). Sub-Unit 2C deposited between ca. 6530 to 4910 cal BP (ca. 5500 to 2960 cal BC), so the incorporation of ^{15}N enriched OM from sewage or N-enriched fertilizers cannot be considered, being the negative shift of $\delta^{15}N$ to values ~0‰ most probably related to hypereutrophication and cyanobacteria bloom episodes and to the development of backswamp environments in the Carrasqueira valley since the Middle Holocene. Recently, the effects of anthropic activities also led to changes in the sediment organic chemistry.

Similarly, in Unit 3, deposited in the last ca. 5000 years, the negative shifts in $\delta^{15}N$ values that occur at ca. 4650 cal BP (ca. 2700 cal BC) and ca. 3525 cal BP (ca. 1575 cal BC) appear to be more related to bacterial activity. Frequent CPI values lower than 1 in Sub-unit 2C and Unit 3 are also indicative of microorganisms, bacterial communities and degraded OM (Figure 4.28; e.g., Bray and Evans, 1961), and Ph/Pr changes between values > and <1 (Table 3.3 and Figure 4.28) point to the alternation between oxic and anoxic environments suitable for the degradation of organic matter and eutrophication events. Only the more recent $\delta^{15}N$ negative peak (ca. 790 cal BP; 1160 cal AD; Figure 4.24) can be associated with anthropic activities. Indeed, between the top-most negative $\delta^{15}N$ shifts, $\delta^{15}N$ values increase to values higher than 6‰ (Figure 4.24) that can be related with organic matter derived from algae (+8.5‰; e.g., Meyers, 2003), but also from heavy nitrate fertilizers and human sewage (e.g., Teranes and Bernasconi, 2000). Unit 3 deposited above present-day MSL, and despite the possibility of being flooded during high tides, the presence of marine algae influencing $\delta^{15}N$ is not plausible, once in-depth $\delta^{15}N$ are lower even during higher marine influence episodes (Unit 1; Figure 4.24). The alluvial plain of Carrasqueira stream, where Arez3 was collected is nowadays used for agriculture practices, particularly rice production, and similarly to the Sado channel alluvial area. The $\delta^{13}C$ higher values measured in the top of Unit 3 can also be related with the input of N-fertilizers once changes in the $\delta^{13}C$ values are known to occur by the input of mineral N-fertilizers (e.g., Bogaard et al., 2013).

In Laxique, the sandy gravel sediment from Unit 0 lacks in organic materials and its source can only be achieved based on the characterization of clasts. The presence of angular centimetric clasts containing essentially quartz and quartzite with the presence of greywacke, granite, shale and sandstone point to the proximity of the source area and to the important influence that Xarrama river, that crosses rocks from the South Portuguese Zone (*Pulo do Lobo* formation) and from Ossa-Morena Zone (granites, diorites and gabbros; Figure 2.10 and 2.11), has concerning the supply of material to the Sado, at least, before 4400 cal BP (2450 cal BC).

In this sediment core, $\delta^{15}N$ presents small variations with depth (Figure 4.21). The correlation between OM and C_{org} and N is positive and very significant, with R^2 values of 0.96 and 0.95, respectively, reflecting mainly an organic source for the materials in spite of dependent on sediment particle size or other sources (e.g., Rumolo et al., 2011; Gao et al., 2012; Figure 5.9A). Similarly, the correlation between C_{org} and N is positive and very significant for all the defined Units reflecting the same source of both organic components within each Unit (Figure 5.9A). $\delta^{13}C$ values vary between -26.8‰ and -25.6‰, C/N between 7.9 and 10.8 (Figure 4.20) and $\delta^{15}N$ between 4.6‰ and 7.4‰ in Units 1 to 5 (Figure 4.21; Table 4.3) pointing to materials originating mainly in terrestrial and freshwater environments (e.g., Lamb et al., 2006; Castro et al., 2010; Figure 5.9B and 5.9C). Comparing the Laxique isotopic values and C/N ratio with the data obtained from ALC-S (Figure 5.9) and Arapouco (Figure 5.10), they are quite similar to the values determined for the sediments accumulated in the alluvial plain (Arapouco Unit 5) and differ from the values determined for the ancient (Arapouco Unit 2 to 4; see below) and current intertidal areas (Arapouco superficial sample and ALC-S), confirming the strong influence of freshwater and terrestrial organic materials reaching Laxique in the early Late Holocene.

Despite the similarity, in Unit 5 $\delta^{13}C$ values are lower than in Units 1 to 4 (Figure 4.20) and seem to reflect an increase in the contribution of organic matter from terrestrial plants and freshwater phytoplankton (Figure 5.9B and 5.9C). In Unit 6 the isotopic values and C/N ratio deviate from the values determined for the Units below (Units 1 to 5) showing higher $\delta^{13}C$ and $\delta^{15}N$ values and lower C/N ratios that most probably are related to the anthropic manipulation of the area, by the addition of manure and fertilizers in agriculture and the discharge of wastewaters into rivers and coastal areas. Despite the relative homogeneity in C and N values, changes in nutrients, suggest modifications in the environmental condition between Units 1 and 4. Their contents are not related to texture (R^2 <0.2), OM (R^2 <0.05) or C_{org} (R^2 <0.1). However, the chemistry of nutrients in aquatic sediments is complex and thus, good correlations with other sediment components are not always found. For instance, the lack of correlation between the distribution of P and the OM could be related to the low C_{org} content, to the complex nature of the organic matter itself, to the predominance of inorganic-P forms and to the intricate relationship among the different sediment components (coating formation, particle cementation, competition for adsorption sites, among others), as observed by Pardo et al. (2003). Phosphorus, in phosphate (PO_4^{-3}) and total forms (P_t) may reflect the importance of minerals inherited from the setting lithologies. The geology of the drainage area of the Sado river, characterized by a high diversity of sedimentary rocks with carbonate nature (sandstones, conglomerates, limestones and marls) and a high diversity of igneous, metamorphic and metavolcanic rocks (Figure 2.11), a few of them

bearing massive sulphide polymetallic deposits, may represent a greater source of P, from mineralogical forms as apatite (Ca-P), to phosphate anions fixed/adsorbed in/on sheet silicates and Fe-, Al-oxi-hydroxides (e.g., Zhang and Kovar, 2000; Slomp, 2011; Koziorowska et al., 2018), common weathering products of the aforementioned lithologies (Fonseca et al., 2011). Given this, in-depth changes in P and PO_4^{-3} will point essentially to high/lower river flows and sediment load to the estuary. Other nutrients and also, at a lesser extent, P and PO_4^{-3} content changes in the sedimentary column are most likely dependent on nutrient biogeochemical processes.

Unit 1 (ca. 4400 and 4350 cal BP; ca. 2450 and 2400 cal BC) is coarser (Figure 4.19A), with Fe-oxides precipitations in some quartz grain surfaces and the presence of Fe-minerals, P and PO_4^{-3} with low concentration such as organic materials (Figures 4.20 and 4.21) pointing to higher fluvial influence and relative higher energetic conditions. Magnetic particles, sourced from the Iberian Pyrite Belt (Figure 2.11), are also transported and accumulated in the area (Figure 4.19). The deposition of Unit 1 can results from high precipitation events, in a prevailing drier climate (e.g., Fletcher et al., 2007) that increased river transport competence. Accordingly, the fluvial and terrestrial POC combined adds up to more than 80%, according to the values determined by the equations used by Alonso-Hernandez et al. (2017) (Figure 4.20), with ca. 60% POC derived from freshwater sources. High river discharges during high precipitation events are typical of Mediterranean rivers and the occurrence of such conditions during the deposition of Unit 1 allows to characterize the Sado as a river with a strong Mediterranean character, at least, since the end of the Middle Holocene.

In Unit 2 (ca. 4350 and 4300 cal BP; 2400 and 2350 cal BC) coarse materials decrease to the top such as the magnetic materials (Figure 4.19) while organic compounds increase, reaching to maximum values in OM, C_{org} (Figure 4.20) and N (Figure 4.21), reflecting a low energy environment with limited fluvial inputs. Organic matter sourced in freshwater organic materials seem to have a higher abundance in the total organic matter content, slightly decreasing the organic matter with terrestrial origin (Figure 5.9). The presence of gypsum in Unit 2 is indicative of dry conditions.

In both Units 1 and 2 diatoms are absent, but bioturbation and macro-plant remains were identified. This upward fine succession accumulated between -195 and -130 cm (Units 1 and 2, total 65 cm thickness) may result from deposition in a tidal flat (sandflat to mudflat) / C3 marsh environment (Figure 5.9D; Khan et al., 2015), in the transition zone between the fluvial-estuarine boundary and the limit of tidal influence with very low to absent salinity contents, receiving essentially organic material from terrestrial and freshwater sources.

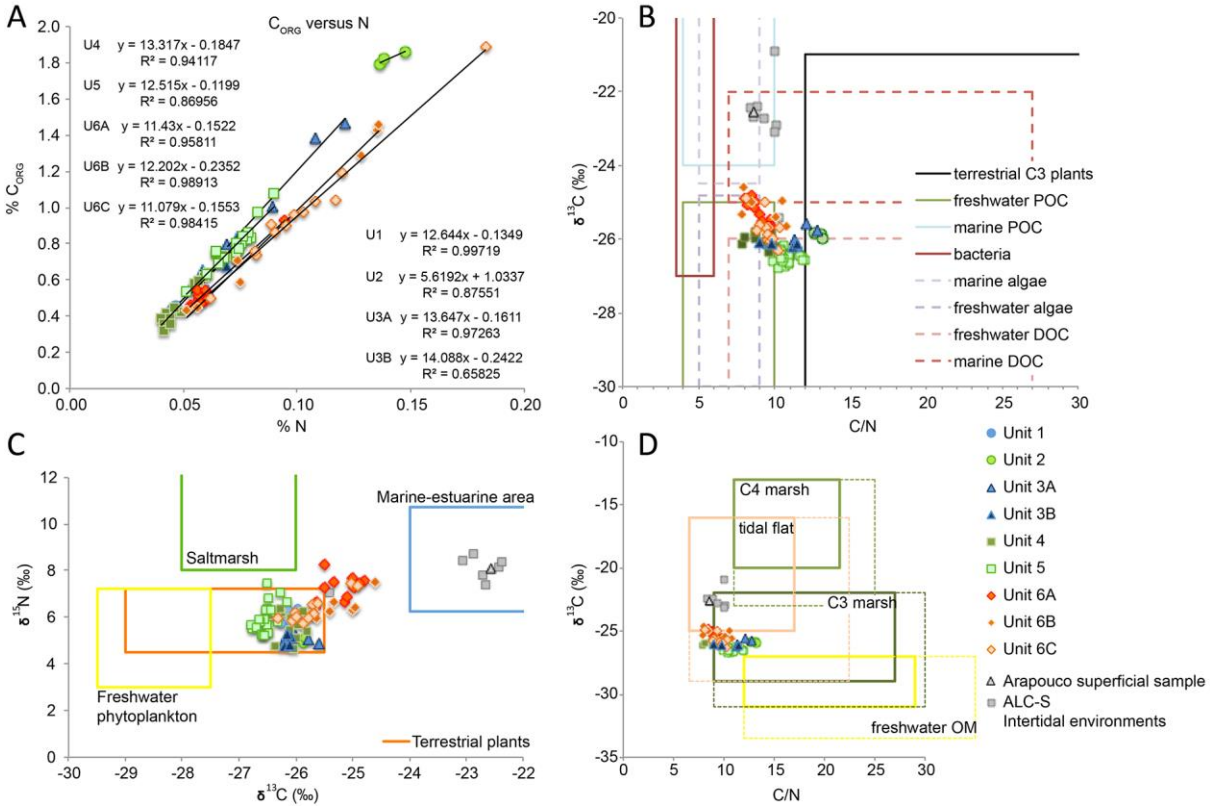

Figure 5.9 - A - Correlation between % C_{org} and % N; B - Source of organic materials according to Lamb et al., 2006; C - Source of organic materials according Castro et al., 2010; D - Source of organic materials according to Khan et al., 2015. Dashed lines in Khan et al.'s chart indicates shift in values from modern to Mid-Early Holocene organic compounds due to early degradation processes.

Assuming a MSL rise rate of 0.31 mm yr^{-1} (Costas et al., 2016a), a MSL placed at -140 to -130 cm below the present-day MSL during the interval between 4400 to 4300 cal BP and considering tidal characteristics similar to the present, the development of tidal flat areas is expected. Presently, the Sado intertidal platforms develop between -1.8 and 2 m MSL (Moreira, 1992).

In addition, both Units present the highest contents of NO_3^- of the sedimentary succession and high contents of PO_4^{-3} and P (Figure 4.21). The high concentration of NO_3^- can result from high rates of atmospheric N fixation by aquatic organisms. In upper estuarine shallow environments turbidity conditions and light restrictions limit the uptake of nitrate by benthic nitrifying communities. In such conditions NO_3^- can be buried in sediments under the presence of oxidizing conditions (e.g., Scanes et al., 2017). It can also result from NO_3^- and NH_4^+ fluvial inputs into the system, followed by high nitrification rates in the estuarine superficial sediments and rapid burial and storage due to high SR. In coastal shallow waters nitrification is enhanced,

for instance, by the input of organic materials (e.g., Henriksen and Kemp, 1988). As mentioned above, the high concentration of P and PO_4^{-3} can derive from higher fluvial activity (Fonseca et al., 2011).

Unit 3A (ca. 4300 and 4250 cal BP; ca. 2350 and 2300 cal BC) is characterised by high contents of SO_4^{-2} and by the presence of gypsum at the base, by the presence of diatoms, see below; Figure 4.19B), while NO_3^-, PO_4^{-3} and P decrease to minimum values (Figure 4.21) pointing to the flooding of marine waters. The diatoms in this Sub-unit indicate initial tidal conditions, moving in the uppermost part to a subtidal environment characterized by the dominance of the marine semi planktonic *Cymatosira belgica* which outnumbers benthic/epiphytic diatoms (Figure 4.22).

Nowadays the fluvial-estuarine boundary is placed near Arapouco (Figure 2.4; Bettencourt and Ramos, 2003), but only influences the present-day Sado channel, a narrow channel incised in the alluvial sediments that are essentially fed by the fluvial network during flooding episodes. Estuarine conditions were present at Arapouco until ca. 3240 cal BP (see below), being the fluvial-estuarine boundary by that time located at upstream reaches of the Sado still unknown.

According to palaeocological and palaeoenvironmental data and taking into consideration the depth of the Unit (-130 to -90 MSL) and contemporary MSL (ca. -130 cm MSL assuming a MSL rise of 0.31 mm yr^{-1}; Costas et al., 2016a), at the time of deposition of Unit 3A the fluvial-estuarine boundary was located near Laxique, allowing for the occasional flooding of the area by marine waters. Even under marine influence, organic source indicators (C_{org}, N, $\delta^{13}C$, $\delta^{15}N$) point to the prevalence of terrestrial and freshwater organic materials, being the incorporation of marine organic matter recorded by a slightly increase in the $\delta^{13}C$ values (Figure 4.19 and 5.9), reflecting the proximity of the freshwater and terrestrial organic sources to the study area and indicating the very upstream limit of the estuarine area at the beginning of the Late Holocene.

Unit 3B (ca. 4250 and 4200 cal BP; ca. 2300 and 2250 cal BC) is characterized by new fluvial inputs reflected by the increase in the sand content (Figure 4.19A). Nitrate, PO_4^{-3} and P increase while SO_4^{-2} decrease pointing to the regression of the fluvial-estuarine boundary and to the establishment of more fluvial conditions. However, diatom assemblages indicate to some extent still the influence of marine water (Figure 4.22). Diatom assemblages are made by common benthic and widespread species in intertidal zones of estuaries and marine coasts worldwide. Assemblage is dominated by large mobile epipelic species characteristic of mudflats environments (Figure 4.22).

Unit 4 (ca. 4200 and 4000 cal BP; ca. 2250 and 2050 cal BC) marks the transition to the upper intertidal environments. It is characterized by episodes of fluvial sediment loads reflected by the increase of sandy sediments (Figure 4.20) and the slightly increase in MS values. Nitrate, PO_4^{-3}, P

and SO_4^{-2} contents are similar to Sub-unit 3B decreasing in the top of the Unit (Figure 4.21), probably in response to the increase of coarse particles. The sharp variations of PO_4^{-3} at the transition to Unit 5 is most probably reflecting the influence of biogeochemical changes (ancient redox boundaries) in the sediment profile than environmental changes once PO_4^{-3} tend to be retained in the sediment in the presence of oxidizing conditions and released to the water (and transported downstream) under reducing conditions (e.g., Scanes et al., 2017). The presence of shallow and sharp redox potential boundary in the sediment can point to high organic matter supply and to low bioturbation, indicating eutrophic conditions at ca. 4000 cal BP (2050 cal BC).

Unit 4 is a threshold considering the marine influence at Laxique. From 4000 cal BP onwards, sedimentation occurs essentially under fluvial conditions with sedimentation contributing to the aggradation of the alluvial plain. Since 4000 years ago the progradation rate of the sand spit increased and barrier grew north (Costas et al., 2015) certainly reducing the water exchange between the sea and the river and allowing for the progradation of fluvial environments.

According to sediment depths of Units 3 and 4 (-130 to 88 cm MSL) and the projected depth for the MSL at that time (-130 to -120 cm MSL) the environmental conditions changed from a tidal flat to an upper intertidal area offering conditions for the development of saltmarshes. But the presence of a saltmarsh at the beginning of the Late Holocene at Laxique is difficult to access. $\delta^{13}C$ determined for Units 3 and 4 are quite similar with the values measured for the Units 1 and 2 (below), reflecting essentially organic materials sourced in terrestrial and freshwater environments. The Sado channel margins at Alcácer do Sal, that represent the present-day fluvial-estuarine boundary and where low salinity values of 0 to 0.5 ‰ are present derived mostly from tidal processes (e.g., Ferreira et al., 2003), are essentially colonized by *Phragmites australis* (C3 photosynthetis pathway) (Moreira, 2016), an autochthonous cosmopolitan species that tolerates a high variety of environments. Freshwater marshes are not described at present in the Sado but could have existed in the past as described between 6700 and 5800 cal BP in the Muge stream, a Tagus tributary (van der Schriek et al., 2007b). At present, Sado riverine margins are highly anthropized, frequently used as agriculture fields, mostly rice crops (Figure 2.6) and most possible inhibit the development of natural freshwater environments. Organic chemical data produced from sediments collected in Alcácer do Sal (ALC-S) present higher C/N, $\delta^{13}C$ and $\delta^{15}N$ values than the values determined for Units 1 to 4 (Figure 5.9). The differences in these values can result from: i) post-depositional processes such as bioturbation, diagenesis or microbial degradation that are known to affect sediment chemical signals through time, with most expression at a scale of thousands of years, i.e., Early-Mid Holocene records (e.g., Khan et al., 2015); and ii) a higher contribution of local C3 (saltmarsh) plants and terrestrial/freshwater organic materials (lower

$\delta^{13}C$, $\delta^{15}N$ and N) in relation to marine organic matter (higher $\delta^{13}C$, $\delta^{15}N$ and N). However, considering the present-day similar environmental characteristics for intertidal areas of Alcácer do Sal that was taken as analogue for Laxique Units 3 and 4, the difference in the values do not support the existence of a saltmarsh most probably resulting from an intertidal area with strong fluvial influence, despite the influence of marine waters.

Unit 5 accumulated between 4000 and 960 cal BP (ca. 2050 cal BC and 980 cal AD), corresponds to the aggradation of the alluvial plain. Sediments represent a fine-up sequence constituted by sandy mud to mud with low MS pointing to low fluvial activity (peak discharges). Similar conditions of low fluvial activity (low peak fluvial discharges) under general wet conditions were described for the Tagus between 3500 to 1000 cal BP (Vis et al., 2010). A marked aridity event was defined for the Guadiana at 3100 cal BP (Fletcher et al., 2007). $\delta^{13}C$ values are low and C/N ratio higher than 10 reflecting the terrestrial/fluvial source of the OM (e.g., Lamb et al., 2006, Khan et al., 2015; Figures 4.20, 4.21 and 5.9). Phosphate and P contents increase in Unit 5 (Figure 4.21). The transfer of phosphorus to estuaries is mostly made through surface runoff that mobilizes particulate and dissolved P forms from land. In addition, the erosion of soils in areas with forest retreat greatly increased the contents of P that are transported to rivers and estuaries once most soils highly contribute to retain P (e.g., Slomp, 2011). Palynological evidence from SW Iberia indicate a retreat in the forest cover and progressive expansion of shrublands and heathlands since ca. 5000 cal BP (3050 cal BC; e.g., Fletcher et al., 2007; 2013; Chabaud et al., 2014; Gomes et al., 2020) that certainly allowed for soil erosion and the transport of sediments by surface runoff to the river. Evidence of anthropic influence on the landscape was recognized in both the Tagus (ca. 6000 cal BP; 4050 cal BC) and the Guadiana (ca. 5000 cal BP; 3050 cal BC) surrounding areas since the Middle Holocene (Fletcher et al., 2007; Vis et al., 2010). The palynological analyses performed in Arez3 also confirm a retreat in the vegetation in the study area since ca. 7000 cal BP (ca. 5050 cal BC; Figures 4.29).

Unit 6 also corresponds to the aggradation of the alluvial plain accumulated during the last 1000 years. $\delta^{13}C$ increase reaching values higher than -25‰ particularly in Sub-Units 6A and 6B (Figure 4.20). In pristine estuarine environments higher $\delta^{13}C$ values point to marine influence, with contribution of marine organic materials to the bulk organic matter (Lamb et al., 2006; Khan et al., 2015). However, Unit 6 correspond to the top 3 meters of the sedimentary succession, accumulated at depths between 290 to 610 cm above present-day MSL, where the intrusion of marine water is not possible considering present-day local tidal conditions. As mentioned above, $\delta^{13}C$ and $\delta^{15}N$ values of plant and soils are known to be affected by the application of manure and mineral fertiliser in crop areas (e.g., Senbayram et al., 2008; Treasure et al., 2016). Usually,

soils with high contribution of organic N (e.g., manure) present higher $\delta^{15}N$ values than unfertilized soils or mineral-fertilised soils (e.g., Senbayram et al., 2008; Fiorentino et al., 2015). $\delta^{13}C$ values can also be affected by the input of N-fertilisers, with soil $\delta^{13}C$ values decreasing with the application of manure (e.g., Bol et al., 2005; Senbayram et al., 2008). Notwithstanding, plant $\delta^{13}C$ values seem not to be affected by manuring increase with the application of mineral-N fertilisers (e.g., Bogaard et al., 2013), but are strongly influenced by environmental conditions, particularly by water availability (e.g., Jenkinson et al., 1995; Senbayram et al., 2008) making isotopic studies relevant considering past environmental conditions (e.g., Bogaard et al., 2013; Fiorentino et al., 2015). In dry years (drought), $\delta^{13}C$ tend to be lower and in optimal environmental conditions (water availability) $\delta^{13}C$ is higher (e.g., Senbayram et al., 2008; Bogaard et al., 2013; Fiorentino et al., 2015). In Laxique, both $\delta^{13}C$ and $\delta^{15}N$ present high values (Figures 4.20 and 4.21), pointing to the inclusion of fertilisers in the study area since, at least, ca. 700 cal BP (1250 cal AD). Additionally, MS and the sand content increase, pointing to high fluvial activity, and possibly to wetter conditions that contribute to higher $\delta^{13}C$ values in the bulk organic sediment, particularly between ca. 625 and 280 cal BP (1325 and 1670 cal AD; Sub-Unit 6A) and the last 50 years (Sub-Unit 6C). Records point to rice production in the Sado since, at least, the 18th century, nevertheless, it probably started before (Carmo et al., 2020). At present in the Sado area, rice is produced in continuous flooding conditions, where the soil is maintained waterlogged for several months and N-fertilisers added to soils (e.g., Figueiredo et al., 2014). The continuous flooding of soils and the addition of N can contribute to the high $\delta^{13}C$ values determined at the top core meters. Recent anthropogenic influence (Sub-Unit 6C, accumulated during the last 50 years) is also attested by the presence of polyethylene fragments within the sediment (Figure 4.19), at ca. 25 cm depth. Polyethylene began to be produced in the late 1930's and 40's, its expansion and usage diversification started at ca. '50s and it's still produced nowadays (e.g., Zalasiewicz et al., 2016).

In Arapouco 2/3 all source-sensitive organic indicators (i.e., C, N, $\delta^{13}C$) show that Units 2, 3 and 4 are different from Unit 5 in what concerns the origin of organic material incorporated in sediment (Figure 5.10). Considering that OM displayed a mean value of 8.5% in Units 2 to 4 and that the mean value of OM is of 5% in Unit 5 there is a clear indication of a shift in the organic matter input from 0 m MSL upwards (Figure 4.15). $\delta^{13}C$ decreases from the core base to the top (-23‰ to -27‰), with mean $\delta^{13}C$ values of -24‰ in Units 2 and 3, -25‰ in Unit 4 and -26‰ in

Unit 5 (Figure 4.15). This change reflects an increase of the contribution of organic matter from terrestrial plants and freshwater phytoplankton to the sediment through time.

The organic material of Units 2, 3 and 4 represent a mixture between marine dissolved organic carbon (marine DOC; Figure 5.10) and carbon sourced in C3 terrestrial plants and freshwater dissolved organic carbon (freshwater DOC; Figure 5.10). Units 2 and 3 sediments received a higher contribution of marine DOC (Figure 5.10), reflecting estuarine conditions with higher marine influence. At Unit 2, the increase in abundance of the diatom *Cyclotella meneghiniana*, a brackish/freshwater planktonic species, correlates well with high freshwater influence in the estuarine environment (DAZ 1; Figure 4.17). Its decrease at Unit 3 (DAZ 2; Figure 4.17) may be indicative of reduced allochthonous input from upstream and indicative of reduced tidal mixing (Weckström, 2006).

Within Unit 4 the contribution of freshwater DOC and C3 terrestrial plants (Figure 5.10) increases, pointing to a higher contribution of freshwater/terrestrial organic materials. C/N versus $\delta^{13}C$ in Unit 5 indicate a shift to organic material originated in freshwater components, initially essentially freshwater DOC and later freshwater particulate organic carbon (POC) and algae (Figure 5.10). C/N and $\delta^{13}C$ for Arapouco superficial sample are also represented in Figure 5.10.

The diatom *Thalassiosira decipiens* decreases and *C. meneghiniana* increases in Unit 4 (DAZ 3; Figure 4.17) indicating a decline in salinity that could be caused by a stronger freshwater influence and increasing eutrophication (Weckström, 2006). *T. decipiens* frequently appears throughout the present-day estuary with its highest development during the winter-early spring period with polyhaline conditions (Coutinho, 2003). It has been reported from vast inland seas, estuaries, bays, shallow coastal waters and rivers with tidal influence (Hasle and Sylversten, 1996) and is especially abundant in tidal inlets and large tidal channels (Vos and De Wolf, 1988). This broad distribution through rivers, estuaries, inland salt waters, and marine localities, suggests an ecologically diverse and tolerant taxon. Tide transported planktonic diatoms are often found in tidal-channel and tidal-inlet sediments (Vos and De Wolf, 1993), a fact that should be taken into consideration. Most of the benthic community of Unit 4 consists of epipelic and epiphytic diatoms (Figure 4.17). *Nitzschia sigma* is an epipelic taxon, dominant at the top of the sequence. It usually appears in high proportions within the intertidal zone or (shallow) subtidal zone in salinities of 5-17 ‰ and adapted to higher turbidity (Coutinho, 2003). Brackish epiphyte taxa are significant towards the top of the core. Accompanied by marine plankton, these assemblages are characteristic of mudflats and low-energy environments that are permanently submerged (Vos and De Wolf, 1993); they live on macroalgae and water plants.

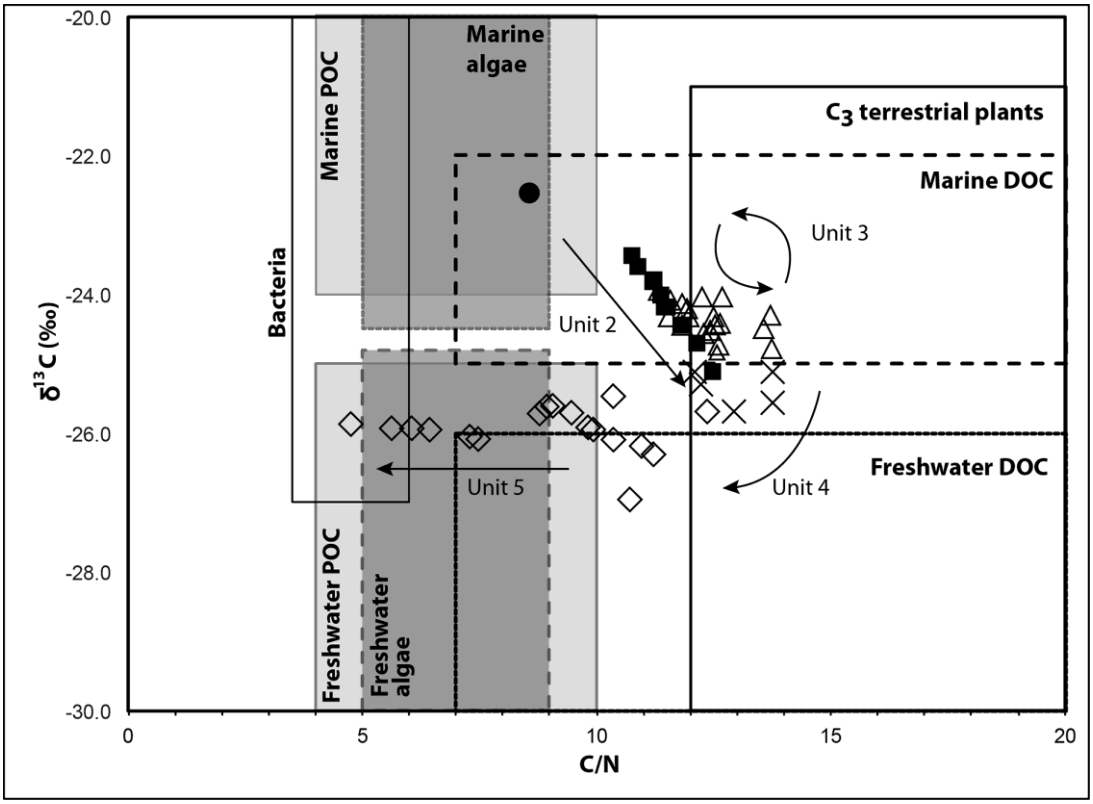

Figure 5.10 - C/N vs. $\delta^{13}C$ results plotted at adapted Lamb et al.'s graph (2006). Black filled squares represent Unit 2; black triangles represent Unit 3; black crosses represent Unit 4, and black diamonds represent Unit 5. The black circle represents the sediment collected in the main channel at Arapouco in 2017.

In addition, figures 5.11a and 5.11b show the correlation between OM versus N and OM versus C_{org}, respectively. In Units 2, 3 and 4 (i.e., below 0 m MSL) OM correlates with N and C_{org} (r^2 = 0.55, n = 49, considered significant for p = 0.05 using F-test in both cases) suggesting that both organic elements share a similar origin and vary in agreement with the OM. In Unit 5, OM presents no correlation at all with either N (Figure 5.11a) or C_{org} (Figure 5.11b) suggesting that these organic elements vary independently from OM. In fact, OM decreases gradually from the base to the top of Unit 5, and both C_{org} and N decrease abruptly at the base and remain almost constant along the remnant of the unit. The decrease in the organic compounds is interpreted as related to oxidation processes that favoured the loss of these organic elements, eventually enhanced by agriculture practices including rice production.

Nitrogen and C_{org} are correlated (r^2 = 0.85, n = 49, considered significant for p = 0.05 using F-test) in Units 2, 3 and 4 and in Unit 5 (r^2 = 0.86; n = 9, considered significant for p = 0.05 using F-test) (Figure 5.11c) pointing to the same source of both organic components in these units.

Three anomalous N values were measured between 0 cm and 100 cm MSL that are most probably related to additional inputs of N-fertilizers associated with rice production.

Based in our data, one can assume that the organic material is typical of an estuarine area, with contributions from both terrestrial/freshwater and marine organic compounds, between the core base (ca. 425 cm MSL) and 0 m MSL, corresponding to Units 2, 3 and 4 previously described. The basal units (Units 2 and 3) reflect the higher influence of marine water and Unit 4 seems to reflect the transition to a more terrestrial / freshwater influenced environment. Above 0 m MSL (Unit 5), organic material shows a higher contribution of freshwater phytoplankton, which is consistent with the aggradation of an alluvial plain (Figures 5.10 and 5.13). The existence of *S. plana* shells considered to be *in situ* in Units 2 and 3 are also indicative of prevailing estuarine conditions (tidal flat or high subtidal zone) in this area.

The $\delta^{13}C$ values determined for the prospecting sediment cores recovered from Vale do Guizo and São Bento, whose base is dated to ca. 3000 cal BP (1050 cal BC; Table 4.1), with mean values of -24.7‰ (Figure 4.11), also reflect an estuarine area receiving organic matter from marine (marine dissolved organic carbon (DOC)) and terrestrial (C3 land plants)/fluvial (freshwater DOC) environments during the Late Holocene. Diatom assemblages in Vale do Guizo are dominated by the marine tychoplanktonic *Cymatosira belgica,* while in São Bento, diatom assemblages are composed by planktonic species common in fresh and brackish waters (Figure 4.12), despite the presence of *C. belgica*. This diatom is a cosmopolitan species found both in plankton and in the benthos, frequently found in sandy beaches but also very abundant in silty sediments (Figures 4.12 and 4.13).

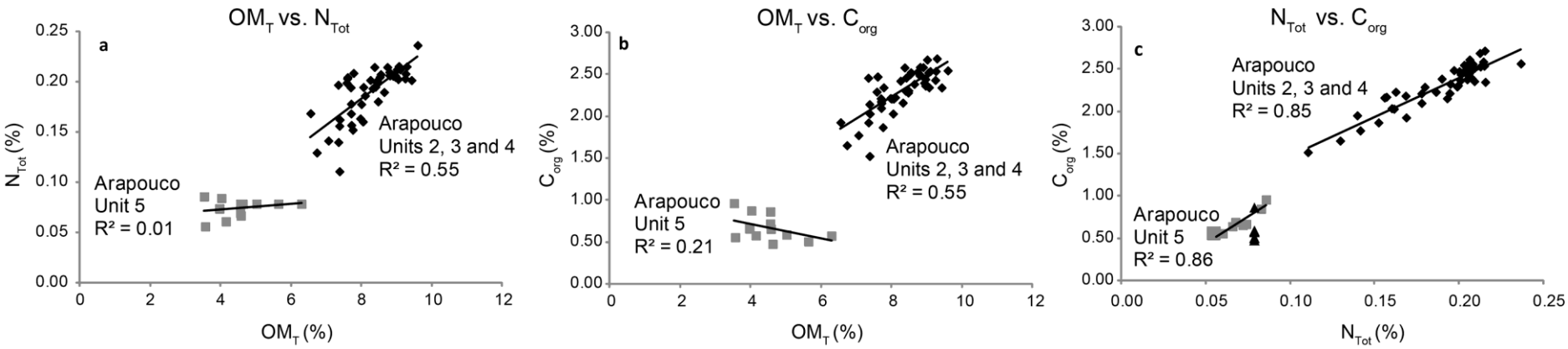

Figure 5.11 – Correlation between: a - OM and N; b - OM and C_{org}; c - N and C_{org} (c). Black diamonds represent samples from Units 2, 3 and 4 and grey squares represent samples from Unit 5. Black triangles (c) represent samples enriched in N.

The interpretations presented above, based on organic chemical compounds and palaeoecological indicators allowed to propose a schematic model for the environmental evolution and fluvio-estuarine boundary changes of the Sado estuary through the Holocene (since 8850 cal BP; 6900 cal BC; Figure 5.12).

During the Early Holocene, the high sea level rise rate promoted the flooding of the deep incised Sado basin (between - 38 and -23 m MSL) forming an extensive estuarine area as pointed out by the Arez3 sedimentary record. The oldest tidal deposits identified in this work are dated back to ca. 8850 cal BP (6900 cal BC) at the Carrasqueira valley bottom, located ca. 52 km distant the present-day inlet, at ca. -1060 m MSL (Figure 5.12A). Tidal environments certainly developed in the Sado valley bottom in a previous date, but the base of the Holocene infilling was not achieved in this channel. Estuarine conditions continued in the Carrasqueira valley until 7040 cal BP (5090 cal BC) when freshwater environments seem to take place, but the higher marine influence was detected until ca. 7500 cal BP (5550 cal BC), as evidenced by the higher contents of Chenopodiaceae and the presence of foraminifera (assemblage identification on-going).

The environmental change at 7500 cal BP (5550 cal BC) is coincident with the decrease of sea level rise identified by García-Artola et al. (2018) that changes from 0.81 ± 0.07 cm yr^{-1} to 0.34 ± 0.10 cm yr^{-1} at that time. A peak of marine influence was also identified at the Muge valley around that date (Van der Schriek et al., 2007a).

By then, the estuary extended, at least, until São Bento, as evidenced by the deep palaeovalley (-34 m MSL) and by the date determined at the base of São Bento (prospecting) core of 2288-1995 cal BP at a depth of -9.4 m MSL (Figure 5.12A). Notwithstanding, shallow valleys such as the Vale dos Açudes, were not flooded during this transgression (Figure 5.12A).

The maximum extension of the estuarine area is still difficult to identify. At Laxique, located ca. 65 km from the sea at present, a deep valley reaching -23 m MSL occurs, deeper than the Early Holocene MSL (ca. -11.85 m MSL at 8850 cal BP). Nevertheless, the valley infilling is coarse, difficult to sample by manual and mechanical meanings and only the top 8.1 m, corresponding to the Late Holocene, was recovered. The coarse sediments in depth could result from the accumulation of alluvial fan deposits or correspond to a bay-head delta forming at the limit of tidal influence.

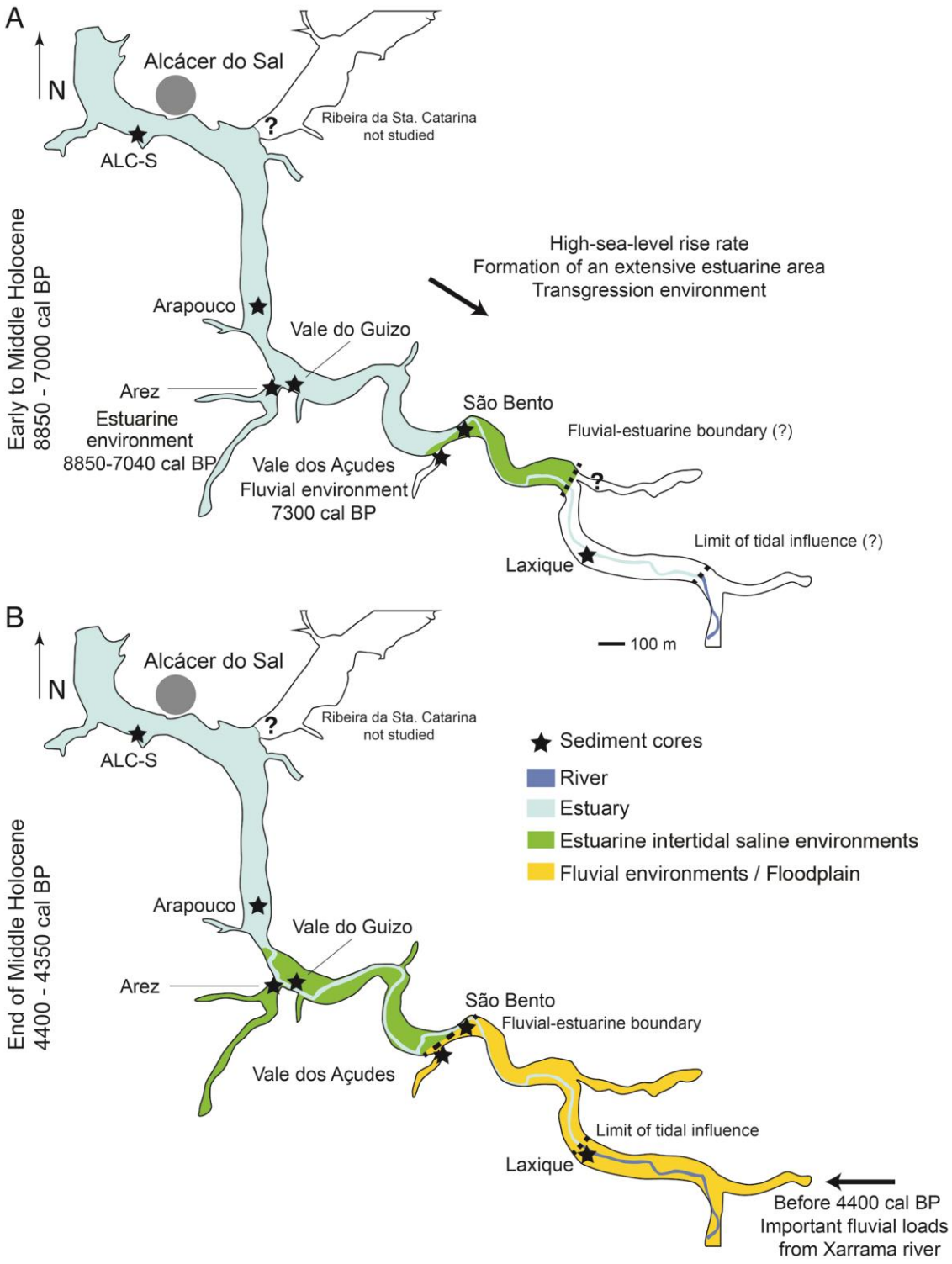

Figure 5.12 - Schematic model proposed for the palaeoenvironmental evolution and fluvial-estuarine boundary changes of the Sado estuary since 8850 cal BP (to be continued). A - Early to Middle Holocene; B - End of the Middle Holocene.

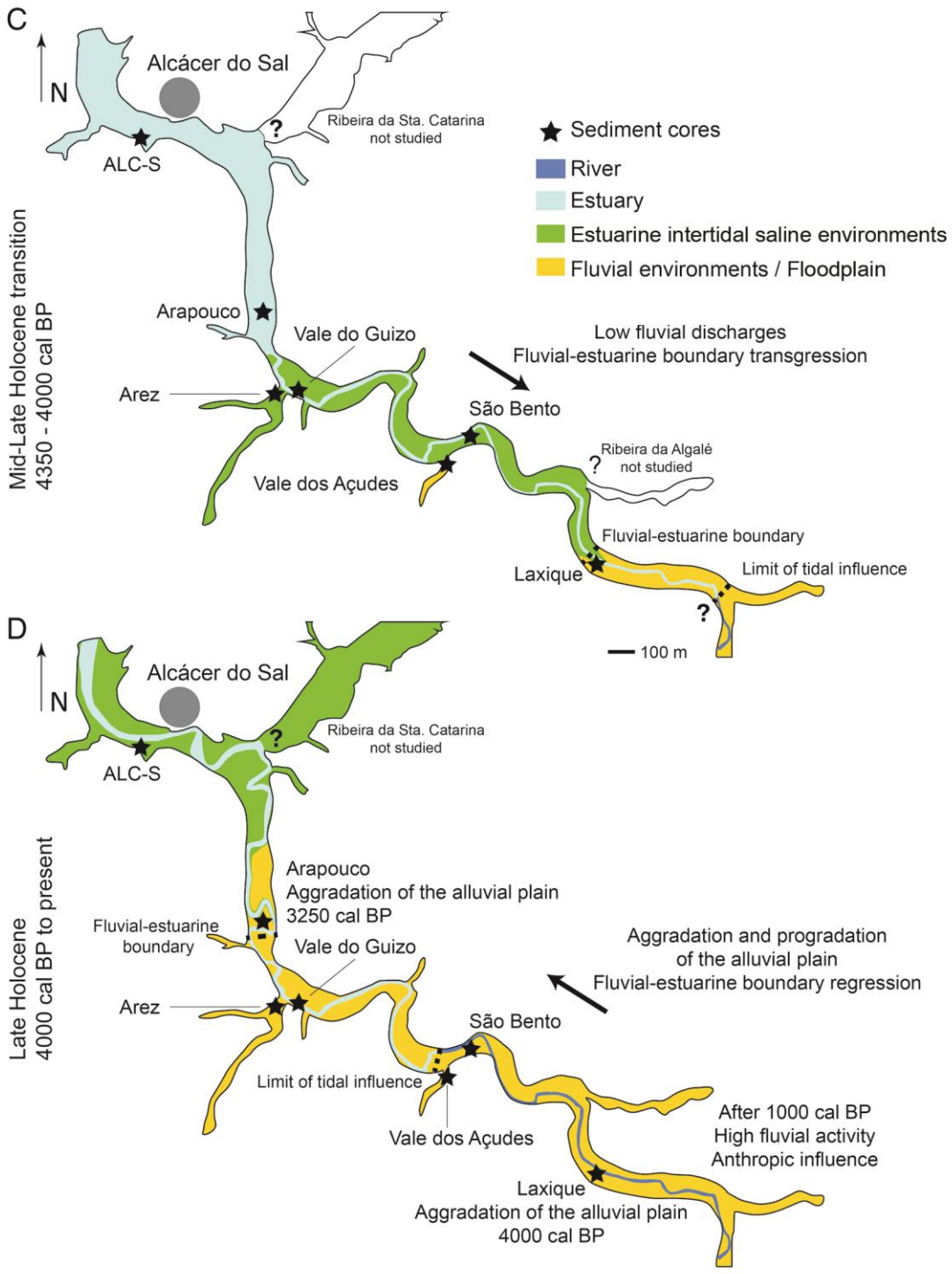

Figure 5.12 - Schematic model proposed for the palaeoenvironmental evolution and fluvial-estuarine boundary changes of the Sado estuary since 8850 cal BP (continuation). C - Mid-Late Holocene transition; D - Late Holocene to present.

During the Middle Holocene (7040 to 4910 cal BP; 5090 to 2960 cal BC), after the deceleration of the MSL rise rate, the Arez3 record points to higher fluvial influence and to the expansion of freshwater wetlands in detriment of brackish environments as suggested by the increase in the contribution of OM from terrestrial plants and freshwater phytoplankton (Figure 5.12B). Since then, and particularly during the Late Holocene, the fluvial/estuarine responses seem to be primarily related to prevalent dry climatic conditions (Figure 5.13; see discussion below). This fact is evident in the constant advances and retreats of the fluvial-estuarine boundary recorded in the Laxique and Arapouco sedimentary succession (Figure 5.13). Indeed, western Mediterranean Late Holocene is characterised by prevailing drier climatic conditions since ca. 5000-4000 cal BP (3050-2050 cal BC; Fletcher et al., 2007; 2013; Carrión et al., 2010; Chabaud et al., 2014; Gomes et al., 2020) with peaks of high fluvial activity that promote regular to sporadic inundation of distal estuarine areas in South Iberia (Vis et al., 2010; Figure 5.13). High inputs of organic materials seem to occur around 4000 cal BP at Laxique leading to the development of a redox boundary preserved in depth (Figure 5.13). The availability of sediment can also result from vegetation retreat due to the establishment of drier climatic conditions (e.g., Fletcher et al., 2007; 2013; Carrión et al., 2010; Chabaud et al., 2014; Gomes et al., 2020). Previously to 4400 cal BP (2450 cal BC) important fluvial loads, particularly from the Xarrama stream, were identified in the Laxique record (Figure 5.12B). Later, between 4350 and 4000 cal BP (2400 and 2050 cal BC), the fluvial-estuarine boundary retreated to Laxique, as evidenced by the presence of marine and brackish diatom assemblages at this location (Figure 5.12C). A retreat of the fluvial-estuarine boundary was also identified at Arapouco, between 3400 and 3300 cal BP (1450 and 1350 cal BC). From 4000 cal BP (2050 cal BC) onwards the aggradation of the alluvial plain started in Laxique as well as its downstream progradation. The installation of the alluvial plain took place at Arapouco at ca. 3250 cal BP (1300 cal BC; Figure 5.12D). According to Moreira (1992) saltmarshes started to develop since, at least, 2700 cal BP (750 cal BC) at the intertidal margins of the present-day estuary. At Alcácer do Sal the subtidal margins were silted-up between the 13th and 14th centuries, allowing for the development of present-day saltmarshes (Moreira, 2016). At present saltmarshes develop in intertidal environments of the estuary occupying an area of ~7.2 km^2 (Moreira, 1992). Anthropic activities and the use of fertilizers for agriculture purposes are imprinted in the top sediments of the Sado infilling and were identified in all the studied sediment cores: Arez3, Laxique and Arapouco (Figure 5.13).

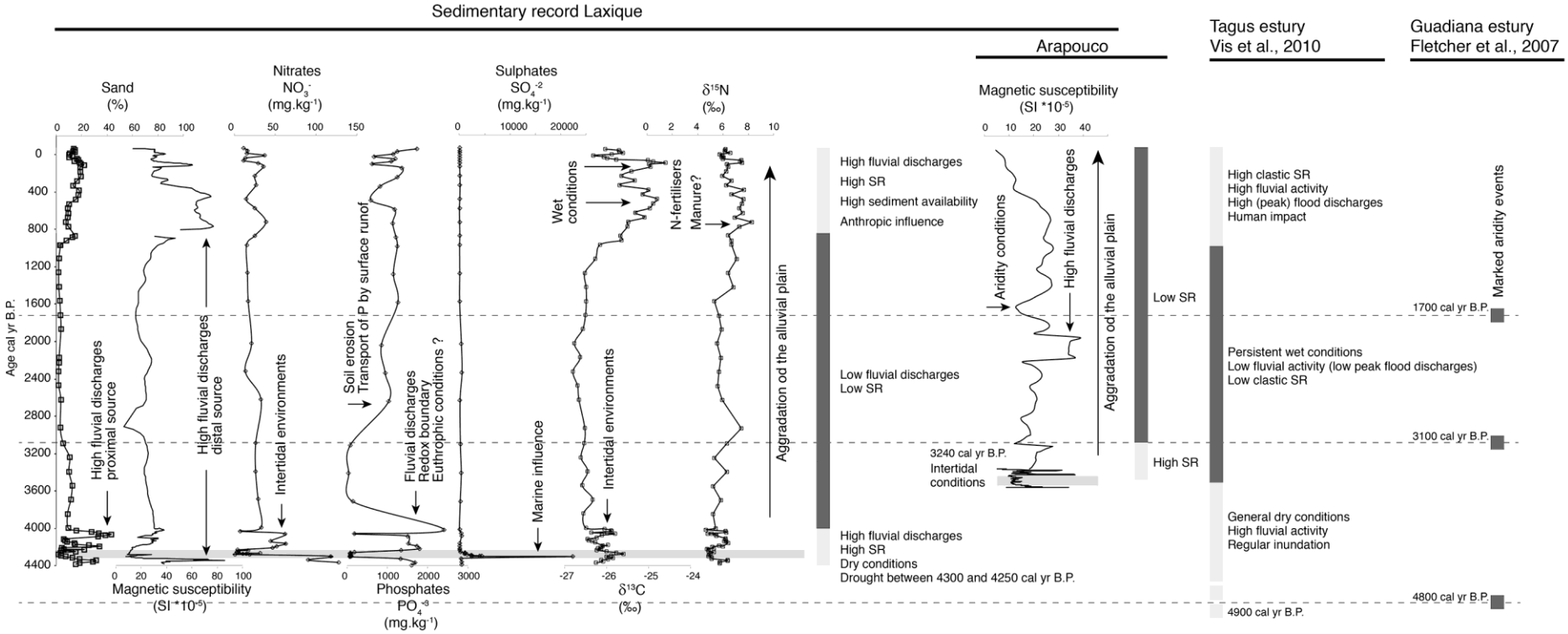

Figure 5.13 - Summary of environmental changes at Laxique and Arapouco in the Sado, the Tagus (Vis et al., 2010) and the Guadiana (Fletcher et al., 2007) valleys. Analysed proxies plotted against age cal BP.

Sedimentation rates and sedimentation triggers and constraints

Estuaries are transitional areas actively controlled by river discharge, flooding and sediment availability (e.g., Brown, 1997) and are very sensitive to global and regional sea level oscillations (e.g., Wong et al., 2014; Little et al., 2017). Sedimentation rates in estuaries are also highly dependent on sediment availability and accommodation space (e.g., Brown, 1997). As mentioned in the previous discussion, Sado has a deep incised palaeovalley reaching -40 m MSL at Alcácer do Sal and -23 m MSL at Laxique (Figure 5.3) offering accommodation space for the deposition of sediments through the Holocene. In this case, the extension of the estuary relies mostly on the sea level rise rate and contemporary sedimentation rates; sedimentation rates, by its turn, are essentially dependent on sediment availability, river discharges and fluvial loads.

The sedimentation rates determined for the all the cores collected in the Sado valley indicate high rates in depth, for sediments accumulating under subtidal and intertidal conditions below or at the MSL, and lower rates for sediments deposited above MSL corresponding to high intertidal areas and to the aggradation of fluvial materials and building-up of the alluvial plain (Figure 5.14). The sedimentary infilling pattern of the Sado valley seems to follow the same depositional characteristics of other SW Iberian estuaries (e.g., Dabrio et al., 2000; Boski et al., 2002; 2008; Lario et al., 2002; Vis et al., 2008; Camacho et al., 2016; Table 5.1) with sedimentation rates surpassing mean sea level rise rates at ca. 7000 cal BP, but with higher mean sedimentation rates, reflecting the strong Mediterranean character of the Sado river (Table 5.1 and references).

During the Early and the beginning of the Middle Holocene the sea level was rising at a rate (0.81 ± 0.07 cm; García-Artola et al., 2018) higher than the sedimentation rates determined, at least, in Arez3 (between 0.22 and 0.64 cm yr^{-1}; Figure 5.14) being the sea level the main factor responsible for the extensive flooding of the area.

The sedimentation rates only surpassed the MSL rise rate between 7120 and 6800 cal BP (between 5170 and 4850 cal BC; Figure 5.14), after the deceleration of the sea level rise (Costas et al., 2016a; García-Artola et al., 2018), achieving high values of 1.2 cm yr^{-1} (Figure 5.14) and promoting the rapid vertical accretion of the valley bottom and estuarine basin from that date onwards. The Carrasqueira is a high-gradient stream with torrential hydraulic regime (Arcão river in the Geological Map of Portugal; Gonçalves and Antunes, 1992) and, in such conditions, it is an important contributor of sediments to the lower section of the valley and to the Sado river that certainly played a role for the high sedimentation rate estimated for the Middle Holocene. A generalised forest decline was identified in diverse sequences of SW Iberia from 7000 cal BP onwards (Cambourieu-Nebout et al., 2009; Chabaud et al., 2014; Fletcher et al., 2007; Fletcher

and Sánchez-Goñi, 2008; Gomes et al., 2020; Vis et al., 2010). The loss of vegetation cover certainly allowed for soil erosion and the transport of sediments by surface runoff to the river.

Table 5.1 - Estimated sedimentation rates for SW Iberian estuaries.

	Core location	Mean SR cm yr^{-1}	SR determination method	Temporal interval	Reference
Portugal	VAL core (Tagus estuary)	0.19	Linear regression using AMS ^{14}C dates	Last 3500 years	Vis et al., 2016
	Corroios saltmarsh (Tagus estuary)	0.15	Linear regression using AMS ^{14}C dates	80-240 CE to present day	Silva, 2013
		0.60 to 0.90	Exponential regression using ^{210}Pb values	Last 150 years	
	Pancas saltmarsh (Tagus estuary)	0.22	Linear regression using AMS ^{14}C dates	560-680 CE to present day	Silva, 2013
		2.20	Exponential regression using ^{210}Pb values	Last 150 years	
	Mouchão da Póvoa saltmarsh (Tagus estuary)	0.29	Linear regression using AMS ^{14}C dates	1350-1290 cal BP to present day	Silva, 2013
		1.41 to 1.55	Exponential regression using ^{210}Pb values	Last 150 years	
	ALC-S (Sado estuary)	2.2	AMS ^{14}C dates using CLAM 2.3.2 (updated in this work)	685-600 cal BP	Moreira, 2016
		0.13		last 1350 years	
	Arapouco (Sado estuary)	2.2	AMS ^{14}C dates using CLAM 2.3.2	3570-3240 cal BP	This work
		0.06		Since 3240 cal BP	
	Laxique (Sado estuary)	0.75	AMS ^{14}C dates using CLAM 2.3.2	4400-4000 cal BP	This work
		0.07		4000-970 cal BP	
		0.2		Since 970 cal BP	
		0.74		Last 140 years	
	Arez3 (Sado estuary)	0.45	AMS ^{14}C dates using CLAM 2.3.2	8850-8550 cal BP	This work
		0.22		8550-7470 cal BP	
		0.64		7470-7120 cal BP	
		1.2		7120-6800 cal BP	
		0.02		6800 -1170 cal BP	
		0.14		Since 1170 cal BP	
	Guadiana estuary	0.07	Linear interpolation using AMS ^{14}C median dates	prior to ca. 7300 cal BP	Fletcher et al. 2007
		0.012		after ca. 7300 cal BP	
Spain	Odiel estuary	0.1	SR derived from ^{14}C dating	Since 6500 cal BP, following sea level rise deceleration	Lario et al., 2002
	Guadalquivir estuary	<0.25	SR derived from ^{14}C dating	Since 6500 cal BP, following sea level rise deceleration	Lario et al., 2002
	Guadalete estuary	0.1-1.5	SR derived from ^{14}C dating	Since 6500 cal BP, following sea level rise deceleration	Lario et al., 2002

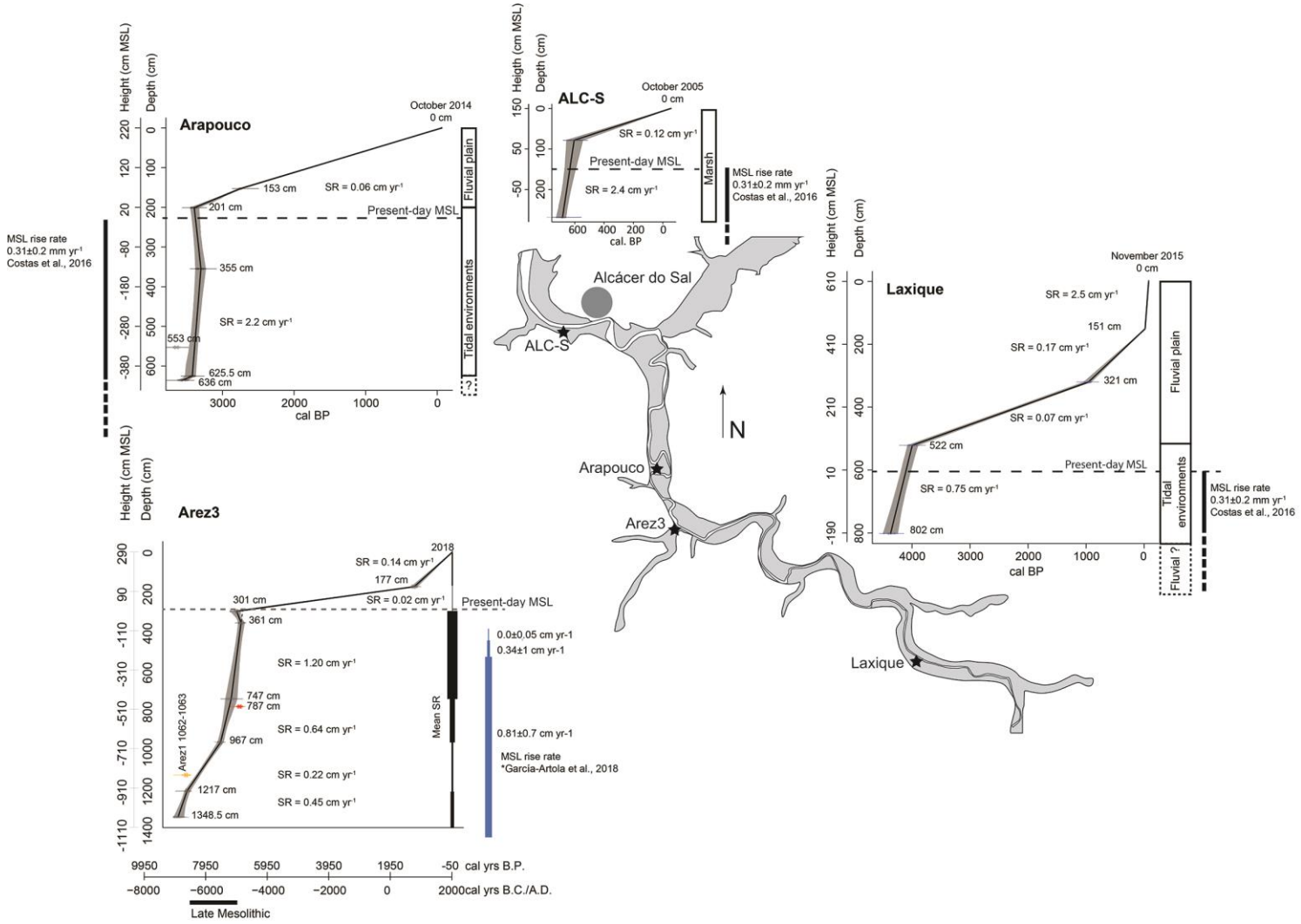

Figure 5.14 - Sedimentation rates (SR) determined for the sediment cores Arez3, Laxique, Arapouco and ALC-S (age-model updated from the one published in Moreira, 2016).

During the Middle to Late Holocene, under prevailing low sea level rise rates (e.g., Costas et al., 2016a; García-Artola et al., 2018) the sedimentation is mostly dependent on river flows and sediment availability. Despite the general drier conditions at the beginning of the Late Holocene that could increase the sediment availability due to vegetation retreat, storminess periods were also documented on the NW Mediterranean (e.g., Sabatier et al., 2012), southern Spain (e.g., Rodríguez-Ramírez et al., 2015) and along the Portuguese coast (e.g., Costas et al., 2015) certainly influencing river discharges. Higher precipitation will increase the river transport competence allowing for the higher proportion of magnetic particles sourced in the Iberian Pyrite Belt to reach and accumulate in the core sediment (e.g., Ellwood et al., 2001). Several MS peaks were identified in all sediment cores (Figures 4.15, 4.19, 4.25 and 5.14) as a response to episodes of intensification of terrestrial input, likely favoured by short episodes of intense precipitation. Mediterranean rivers can experience extreme floods during prevalent continental wet conditions (e.g., Thornes et al., 2009; Cid et al., 2017) and are strongly influenced by seasonal precipitation variability, with maximum discharges usually occurring during the autumn and winter, and minimum flows occurring during the summer (e.g., Thornes et al., 2009; Benito et al., 2015).

At Laxique, sediments accumulated between 4200 and 4000 cal BP (2250 and 2050 cal BC), are characterized by episodes of fluvial sediment loads reflected by the increase of sandy sediments and the slightly increase in MS values (Figures 4.19 and 5.14). The presence of FeO minerals and quartz grains with Fe coating will likely be influencing the magnetic response of the sediments.

At Arapouco, 15 km downstream, the higher intensity of MS peaks identified between 3570 and 3400 cal BP (1620 and 1450 cal BC) also point to higher inputs of terrigenous material. In this interval, the MS peaks correspond to the occurrence of coarse (sandy) sediment layers mostly constituted by quartz grains brought to the area by the fluvial network. Quartz is a diamagnetic mineral (Hayes, 2015) and thus responds to magnetization yielding negative values. Iron-coating on the sand grains were not observed in morphoscopic analysis of this samples, and it is reasonable to conclude that the peaks in MS are probably related to the finer constituents (size fraction <63 μm). According to these results, under high stream discharges coarse sediments accumulate at the upstream reaches of the estuarine area while finer sediments with magnetic particles are transported and accumulated more downstream. At this location, several MS peaks were also identified between 3300 and 3240 cal BP (1350 and 1290 cal BC; Figures 4.15 and 5.14) reflecting higher terrigenous inputs with high frequency (each ~50 cm). The high terrigenous input and the high SR at that time (Table 5.1) promoted the fast silting-up of the area and the transition from an aggradational subtidal-intertidal mudflat to an alluvial plain. In addition, MS peaks were obtained for the last 175 years (Figures 4.15 and 5.14) reflecting higher inputs of

terrigenous material with higher contents of coarse material in sediments accumulated at a low sedimentation rate. The later MS peaks are probably related with the silting up of the area and the decrease of accommodation space, the sedimentation being mostly dependent on repetitive fluvial floods.

Similarly to Laxique and Arapouco, the high SR determined during the 13th and 14th centuries in the Alcácer do Sal core (Moreira, 2016) could correspond to high terrestrial inputs promoting the silt-up of this subtidal area. The decrease in the sedimentation rate for the top sections of the core (>40 cm MSL) could be related to the higher altitude and reduction of the accommodation space forming conditions for the development of a saltmarsh.

By opposition, upstream retreats of the fluvio-estuarine boundary were identified in both Laxique and Arapouco between 4350 and 4000 cal BP (2400 and 2050 cal BC) and 3400 and 3300 cal BP (1450 and 1350 cal BC), respectively. Sediments during those periods are characterized by low MS values (Figures 4.15, 4.19 and 5.14), suggesting lower terrestrial inputs. This higher marine influence in the innermost and marginal areas of the estuary can be triggered by diverse factors such as tsunami events, sea level oscillations, storminess episodes or changes in river flow.

High-energy events were recorded at the Guadalquivir estuary/sandy barrier at 4000, 3550 and 3150 cal BP (2050, 1600 and 1200 cal BC; Rodríguez-Ramírez et al., 2015). Both 4000 and 3150 cal BP events were correlated with storminess conditions, but the 3550 cal BP event was related to a seismic event that occurred at the SW Portuguese margin catalogued by Lario et al. (2011) as a tsunami-generated event (Rodríguez-Ramírez et al., 2015). However, evidence for this event has only been reported in some areas of the Gulf of Cadiz, and it was considered as a seismic event that generated a local tsunami (Lario et al., 2011). Also, evidence of barrier permeability and an increase of marine influence around this period were found on sedimentary sequences sampled along the SW Portuguese coast at Albufeira, Melides and Santo André coastal lagoons (Figure 2.8): Albufeira lagoon between 4900 and 3400 cal BP (2950 and 1450 cal BC); Melides lagoon after 3950 cal BP (2000 cal BC); and Santo André lagoon between 3770 and 1500 cal BP (1820 cal BC and 450 cal AD; Freitas et al., 2002).

Positive oscillations of sea level rise rate promoted by regional climatic factors (e.g., Church et al., 2013) and enhanced storminess periods, can also affect the position of the fluvial-estuarine boundary. Long-term regional oscillations of the relative sea level can be brought about by changes in the wind regime, ocean heat, freshwater content and atmospheric pressure (Church et al., 2013). Costas et al. (2016a) reported small oscillations of the sea level rise curve in the last 6500 years in the Sado area, most probably associated with climate variability, which induced a

small positive change of the sea level ca. 3600 cal BP (1650 cal BC). Also, an enhanced storminess period affecting southern Europe, and particularly the Western Portuguese central coast, SW France coast and the western Mediterranean seems to have occurred in the time interval of 4000-3000 cal BP (2050 and 1050 cal BC; Costas et al., 2016b and references therein). Costas et al. (2015) mentioned an episode of shoreline retreat at the Tróia spit ca. 4000 cal BP (2050 cal BC) and, according to these authors, the barrier enclosing the Sado estuary was much less robust until ca. 3250 cal BP (1300 cal BC).

Fluctuations on the MSL rise rate have not yet been identified in the curves draw for the Tagus estuary. Notwithstanding, the record of changes in the MSL rise rate and the influence of such oscillations in the environmental conditions of both estuaries can also be dependent on these two river hydrological parameters that differ severely, at least, considering their natural mean annual flows.

In what respects influence of river discharge on salinity changes in estuaries, several accounts have been published (e.g., Liu et al., 2007; Shaha and Cho, 2016; Robins et al., 2018). For the north Portuguese estuaries, the results point to an increase in salinity during periods with low river flows (Douro estuary - Azevêdo et al., 2010; Mondego estuary - Baptista et al., 2010). For the Tagus estuary, although variation in salinity over the estuarine area for wet (>300 $m^3 s^{-1}$) and dry (<300 $m^3 s^{-1}$) years has not been published, a higher density of marine occasional species has been reported in the dry years for the upper estuary (Costa et al., 2007) probably reflecting higher salinity conditions.

For the Sado estuary, no data was available until now but, at present, due to the low river discharge, as a consequence of the flow control (water retention by dams) and the severe drought felt in Portugal during 2017, the marine influence is present in the channel at Arapouco, where organic matter is represented by Marine POC and Marine algae (Figure 5.11) (information from Index SPI 12 months at IPMA).

Drier climatic conditions were defined for the northern littoral area of Alentejo (south Portugal) during the Late Holocene, based on palaeoecological analysis of sediment cores collected on littoral lagoons and peat bogs (Queiroz, 1999). Drier conditions were also identified in other geographical areas of SW Europe (e.g., Fletcher et al., 2007, 2013; Carrión et al., 2010; Danielsen et al., 2012; Chabaud et al., 2014). In SW Portugal the drier conditions led to meagre sedimentation rates estimated in peat bogs at the SW Portuguese coast, such as Poços do Barbaroxa (Figure 2.8; Leira et al., 2019). The low MS values point to low fluvial activity (peak discharges). Similar conditions of low fluvial activity (low peak fluvial discharges) under general wet conditions were described for the Tagus between 3500 to 1000 cal BP (1550 cal BC and 950

cal AD; Vis et al., 2010). A marked aridity event was defined for the Guadiana at 3100 cal BP (1150 cal BC; Fletcher et al., 2007; Figure 5.13).

5.3 The Sado Late Mesolithic environments and implications for the last hunter gatherer communities

The Sado valley environment during the Late Mesolithic occupation

Late Mesolithic occupation in the Sado valley took place between 8400 and 7000 cal BP (6450 and 5050 cal BC; e.g., Arias et al., 2017; Peyroteo-Stjerna, 2020). The occupation is contemporaneous of the deposition of Arez3 Unit 1 and Sub-unit 2A (8850 to 7040 cal BP; 6900 and 5090 cal BC; Figure 4; Table 2). During this time span MSL was rising at a high rate in the SW Atlantic Portuguese margin (García-Artola et al., 2018) allowing for the flooding of the incised Sado and Carrasqueira valleys, and certainly other similar tributaries of the Sado. By then the estuary was still an open bay and Late Mesolithic sites were located between ca. 25 (Arapouco) and 45 km (Vale de Romeiras and Cabeço do Pez) from the open sea (Figure 5.15).

The sea level position and the chronology of sediments at ca. 8400 cal BP (6450 cal BC) point to an extensive drowned area at Arez3, probably reaching upstream areas of the Sado (Figures 5.13A and 5.16). Higher marine influence was detected until ca. 7500 cal BP (5550 cal BC), when freshwater environments started to increase. Between this time-period, the high intertidal areas of the Carrasqueira stream (developing in the shallow margins; Figure 5.16) and other similar valleys were certainly colonised by saltmarsh communities (Figure 5.16), as indicated by the organic chemistry results (presented above) and the palynological content of Arez3, with high percentages of Chenopodiaceae (saltmarsh). In the emerged landscape, mesophilous trees (mainly deciduous *Quercus*) are more abundant than other arboreal taxa, suggesting mostly the existence of a moist climate during the Late Mesolithic occupation. High-mountain pines (*Pinus sylvestris-nigra* type), usually related to continental climate, also occur but with low representation. Mediterranean pines, such as *Pinus halepensis-pinea* type and *Pinus pinaster*, are also represented (Figure 4.29), probably distributed across the interdune depressions.

Between 7450 and 7040 cal BP (5500 and 5090 cal BC; Arez3 Sub-unit 2A) Chenopodiaceae decreases, Asteraceae Cichorioideae slightly declines while *Isoetes* slightly increases reflecting the development of freshwater marshes, although estuarine conditions were still present in the area. A slightly rise of Mediterranean trees occurs, indicating the presence of temperate elements within the forests.

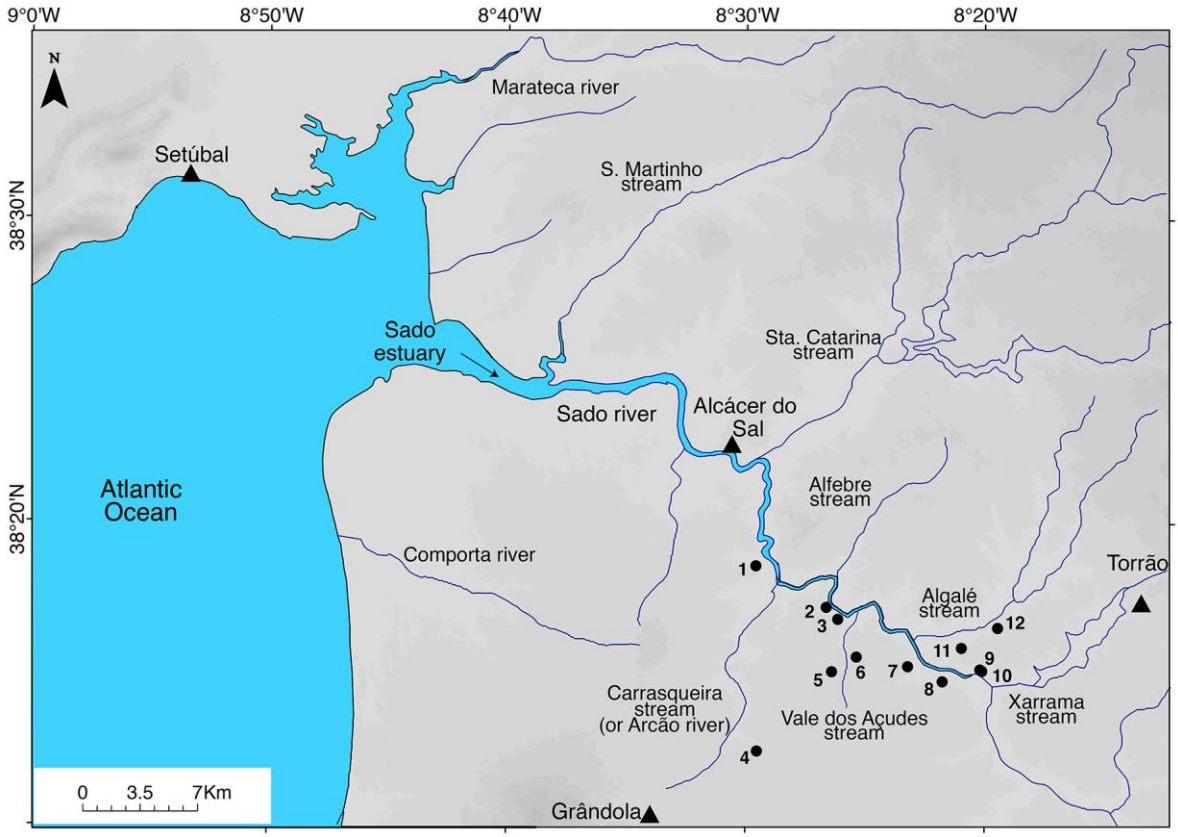

Figure 5.15 - Location of the Late Mesolithic shell middens and contemporary estuarine Sado area (ca. 8400 to 7000 cal BP; ca. 6450 to 5050 cal BC). Palaeoenvironmental evolution represented in figure 5.13. 1 - Arapouco; 2 - Cabeço do Rebolador; 3 - Barreirões; 4 - Barranco da Moura; 5 - Poças de São Bento; 6 - Fonte da Mina; 7 - Barrada das Vieiras; 8 - Cabeço das Amoreiras; 9 - Vale de Romeiras; 10 - Cabeço do Pez; 11- Várzea da Mó; 12 - Barrada do Grilo.

Such conditions were suitable for the occurrence of *Scrobicularia plana* and *Cerastoderma edule* at the Carrasqueira valley (and certainly in other similar valleys) during the Late Mesolithic occupation, allowing their exploitation by the Mesolithic groups. At present, despite not being abundant, *S. plana* and *C. edule* still occur in the Sado estuary. *Scrobicularia plana* is essentially present in the Alcácer do Sal channel in mud to fine sand sediments with lower salinity contents. Likewise, *Cerastoderma* spp. is present in the Alcácer channel, but also in the central estuarine basin, being salinity (values between 17 and 30 ‰), grain-size (fine sediments), OM content, and water depth (shallower areas) the most important factors contributing to its distribution (Santos, 2019). *Scrobicularia plana* shell fragments were described in Arez3 sediments, particularly between the base of the core and -360 cm MSL (Unit 1, Sub-unit 2A and partially Sub-unit 2B) confirming the presence of this species at this location of the Sado valley during the Early-Middle Holocene.

The Carrasqueira valley would also present suitable conditions for the presence of fish explored by Mesolithic groups. In the wider array of species identified in Arapouco and Poças de São

Bento shell middens, marine taxa show higher percentages. The identified taxa (e.g., *Chellon labrosus*, *S. aurata*, *A. regius* and *Dicentrarchus* sp.) still occur in the estuary (Sobral, 1993; Cabral, 1999; Cunha et al. 2014), feeding on various kinds of bottoms. The young form school and feed chiefly on invertebrates, molluscs, and also on fishes. Assuming fish behaviour has not changed since Mesolithic times, and considering individual size estimates from archaeological bone, one can assume that Mesolithic communities exploited the surrounding environments targeting large schools of young fish (e.g., *A. regius* and *Dicentrarchus* sp.; Gabriel et al., 2012; Gabriel, unpub. data).

Suitable areas for the collection of shellfish during the Mesolithic in the Sado valley

The Alcácer do Sal (palaeo)intertidal area was pointed out as the local used by Mesolithic groups for the collection of shellfish, based on the presence of foraminifera shells and calcareous pebbles among the content of Poças de São Bento shell midden (Duarte et al., 2019; Figure 5.15). According to our data, suitable conditions for the collection of shellfish were also present at the Carrasqueira valley, located ca. 7 km upstream Alcácer do Sal, but such conditions certainly extended to other similar valleys.

Based on morphological analysis (length and width of the alluvial plain) and on palaeovalleys depth and morphology, other tributaries of the Sado upstream Alcácer do Sal such as Santa Catarina and Alfebre streams (Figure 5.15) could have suitable environmental conditions for the development of molluscs and thus conditions for their exploitation by Mesolithic people.

By opposition, results performed at Vale dos Açudes located ca. 6.5 km upstream Carrasqueira (Figure 5.15), revealed a very shallow palaeovalley without marine influence. Similarly, brackish conditions in shallow tributaries of the Sado located upstream Vale dos Açudes should be absent. The Algalé (or Alcaçovas) stream is longer and has a larger alluvial plain pointing to a deeper palaeovalley, but the scarcity of data in this section of the Sado valley prevent us to characterize its environmental conditions.

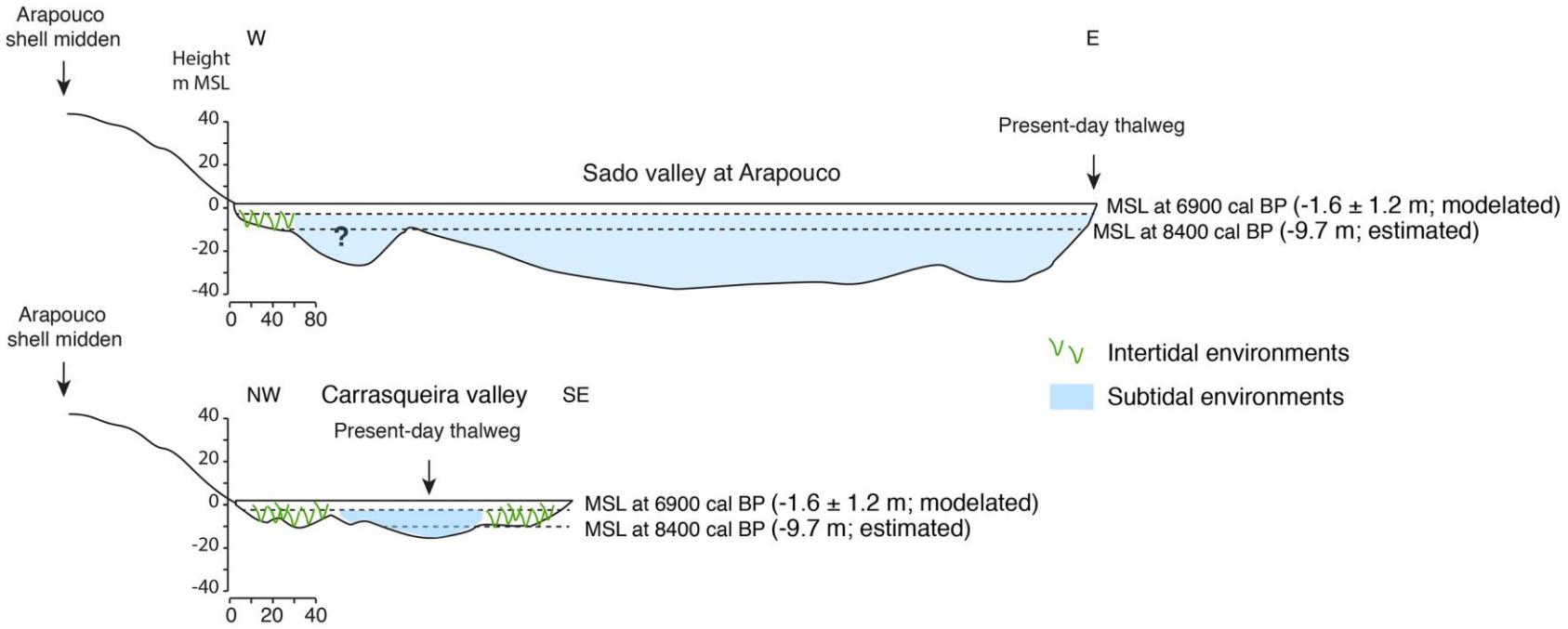

Figure 5.16 - Schematic environmental characterization of the Sado valley at Arapouco (above) and the Carraqueira valley (below) for the Late Mesolithic occupation and altimetric position of the Arapouco shell middens (Table 1.6). The information for mean sea level at 8400 and 6900 cal BP (6450 and 4950 cal BC) was retrieved from García-Artola et al. (2018).

The morphology of the Sado channel as characterized by ERT data seems to have deep steep margins, presenting less suitable conditions for the development of extensive marshes and/or tidal flats. However, less incised upstream areas of the Sado river would certainly have offered conditions for the establishment of intertidal environments. Notwithstanding, the maximum limit of marine inundation during the Early and Middle Holocene in the Sado channel is still unknown. Estuarine conditions were confirmed during the Mid-Late Holocene transition (between 4350 and 4000 cal BP; 2400 and 2050 cal BC) at Laxique, at the proximity of Cabeço das Amoreiras. The distance to the open sea was shorter during the Late Mesolithic occupation than at present, ca. 40 km during the Early to Middle Holocene, instead of ca. 65 km as nowadays, once the Tróia spit was not formed yet. The ERT profile reflects the existence of coarse sediments in depth that could have resulted from the formation of a bay-head delta (not visible today) at the limit of maximum marine flooding. In this case, intertidal environments could have occurred. However, the coarse sediments can also be the result of alluvial fan deposits that inhibited the marine flooding in the area. Further studies of deep sediment cores covering the Holocene sedimentary sequence at this location are crucial to evaluate the marine inundation previously to 4350 cal BP (2400 cal BC) at the upstream limits of the Sado estuary.

The difference in human diets identified between downstream (Arapouco and Poças de São Bento) and upstream shell middens (Cabeço das Amoreiras, Vale de Romeiras and Cabeço do Pez) have been, to some extent, interpreted as the result of different environmental contexts offered to the Mesolithic groups (Diniz and Arias, 2012; Guiry et al., 2015; Peyroteo-Stjerna, 2016). To our understanding, full estuarine conditions extended, at least, until São Bento, located ca. 9 km from Vale de Romeiras and Cabeço do Pez, the most upstream Sado shell middens, and likely extended to more upstream areas of the valley between São Bento and Laxique (Figures 5.3 and 5.13A). At present, marine and tidal influence extend through 50 and 57 km from the estuary inlet (Figure 2.4) with river low mean annual flows of ca. 7 $m^3 s^{-1}$ (Bettencourt and Ramos, 2003). During the last 60 years south European rivers flows have decreased following the trend in warming and drying climate and to more intense and long meteorological droughts (e.g., Sousa et al., 2011; Jiménez Cisneros et al., 2014; Kovats et al., 2014). In the Early to Middle Holocene (ca. 9700 to 7300 cal BP; 7750 and 5350 cal BC) the palynological record of SW Iberia indicates high temperatures, and winter precipitation, but also summer droughts (e.g., Santos and Sánchez Goñi, 2003; Chabaud et al., 2014; Gomes et al., 2020). Despite the lack of information concerning river flows in the past, mean Sado discharges were certainly higher than nowadays, what could have prevented tides (marine and dynamic) to extend for so long. However, by then, São Bento was ca. 34 km and Laxique ca. 40 km upstream the Sado mouth (Figure 5.16), shorter

distances when compared to the extension of the estuary at present, so influence of tides should be considered in these upstream areas of the Sado where, at least, Cabeço das Amoreiras locates.
According to our results, even considering organic early degradation processes, the organic matter present in Laxique have a high terrestrial and freshwater signal (Figure 5.10) while under marine influence, as attested by the presence of marine diatoms between 4350 and 4000 cal BP (2400 and 2050 cal BC). *Scrobicularia plana* has a large range of distribution, occurring today, at the Sado, in low salinity areas that could reach 0.5‰ (Figure 2.4). To our knowledge, the isotopic signal of species living with low salinities was not studied yet and diets were determined based on general terrestrial and marine end-members. Could, somehow, the isotopic signal of shellfish collected in low salinity areas of the estuary, receiving high contents of freshwater and terrestrial organic matter, be influencing the isotopic signal of human collagen? Indeed, $\delta^{13}C$ high values of -6‰ were determined for *S. plana* shells collected in the Arapouco sediment core, dated to ca. 3000 years cal BP (ca. 1050 cal BC; Table 4.1) and values of -9.7 and -10.6‰ determined for *S. plana* shells collected at Vale de Romeiras and dated to ca. 7500 cal BP (ca. 5565 cal BC; Monge Soares, 2004). These low $\delta^{13}C$ point to their occurrence in estuarine conditions, and eventually, with a high contribution of freshwater (Keith and Anderson, 1963; Monge Soares, 2004; McConnaughey and Gillikin, 2008).

The Sado and the Tagus valleys: environmental similarities and differences during the Late Mesolithic

The Tagus and the Sado valleys housed the largest Late Mesolithic shell middens known in Iberia. Sites locate at the inner areas of the major estuaries formed during the Holocene due to sea level rise, establishing estuarine conditions in both valleys suitable for human settlement. Nevertheless, environmental similarities and differences can be pointed out:
i) at the Tagus, sites are placed more than ca. 65 km upstream the estuary inlet, while in the Sado the distance to the contemporary river mouth was shorter, between 25 and 45 km (Figures 1.3 and 5.16), closer to the open sea;
ii) at the Tagus, sites border three tributaries, the Magos, Muge and Fonte da Moça streams, while in the Sado sites locate mainly in the top of steep slopes margining the channel (Figures 1.4 and 5.16). Howsoever, it is important to mention that the Sado, despite being one of the most important rivers of South Portugal with a length of ca. 175 km, is a small river when compared to the Tagus (ca. 1000 km). In addition, despite forming the second larger Portuguese estuary (at present 140-150 km^2), the estuarine area of the Sado occupies half the area of the Tagus estuary

(at present ca. 325 km^2). The width of the valley in the section occupied by Mesolithic groups is ca. 1 km, being similar to the widths of the Magos and Muge valleys (Figures 1.4, 1.9, 1.10 and Figure 5.16). This similarity - visibility to the other bank - should be a precondition for choosing the site to settle;

iii) both in Tagus and Sado, shell middens locate at the edge of slopes facing the estuary/river (except for Poças de São Bento, Fonte da Mina and Barranco da Moura in the Sado, that are placed at greater distances), despite the difference in heigths (from 10 to 20 m MSL for the Tagus; Table 1.1; from 40 to 60 m MSL for the Sado; Table 1.6). However, all streams present steep slopes, which eventually constrained the occupation of other areas of the slope closer to the river;

iv) the presence of *S. plana* banks in the Muge (Tagus valley; van der Schriek et al., 2007b) and Carrasqueira (Sado valley) streams during the Mesolithic occupation is attested by the natural occurrence of this species in the contemporary sedimentary records. Both areas had suitable conditions for the development of mollusc banks between 8400 and 7000 cal BP (6450 and 5050 cal BC).

v) in both the Muge (van der Schriek et al., 2007b) and the Carrasqueira streams, maximum influence was present until ca. 7500 cal BP (5550 cal BP), coincident with a decrease in the sea level rise rate identified by García-Artola et al. (2018).

The Sado valley environment and the Neolithic occupation

At ca. 7000 cal BP (ca. 5050 cal BC), when shell middens were abandoned by the Late Mesolithic communities, important changes were observed in the environmental conditions, with intertidal areas occupying previous drowned areas and high sedimentation rates promoting the fast silting-up of the valley. Furthermore, the Tróia sandspit started to grow northwards, protecting the estuary from the open sea and increasing the distance from sites to open marine environments (Figure 5.17).

The arrival of the first Neolithic farmers to central and south Portugal is estimated to ca. 7450-7250 cal BP (ca. 5500-5300 cal BC; Carvalho, 2010). The human presence in the Sado shell middens during the Neolithic is attested by the presence of sherds in the upper levels of some of the Late Mesolithic shell middens (Diniz, 2010; Diniz and Cubas, 2015; Arias et al., 2021). However, the low density of Neolithic archaeological remains in the sites do not allow to infer about the nature and causes of this occasional Neolithic presence in the area (Arias et al., 2021). Cabeço do Pez seems to have been used for the burial of a child (ca. 6446-6220 cal BP; ca 4496-

4270 cal BC; Table 1.10) during the Middle Neolithic, coeval with some other domestic activities identified at the site (Arnaud, 2000), suggesting that some shell middens may have been used occasionally after their abandonment by the Mesolithic groups ((Peyroteo-Stjerna, 2020). It is however much further downstream of the estuary that these Neolithic and also Chalcolithic communities will settle, exploiting the estuarine resources alongside the cultivation of plants and the domestication of animals. These much recent (ca. 5850 and 4750 cal BP; ca. 3900 and 2800 cal BC; e.g., Silva et al., 1986; Soares and Silva, 2013) were accumulated within Holocene sand dunes present near Comporta, at the right margin of the Comporta channel, margining the estuarine area (Antunes et al., 1983; Figure 5.17). These sites are rich in malacofauna remains, particularly the *Ruditapes decussatus* shells (e.g., Soares and Silva, 2013), probably the most available mollusc species during these Neolithic times.

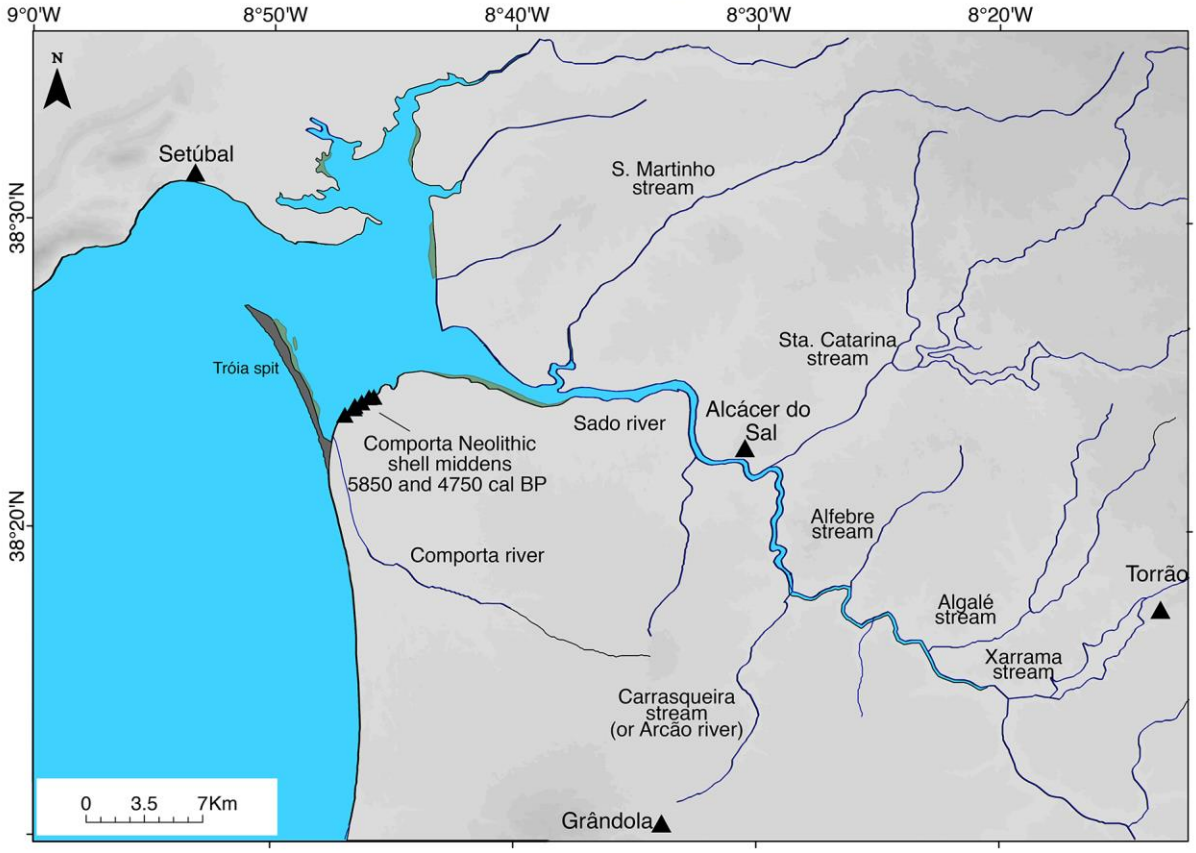

Figure 5.17 - Location of recent Prehistoric sites from the Comporta complex and contemporary palaeocoastal morphology and environment. Greenish colours represent salt marsh areas starting to develop. Dark-grey area represent the Tróia spit formed between 6500-4000 cal BP (Costas et al., 2015; see Figure 5.6).

6. CONCLUSIONS

6. Conclusions

The multiproxy analysis of the Arez3 sedimentary succession recovered from the Carrasqueira stream, a tributary of the Sado valley located at ca. 52 km upstream the present-day estuarine inlet, and near the most downstream shell midden, revealed to be a source of information concerning environmental conditions of the Sado valley during the Early to the Middle Holocene. Estuarine conditions, similar to the present-day central estuarine basin, characterized the Carrasqueira valley, at least, between ca. 8850 and 7450 cal BP (6900 and 5500 cal BC) and prevailed until ca. 7040 cal BP (5090 cal BC), despite the higher freshwater influence. The marine flooding certainly extended to upstream areas of the Sado channel during this time period, considering i) the depth of the palaeovalley (ca. -34 m to -23 m MSL, at ca. 5 km and 13 km upstream the Carrasqueira valley, respectively), ii) the recent radiocarbon dates determined at -9.4 m MSL (São Bento; 2288-1995 cal BP; 339-46 cal BC) and iii) -3 m MSL (Vale do Guizo; 2930-2766 cal BP; 981-817 cal BC) in sediments from the Sado channel, and iv) the results of geochemical and palaeoecological proxies of these sediments. Estuarine intertidal environments (tidal flats and saltmarshes) most probably developed in the shallower margins of the Sado.

The estuarine conditions allowed for the development of mollusc banks, such as *Scrobicularia plana* and *Cerastoderma edule*, as corroborated by the present of *S. plana* and *C. edule* shells and shell fragments in the natural sedimentary successions.

Other valleys with extensions and morphologies comparable to the Carrasqueira valley should present similar environmental conditions during the Early to the Middle Holocene. The Santa Catarina and Alfebre streams, located between Alcácer do Sal and São Bento, are proposed as streams with similar conditions to the Carrasqueira stream in this work. For the Algalé stream, located upstream Vale dos Açudes (i.e., upstream Poças de São Bento shell midden), further studies are required.

Since ca. 7040 cal BP the sedimentation rates surpassed the sea level rise rates, promoting the silting-up of the Carrasqueira valley (and certainly other similar Sado tributaries), allowing for the progressive progradation of freshwater environments downstream the Sado basin.

The maximum extension of the estuarine basin during the maximum marine flooding is still unknown and further analyses are needed to establish the fluvio-estuarine boundary and the limit of tidal influence during the Early and the Middle Holocene. Nevertheless, the multiproxy analysis performed in the Laxique and Arapouco (located more than 50 km upstream the Sado present estuarine inlet) sedimentary successions revealed to be a source of information

concerning palaeoenvironmental characterization and fluvial responses to climate variability during the Middle to Late Holocene in this Mediterranean river.

During the Mid-Late Holocene transition and through the Late Holocene the Sado estuary experienced significant changes in the fluvial-estuarine boundary. The occurrence of marine diatoms at Laxique between 4300 and 4200 cal BP (2350 and 2250 cal BC) locates the fluvial-estuarine boundary ca. 65 km upstream the present-day estuary inlet and ca. 15 km upstream the present-day boundary, at Arapouco. Even during periods with higher marine influence, the organic matter at the fluvial-estuarine boundary seems to be transported by the fluvial network and mostly sourced in terrestrial and freshwater environments, similar to present-day conditions where low to very low salinity contents are attested.

New changes in the fluvial-estuarine boundary were attested in Arapouco, at the proximity of the present-day fluvial-estuarine boundary, between ca. 3570 and 3240 cal BP (1620 and 1290 cal BC). During this period, the high-sedimentation rates (mean sedimentation rates of ~2.2 cm yr^{-1}) and changes on the primary source of sediment reflect changes on the precipitation regime and, to a much lesser extent, regional oscillations in sea level related to climate variability. Between 3570 and 3240 cal BP (1620 and 1290 cal BC), sediments were influenced by marine/brackish water with a high contribution of marine contents to the OM. The sedimentation in the area is compatible with an intertidal flat. The estuarine-fluvial boundary retreated upstream for ca. 100 years. From this moment onwards, the marine influence decreased while fluvial/terrestrial influence increased in the sedimentation pattern, and deposition took place in the intertidal zone under high contribution of terrigenous materials.

The high sedimentation rates determined in all cores, below MSL, were responsible for the fast silting-up of the valleys (Sado channel and tributaries) and the aggradation of an alluvial plain took place above MSL. The high SR rates calculated at Arez3, Laxique, Arapouco and Alcácer do Sal show that the sediment depocenter migrate downstream after the filling of the accommodation space in upstream areas. The aggradation and progradation of the alluvial plain occurred since ca. 4000 cal BP (2050 cal BC) at Laxique and at ca. 3240 cal BP (1290 cal BC) at Arapouco.

As typical of the Mediterranean rivers, prevalent Late Holocene dry climatic condition, also attested in Laxique by the presence of gypsum precipitation in depth, and consequent general retreat of vegetation, low river discharges and sediment availability are the main responsible for the modifications of the fluvial-estuarine boundary location.

The fluvial activity and the anthropic influence increased during the last 1000 years, as also attested for the Tagus estuary.

According to our results, estuarine conditions prevailed in the Sado valley during the Mesolithic occupation (ca. 8400 to 7000 cal BP; 6450 to 5050 cal BP) offering suitable conditions for the exploitation of bivalves, gastropods and fish. Intertidal areas (saltmarshes and tidal flats) developed in the Carrasqueira stream, as pointed out by the high percentages of Chenopodiaceae pollen, certainly in other similar valleys (e.g., Alfebre and Santa Catarina streams) and upstream shallower areas of the Sado, despite the maximum limit of marine flooding is still unknown. By then, shell middens were located between 25 km (Arapouco) and 45 km (Vale de Romeiras and Cabeço do Pez) from the open sea, closer to marine environments than at present. Taking into consideration the extension of the tidal and marine intrusions nowadays, that reach 50 km and 57 km upstream the estuarine inlet, respectively, the estuary extended until Laxique, near the most upstream shell middens identified in the Sado valley. Notwithstanding, river hrydological conditions were surely different, responding to high precipitation values during the Early and the beginning of the Middle Holocene, which can prevent the presence of marine water at these upstream locations of the valley. Indeed, in the emerged landscape, the abundance of mesophilous trees, such as evergreen and deciduous *Quercus*, suggest mostly the existence of a moist climate during the Late Mesolithic occupation. Despite the prevalence of *Quercus* forests, Mediterranean pines, such as *Pinus pinaster* and *Pinus halepensis-pinea* type, distributed across the interdunal depressions nd coastal areas. On the river banks, riparian communities were primarily composed by alders.

The different human dietary pattern identified between the shell middens located downstream São Bento (i.e., Arapouco and Poças de São Bento) and upstream São Bento (i.e., Cabeço da Amoreira, Vale de Romeiras, Cabeço do Pez and Várzea da Mó) do not seem to be the result from different environmental conditions offered to these hunter-gatherer groups. Instead, it can derive from the isotopic signal of shellfish collected in low salinity areas of the estuary, that usually have lower values than shells living in full marine conditions.

The environmental conditions of the Sado and the Tagus valleys during the Late Mesolithic occupation seem to be quite similar, with estuarine environments being present at the proximity of the sites, at least, considering the sedimentary record of the Muge valley (Tagus basin). In both areas, most sites are located at the edge of steep slopes, facing the estuary, with the exception of Barranco da Moura, Poças de São Bento and Fonte da Mina that locate far away from the estuarine environments. In addition, the Sado valley width, is similar to the ones of the Magos and Muge valleys, reflecting similar morphological settings for the location of the sites.

Concomitant to the abandonment of the sites by the Mesolithic communities, at ca. 7000 cal BP, environmental conditions changed with freshwater environments increasing, while saltmarshs

and tidal flats retreated to downstream areas of the Sado and its tributaries. The MSL rise decelerated and sedimentation rates surpassed the MSL rise rate contributing to the silting-up of the Sado tributary valleys. Notwithstanding, estuarine conditions prevailed in the main channel and the fluvial-estuarine boundary was still near Laxique at the transition to the Late Holocene. By then, Neolithic farmers occupied the Sado (5850 and 4750 cal BP; 3900 and 2800 cal BC) and, among other activities, have also exploited the estuarine area for the collection fish and shellfish. At that time, however, the estuary would already have a different configuration with the growth to north of the (still narrow) Tróia spit.

REFERENCES

References

Aldeias V, Bicho N (2016) Embedded behavior: Human activities and the construction of the Mesolithic shellmound of Cabeço da Amoreira, Muge, Portugal. Geoarchaeology: An International Journal 31(6), 530-549. https://doi.org/10.1002/gea.21573.

Alonso-Hernandez CM, Garcia-Moya A, Tolosa I, Diaz-Asencio M, Corcho-Alvarado JA, Morera-Gomez Y, Fanelli E (2017) Tracing organic matter sources in a tropical lagoon of the Caribbean Sea, Continental Shelf Research 148, 53-63. http://dx.doi.org/10.1016/j.csr.2017.08.001.

Álvarez-Blanco I, Blanco S (2014) Benthic diatoms from Mediterranean coasts. Bibliotheca Diatomologica. Stuttgart: Gebrüder Borntraeger Verlagsbuchhandlung.

Álvarez-Fernandéz E, Arias P, Diniz M, Simões T (2012) Marine Resource exploitation during the Mesolithic and the early Neolithic in Portugal: Preliminary data from Poças de São Bento (Alcácer do Sal) and Lapiás das Lameiras (Sintra). Advancing Method, Enhancing Understanding: Technique and Narrative in Archaeomalacology, 3rd Meeting of the ICAZ Archaeomalacology Working Group, Cairns, Queensland, Australia.

Andrade C, Freitas MC (2001) Transformação litoral e equilibrios perturbados: Exemplos do litoral português. Homenagem (in honorium) Professor Doutor Gaspar Soares de Carvalho. In: Moreira MA, Moura AC, Granja HM, Noronha F (Eds.). Braga, pp. 195-212.

Andrade C, Freitas MC, Brito P, Amorim A, Barata A, Cabaça G (2006a) Estudo de caso da região do Sado, zonas costeiras. Alterações Climáticas em Portugal Cenários, Impactos e Medidas de Adaptação, Projecto SIAM II. FD Santos e P Miranda (Coord.). Lisboa, Gradiva, pp. 423-436.

Andrade C, Rebelo L, Brito PO, Freitas MC (2006b) Processos Holocénicos; Aspectos da geologia, geomorfologia e dinâmica sedimentar do troço litoral Tróia-Sines. *In*: Dias R, Araújo A, Terrinha P, Kullberg JC (Eds.), Geologia de Portugal no Contexto da Ibéria, Universidade de Évora, Évora, 397-418.

Andrade C, Rebêlo L, Brito PO, Freitas MC (2013) III.7 Processos holocénicos; aspectos da geologia, geomorfologia e dinâmica sedimentary do troço litoral Tróia-Sines. In: Geologia de Portugal, Volume II - Geologia Meso-Cenozóica de Portugal, Dias R, Araújo A, Terrinha P, Kullberg JC (Eds.), Escolar Editora, 533-571.

Antunes MT (1983) Notícia explicativa da Folha 39-C Alcácer do Sal, Carta Geológica de Portugal 1:50000. Lisboa: Serviços Geológicos de Portugal.

Antunes MT, Pais J, Lopes JC (1983) Carta Geológica de Portugal 1:50000 Folha 39C Alcácer do Sal. Serviços Geológicos de Portugal, Direcção Geral de Geologia e Minas.

Antunes MT, Pais J, Gonçalves F, Oliveira JT, Peleja AF, Barroso JP, Romão JA, Lopes JC, Casimiro J (1991) Carta Geológica de Portugal 1:50000 Folha 39D Torrão. Serviços Geológicos de Portugal, Direcção Geral de Geologia e Minas.

Araújo AC (1995-1997) A indústria lítica do concheiro de Poças de S. Bento (vale do Sado) no seu contexto regional. O Arqueólogo Português 13/15, série IV, Lisboa, 87-159.

Araújo AC (2015) A few steps backwards... In search of the origins of the Late Mesolithic. In: Bicho N, Detry C, Price D, Cunha E (Eds.), Muge 150th: The 150th anniversary of the discovery of Mesolithic shellmiddens. Volume 2. Cambridge: Cambridge Scholars Publishing, 1-15.

Araújo AC (2016a) The significance of Marine Resources during the Early Mesolithic in Portugal. *In*: Dupont C, Marchand G (Eds.) Archéologie des chasseurs-cuilleurs maritimes. De la function des habitats à lórganisation de léspace littoral, Rennes. Paris, Bulletin de la Société Préhistorique française (Séances de la sociéte Préhistorique française, 6), pp. 127-143.

Araújo AC (2016b) Une histoire des premières communautés mésolithiques au Portugal. Oxford, Archaeopress (BAR, International Series 2782), pp. 265.

Araújo AC, Arias P, Diniz M (2015) Lithics in a Mesolithic shell midden: new data from Poças de São Bento (Portugal). In: Bicho N, Detry C, Price D, Cunha E (Eds.) Muge 150th: The 150th anniversary of the discovery of Mesolithic shellmiddens. Volume 1. Cambridge: Cambridge Scholars Publishing, 361-373.

Araújo AC, Costa AM, Costas S, Naughton F (2021) The impact of shoreline changes over Mesolithic populations of Western Iberia (11500 to 7000 cal BP). EAA Annual Meeting 2021, online, 8-11 September 2021.

Araújo AC, Moreno M, Gabriel S (2014) Para além de Toledo. Outros dados, novas revisões e algumas reflexões sobre o Mesolítico antigo do litoral da Estremadura. Revista Portuguesa de Arqueologia 17, 5-34.

Araújo AC, Piga G, Gonçalves D (2019) Fragmentary bodies or fragmentary perceptions? Mortuary practices of early mesolithic communities in South-western Iberia (c. 11,200-8500 cal BP). Journal of Archaeological Science: Reports 28, 102052.

Arias P, Diniz MT, Araújo AC, Armendariz Á, Teira LC (2015) At the edge of the marshes: New approaches to the Sado valley Mesolithic (southern Portugal). In: Bicho N, Detry C, Price D, Cunha E (Eds.) Muge 150th: The 150th anniversary of the discovery of Mesolithic shellmiddens. Volume 1. Cambridge: Cambridge Scholars Publishing, 301-319.

Arias P, Diniz MT, Araújo AC, Armendariz Á, Teira L (2021) New perspectives on the Mesolithic of the Sado Valley (Southern Portugal): Preliminary results of the Sado Meso project. In: Borić D, Antonović D, Mihaiilović B (Eds.) Foraging Assemblages Vol 1, Serbian Archaeological Society, Belgrade, Republic of Serbia and The Italian Academy for Advances Studies in America, Columbia University, New York, USA, 274-280.

Arias P, Diniz MT, Cubas M, Duarte C, Iriarte E, Salzmann C, Teichner F, Teira LC (2017) Looking for the traces of the last hunter-gatherers: Geophysical survey in the Mesolithic shell middens of the Sado valley (southern Portugal). Quaternary International 435(B), 61-70.

Arnaud JM (1987) Os concheiros dos vales do Tejo e Sado: semelhanças e diferenças. Arqueologia 15, 53-63.

Arnaud JM (1989) The Mesolithic communities of the Sado valley (Portugal) in their ecological setting. In: Bonsall, C. (Eds.), The Mesolithic in Europe, Papers presented at the III International Symposium. John Donald, Edinburgh, pp. 614-631.

Arnaud JM (2000) Os concheiros mesolíticos do vale do Sado e a exploração dos recursos estuarinos (nos tempos pré-históricos e na actualidade). Trabalhos de Arqueologia 14, Instituto Português de Arqueologia, Lisboa, 21-43.

Astrup P, Skriver C, Benjamin J, Stankiewick F, Ward I, MacCarthy, Ross P, Baggaley P, Ulm S, Bailey G (2020) Underwater shell middens: Excavation and remote sensing of a submerged Mesolithic site at Hjarnø, Denmark. The Journal of Island and Coastal Archaeology 15(4), 457-476. https://doi.org/10.1080/15564894.2019.1584135.

Azevêdo IC, Bordalo AA, Duarte PM (2010) Influence of river discharge patterns on the hydrodynamics and potential contaminant dispersion in the Douro estuary (Portugal). Water Research 44, 3133-3146.

Baines D, Smith DG, Froese DG, Bauman P, Nimeck G (2002) Electrical resistivity ground imaging (ERGI): a new tool for mapping the lithology and geometry of channels-belts and valley-fills. Sedimentology 49, 441-449.

Baptista J, Martinho F, Dolbeth M, Viegas I, Cabral H, Pardal M (2010) Effects of freshwater flow on the fish assemblage of the Mondego estuary (Portugal): comparison between drought and non-drought years. Marine and Freshwater Research 61, 490-501.

Bardhan P, Naqvi SWA, Karapurkar SG, Shenoy DM, Shenoy DM, Kurian S, Naik H (2017) Isotopic composition of nitrate and particulate organic matter in a pristine dam reservoir of westen India: implications for biogeochemical processes. Biogeoscences 14, 767-779. https://doi.org/10.5194/bg-14-767-2017.

Barradas L (1936) Concheiros do Vale do Sado. Anais da Faculdade de Ciências do Porto, XXI, 175-179.

Benito G, Macklin MG, Zielhofer C, Jones AF, Machado MJ (2015) Holocene flooding and climate change in the Mediterranean. Catena 130, 13-33. https://doi.org/10.1016/j.catena.2014.11.014.

Benito G, Sopena A, Sanchez-Moya Y, Machado MJ, Perez-Gonzalez A (2003) Palaeoflood record of the Tagus River (Central Spain) during the Late Pleistocene and Holocene. Quaternary Science Reviews 22, 1737-1756. https://10.1016/S0277-3791(03)00133-1.

Bettencourt A, Ramos L (Eds.) (2003) – Estuários Portugueses. Lisboa: Direcção de Serviços do Planeamento, Instituto da Água, Ministério das Cidades, Ordenamento do Território e Ambiente.

Bicho N (2004) As comunidades humanas de caçadores-recolectores do Algarve Ocidental. In: Tavares A, Tavares M, Cardoso J (Eds). Actas do Congresso Evolução Geohistórica do Litoral Português e Fenómenos Correlativos: Geologia, História, Arqueologia e Climatologia. Lisboa: Universidade Aberta, pp. 359-396.

Bicho N (2009) Sistemas de povoamento, subsistência e relações sociais dos últimos caçadores-recoletores do vale do Tejo. Estudos Arqueológicos de Oeiras 17, 133-156.

Bicho N, Cascalheira J, Marreiros J, Pereira T (2011) The 2008-2010 excavations of Cabeço da Amoreira, Muge, Portugal. Mesolithic Miscellany 21(2), 3-13.

Bicho N, Cascalheira J, Marreiros J, Gonçalves C, Pereira T, Dias R (2013a) Chronology of the Mesolithic occupation of the Muge valley, central Portugal: The case of Cabeço da Amoreira. Quaternary International 308-309, 130-139. https://doi.org/10.1016/j.quaint.2012.07.223.

Bicho N, Manne T, Marreiros J, Cascalheira J, Pereira T, Tátá F, Évora M, Gonçalves C, Infantini L (2013b) The Ecodynamics of the First Modern Humans in Southwestern Iberia. The Case of Vale Boi, Portugal. Quaternary International 318, 102-116. https://doi.org/10.1016/j.quaint.2013.06.029.

Bicho N, Umbelino C, Detry C, Pereira T (2010) The Emergence of Muge Mesolithic Shell Middens in Central Portugal and the 8200 cal yr BP Cold Event, The Journal of Island and Coastal Archaeology 5, 86-104. https://doi.org/ 10.1080/15564891003638184.

Biguino B, Sousa F, Brito AC (2021) Variability of currents and water column structure in a temperate estuarine system (Sado estuary, Portugal). Water 13, 187. https://doi.org/10.3390/w13020187.

Blaauw M (2010) Methods and code for 'classical' age-modelling of radiocarbon sequences. Quaternary Geochronology 5(5), 512-518.

Blott S (2000) GRADISTAT version 4.0. A Grain Size Distribution and Statistics Package for the Analysis of Unconsolidated Sediments by Sieving or Laser Granulometer.

Blum P (1997) Magnetic susceptibility. In: Ocean Drilling Program - ODP (Eds.) Physical properties handbook: a guide to the shipboard measurement of physical properties of deep-sea cores, 1-10.

Bogaard A, Fraser R, Heaton THE, Wallace M, Vaiglova P, Charles M, Jones G, Evershed RP, Styring AK, Andersen NH, Arbogast R-M, Bartosiewicz L, Gardeisen A, Kanstrup M, Maier U, Marinova E, Ninov L, Shäfer M, Stephan E (2013) Crop manuring and intensive land management by Europe's first farmers. Proceeding of the National Academy of Sciences of the United States of America 110 (31), 12589-12594. https://doi.org/10.1073/pnas.13059181110.

Bol R, Eriksen J, Smith P, Garnett MH, Coleman K, Christensen BT (2005) The natural abundance of 13C, 15N, 34S and 14 C in archived (1923-2000) plant and soil samples from the

Askov long-term experiments on animal manure and mineral fertilizer. Rapid Communications in Mass Spectrometry 19(22), 3216-3226. https://doi.org/10.1002/rcm.2156.

Boski T, Camacho S, Moura D, Fletcher WJ, Wilamowski A, Veiga-Pires CC, Correia V, Loureiro C, Santana P (2008) Chronology of the sedimentary processes during the postglacial sea level rise in two estuaries of the Algarve coast, southern Portugal. Estuarine, Coastal and Shelf Science 77, 230-244. https://doi.org/10.1016/j.ecss.2007.09.012.

Boski T, Moura D, Veiga-Pires C, Camacho S, Duarte D, Scott DB, Fernandes SG (2002) Postglacial sea level rise and sedimentary response in the Guadiana Estuary, Portugal/Spain border. Sedimentary Geology 150, 103-122. https://doi.org/10.1016/S0037-0738(01)00270-6.

Bray EE, Evans ED (1961) Distribution of n-paraffins as a clue to recognition of source beds. Geochimica et Cosmochimica Acta 22(1), 2-15. https://doi.org/10.1016/0016-7037(61)90069-2.

Brito P (2009) Impactos da elevação do nível médio do mar em ambientes costeiros: o caso do estuário do Sado. PhD thesis, Departamento de Geologia da Faculdade de Ciências, Universidade de Lisboa, Portugal.

Brock F, Higham T, Ditchfield P, Bronk Ramsey C (2010) Current pretreatment methods for AMS radiocarbon dating at the Oxford Radiocarbon Accelerator Unit (ORAU). Radiocarbon 52(1), 103–112.

Brown AG (1997) Alluvial geoarchaeology. Floodplain archaeology and environmental change. Cambridge Manuals in Archaeology.

Cabral H (1999) Ictiofauna do Estuário do Sado. Relatórios Científicos e Técnicos (47). Instituto de Investigação das Pescas e do Mar.

Cabral MC, Lord AR, Dambeck R, Kunst M (2016) Ostracod evidence for the Neolithic environment of Rio Sizandro, Portugal: Part 2. Palaeobiodiversity and Palaeoenvironment 96, 541-557. https://doi.org/10.1007/s12549-016-0240-5.

Caeiro S, Costa MH, Ramos TB, Fernandes F, Silveira N, Coimbra A, Medeiros G, Painho M (2005) Assessing heavy metal contamination in Sado Estuary sediment: An index analysis approach. Ecological Indicators 5(2), 151-169.

Camacho S, Boski T, Moura D, Scott D, Connor S, Pereira L (2016) Paleoenvironmental evolution of the Guadiana Estuary, Portugal, during the Holocene: A modern foraminifera analog approach. The Holocene 27(2), 197-235. https://doi.org/10.1177/0959683616658526.

Cambourieu-Nebout N, Peyron O, Dormoy I (2009) Rapid climatic variability in the west Mediterranean during the last 25 000 years from high resolution pollen data. Climate of the Past 5, 503–521. https://doi.org/10.5194/cpd-5-671-2009.

Cardoso JL, Rolão JM (1999-2000) Prospecções e escavações nos concheiros mesolíticos de Muge e Magos (Salvaterra de Magos): Contribuição para a história dos trabalhos arqueológicos efectuados. Estudos Arqueológicos de Oeiras 8, 83-240.

Carmo M, Sousa J, Varela P, Ventura R, Bivar M (2020) African knowledge transfer in Early Modern Portugal: Enslaved people and rice cultivation in Tagus and Sado rivers. Diacronie. Studi di Storia Contemporanea: "Can the subaltern speak" attraverso l'ambiente? 44, http://www.studistorici.com/2020/12/29/sousa-bivar-carmo-varela-ventura_numero_44/.

Carrión JS, Fernández S, González-Sampériz P, Gil-Romera G, Badal E, Carrión-Marco Y, López-Merino L, López-Sáez JA, Fierro E, Burjachs F (2010) Expected trends and surprises in the Lateglacial and Holocene vegetation history of the Iberian Peninsula and Balearic Islands. Review of Palaeobotany and Palynology 162, 458-475.

Carvalho AF (2009) O Mesolítico Final em Portugal, El Mesolítico Geométrico en la Península Ibérica, Monografías Arqueológicas 44, 33-68.

Carvalho AF (2010) Chronology and geography of the Mesolithic-Neolithic transition in Portugal. In: Armbruester T, Hegewisch M (Eds.) On pre- and earlier history of Iberia and central Europe. Studies in honour of Philine Kalb. Bonn: Habelt-Verlag. (Studien zur Archäologie Europas), p. 45–61.

Carvalho AF, Valente MJ (2005) Novos contextos conquíferos pré-históricos na Costa Vicentina, 2º Encontro de Arqueologia do Algarve (Xelb 5), Silves, 9-26.

Cascalheira J, Paixão E, Marreiros J, Pereira T, Bicho N (2015) Preliminary techno-typological analysis of the lithic materials from the Trench área of Cabeço da Amoreira (Muge, Central Portugal)". In: Muge 150th: The 150th Anniversary of the Discovery of Mesolithic Shellmiddens, Bicho N, Detry C, Price D, Cunha E (Eds.). Cambridge Scholar Publishing, pp. 119-133.

Castro DF, Rossetti DF, Pessenda LCR (2010) Facies, δ13C, δ15N and C/N analyses in a late Quaternary compound estuarine fill, northern Brazil and relation to sea level. Marine Geology 274, 135-150. https://doi.org/10.1016/j.margeo.2010.03.011.

Cearreta A, Cachão M, Cabral MC, Bao R, Ramalho MJ (2003) Lateglacial and Holocene environmental changes in Portuguese coastal lagoons 2: microfossil multiproxy reconstruction of the Santo André coastal area. The Holocene 13(3), 447-458.

Chabaud L, Goñi MFS, Desprat S, Rossignol L (2014) Land – sea climatic variability in the eastern North Atlantic subtropical region over the last 14,200 years: Atmospheric and oceanic processes at different timescales. The Holocene 24, 787–797. https://doi.org/10.1177/0959683614530439.

Chaumillon E, Tessier B, Reynaud J-Y (2010) Stratigraphic records and variability of incised valleys and estuaries along French coasts. Bulletin de la Societe Geologique de France 181 (2), 75-85. https://doi.org/10.2113/gssgfbull.181.2.75.

Chambers JE, Wilkinson PB, Wardrop D, Hameed A, Hill I, Jeffrey C, Loke MH, Meldrum PI, Kuras O, Cave M, Gunn DA (2012) Bedrock detection beneath river terrace deposits using three-dimensional electrical resistivity tomography. Geomorphology 177-178, 17-25.

Church JA, Clark PU, Cazenave A, Gregory JM, Jevrejeva S, Levermann MA, Merrifield MA, Milne GA, Nerem RS, Nunn PD, Payne AJ, Pfeffer WT, Stammer D, Unnikrishnan AS (2013) Sea Level Change. *In* Stocker TF, Qin D, Plattner G-K, Tignor M, Allen SK, Boschung J, Nauels A, Xia Y, Bex V, Midgley PM (Eds.) Climate Change 2013: The Physical Science Basis. Contribution of Working Group I to the Fifth Assessment Report of the Intergovernmental Panel on Climate Change. United Kingdom and New York, USA: Cambridge University Press, 1137-1216.

Cid N, Bonada N, Carlson SM, Grantham TE, Gasith A, Resh VH (2017) High Variability Is a Defining Component of Mediterranean-Climate Rivers and Their Biota. Water 9(1), 52. https://doi.org/10.3390/w9010052.

Clark PU, Dyke AS, Shakun JD, Carlson AE, Clark J, Wohlfarth B, Mitrovica JX, Hostetler SW, McCabe AM (2009) The Last Glacial Maximum. Sience 325, 710-714. https://doi.org/10.1126/science.1172873.

Coleman M, Meier-Augenstein W (2014) Ignoring IUPAC guidelines for measurement and reporting of stable isotope abundance values affects us all, Letter to the Editor, Rapid Communications in Mass Spectrometry 28, 1953-1955.

Colman SM, Baucom PC, Bratton JF, Cronin TM, McGeehin JP, Willard D, Zimmerman AR, Vogt PR (2002) Radiocarbon dating, chronological framework, and changes in accumulation rates of Holocene estuarine sediments from Chesapeake bay. Quaternary Research 57, 58-70.

Connolly RM, Gorman D, Hindell JS, Kildea TN, Schlacher TA (2013) High congruence of isotope sewage signals in multiple marine taxa. Marine Pollution Bulletin 71, 152-158. https://doi.org/10.1016/j.marpolbul.2013.03.021.

Cooper SR (1999) Estuarine palaeoenvironmental reconstructions using diatoms. In: Stoermer, E.F. and Smol, J.P. (Eds.) The diatoms: applications for the environmental and earth sciences. Cambridge: Cambridge University Press, pp. 352-373.

Cortesão C, Vale C (1995) Metals in sediments of the Sado Estuary, Portugal. Marine Pollution Bulletin 30(1), 34-37.

Costa MJ, Vasconcelos R, Costa JL, Cabral HN (2007) River flow influence on the fish community of the Tagus estuary (Portugal). Hydrobiologia 587, 113-123.

Costas S, Ferreira O, Plomaritis TA, Leorri E (2016a) Coastal barrier stratigraphy for Holocene high-resolution sea-level reconstruction. Scientific Reports 6: 38726.

Costas S, Naughton F, Goble R, Renssen H (2016b) Windiness spells in SW Europe since the last glacial maximum. Earth and Planetary Science Letters 436, 82-92.

Costas S, Rebêlo L, Brito P, Fitzgerald D (2015) The Joint History of Tróia Península and Sado Ebb-Delta. *In*: Randazzo G, Jackson DWT, Cooper JAG (eds.) Sand and Gravel Spit. Spinger, pp. 79-102.

Costas S, Araújo AC, Costa AM, Naughton F (2021) Changes in human settlement during the Mesolithic of SW Iberia motivated by the rapid inundation of the coast, EGU General Assembly 2021, online, 19–30 April 2021, EGU21-12389, https://doi.org/10.5194/egusphere-egu21-12389.

Coutinho MTP (2003) Comunidade fitoplanctónica do estuário do Sado. Estrutura, Dinâmica e Aspectos Ecológicos. IPIMAR research Thesis.

Crann CA, Murseli S, St-Jean G, Zhao X, Clark ID, Kieser WE (2017) First status report on radiocarbon sample preparation at the A.E. Lalonde AMS Laboratory (Ottawa, Canada). Radiocarbon 59, 695-704. http://doi.org/10.1017/RDC.2016.55

Cunha AH, Erzini K, Serrão EA, Gonçalves E, Borges R, Henriques M, Guerra M, Duarte C, Marbá N, Fonseca M (2014) Biomares, a LIFE project to restore and manage the biodiversity of Prof. Luiz Saldanha Marine Park. Journal of Coastal Conservation 18(6), 643–655. https://www.jstor.org/stable/i24760666.

Cunha E, Cardoso F (2001) The osteological series from Cabeço da Amoreira (Muge, Portugal). Bulletin et Mémoires de la Société d'Anthropologie de Paris 13(3-4), 323-333.

Cunha E, Cardoso F (2002-2003) New data on Muge shell middens: a contribution to more accurate numbers and dates. Estudos Arqueológicos de Muge 1, 171-183.

Cunha E, Cardoso F, Umbelino C (2003) Inferences about Mesolithic lifestyle on the basis of anthropological data. The case of the Portuguese shell middens. In: Larsson L, Kindgren H, Knutsson K, Loeffer, Akerlund A (Eds.), Mesolithic on the Move. Proceedings of the 6th International Symposium on the Mesolithic in Europe in Stockholm 2000, 184-188. Okford: Oxbow Books.

Cunha E, Umbelino C (1995-1997) Abordagem antropológica das comunidades mesolíticas dos concheiros do Sado. O Arqueólogo Portugês S4 (13-15), 161-179.

Cunha E, Umbelino C (2001) Mesolithic People from Portugal: an approach to Sado osteological séries. Anthropologie 39 (2-3), 125-132.

Cunha E, Umbelino C, Cardoso F (2002) New anthropological data on the Mesolithic communities from Portugal: the shell middens from Sado. Human Evolution 17, 187-198. https://doi.org/10.1007/BF02436370.

Dabrio CJ, Zazo C, Goy JL, Sierro FJ, Borja F, Lario J, González JA, Flores JA (2000) Depositional history of estuarine infill during the last postglacial transgression (Gulf of Cadiz, Southern Spain). Marine Geology 162, 381-404. https://doi.org/10.1016/S0025-3227(99)00069-9.

Danielsen R, Castilho AM, Dinis PA, Almeida AM, Callapez PM (2012) Holocene interplay between a dune field and coastal lakes in the Quiaios-Tocha region, central littoral Portugal. The Holocene 22(4), 383-395.

Denys L, De Wolf H (1999) Diatoms as indicators of coastal paleoenvironments and relative sea-level change. In: Stoermer EF and Smol JP (Eds.) The diatoms: applications for the environmental and earth sciences. Cambridge, Cambridge University Press, 277-297.

Detry C (2007) Paleoecologia e Paleoeconomia do Baixo Tejo no Mesolítico Final: O contributo do estudo dos mamíferos dos concheiros de Muge. PhD thesis. Universidade de Salamanca and Universidade Autónoma de Lisboa.

Detry C (2008) Vertebrates from Cabeço dos Morros: a Mesolithic Shell midden near Salvaterra de Magos, in the lower Tagus valley, Portugal. Promontoria 6, 51-71.

Detry C, Cardoso JL (2010) On some remains of dog (Canis familiaris) from the Mesolithic Shell-middens of Muge, Portugal. Journal of Archaeological Science 37, 2762-2774.

Dias JM, Boski T, Rodrigues A, Magalhães F (2000) Coast line evolution in Portugal since the Last Glacial Maximum until present - a synthesis. Marine Geology 170, 177-186. https://doi.org/10.1016/S0025-3227(00)00073-6.

Dias RP (Coord.) (2011) Carta Geológica de Portugal 1:50000 Folha 42A Grândola. Unidade de Geologia e Cartografia Geológica, Laboratório de Geologia e Minas.

Dias R, Detry C, Bicho N (2016) Changes in the exploitation dynamics of small terrestrial vertebrates and fish during the Pleistocene-Holocene transition in the SW Iberian Peninsula: A review. The Holocene 26(6), 964-984. https://doi.org/10.1177/0959683615622547.

Dias R, Estrella-Martínez J, Butler P, Nederbragt A, Hall IR, Barrulas P, Maurer AF, Cardeira AM, Mirão J, Detry C, Bicho N (2019) Mesolithic human occupation and seasonality: sclerochronology, $\delta^{18}O$ isotope geochemistry, and diagenesis verification by Raman and LA-ICP-MS analysis of *Argyrosomus regius* (meagre) sagitae otoliths from layer 1 of Cabeço da Amoreira Mesolithic shell midden (Muge, Portugal). Archaeological and Anthropological Sciences 11, 409-432. https://doi.org/10.1007/s12520-017-0569-3.

Diniz M (2010) O concheiro mesoliÅLtico do Cabeco das Amoreiras (S. Romao do Sado, Alcálcer do Sal): um (outro) paradigma perdido? In: Gibaja JF and Carvalho AF (Eds.) Os

últimos caçadores-recolectores e as primeiras comunidades produtoras do sul da Península Ibérica e do norte de Marrocos. Actas do Workshop (Faro, 2–4 de Novembro de 2009). Faro, Faculdade de Ciências Humanas e Sociais da Universidade do Algarve, p. 49–61.

Diniz M, Arias P (2012) O povoamento humano do paleo-estuário do Sado (Portugal): Problemáticas em torno da ocupação dos concheiros Mesolíticos. In: Almeida AC, Bettencourt AMS, Moura D, Monteiro–Rodrigues S, Alves MIC (Eds.). Mudanças ambientais e interação humana na fachada atlântica ocidental. Coimbra: APEQ/CITCEM/CEGT/CGUP/CCT, pp. 139-157.

Diniz M, Cubas M (2015) Pots for Thought: Neolithic Pottery in the Sado Mesolithic Shell Middens. In: Bicho N, Detry C, Price TD, Cunha E (Eds.). Muge 150th: the 150th anniversary of the discovery of Mesolithic shellmiddens. Vol. 1. Cambridge: Cambridge Scholars Publishing. p. 375–390.

Diniz M, Nukushima D (2014) Caçadores-Recolectores no Vale do Sado. Ambiente, Recursos e Tecnologia Lítica: o caso de Arapouco (Alcácer do Sal). Estudos do Quaternário 11, 27-38.

Duarte C (2019) The formation of Shell middens in Atlantic Iberia during the Mesolithic. A geoarchaeological and micromorphological approach to the coastal adaptations of the Holocene hunter-gatherers. PhD thesis, Escuela de Doctorado de la Universidad de Cantabria, Spain.

Duarte C, Costa AM, Aldeias V (2017) Recosntruir atividades humanas e formação de contextos conquíferos: microfácies sedimentares do Cabeço da Amoreira (Muge) e das Poças de São Bento (Sado) e o seu potencial interpretativo nos padrões de comportamento humano no Mesolítico. In: Arnaud J, Martins A (Eds.), Arqueologia em Portugal, 2017 - Estado da Questão, Actas II Congresso da AAP, 419-432.

Duarte C, Iriarte E, Diniz M, Arias P (2019) The microstratigraphy record of human activities and formation processes at the Mesolithic Shell midden of Poças de São Bento (Sado Valley, Portugal). Archaeological and Anthropological Sciences 11, 483-509. https://doi.org/10.1007/s12520-017-0519-0.

Dupont C (2011) Les invertébrés marins du « concheiro » de Toledo (Lourinhã, Portugal). In: Araújo AC (Ed.) O concheiro de Toledo no contexto do Mesolítico Inicial do litoral da Estremadura. Trabalhos de Arqueologia, 51. Lisboa, Igespar, pp. 185-227.

Dupont C (2016) Could occupation durantion be related to the diversity of faunal remains in Mesolithic Shell middens along the European Atlantic seaboard? Quaternary International 407(B), SI Time for the tide: New perspectives on hunter-fisher-gathetrer exploitation on intertidal resources in Atlantic Europe and Mediterranean regions, Gutiérrez-Zugasti I, Cuenca Solana D, Colonese AC, Fernández-López de Pablo J (Eds.), 145-153. http://dx.doi.org/10.1016/j.quaint.2016.01.039.

Dupont C, Marchand G (2021) New paradigms in the exploitation of Mesolithic Shell middens in Atlantic France: The exemple of Beg-er-Vil, Britanny. Quaternary International 584, SI Coastal Prehistory and Submerged Landscapes: Molluscan Resources, Shell-Middens and Underwater Investigations, Bailey G, Hardy K (Eds.), 59-71. https://doi.org/10.1016/j.quaint.2020.09.043.

Elfadly AA, Ahmed OE, El Nady MM (2017) Assessing of organic content in surface sediments of Suex Gulf, Egypt depending on normal alkanes, terpanes and steranes biological markers indicators. Egyptian Journal of Petroleum 26, 969-979. https://doi.org/10.1016/j.ejpe.2016.11.007.

Ellwood BB, Harrold FB, Benoist SL, Straus LG, Morales MG, Petruso K, Bicho NF, Zilhão J, Soler N (2001) Paleoclimate and intersite correlations from Late Pleistocene/Holocene cave sites: Results from Southern Europe. Geoarchaeology: An International Journal 16 (4), 433-463.

ENGIVIA, Consultores de Engenharia Lda. (1995), A2, Auto-estrada do Sul. Sublanço Alcácer do Sal / Grândola Norte, PE1-Terraplanagens, Parte 1.4-Geologia e geotecnia, Volume V.

Evans MJ (2021) Hunter-gatherer and Environmental Relations during the Mesolithic of Atlantic Europe., Durham theses, Durham University. Available at Durham E-Theses Online: http://etheses.dur.ac.uk/14020/.

Fatela F, Moreno J, Antunes C, Leorri E, Taborda R, Silva A, Andrade C, Cearreta A (2009a) Foraminiferal assemblages distribution across the Sado estuary tidal marshes (SW Portugal): local assessment of regional palaeoenvironmental value, 6º Simposio sobre el Margen Ibérico Atlântico, MIA 2009, Oviedo, 345-348.

Fatela F, Moreno J, Moreno F, Araújo MF, Valente T, Antunes C, Taborda R, Andrade C, Drago T (2009b) Environmental constraints of foraminiferal assemblages distribution across a brackish tidal marsh (Caminha, NW Portugal). Marine Micropaleontology 70, 70-88. https://doi.org/10.1016/j.marmicro.2008.11.001.

Fernández-López de Pablo J, Gabriel S (2016) El Collado shell middens and the exploitation patterns of littoral resources during the Mesolithic in the Eastern Iberian Península. Quaternary International 407(B), SI Time for the tide: New perspectives on hunter-fisher-gathetrer exploitation on intertidal resources in Atlantic Europe and Mediterranean regions, Gutiérrez-Zugasti I, Cuenca Solana D, Colonese AC, Fernández-López de Pablo J (Eds.), 106-117. https://doi.org/10.1016/j.quaint.2015.11.100.

Ferreira JG, Simas T, Nobre A, Silva MC, Shifferegger K, Lencart, Silva J (2003) Identification of areas and vulnerable zones in transitional and coastal portuguese systems, Application of the United States national estuarine eutrophication assessment to the Minho, Lima, Douro, Ria de Aveiro, Mondego, Tagus, Sado, Mira, Ria Formosa. Instituto da Água & Institute of Marine Research, pp. 151.

Ficken KJ, Li B, Swain DL, Eglinton G (2000) An n-alkane proxy for the sedimentary input of submerged/floating freshwater aquatic macrophytes. Organic Geochemistry 31(7), 745-749. https://doi.org/10.1016/S0146-6380(00)00081-4.

Figueiredo N, Carranca C, Coutinho J, Trindade H, Pereira J, Prazeres A, Marques P (2014) Climate change on ammonium "fixation" in flooded rice (Oryza sativa) soils. Actas do Encontro Anual da SPCS 2013, Oeiras, 22-28.

Fiorentino G, Ferrio JP, Bogaard A, Araus JL, Riehl S (2015) Stable isotopes in archaeobotanical research. Vegetation History and Archaeobotany 24, 215-227. https://doi.org/10.1007/s00334-014-0492-9.

Flemming B (2000) A revised textural classification of gravel-free muddy sediments on the basis of ternary diagrams. Continental Shelf Research 20, 1125–1137. doi:10.1016/S0278-4343(00)00015-7.

Fletcher W, Boski T, Moura D (2007) Palynological evidence for environmental and climatic change in the lower Guadiana valley, Portugal, during the last 13000 years. The Holocene 17 (4): 481-494. https://doi.org/10.1177/0959683607077027.

Fletcher WJ, Debret M, Sanchez Goñi MF (2013) Mid-Holocene emergence of a low frequency millennial oscillation in western Mediterranean climate: Implications for past dynamics of the North Atlantic atmospheric westerlies. The Holocene 23, 153-166.

Fletcher WJ, Sánchez Goñi MF (2008) Orbital- and sub-orbital-scale climate impacts on vegetation of the western Mediterranean basin over the last 48,000 yr. Quaternary Research 70, 451–464. https://doi.org/10.1016/j.yqres.2008.07.002.

Folk RL (1954) The distinction between grain size and mineral composition in sedimentary-rock nomenclature. Journal of Geology 62, 344-359.

Fontanals-Coll M, Subirà ME, Marín-Moratalla N, Ruiz J, Gibaja JF (2014) From Sado Valley to Europe: Mesolithic dietary practices through different geographic distributions. Journal of Archaeological Science 50, 539-550. https://doi.org/10.1016/j.jas.2014.07.028.

Fonseca R, Canário T, Morais M, Barriga FJAS (2011) Phosphorus sequestration in Fe-rich sediments from two Brazilian tropical dam reservoirs. Applied Geochemistry 26, 1607-1622. https://doi.org/10.1016/j.apgeochem.2011.04.017.

Fortunato AB, Oliveira A, Baptista AM (1999) On the effect of tidal flats on the hydrodynamics of the Tagus estuary. Oceanologica Acta 22(1), 31-44. https://doi.org/10.1016/S03991784(99)80030-9.

Freitas MC, Andrade C (2005) Global vs local forcing factores and paleoenvironmental changes of estuaries and lagoons of SW Portugal since the late glacial. Iberian coastal holocene paleoenvironmental evolution, Costal Hope 2005, Lisboa, 64-70.

Freitas C, Andrade C (2008) O estuário do Sado. In: Soares J (Coord.), Embarcações tradicionais. Contexto físico-cultural do estuário do Sado. Setúbal: Museu de Arqueologia e Etnografia do Distrito de Setúbal / Administração dos Portos de Setúbal e Sesimbra, 21-29.

Freitas MC, Andrade C, Cruces A (2002) The geological record of environmental changes in southwestern Portuguese coastal lagoons since the Lateglacial. Quaternary International 93-94, 161-170. https://doi.org/10.1016/S1040-6182(02)00014-9.

Freitas MC, Andrade C, Cruces A, Munhá J, Sousa MJ, Moreira S, Jouanneau JM, Martins L (2008) Anthropogenic influence in the Sado estuary (Portugal): A geochemical approach. Journal of Iberian Geology 34(2), 271-286.

Freitas MC, Andrade C, Pimentel N, Silva CM, Fatela F, Costa AM, Diniz M, Arias P (2013) Holocene evolution of the Sado estuary - preliminary data and implications on Mesolithic shell

middens, Proceedings, MUGE 150th, 150th Anniversary of the Discovery of the Mesolithic Shell Middens.

Freitas MC, Andrade C, Rocha F, Tassinari C, Munhá JM, Cruces A, Vidinha J, Silva C M (2003) Lateglacial and Holocene environmental changes in Portuguese coastal lagoons: 1. The sedimentological and geochemical records of the Santo André coastal area (SW Portugal). The Holocene 13(3) 433-446. https://doi.org/10.1191/0959683603hl636rp.

Gabriel S (2011) A exploração dos recursos ictícos. In: Araújo AC (Ed.), O concheiro de Toledo no contexto do Mesolítico inicial do litoral da Estremadura, Trabalhos de Arqueologia, 51. Lisboa, Igespar, pp. 127-144.

Gabriel S, Prista N, Costa MJ (2012) Estimating meagre (Argyrosomus regius) size from otoliths and vertebrae. Journal of Archaeological Science 39, 2859-2865. https://doi.org/10.1016/j.jas.2012.04.046.

Gao X, Yang Y, Wang C (2012) Geochemistry of organic carbon and nitrogen in surface sediments of coastal Bohai Bay inferred from their ratios and stable isotopic signatures. Marine Pollution Bulletin 64, 1148-1155.

García-Artola A, Stephan P, Cearreta A, Kopp RE, Khan, SN, Horton BP (2018) Holocene sea-level database from the Atlantic coast of Europe. Quaternary Science Reviews 196, 177–192.

Golubkov MS, Nikulina VN, Tiunov AV, Golubkov SM (2020) Stable C and N isotope composition of suspended particulate organic matter in the Neva estuary: the role of abiotic factors, productivity, and phytoplankton taxonomic composition. Journal of Marine Science and Engineering 8, 959. https://doi.org/10.3390/jmse120959.

Gomes SD, Fletcher WJ, Rodrigues T, Stone A, Abrantes F, Naughton F (2020) Time-transgressive Holocene maximum of temperate and Mediterranean forest development across the Iberian Peninsula reflects orbital forcing. Palaeogeography, Palaeoclimatology, Palaeoecology 550, 109739. https://doi.org/10.1016/j.palaeo.2020.109739.

Gonçalves C (2014) Modelos preditivos de ocupação do território no Mesolítico entre os vales do Tejo e do Sado. PhD thesis, Faculdade de Ciências Humanas e Sociais, Universidade do Algarve, Portugal.

Gonçalves F, Antunes MT (1992) Notícia explicativa da Folha 39-D Torrão, Carta Geológica de Portugal 1:50000. Lisboa: Serviços Geológicos de Portugal.

Gourry J-C, Vermeersch F, Garcin M, Giot D (2003) Contribution of geophysics to the study of alluvial deposits: a case study in the Val d'Avaray area of the River Loire, France. Journal of Applied Geophysics 54, 35-49.

Gu B (2009) Variations and controls of nitrogen stable isotopes in particulate organic matter of lakes. Oecologia 160, 421-431. https://doi.org/10.1007/s00442-009-1323-z.

Gutiérrez-Zugasti I, Andersen SH, Araújo AC, Dupont C, Milner N, Monge-Soares AM (2011) Shell middens research in Atlantic Europe: State of the art, research problems and perspectives of the future. Quaternary International 239, 70-85. https://doi.org/10.1016/j.quaint.2011.02.031.

Guiry EJ, Hillier M, Richards MP (2015) Mesolithic dietary heterogeneity on the European Atlantic coastline: stable isotope insights into huntergatherer diet and subsistence in the SadoValley, Portugal. Current Anthropology 56(3), 460-470. https://doi.org/10.1086/680854.

GRID, Consultas Estudos e Projectos de Engenharia (1989) IP1-Variante de Alcácer do Sal, Ponte sobre o rio Sado e seus viadutos de acesso. Anexo 1-Travessia da baixa aluvionar. Gráficos das sondagens e ensaios "in situ".

Hasle GR, Syvertsen EE (1996) Marine diatoms. In: Tomas CR (Ed.) Identifying marine phytoplankton. San Diego, CA: Academic Press, 5-383.

Hayes WM (Ed.) (2015) CRC Handbook of Chemistry and Physics 96th Edition. CRC press.

Heaton T, Köhler P, Butzin M, Bard E, Reimer R, Austin W, Bronk Ramsey C, Grootes P, Hughen K, Kromer B, Reimer P, Adkins J, Burke A, Cook M, Olsen J, Skinner L (2020) Marine20 - the marine radiocarbon age calibration curve (0–55,000 cal BP). Radiocarbon 62, 779-820. https://doi.org/10.1017/RDC.2020.68.

Henriksen K, Kemp WM (1988) Nitrification in Estuarine and Coastal Marine Sediments. In: Nitrogen Cycling in Coastal Marine Environments, Chapter 10, Blackburn TH and Sørensen J (Eds.). SCOPE, John Wiley & Sons Lds, 207-250.

Herbert RA (1999) Nitrogen cycling in coastal marine ecosystems. FEMS Microbiology Reviews 23, 563-590. https://doi.org/10.1111/j.1574-6976.1999.tb00414.x.

Hijma MP, Cohen KM, Hoffmann G, Van der Spek AJF, Stouthamer E (2009) From river valley to estuary: the evolution of the Rhine mouth in the early to middle Holocene (western Netherlands, Rhine-Meuse delta). Netherlands Journal of Geosciences 88(1), 13-53. https://doi.org/10.1017/S0016774600000986.

Hua Q, Barbetti M, Rakowski AZ (2013) Atmospheric radiocarbon for the period 1950-2010. Radiocarbon 55, 2059-2072. doi:10.2458/azu_js_rc.v55i2.16177.

Hughes WB, Holba AG, Dzou IP (1995) The ratios of dibenzothiophene to phenanthrene and pristana to phytane as indicatiors of depositional environment and lithology of petroleum source rocks. Geochimica et Cosmochimica Acta 59 (17), 3581-3598. https://doi.org/10.1016/0016-7037(95)00225-O.

INE (2007) Anuário Estatístico da Região do Alentejo, Lisboa, INE.

Inverno C, Manuppella G, Zbyszewski G, Leandro A, Rodrigues A, Rodrigues L, Oliveira J, Barroso J, Moreira P, Ribeiro ML (1986) Carta Geológica de Portugal 1:50000 Folha 42C Santiago do Cacém. Serviços Geológicos de Portugal, Direcção Geral de Geologia e Minas.

Jackes MP, Alvim JAA, Roksandic A (2014) New photographic evidence on the 1954 excavations at Moita do Sebastião, Muge, Portugal. In: The cultural dynamics of shell-matrix sites, Roksandic M, Souza SN, Eggers S, Burchell M, Klökler D (Eds.), 131-49. Albuquerque: University of New Mexico Press.

Jackes M, Lubell D (2012) Mortuary archaeology of the Muge shell middens. In: Gibaja JF, Carvalho AF, Chambon P (Eds.) Funerary practices in the Iberian Peninsula from the Mesolithic to the Chalcolithic. Oxford: Archaeopress (BAR International Series), 67-76.

Jackes M, Meiklejohn C (2008) The palaeodemography of central Portugal and the Mesolithic-Neolithic transition. In: Recent advances in Palaeodemography: data, techniques, pattterns, Bocquet-Appel J-P (Ed.), 209-258.

Jarzen DM, Elsik WC (1986) Fungal palynomorphs recovered from recent river deposits, Luangwa valley, Zambia. Palynology 10, 35-60. https://doi.org/10.1080/01916122.1986.9989302.

Jenkinson DS, Coleman K, Harkness DD (1995) The influence of fertilizer nitrogen and season on the carbon-13 abundance of wheat straw. Plant and Soil 171, 365-367. https://doi.org/10.1007/BF00010293.

Jiménez Cisneros BE, Oki T, Arnell NW, Benito G, Cogley JG, Döll P, Jiang T, Mwakalila SS (2014) Freshwater resources. *In* Field CB, Barros VR, Dokken DJ, Mach KJ, Mastrandrea MD, Bilir TE, Chatterjee M, Ebi KL, Estrada YO, Genova RC, Girma B, Kissel ES, Levy AN, MacCracken S, Mastrandrea PR, White LL (Eds.) Climate Change 2014: Impacts, Adaptation, and Vulnerability. Part A: Global and Sectoral Aspects. Contribution of Working Group II to the Fifth Assessment Report of the Intergovernmental Panel on Climate Change. Cambridge, United Kingdom and New York, NY, USA: Cambridge University Press, 229-269.

Johnson ME, Baarli BG, Cachão M, Silva CM, Ledesma-Vázquez J, Mayoral E, Ramalho RS, Santos A (2012) Rhodoliths, uniformitarism and Darwin: Pleistocene and Recent carbonate deposits in the Cape Verde and Canary archipelagos. Palaeogeography, Palaeoclimatology, Palaeoecology 329-330, 83-100.

Khan NS, Vane CH, Horton BP (2015) Stable carbon isotope and C/N geochemistry of coastal wetland sediments as a sea-level indicator, chapter 20. In: Handbook of Sea-Level Research, First Edition. Ian Shennan, Antony J. Long, and Benjamin P. Horton (Eds.), John Wiley & Sons, Ltd., 295-311.

Keith ML, Anderson GM (1963) Radiocarbon dating: Fictitious results with mollusk shells. Science 141, 634-637.

Kopprio GA, Dutto MS, Garzón Cardona JE, Gärdes A, Lara RJ, Graeve M (2018) Biogeochemica markers across a pollution gradient in a Patagonian estuary: A multidimensional approach of fatty acids and stable isotopes. Marine Pollution Bulletin 137, 617-626. https://doi.org/10.1016/j.marpolbul.2018.10.059.

Kovats RS, Valentini R, Bouwer LM, Georgopoulou E, Jacob D, Martin E, Rounsevell M, Soussana J-F (2014) Europe. In: Barros VR, Field CB, Dokken DJ, Mastrandrea MD, Mach KJ, Bilir TE, Chatterjee M, Ebi KL, Estrada YO, Genova RC, Girma B, Kissel ES, Levy AN, MacCracken S, Mastrandrea PR, White LL (Eds.) Climate Change 2014: Impacts, Adaptation, and Vulnerability. Part B: Regional Aspects. Contribution of Working Group II to the Fifth

Assessment Report of the Intergovernmental Panel on Climate Change. Cambridge, United Kingdom and New York, NY, USA: Cambridge University Press, 1267-1326.

Koziorowska K, Kuliński K, Pempkowiak J (2018) Deposition, return flux, and burial rates of nitrogen and phosphorus in the sediments of two high-Arctic fjords. Oceanologia 60(4), 431-445. https://doi.org/10.1016/j.oceano.2018.05.001.

Kristensen E (1990) Characterization of biogenic organic matter by stepwise thermogravimetry (STG). Biogeochemistry 9, 135-159.

Lamb AL, Wilson GP, Leng MJ (2006) A review of coastal palaeoclimate and relative sea-level reconstructions using $\delta^{13}C$ and C/N rations in organic material. Earth-Science Reviews 75, 29-57.

Lambeck K, Rouby H, Purcell A, Sun Y, Sambridge M (2014) Sea level and global ice volumes from the Last Glacial Maximum to the Holocene. PNAS 111(43), 15296-15303. https://doi.org/10.1073/pnas.1411762111.

Lario J, Zazo C, Goy JL, Dabrio CJ, Borja F, Silva PG, Sierro F, González A, Soler V, Yll E (2002) Changes in sedimentation trends in SW Iberia Holocene estuaries (Spain). Quaternary International 93–94, 171–176. https://doi.org/10.1016/S1040-6182(02)00015-0.

Lario J, Zazo C, Goy JL, Silva PG, Bardaji T, Cabero A, Dabrio CJ (2011) Holocene palaeotsunami record of SW Iberia. Quaternary International 242, 196-200.

Larsson L (1996) Late Atlantic settlements in Southern Portugal. Results of an excavation of a Mesolithic shell midden by the River Sado. Current Swedish Archaeology 4, 123-139.

Larsson L (2010) Shells in the sand: Poças de S. Bento – a Mesolithic shell midden by the River Sado, Southern Portugal. In: Armbruester T, Hegewisch M (Eds.) On Preand Earlier History of Iberia and Central Europe. Studies in honour of Philine Kalb. Bonn: Verlag Dr. Rudolf Habelt Gmbrl. (Studien zur Archäologie Europas, 11), 29-43

Laussaque J, Lepoint G, Thibaut T, Francour P, Meinesz A (2010) Tracing sewage and natural freshwater input in a Northwest Mediterranean bay: Evidence obtained from isotopic ratios in marine organisms. Marine Pollution Bulletin 60, 843-851. https://doi.org/10.1016/j.marpolbul.2010.01.008.

Le Gall O, Altuna Extabe J, Straus L (1994) Les faune mésolithique et néolithique de Vidigal. Archaeozoologia 7(1), 59-72.

Le Gall O, Straus LG, Vierral B, Altuna Etxabe J (1992) Ichtyofaunas and seasonality at Vidigal. Mesolithic Miscellany 13(2), 13-18.

Leira M, Freitas MC, Ferreira T, Cruces A, Connor S, Andrade C, Lopes V, Bao R (2019) Holocene sea level and climate interactions on wet dune slack evolution in SW Portugal. A model for future scenarios?. The Holocene 29(1), 26-44.

Lentacker A (1986) Preliminary results of the fauna of Cabeço da Amoreira and Cabeço de Arruda (Muge, Portugal). Trabalhos de Antropologia e Etnologia 26 (1-4), 9-26.

Leorri E, Cearreta A, Milne G (2012) Field observations and modelling of Holocene sea-level changes in the southern Bay of Biscay: implication for understanding current rates of relative sea-level change and vertical land motion along the Atlantic coast of SW Europe. Quaternary Science Reviews 42, 59-73. http://dx.doi.org/10.1016/j.quascirev.2012.03.014.

Lepoint G, Dauby P, Gobert S (2004) Applications of C and N stable isotopes to ecological and environmental studies in seagrass ecosystems. Marine Pollution Bulletin 49, 887-891. https://doi.org/10.1016/j.marpolbul.2004.07.005.

Li Z, Sun Y, Nie X (2020) Biomarkers as a soil organic carbon tracer of sediment: Recent advances and challenges. Earth-Science Reviews 208, 103277. https://doi.org/10.1016/j.earscirev.2020.103277.

Little S, Wood PJ, Elliott M (2017) Quantifying salinity-induced changes on estuarine benthic fauna: The potential implications of climate change. Estuarine, Coastal and Shelf Science 198, 610-625.

Liu W-C, Chen W-B, Cheng RT, Hsu M-H, Kuo AY (2007) Modeling the influence of river discharge on salt intrusion and residual circulation in Danshuei River estuary, Taiwan. Continental Shelf Research 27, 900-921. https://doi.org/10.1016/j.csr.2006.12.005.

Loh PS, Miller AEJ, Reeves AD, Harvey SM, Overnell J (2008) Assessing the biodegradability of terrestrially-derived organic matter in Scottish sea loch sediments. Hydrology and Earth System Sciences 12, 811-823.

López-Doriga I, Diniz M, Arias P (2016) Macrobotanical remains and shell-midden formation processes, are they related? The case of Poças de São Bento (Portugal). Archaeological and Anthropological Sciences 11, 469-481. https://doi.org/10.1007/s12520-016-0429-6.

López-Sáez JA, van Geel B, Martín Sánchez M (2000) Aplicación de los microfósiles no polínicos en Palinología Arqueológica. Contributos das Ciências e das. Tecnologias para a Arqueologia da Península Ibérica. Actas 3° Congresso de Arqueologia Peninsular IX. Adecap, Porto, 11-20.

Lord A, Cabral MC, Dambeck R, Kunst M (2011) Ostracod evidence for the Neolithic environment of Rio Sizandro, Portugal. Palaeobiodiversity and Palaeoenvironments 91, 215-228. https://doi.org/10.1007/s12549-011-0055-3.

Lubell D, Jackes M (1988) Portuguese Mesolithic-Neolithic subsistence and settlement. Rivista di Antropologia. Roma. Supplemento Vol. 66, 231-248.

Lubell D, Jackes M, Schwarcz H, Meiklejohn C (1986) New radiocarbon dates for Moita do Sebastião. Arqueologia 14, 34-36.

Lubell D, Jackes M, Schwarcz H, Knyf M, Meiklejohn C (1994) The Mesolithic-Neolithic transition in Portugal: isotopic and dental evidence of diet. Journal of Archaeological Science 21, 201-216. https://doi.org/ 10.1006/jasc.1994.1022.

Maillet GM, Rizzo E, Revil A, Vella C (2005) High resolution electrical resistivity tomography (ERT) in a transition zone environment: Application for detailed internal architecture and infilling processes study of the Rhône River paleo-channel. Marine Geophysical Researches 26, 317-328.

Marchand G (2001) Les traditions techniques du Mésolithique final dans le sud de Portugal: les industries lithiques des amas coquilliers de Várzea da Mó et de Cabeço do Rebolador (fouilles M. Heleno). Revista Portuguesa de Arqueologia 4, 47-110.

Marchand G (2005) Interpretar as mudanças dos sistemas técnicos do Mesolítico final em Portugal. O Arqueólogo Português, Série IV, 23, 171-196.

Marino RW, Howarth R (2009) Nitrogen fixation. In: Encyclopedia of Inland Waters, Inorganic Chemicals: Cycles and Dynamics. Likens GE (Ed.), Academic Press, Elsevier Science (Verlag), 65-72.

Martins AA, Cunha PP (2009) Terraços do rio Tejo em Portugal, sua importância na interpretação da evolução da paisagem e da ocupação humana. In Arqueologia do Vale do Tejo: 163-176. Lisboa, Centro Português de Geo-História e Pré-História.

Martins AA, Cunha PP, Huot S, Murray AS, Buylaert JP (2009) Geomorphological correlation of the tectonically displaced Tejo River terraces (Gavião-Chamusca area, central Portugal) supported by luminescence dating. Quaternary International 199, 75-91. https://doi.org/10.1016/j.quaint.2009.01.009.

Martins F, Leitão P, Silva A, Neves R (2000) 3D modelling in the Sado estuary using a new generic vertical discretization approach. Oceanologica Acta 24 (supplement), S51-S62.

Martins JMM, Carvalho AF, Monge Soares AM (2008) A calibração das datas de radiocarbono dos esqueletos humanos de Muge. Promontoria Monográfica 6, 73-93.

Matos JX, Oliveira V (2003) Mina do Lousal (Faixa Piritosa Ibérica) - Percurso geológico e mineiro pelas cortas e galerias da antiga mina. IGME, Pub. Museo Geominero, n. 2, 117-128.

McConnaughey TA, Gillikin DP (2008) Carbon isotopes in mollusk shell carbonates. Geo-Marine Letters 28, 287-299.

McLaughlin TR, Gómez-Puche M, Cascalheira J, Bicho N, Fernández-López de Pablo J (2021) Late Glacial and Early Holocene human demographic responses to climatic and environmental change in Atlantic Iberia. Philosophical Transactions B 376, 20190724. https://dx.doi.org/10.1098/rstb.2019.0724.

Meiklejohn C, Roksandic M, Jackes M, Lubell D (2009) Radiocarbon dating of Mesolithic human remains in Portugal. Mesolithic Miscellany 20(1), 4-16.

Meyers PA (1994) Preservation of elemental and isotopic source identification of sedimentary organic matter. Chemical Geology 144: 289-302.

Meyers PA (1997) Organic geochemical proxies of paleoceanographic, paleolimnologic, and paleoclimatic processes. Organic Chemistry 27 (5-6), 213-250. https://doi.org/10.1016/S0146-6380(97)00049-1.

Meyers PA (2003) Applications of organic geochemistry to paleolimnological reconstructions: a summary of examples from the Laurentian Great Lakes. Organic Geochemistry 34, 261-289. PII: S0146-6380(02)00168-7.

Milner N, Woodman P (Eds.) (2005) Mesolithic Studies at the Beginning of the 21st Century. Oxbow Books, pp.224.

Miola A (2012) Tools for Non-Pollen Palynomorphs (NPPs) Analysis: A List of Quaternary NPP Types and Reference Literature in English Language (1972–2011). Review of Palaeobotany and Palynology 186, 142-161. https://doi.org/10.1016/j.revpalbo.2012.06.010.

Mita H, Shimoyama A (1999) Characterization of n-alkanes, pristine and phytane in the Cretaceous/Tertiary boundary sediments at Kawaruppu, Hokkaido, Japan. Geochemical Journal 33, 285-294. https://www.jstage.jst.go.jp/article/geochemj1966/33/5/33_5_285/_pdf.

Moore PD, Webb JA, Collinson ME (1991) Pollen Analysis. Blackwell Scientific Publications, Oxford.

Monge Soares AM (2004) Variabilidade do "upwelling" costeiro durante o Holocénico nas margens atlânticas ocidental e meridional da Península Ibérica, PhD thesis, Faculdade de Ciências do Mar e do Ambiente, Universidade do Algarve, Portugal.

Monge Soares AM (2008) O. da Veiga Ferreira e as primeiras datações de radiocarbono para a aqueologia portuguesa. Estudos Arqueológicos de Oeiras 16, 377-382.

Monge Soares AM, Dias J (2006) Coastal upwelling and radiocarbon—evidence for temporal fluctuations in ocean reservoir effect off Portugal during the Holocene. Radiocarbon 48(1), 45–60.

Moreira ME (1992) Recent saltmarsh changes and sedimentation rates in the Sado estuary, Portugal. Journal of Coastal Research 8, 631-640. https://www.jstor.org/stable/4298012.

Moreira S (2016) Contributo da geoquímica e sedimentologia na caracterização de influências antrópicas em ambientes estuarinos. PhD Thesis, Departamento de Geologia da Faculdade de Ciências, Universidade de Lisboa, Portugal.

Moreno J, Valente T, Moreno F, Fatela F, Guise L, Patinha C (2007) Occurrence of calcareous foraminifera and calcite-carbonate equilibrium conditions - a case study in Minho/Coura estuary (Northern Portugal). Hydrobiologia 587, 177-184. https://doi.org/10.1007/s10750-007-0677-7.

Moreno M (2011) Exploração de recursos faunísticos de origem terrestre. In: Araújo A (Ed.), O concheiro do Toledo no contexto do Mesolítico inicial do litoral da Estremadura. Trabalhos de Arqueologia 51. Lisboa. Igespar, 99-124.

Mota R (2013) Prospeção geofísica pelo método da resistividade elétrica no âmbito do projeto de investigação "shell middens and agriculture", LNEC - Proc. 504/19/18816. Relatório 248/2013 – DG/NGEA.

Mota R (2017) Prospeção geofísica pelo método da resistividade elétrica no âmbito do projeto de investigação "Sociedades costeras en un mundo cambiante: studio diacrónico comparado de la prehistoria del SW de Europa desde el Paleolítico final al Neolítico". Proc. 504/111/21271. Relatório 460/2017 – DG/NGEA.

Murphy J, Riley JP (1962) A modified single solution method for the determination of phosphate in natural waters. Analytical Chimica Acta 27, 31-36.

Neves FS (2010) Dynamics and hydrology of the Tagus estuary: results from in situ observations. 210p, PhD thesis, Universidade de Lisboa, Portugal. Unpublished. Available on-line at http://repositorio.ul.pt/handle/10451/2003.

Nukushima D (2015) Geometric microliths and cultural markers in the Sado Shell middens? Reflections from Amoreiras (Alcácer do Sal, Portugal). NAILOS, Estudios Interdisciplinares de Arqueología 2, 89-122.

Oliveira JT (Coord.) (2006) Carta Geológica de Portugal 1:50000 Folha 42B Azinheira de Barros. Departamento de Geologia, Instituto Nacional de Engenharia, Tecnologia e Inovação.

Oueslati O, Girolamo AM, Abouabdillah A, Kjeldsen TR, Lo Porto A (2015) Classifying the flow regimes of Mediterranean streams using multivariate analysis. Hydrological Processes 29, 4666–4682. https://doi.org/10.1002/hyp.10530.

Ouyang X, Guo F, Bu H (2015) Lipid biomarkers and pertinent indices from aquatic environment record paleoclimate and paleoenvironment changes. Quaternary Science Reviews 123, 180-192. http://dx.doi.org/10.1016/j.quascirev.2015.06.029.

Paço A (1938) Novos concheiros do vale do Tejo. Brotéria 27(1), 66-75.

Pais J, Cunha P, Legoinha P, Dias RD, Pereira D, Ramos A (2013) Cenozóico das Bacias do Douro (sector ocidental), Mondego, Baixo Tejo e Alvalade. In: Dias R, Araújo A, Terrinha P, Kullberg JC (Eds.) Geologia de Portugal, Volume II, Geologia Meso-Cenozóica de Portugal, Escolar Editora.

Pals JP, van Geel B, Delfos A (1980) Paleoecological studies in the Klokkeweel bog near Hoogkarspel (Prov. of Noord-Holland). Review of Palaeobotany and Palynology 30, 371-418. https://doi.org/10.1016/0034-6667(80)90020-2.

Pansu M, Gautheyrou J (2006) Handbook of Soils Analysis – Mineralogical, Organic and Inorganic Methods, Springer.

Pardo P, Rauret G, López-Sánchez J (2003) Analytical approaches to the determination of phosphorus partitioning patterns in sediments. Journal of Environmental Monitoring 5, 312-318. https://doi.org/10.1039/B210354K.

Peyroteo-Stjerna R (2016) On Death in the Mesolithic. Or the Mortuary Practices of the Last Hunter Gatherers of the South Western Iberian Peninsula, 7th–6th Millennium BCE. PhD dissertation. Uppsala University. Occasional Papers in Archaeology 60.

Peyroteo-Stjerna R (2020) Chronology of the burial activity of the last hunter-gatherers in the southwestern Iberian Peninsula, Portugal. Radiocarbon 63(1), 265-299. https://doi.org/10.1017/RDC.2020.100.

Philippsen B (2013) The freshwater reservoir effect in radiocarbon dating. Heritage Science1(24), 19pp.

Pimentel NL (2002) Pedogenic and early diagenetic processes in Palaeogene alluvial fan and lacustrine deposits from the Sado Basin (S Portugal). Sedimentary Geology 148(1-2), 123-138.

Pimentel N, Nukushina D, Diniz MT, Arias P (2015) Lithic materials in the Sado River's shell middens – geological provenance and impact on site location. In: Bicho NF, Detry C, Price TD, Cunha E (Eds.) Muge 150th: The 150th Anniversary of the Discovery of Mesolithic Shellmiddens, Vol. 1. Newcastle upon Tyne, Cambridge Scholars Publishing, 321-332.

Pimentel NLV, Pimentel PRV, Azevêdo TM, Andrade C, Freitas MC, Pereira DI (2001) Estudo sedimentológico e geoquímico de depósitos holocénicos do rio Sado. V REQUI / I CQPLI, Lisboa, 125-127.

Pizzolla PF (2002) *Scrobicularia plana* Peppery furrow shell. In: Tyler-Walters H. and Hiscock K. (Eds.) Marine Life Information Network: Biology and Sensitivity Key Information Reviews, [on-line]. Plymouth: Marine Biological Association of the United Kingdom. Available from: http://www.marlin.ac.uk/species/detail/1507.

Powell TG (1988) Pristane/phytane ratio as environmental indicator. Nature 333, 604.

Preston T, Owens NJP (1983) Interfacing an automatic elemental analyser with an isotope ratio mass spectrometer: the potential for fully automated total nitrogen and nitrogen-15 analysis. Analyst 108, 971-977.

Psuty NP, Moreira MA (2000) Holocene sedimentation and sea level rise in the Sado estuary, Portugal. Journal of Coastal Research 16(1), 125-138.

Queiroz P (1999) Ecologia histórica da paisagem do noroeste alentejano. PhD thesis, Universidade de Lisboa, Portugal.

Quevauviller P, Lavigne R, Cortez L (1989) Impact of industrial and mine drainage wastes on the heavy metal distribution in the drainage basin and estuary of the Sado River (Portugal). Environmental Pollution 59(4), 267-286.

Reille M (1992) Pollen et Spores d'Europe et d'Afrique du nord. Laboratoire de Botanique Historique et Palynologie, CNRS. Marseille.

Reille M (1995) Pollen et Spores d'Europe et d'Afrique du Nord (Supplément 1). Laboratoire de Botanique Historique et Palynologie, CNRS. Marseille.

Reimer P, Austin W, Bard E, Bayliss A, Blackwell P, Bronk Ramsey C, Butzin M, Cheng H, Edwards R, Friedrich M, Grootes P, Guilderson T, Hajdas I, Heaton T, Hogg A, Hughen K, Kromer B, Manning S, Muscheler R, Palmer J, Pearson C, van der Plicht J, Reimer R, Richards D, Scott E, Southon J, Turney C, Wacker L, Adolphi F, Büntgen U, Capano M, Fahrni S, Fogtmann-Schulz A, Friedrich R, Köhler P, Kudsk S, Miyake F, Olsen J, Reinig F, Sakamoto M, Sookdeo A, Talamo S (2020) The IntCal20 Northern Hemisphere radiocarbon age calibration curve (0–55 cal kBP). Radiocarbon, 62. https://doi.org/10.1017/RDC.2020.41.

Reimer PJ, Baillie MGL, Bard E, Bayliss A, Beck JW, Bertrand CJH, Blackwell PG, Buck CE, Burr GS, Cutler KB, Damon PE, Edwards RL, Fairbanks RG, Friedrich M, Guilderson, TP, Hogg AG, Hughen KA, Kromer B, McCormac G, Manning S, Bronk Ramsey C, Reimer RW, Remmele S, Southon JR, Stuiver M, Talamo S, Taylor FW, van der Plicht J, Weyhenmeyer CE (2013) INTCAL04 Terrestrial radiocarbon age calibration, 0-26 Cal Kyr BP. Radiocarbon 46, 1029-1058.

Reimer PJ, Brown TA, Reimer RW (2004) Discussion: reporting and calibration of post-bomb 14C data. Radiocarbon 46(3), 1299-1304. https://doi.org/ 10.1017/S0033822200033154.

Renberg I (1990) A procedure for preparing large sets of diatom slides from the sediment cores. Journal of Paleolimnology 4, 87-90.

Riera P, Stal LJ, Nieuwenhuize J, Richard P, Blanchard G, Gentil F (1999) Determination of food sources for benthic invertebrates in a salt marsh (Aiguillon, France) by carbon and nitrogen stable isotopes: importance of locally produced sources. Marine Ecology Progress Series 187, 301-307.

Robins PE, Lewis MJ, Freer J, Cooper DM, Skinner CJ, Coulthard TJ (2018) Improving estuary models by reducing uncertainties associated with river flows. Estuarine, Coastal and Shelf Science 207, 63-73. https://doi.org/10.1016/j.ecss.2018.02.015.

Roche J (1951) L'industrie préhistorique du Cabeço d'Amoreira (Muge). Lisboa: Imprensa Portuguesa, pp.159.

Roche J (1970) L'industrie de l'amas conquiller mésolithique de Cabeço da Amoreira, Muge (Portugal). Actes du VII ème congrès International des Sciences Préhistorique et Protohistorique. Prague, vol. I, 368-373.

Roche J (1972) Le gisement mésolithique de Moita do Sebastião (Muge - Portugal). Archéologie. Lisboa: Instituto de Alta Cultura.

Roche J (1989) Spatial organization in the Mesolithic sites of Muge, Portugal. In: The Mesolithic in Europe. Third International Symposium, Bonsall C (Ed.), 607-613. Edinburgh: John Donald.

Roche J, Veiga Ferreira O (1957) Nota sobre a estratigrafia dos concheiros de Muge. Comunicações dos Serviços Geológicos de Portugal 38 (2), Lisboa, 261-268.

Roche J, Veiga Ferreira O (1972-1973) Seconde datation par le C14 de l'amas coquillier mésolithique de Moita do Sebastião (Muge). Comunicações dos Serviços Geológicos de Portugal VI, 471-474.

Rodrigues AMJ (1992) Avaliação do estado ambiental de um estuário de uso múltiplo, através da análise de comunidades biosedimentares. Estuário do Sado, Portugal. Department of Biological and Molecular Sciences, University of Stirling, Scotland, pp. 364.

Rodríguez-Ramírez A, Pérez-Asensio JN, Santos A, Jiménez-Moreno G, Villarías-Robles JJR, Mayoral E, Celestino-Pérez S, Cerrillo-Cuenca E, López-Sáez JA, Léon A, Contreras C (2015) Atlantic extreme wave events during the last four millennia in the Guadalquivir estuary, SW Spain. Quaternary Research 83, 24-40.

Roksandic M (2006) Analysis of burials from the new excavations of the sites Cabeço da Amoreira and Cabeço da Arruda (Muge, Portugal). In: Bicho N and Veríssimo H (Eds.), Do Epipalaeolítico ao Calcolítico na Península Ibérica, Actas do IV Congresso de Arqueologia Peninsular. Promontória Monográfica 4, 43-54. Faro: Universidade do Algarve.

Rolão J, Joaquinito A, Gonzaga M (2006) O complexo mesolítico de Muge: novos resultados sobre a ocupação do Cabeço da Amoreira. In Bicho N, Veríssimo (Eds.), Do Epipaleolítico ao Calcolítico na Península Ibérica. Actas do IV Congresso de Arqueologia Peninsular. Promontória Monográfica 4, 27-42. Faro: Universidade do Algarve.

Rolão J, Roksandic M (2007) The Muge Mesolithic complex: new results from the excavations of Cabeço da Amoreira 2001-2003. In: Shell middens in Atlantic Europe, Milner N, Craig OE, Bailey GN (Eds.), 78-85. Oxford: Oxford Books.

Rowley-Conwy P (2015) The Late Mesolithic of southwest Portugal: a zooarchaeological approach to resource exploitation and settlement patterns. In: Bicho N, Detry C, Price D, Cunha E (Eds.) Muge 150th: The 150th anniversary of the discovery of Mesolithic shellmiddens. Volume 1. Cambridge: Cambridge Scholars Publishing, 255-272.

Rowntree KM, van der Wall B W, Pulley S (2017) Magnetic susceptibility as a simple tracer for fluvial sediment source ascription during storm events. Journal of Environmental Management 194, 54-62.

Rumolo P, Barra M, Gherardi S, Marsella E, Sprovieri M (2011) Stable isotopes and C/N ratios in marine sediments as a tool for discriminating anthropogenic impact. Journal of Environmental Monitoring 13, 3399-3408.

Sabatier P, Dezileau L, Colin C, Briqueu L, Bouchette F, Martinez P, Siani G, Raynal O, Grafenstein UV (2012) 7000 years of paleostorms activity in the NW Mediterranean Sea in response to Holocene climate events. Quaternary Research 77, 1-11.

Santos MF (1967) Notícia: o concheiro mesolítico do Barranco da Moura, Grândola. O Arqueólogo Português S3(1), 113-114.

Santos MF (1968) Notícia: o concheiros mesolítico da Fonte da Mina, Grândola. O Arqueólogo Português S3(2), 183.

Santos CS (2019) Estado atual das populações de berbigão (*Cerastoderma* spp.) no estuário do Sado. Mestrado em Ecologia e Gestão Ambiental, Faculdade de Ciências da Universidade de Lisboa.

Santos M, Soares J, Silva C (1972) Campaniforme da Barrada do Grilo, Torrão, Vale do Sado. O Arqueológo Português 3(6), 163-192.

Santos MF, Rolão JM, Marques, MGD (1990) Duas novas jazidas epipalaeoliticas do baixo Tejo, n.os 1 e 2 do Vale da Fonte da Moça (Almeirim), sua exploração arqueológica e salvaguarda. Actas do I Congresso do Tejo, Lisboa em 1988*,* 1, 33-38.

Santos S, Cardoso JFMF, Borges V, Witbeerd R, Luttikhuizen PC, van der Veer H (2012) Isotopic fractionation between seawater and the shell of *Scrobicularia plana* (Bivalvia) and its application for age validation. Marine Biology 159, 601-611.

Santos L, Sánchez Goñi MF (2003) Lateglacial and Holocene environmental changes in Portuguese coastal lagoons 3: vegetation history of the Santo Andre coastal area. The Holocene 13(3), 459-464. https://doi.org/10.1191/0959683603hl638rp.

Scanes P, Ferguson A, Potts J (2017) Estuary Form and Function: Implications for Palaeoecological Studies. In: Applications of Paleoenvironmental Techniques in Estuarine Studies, Weckström K, Saunders KM, Gell PA, Skilbeck CG (Eds.), Part I, Estuaries and Their Management. Springer Nature, 9-44.

Schermerhorn LJ, Stanton WI, Strauss G, Abreu F, Matze K, Zbyszewsky G, Ferreira OV, Andrade RF, Oliveira J, Deus PC, Rodrigues A, Rodrigues L, Nery F, Oliveira V (1984) Carta Geológica de Portugal 1:50000 Folha 42D Aljustrel. Serviços Geológicos de Portugal, Direcção Geral de Geologia e Minas.

Schrader HJ, Gersonde R (1978) Diatoms and silicoflagellates, in Micropaleontological Counting Methods and Techniques: An Exercise on an Eight Metres Section of the Lower Pliocene of Capo Rossello, Sicily, Utrecht Micropaleontol. In W. J. Zachariasse *et al.* (Eds.) Bulletin vol.17, Utrecht, Schotanus and Jens, Odijk, Netherlands. pp. 129–176.

Schubel JR (1982) Estuarine sedimentation. In: Schwartz M (Ed.) Beaches and Coastal Geology. Encyclopedia of Earth Science. Boston, MA: Springer.

Schultz DJ, Calder JA (1976) Organic carbon 13C/12C variations in estuarine sediments. Geochimica et Cosmochimica Acta 40, 381-385.

Scott L (1992) Environmental implications and origin of microscopic Pseudoschizaea Thiergart and Frantz ex R. Potonie emend. in sediments. Journal of Biogeography 19(4), 349-354. https://doi.org/10.2307/2845562.

Senbayram M, Dixon L, Gouding KWT, Bol R (2008) Long-term influence of manure and mineral nitrogen applications on plant and soil 15N and 13C values from the Broadbalk Wheat Experiment. Rapid Communication in Mass Spectrometry 22, 1735-1740. https://doi.org/10.1002/rcm.3548.

Shaha DC and Cho Y-K (2016) Salt plug formation caused by decreased river discharge in a multi-channel estuary. Nature Scientific Reports 6:27176.

Sikes EL, Uhle ME, Nodder SD, Howard ME (2009) Sources of organic matter in a coastal marine environment: Evidence from n-alkanes and their δ13C distributions in the Hauraki Gulf, New Zeland. Marine Chemistry 113, 149-163. https://doi.org/10.1016/j.marchem.2008.12.003.

Silliman JE, Meyers PA, Bourbonniere RA (1996) Record of postglacial organic matter delivery and burial in sediments of Lake Ontario. Organic Geochemistry 24, 463-472. https://doi.org/10.1016/0146-6380(96)00041-1.

Silva CT, Soares J, Cardoso JL, Cruz CS, Reis CAS (1986) Neolítico da Comporta: aspectos cronológicos (datas 14C) e paleoambientais. Arqueologia 14, 59-82.

Silva TA, Freitas MC, Andrade C, Taborda R, Freire P, Schmidt S (2013) Geomorphological response of saltmarshes in the Tagus estuary to sea level rise. Journal of Coastal Research SI65, 582-587. https://doi.org/10.2112/SI65-099.1.

Singh R, Bhumbl DK, Keefer RF (2011) Recommended Soil Sulfate-S Tests. In: The Northeast Coordinating Committee for Soil Testing, (NECC-1312) (eds), Recommended Soil Testing Procedures for the Northeastern United States, Northeastern Regional Publication No. 493, 3rd Edition, pp. 55-62.

Slomp CP (2011) 5.06 - Phosphorus Cycling in the Estuarine and Coastal Zones: Sources, Sinks, and Transformations. In: Treatise on Estuarine and Coastal Science, Wolanski E, McLusky D (Eds.) Academic Press, 201-229. https://doi.org/10.1016/B978-0-12-374711-2.00506-4.

Smith RC, Sjogren DB (2006) An evaluation of electrical resistivity imaging (ERI) in Quaternary sediments, southern Alberta, Canada. Geosphere 2(6), 287-298.

Soares J, Silva CT (2013) Economia agro-marítima na Pré-história do estuário do Sado. Novos dados sobre o Neolítico da Comporta. In: Soares J (Ed.) Pré-história das zonas húmidas. Paisagens de sal / Prehistory of wetlands. Landscapes of salt. MAEDS/ADS - Museu de Arqueologia e Etnografia do Distrito de Setúbal/Assembleia Distrital de Setúbal & SIMARSUL, S.A., pp. 145-170.

Sobral DV (1993) Peixes do estuário do Sado. Estudos de Biologia e Conservação da Natureza (11).

Sousa PM, Trigo RM, Aizpurua P, Nieto R, Gimeno L, Garcia-Herrera R (2011) Trends and extremes of drought indices throughout the 20th century in the Mediterranean. Natural Hazards and Earth System Science 11(1), 33-51.

Stockmarr J (1971) Tablets with spores used in absolute pollen analysis. Pollen Spores 13, 614-621.

Stuiver M, Polach HA (1977) Discussion: reporting of 14C data. Radiocarbon 19(3), 355–63.

Taborda R, Freire P, Silva A, Andrade C, Freitas C (2009) Origin and evolution of Tagus estuarine beaches. Journal of Coastal Research SI56, ICS 2009 Proceedings, 213-217.

Teixeira SB, Gaspar P, Rosa M (2005) Holocene sea-level index points on the Quarteira coast (Algarve, Portugal). Iberian coastal Holocene paleoenvironmental evolution, Proceedings COASTAL HOPE 2005, 125-127.

Teranes JL, Bernasconi SM (2000) The record of nitrate utilization and productivity limitation provided by $\delta^{15}N$ values in lake organic matter - A study of sediment trap and core sediments from Baldeggersee, Switzerland. Limnology and Oceanography 45(4), 801-813.

Thornes J, López-Bermúdez F, Woodward J (2009) Hydrology, River regimes, and sediment yield. In The Physical Geography of the Mediterranean (1st ed., pp. 229-253). Oxford University Press.

Torres, I.C., Inglett, P.W., Brenner, M., Kenney, F., Reddy, K.R., 2012. Stable isotope ($\delta^{13}C$ and $\delta^{15}N$) values of sediment organic matter in subtropical lakes of different trophic status. Journal of Palaeolimnology 47, 693-706. https://doi.org/10.1007/s10933-012-9593-6.

Treasure ER, Church MJ, Gröcke DR (2016) The influence of manuring on stable isotopes (δ13C and δ15N) in Celtic bean (*Vicia faba* L.): archaeolobotanical and palaeodietary implications. Archaeological and Anthropological Sciences 8, 555-562. https://doi.org/10.1007/s12520-015-0243-6.

Tweddle JC, Edwards KJ, Fieller NRJ (2005) Multivariate statistical and other approaches for the separation of cereal from wild Poaceae pollen using a large Holocene dataset, Vegetation History and Archaeobotany 14, 15-30. https://doi.org/10.1007/s00334-005-0064-0.

Umbelino C (2006) Outros Sabores do Passado: As análises de oligoelementos e de isótopos estáveis na reconstituição da dieta das comunidades humanas do Mesolítico Final e do Neolítico Final/Calcolítico do território português, PhD thesis, Faculdade de Ciências e Tecnologia, Universidade de Coimbra, Portugal.

Umbelino C, Cunha E (2012) The Sado shell middens: anthropological and paleodietary description. In: Gibaja JF, Carvalho AF, Chambon P (Eds.) Funerary practices in the Iberian Peninsula from the Mesolithic to the Chalcolithic. Oxford: Archaeopress (BAR International Series), 91-102.

Umbelino C, Pérez-Pérez A, Cunha E, Hipólito C, Freitas M, Cabral J (2007) Outros sabores do passado: um novo olhar sobre as comunidades humanas mesolíticas de Muge e do Sado através de análises químicas dos ossos. Promontoria 5, 45-90.

Vale C, Sundby B (1982) A survey of the elemental composition of bottom sediments in the Sado estuary. Actual problems of oceanography in Portugal, Lisbon, JNICT and NATO.

Valente MJ (2008) As últimas sociedades de caçadores-recolectores no Centro e Sul de Portugal (10000-6000 anos BP): aproveitamento dos recursos animais. PhD Thesis, Faro, Universidade do Algarve, Portugal.

Valente MJ (2014) Mesolithic and Neolithic shell middens in western Algarve: issues in ecology, taphonomie and economy. In: Detry C, Dias R (Eds.) Proceedings of the first Zooarchaeology Conference in Portugal (BAR Int. Ser. S2662), 23-32. Oxford, Hadrian Books.

Valente T, Fatela F, Moreno J, Guise L, Patinha C (2009) A comparative study of the influence of geochemical parameters on the distribution of foraminiferal assemblages in two distinctive tidal marshes. Journal of Coastal Researsh, SI 56, 1439-1443.

van der Schriek T, Passmore DG, Rolão J, Stevenson AC (2007a) Estuarine-fluvial floodplain formation in the Holocene Lower Tagus valley (Central Portugal) and implications for the Quaternary flivial system evolution. Quaternary Science Reviews 26, 2937-2957. https://doi.org/10.1016/j.quascirev.2007.07.020.

van der Schriek T, Passmore DG, Stevenson AC, Rolão J (2007b) The paleogeography of Mesolithic settlement-subsistence and shell midden formation in the Muge valley, Lower Tagus Basin, Portugal. The Holocene 17(3), 369-385. https://doi.org/10.1177/0959683607075839.

van der Schriek T, Passmore DG, Mugica FF, Stevenson AC, Boomer I, Rolão J (2008) Holocene palaeoecology and floodplain evolution of the Muge tributary, Lower Tagus Basin, Portugal. Quaternary International 189, 135-151. https://doi.org/10.1016/j.quaint.2007.09.007.

van Geel B (1978) A palaeoecological study of Holocene peat bog sections in Germany and The Netherlands, based on the analysis of pollen, spores and macro- and microscopic remains of fungi, algae, cormophytes and animals. Review of Palaeobotany and Palynology 25, 1-120.

van Geel B (1986) Application of fungal and algal remains and other microfossils in palynological analyses. In: Handbook of Holocene Palaeoecology and Palaeohydrology, Berglund, B.E. (Ed.), John Wiley & Sons Ltd.: 497-505. Chichester.

van Geel B (1992) Fungal spores as extra indicators for human impact in the past? Abstracts 8th International Palynological Congress, Aix-en-Provence.

van Geel B, Bohncke SJP, Dee H (1981) A palaeoecological study of an upper Late Glacial and Holocene sequence from "De Borchert", The Netherlands. Review of Palaeobotany and Palynology 31, 367-448.

van Geel B, Coope GR, van der Hammen T (1989) Palaeoecology and stratigraphy of the Lateglacial type section at Usselo (The Netherlands). Review of Palaeobotany and Palynology 60, 25-129.

van Geel B, Buurman J, Brinkkemper O, Schelvis J, Aptroot A, van Reenen G, Hakbijl T (2003) Environmental reconstruction of a Roman Period settlement site in Uitgeest (The Netherlands), with specific reference to coprophilous fungi. Journal of Archaeological Science 30, 873–883. https://doi.org/10.1016/S0305-4403(02)00265-0.

van Geel B. (Ed.), 2006. Quaternary Non-Pollen Palynomorphs. Review of Palaeobotany and Palynology 141, 1-2.

Vis G-J, Kasse C, Vandenberghe J (2008) Late Pleistocene and Holocene palaeogeography of the Lower Tagus Valley (Portugal): effects of relative sea level, valley morphology and sediment supply. Quaternary Science Reviews 27, 1682-1709. https://doi.org/10.1016/j.quascirev.2008.07.003.

Vis G-J, Bohncke SJP, Schneider H, Kasse C, Coenraads-Nederveen S, Zuurbier K, Rozema J (2010) Holocene flooding history of the Lower Tagus Valley (Portugal). Journal of Quaternary Science 25(8), 1222-1238. https://doi.org/10.1002/jqs.1401.

Vis G-J, Cornelius K, Kroon D, Vandenberghe J, Jung S, Lebreiro SM, Rodrigues T (2016) Time-integrated 3D approach of late Quaternary sediment-depocenter migration in the Tagus depositional system: From river valley to abyssal plain. Earth-Science Reviews 153, 192-211. https://doi.org/10.1016/j.earscirev.2015.11.002.

Vos P and De Wolf H (1988) Methodological aspects of paleoecological diatom research in coastal areas of the Netherlands. Geologie en Mijnbouw 67, 31-40.

Vos PC, De Wolf H (1993) Diatoms as a tool for reconstructing sedimentary environments in coastal wetlands: methodological aspects. Hydrobiologia 269/70, 285-296.

Wang J-Z, Ni H-G, Guan Y-F, Zeng EY (2008) Occurrence and mass loadings of n-alkanes in riverine runoff of the Pearl River Delta, South China: Global implications for levels and inputs. Environmental Toxicology and Chemistry 27 (10), 2036-2041. https://doi.org/10.1897/08-034.1.

Weckström K (2006) Assessing recent eutrophication in coastal waters of the Gulf of Finland (Baltic Sea) using subfossil diatoms. Journal of Paleolimnology 35, 571-592.

Wilson GP, Lamb AL, Leng MJ, Gonzalez S, Huddart D (2005a) Variability of organic $\delta^{13}C$ and C/N in the Mersey Estuary, U.K. and its implications for sea-level reconstruction studies. Estuarine, Coastal and Shelf Science 64, 685-698. https://doi.org/10.1016/j.ecss.2005.04.003.

Wilson GP, Lamb AL, Leng MJ, Gonzalez S, Huddart D (2005b) $\delta^{13}C$ and C/N as potential coastal palaeoenvironmental indicators in the Mersey Estuary, UK. Quaternary Science Reviews 24, 2015-2029. https://doi.org/10.1016/j.earscirev.2005.10.003.

Witkowski A, Lange-Bertalot H, Metzeltin D (2000) Diatom Flora of Marine Coasts I. Iconographia Diatomologica 7. Koenigstein: A.R.G. Gantner.

Whitlock C, Larsen C (2001) Charcoal as a Fire Proxy. In: Smol, J.P., Birks, H.J.B., Last, W.M., Bradley, R.S., Alverson, K. (Eds.), Tracking Environmental Change Using Lake Sediments. Developments in Paleoenvironmental Research, vol 3. https://doi.org/10.1007/0-306-47668-1.

Wong PP, Losada IJ, Gattuso J-P, Hinkel J, Khattabi A, McInnes KL, Saito Y, Sallenger A (2014) Coastal systems and low-lying areas. In: Field CB, Barros VR, Dokken DJ, Mach KJ, Mastrandrea MD, Bilir TE, Chatterjee M, Ebi KL, Estrada YO, Genova RC, Girma B, Kissel ES, Levy AN, MacCracken S, Mastrandrea PR, White LL (eds.) Climate Change 2014: Impacts, Adaptation, and Vulnerability. Part A: Global and Sectoral Aspects. Contribution of Working Group II to the Fifth Assessment Report of the Intergovernmental Panel on Climate Change. United Kingdom and New York, NY, USA: Cambridge University Press, Cambridge, 361-409.

Yamamuro M, Kayanne H, Yamano H (2003) $\delta^{15}N$ of seagrass leaves for monitoring anthropogenic nutrient increases in coral reef ecosystems. Marine Pollution Bulletin 46, 452-458. https://doi.org/10.1016/S0025-326X(02)00463-0.

Zalasiewicz J, Waters CN, do Sul JI, Corcoran PL, Barnosky AD, Cearreta A, Edgeworth M, Gałuzka A, Jeandel C, Leinfelder R, NcNeill JR, Steffen W, Summerhayes C, Wagreich M, Williams M, Wolfe AP, Yonan Y (2016) The geological cycle of plastic and their use as a stratigraphic indicator of the Anthropocene. Anthropocene 13, 4-17. https://doi.org/10.1016/j.ancene.2016.01.002.

Zbyszewsky G (1939) Essai sur l'hydrologie du bassin du Sado (Portugal). Bulletin du Laboratoire de Géographie Physique de la Faculté des Sciences de l'Université de Paris XII(3), 405-427.

Zbyszewsky G, Veiga Ferreira O (1968) Notícia explicativa da Folha 31-C Coruche, Carta Geológica de Portugal 1:50000. Lisboa: Serviços Geológicos de Portugal.

Zbyszewsky G, Veiga Ferreira O, Deus PC, Oliveira J, Rodrigues L, Rodrigues A, Antunes MT (1972) Carta Geológica de Portugal 1:50000 Folha 39-A Águas de Moura. Direcção Geral de Minas e Serviços Geológicos. Lisboa: Serviços Geológicos de Portugal.

Zbyszewski G, Veiga Ferreira O, Rodrigues A, Rodrigues L (1967) Carta Geológica de Portugal 1:50000 Folha 31-C Coruche. Direcção Geral de Minas e Serviços Geológicos. Lisboa: Serviços Geológicos de Portugal.

Zhan Q, Wang Z, Xie Y, Xie J, He Z (2011) Assessing C/N and δ13C as indicators of Holocene sea level and freshwater discharge changes in the subaqueous Yangtze delta, China. The Holocene 22(6), 697-704.

Zhang H, Kovar J (2000) Phosphorus fractionation. In: Pierzynski GM (Ed.) Methods of phosphorus analysis for soils, sediments, residuals and waters. Southern Cooperative Series Bulletin 396, 50-59.

Zilhão J (2003) Algumas observações acerca do Mesolítico do interior peninsular e do modelo de passagem ao Neolítico através de colonização pioneira por via marítima. Comentário a: Carvalho AF, A emergência do Neolítico no actual território português: pressupostos teóricos, modelos interpretativos e a evidência empírica, O Arqueólogo Português, Volume 21, 108-118.

Zilhão J (2004a) Muge shell middens. In: Bogucki, P., Crabtree, P.J. (Eds.) Ancient Europe 8000 B.C. - A.D. 1000: encyclopedia of the Barbarian World. New York, Charles Scribner's Sons, volume I, 164-166.

Zilhão J (2004b) The Mesolithic of Iberia. In: Bogucki, P., Crabtree, P.J. (Eds.), Ancient Europe 8000 B.C. – A.D. 1000: encyclopedia of the Barbarian World, New York, Charles Scribner's Sons, Vol. 1, 157-164.

Zilhão J, Angelucci DE, Igreja MA, Arnold LJ, Badal E, Callapez P, Cardoso JL, d'Errico F, Daura J, Demuro M, Deschamps M, Dupont C, Gabriel S, Hoffmann DL, Legoinha P, Matias H, Monge Soares AM, Nabais M, Portela P, Queffelec A, Rodrigues F, Souto P (2020). Last Interglacial Iberian Neandertals as fisher-hunter-gatherers. Science 367, 1443. https://doi.org/10.1126/science.aaz7943.

Zvelebil M (Ed.) (1986) Hunters in transition. Mesolithic societies of temperate Eurasia and their transition to farming. New Directions in Archaeology. Cambridge University Press, pp. 194.

Zvelebil M (1986) Mesolithic prelude and neolithic revolution. In : Zvelebil M (Ed.), Hunters in transition. Mesolithic societies of temperate Eurasia and their transition to farming, 5-15.

Web References

AGI - Advanced Geosciences Inc. @ www.agiusa.com. Consulted in November 2021.

Bartington's operation manual OM1131 @ https://manualzz.com/doc/12417892/multisus-operation-manual. Consulted frequently until January 2022.

Beta Analytic laboratories @ https://www.radiocarbon.com/beta-lab.htm. Consulted in January 2021.

Endovelico database (DGPC) @ https://arqueologia.patrimoniocultural.pt/. Consulted frequently until January 2022.

European Environmental Agency @ https://www.eea.europa.eu. Consulted in November 2021.

GeoPortal Energia e Geologia (LNEG) @ https://geoportal.lneg.pt/. Consuted in November 2021.

Geoportal DGPC @ https://patrimoniodgpc.maps.arcgis.com. Consulted in December 2021.

GeoSci Developers, 2015-2018 @ https://em.geosci.xyz/content/physical_properties/electrical_conductivity/electrical_conductivity_values.html. Consulted in January 2022.

Google Earth Pro 7.3.4.8248, 2019, Arapouco, Sado valley (Portugal), lat: 38.320508°, long: -8.484917° [online] @ http://www.google.com/earth/index.html. Consulted in December 2021.

Google Earth Pro 7.3.4.8248, 2019, Laxique, Sado valley (Portugal), lat: 38.253691°, long: -8.375054° [online] @ http://www.google.com/earth/index.html. Consulted in December 2021.

IPMA @ http://www.ipma.pt/pt/oclima/observatorio.secas/spi/monitorizacao/situacaoatual/, Index SPI 12 months. Consulted in January 2022.

MarLIN - The Marine Life Information Network, accessible at www.marlin.ac.uk. Consulted in January 2022.

LIST OF FIGURES

LIST OF TABLES

Este trabajo aborda el estudio del contexto medioambiental del valle del Sado (Portugal) durante las ocupaciones del Mesolítico final (*ca.* 8400-7000 cal BP; 6450-5050 cal BC). Desde al menos 8850 cal BP, se establecieron condiciones salobres en el sector del valle en el que se localizan los concheros mesolíticos situados más abajo, y fueron predominantes hasta *ca*. 7040 cal BP. En esta zona se desarrollaron ambientes estuarinos (marismas, llanuras mareales), que llegaron hasta 10-15 km aguas arriba del límite fluvio-estuarino actual, donde se localizan los concheros más alejados de la costa. Estas condiciones ambientales hicieron posible la presencia de moluscos y peces marinos en la proximidad de las áreas de ocupación y su explotación por parte de las comunidades de cazadores recolectores del SO ibérico. Las condiciones estuarinas se mantuvieron en el canal principal del Sado hasta el comienzo del Holoceno superior, en torno a 4000 cal BP/2050 cal BC, más allá del abandono de los sitios por los grupos mesolíticos.

This work focuses on the environmental context of the Sado valley, Portugal, during the Late Mesolithic occupation (ca. 8400-7000 cal BP; 6450-5050 cal BC). Brackish conditions established in the section of the valley where the most downstream Late Mesolithic shell middens are located, since, at least, 8850 cal BP and prevailed until ca. 7040 cal BP. Estuarine environments, i.e., saltmarshes and tidal flats, developed in the area, reaching 10-15 km upstream the present-day fluvio-estuarine boundary, where the most upstream Late Mesolithic sites were identified. The environmental settings allowed for the occurrence and for the exploitation of marine molluscs and fish by the last hunter-gatherer communities of SW Iberia, at the proximity of the occupation areas. The estuarine environments maintained in the Sado main channel until the beginning of the Late Holocene, long after the abandonment of the sites by the Mesolithic groups.

UAB Universitat Autònoma de Barcelona

UC UNIVERSIDAD DE CANTABRIA Escuela de Doctorado